Catalysis and Sustainable Polymers: Bridging the Homogeneous-Heterogeneous Gap

Howard, Ioli

Award date:
2021

Awarding institution:
University of Bath

Catalysis and Sustainable Polymers: Bridging the Homogeneous-Heterogeneous Gap

submitted by

Ioli C. Howard

for the degree of Doctor of Philosophy

of the

University of Bath

Department of Chemistry

Supervisors: Dr Antoine Buchard & Dr Ceri Hammond

June 2021

COPYRIGHT

.....

Signed on behalf of the Faculty of Science .....

Abstract

Plastics are found everywhere, from electronics to materials, and while these are a revolutionary material, they go hand in hand with significant levels of environmental pollution. To this end, renewable plastics such as aliphatic polyesters, sourced from natural feedstocks with the potential to degrade into non-toxic components, are necessary to replace the non-degradable, fossil fuel-derived plastics; for this reason, poly(lactic acid) (PLA) alone is now produced on a multi-tonne scale each year.

Despite this, the synthesis of polymers such as PLA are plagued with their own challenges, including residual cytotoxic metals from the catalyst which could render the plastic unsuitable for use in biomedical or food packaging applications. Throughout this thesis, renewed efforts to create robust, biocompatible heterogeneous catalysts are explored, leading to plastic with low levels of metal content and offering new strategies for the recovery and reuse of these catalysts, in an effort to contribute to a circular plastic economy.

To begin, Chapter 1 will explore the structure, properties and synthesis of PLA and the current homogeneous catalysts which offer rapid, controlled ring-opening polymerisation (ROP), and discuss their shortcomings. The benefits of heterogeneous catalysis are outlined, along with a summary of heterogeneous catalysts for ROP, and how these can be implemented into a flow reactor for continuous production of polymer. Chapter 2 offers an overall summary of how these topics feed into the thesis work.

Chapter 3 covers the published work (I. C. Howard, C. Hammond, A. Buchard, *Polym. Chem.*, 2019, **10**, 5894-5904), describing the development of a series of metal complexes, immobilised onto an inert poly(styrene) (PS) support. Excellent, rapid conversions within 55 minutes are observed in the solvent-free ROP of *L*-Lactide (LA), with M_{n} up to 35 000 Da and minimal leaching of the metal into the crude polymer (335 ppm). Catalyst reuse is also explored, with up to 7 reuse cycles, suggesting these systems as promising reusable catalysts for the industrial production of metal-free renewable polymers.

These catalysts are used in Chapter 4, covering the ROP of other lactones such as ϵ-caprolactone and ϵ-decalactone and extending to the copolymerisation of these

with *L*-LA. Investigations into copolymer microstructure reveal the formation of amorphous copolymers with random distribution of the monomers throughout the copolymer when a one-pot method is used, while block copolymers form when a sequential monomer addition method was utilised. ABC and ABA triblock copolymers can also be accessed, highlighting the potential to create a thermoplastic elastomers (TPEs) with these heterogeneous catalysts.

Chapters 5 and 6 examine the ROP with heterogeneous organocatalysts. Chapter 5 first looks at the ROP with commercially available PS-immobilised organocatalysts in the melt ROP, with comparisons to their homogeneous analogues. Coupling these with an immobilised urea (PS-U) to improve the activity of the bases is investigated: compared to other bases, an improvement in conversion is possible when PS-U is combined with imidazole (from 64 to 73% conversion). Proximity of the base to the PS-U is necessary to enable cooperativity, with larger bases struggling to access the PS-U active site for bifunctional ROP. This indicates that correct selection of the base and urea combination is needed to improve conversion; the nature of the urea catalyst and the base must be well matched to achieve cooperation between the two components.

Chapter 6 considers the solution-phase ROP using the immobilised (thio)urea catalysts coupled with KOEt, creating a semi-heterogeneous bi-component system. Formation of the active thioimidate ion is confirmed and evidence of modification in base activity by the PS-(T)U is presented, achieving increased levels of ROP control due to the better coordination between the two components in solution-phase. Combination of KOEt with PS-U improved the ROP control compared to the base on its own, with a more reliable increase in conversion over time, reaching 87% in 30 minutes, with a monomodal SEC trace.

Finally, Chapters 7-8 explore the beginnings of an effort to implement these heterogeneous systems into a continuous flow reactor. Chapter 7 concerns the solution-phase ROP in a microreactor is explored, using homogeous organocatalysts, working towards the rapid generation of molecular weight libraries to enable information encryption in unique molecular weight distributions; this work was conducted in collaboration with Professor Tanja Junkers at Monash University, Australia. Judicious choice of base, solvent, concentration and temperature (among other parameters) are all explored, achieving 97% conversion of LA in 2

minutes at 35 °C ($Đ_M$ 1.25, [LA]:[DBU]:[I] = 50:1:1, [LA] = 1 mol L^{-1} in DCM). This is then followed by an increase in reactor scale in Chapter 8, built to accommodate heterogeneous catalysts in a packed-bed; reactor development and initial results from the homogeneous ROP in solution phase – used as a model for future heterogeneous work – are outlined.

Acknowledgements

Writing this thesis was a mammoth task... But I finished! How exciting.

I could not have done any of this project without the help of my supervisor, Antoine Buchard, who created a project that bridged all my interests into one happy (and equally frustrating) project. His ability to come up with solutions and perpetual enthusiasm was so great when I was struggling; I could walk into his office completely confused and leave 15 minutes later with a renewed motivation. I really appreciate it — and all the times his office was open so I could vent all my worries. Merci!

I'm also so grateful to Ceri Hammond and Luca Botti for letting me loose around their lab with a saw in the name of reactor building, and for providing me with invaluable advice so that I did not have to start that process from scratch. Thanks to the Catalysis CDT and the EPSRC for the funding; it would've been impossible otherwise.

Thanks also to Tanja Junkers and her joyful and welcoming group in Monash, in particular Maarten and Camille, who took me under their wing and showed me the way of flow chemistry. (To Emma, too, for sharing a birthday so we could celebrate together on the other side of the world!).

Even though I was the only one working on this project at the beginning, so many other people have supported my project in big and little ways: Martin and Rémi (for all sorts of characterisation), John, Tim and Catherine (NMR) and Phil and Diana (SEM) and all the technical staff. Thank you.

I also want to thank Paul (PDP), Thom and Frances for letting me pick their great brains for all the information I could get. Paul: for all the lab help, but also for cracking out the candle making kits during the lead up to Christmas, which made us all feel like children again. Thom: for running about 6 million DSC samples once I had left the lab to write up, just because he is a good egg. And Frances: for quenching all those awkwardly timed reactions during the Covid Shift Era, then reading and re-reading so many drafts of this thesis.

I have been so lucky to be part of a growing group of wonderful people, including Strachan, Marco, Craig, Jamie, Emma and Matt and so many more. Thanks to

Sophie, too, who joined as I was getting Covid-related burn out to carry on the project and brought a fresh set of eyes and enthusiasm to it.

A huge thank you and even bigger hugs to the OG 3.11 crowd (Oli, Dan, Steffi, Izzy, Jamie and little Rach), the Name the Plant gang and others (Callum!), who have created the biggest bubble of PhDs supporting PhDs and provided endless laughs and stress relieving fun (sometimes literally, when we would play catch in the office with a stress ball in times of collective exasperation).

A more specific shout out to Natalie and Megan. Natalie, who has put up with me for almost 10 years (really?!) since undergrad, even after living together for 2 years. Not sure how you did it, but I'm glad. Meg — thank you for your listening ear, wise advice and also teaching me how to do a cryptic crossword (very important).

Thank you, Drew, for the food you have cooked, the calm and the adventures. I don't have the right words, but you know what I mean.

Finally, thank you to mama and pater and sibling (who has requested to be named by her full name: Danai Carolyn Howard), who have been able to shake some sense into me and remind me to do this because I like it, not because I have to.

List of Abbreviations

4-MeBnOH	4-methylbenzyl alcohol
ATR-FT-IR	Attenuated Total Reflectance-Fourier Transform-Infrared
BnOH	Benzyl alcohol
BZA	Polymer-supported benzylamine (Quadrapure beads)
Cat	Catalyst
Conv.	Conversion
$Đ_{\mathrm{M}}$	Dispersity of molecular weights
DBU	1,8-Diazabicyclo[5.4.0]undec-7-ene
DMAP	4-Dimethylaminopyridine
DMSO	Dimethyl sulfoxide
DVB	Divinylbenzene
ϵ-CL	ϵ-caprolactone
ϵ-DL	ϵ-decalactone
I	Initiator
ICP	Inductively Coupled Plasma
$k_{\mathrm{i/p/tr}}$	Rate of initiation/propagation/transesterification
k_{obs}	Observed rate constant
LA	Lactide
MALDI-ToF	Matrix-Assisted Laser Desorption-Time of Flight
M_{n}	Number average molecular weight $\left(M_{\mathrm{n}} = \frac{\sum N_i \sum M_i}{\sum N_i}\right)$
$M_{\mathrm{n,Theo}}$	Theoretical number average molecular weight
M_{w}	Weight average molecular weight $\left(M_{\mathrm{w}} = \frac{\sum N_i \sum {M_i}^2}{\sum N_i \sum M_i}\right)$
NMR	Nuclear Magnetic Resonance
PCL	Poly(ϵ-caprolactone)
PDL	Poly(ϵ-decalactone)
PLA	Poly(lactic acid) or Poly(lactide)
ppm	Parts *per* million
P_{r}	Probability of heterotactic enchainment
PS	Polystyrene
PS-CH_2NH_2	(Aminomethyl)polystyrene
RI	Refractive index
ROP	Ring-opening polymerisation
SEC [GPC]	Size Exclusion Chromatography [Gel Permeation Chromatography]
$Sn(Oct)_2$	Tin(II) Ethylhexanoate (Octoate)
TBD	1,5,7-Triazabicyclodec-5-ene
TGA	Thermogravimetric analysis
T_{g}	Glass transition temperature
T_{m}	Melting temperature
TOF	Turnover frequency
TON	Turnover number
τ_{r}	Residence time
TU/U	Thiourea/Urea

Contents

Chapter 1

Introduction

1.1 Sustainable polymers

Plastics, with their extremely versatile properties, have revolutionised the materials landscape in the last 70 years. Their strength and malleability, coupled with their low toxicity, has made these materials competitive with others such as iron and steel.[1] As such, plastics have been used in a wide variety of applications, most notably as packaging materials, but also within construction materials, textiles and other consumer products.

While plastics have become an increasingly valuable commodity chemical, approximately 92% of all virgin plastics have been derived from finite fossil fuel resources, which have excellent durability. Yet plastics have typically been single-use items, with product lifetimes ranging from less than 1 to 70 years depending on the application; plastic packaging, for example, has a notoriously short lifetime before it is discarded.[2]

Due in part to a "linear plastic economy", where plastics are synthesised, used and thrown away, waste plastic has accumulated in landfill waste streams, leaching into both terrestrial and aquatic ecosystems.[3] Thus far, an estimated 8 300 million metric tons (Mt) of plastic has been synthesised globally, of which 79% were redirected into landfills post-use, while only 9% were recycled.[2] These values are only set to increase, with projections estimating that by 2050, plastic waste landfill will reach 12 000 Mt. It was reported that up to 500 000 tonnes of plastic

waste leaches into marine environments annually, in the E.U. alone.[4]

Although initially an asset, the durability of plastics is inherently coupled with slow chemical degradation rates and has therefore had serious environmental and ecological consequences. The mechanical breakdown of plastic over time creates microplastics (< 5 mm) and is prone to release other harmful materials into the environment such as dissolved organic carbon (DOC) and plasticizers, which can be taken up into the food chain through ingestion by marine species.[5,6]

In moving away from the linear model, several key policy initiatives and white papers have emerged, such as the EU Green Deal and the adoption of the UN sustainable development goals (SDGs), which have looked towards promoting a circular economy.[4,7,8] Here, reduction, reuse and recycling of plastics, along with a move away from finite feedstocks, are now the required standard for plastic production. In the E.U., this translates to a reduction of marine litter and environmental microplastics by 50 and 30%, respectively, by 2030, according to the E.U. environment strategy.[9]

Results from these initiatives include developments in recycling infrastructure, which saw 2016 as the first year in which recycling of plastics surpassed the amount of plastics disposed of into landfills (31% and 27%, respectively).[10] Yet a difficulty in altering human behaviours (*i.e.* implementing recycling over household waste), lack of widespread and safe infrastructure for thermal degradation and a global reliance on plastic, has meant that reduction of plastic usage and recycling schemes must be supported by a transition to more sustainable options to phase out single-use plastics.

1.2 Sustainable plastics: a case for poly(lactide) (PLA)

Sustainable plastics – those sourced from naturally occurring feedstocks that do not cause adverse harm to the environment – can offer promising end-of-life-opportunities *via* biodegradation into smaller organic components that can readily be reabsorbed into the environment.[11,12] Thorough comparison between sustainable plastics and plastics derived from petroleum sources established that

the former omit far lower levels of greenhouse gases on production.[13]

Sustainable plastics (used interchangeably here with "polymers" to denote materials of an assembly of repeating units, or "monomers") may broadly be divided into two subgroups: naturally available polymers such as cellulose and other lignocellulosic polymers, and those which are synthesised from naturally abundant monomer feedstocks.[14] Often, these polymers have oxygenated backbones made up of ester linkages which can readily be broken down through hydrolysis.

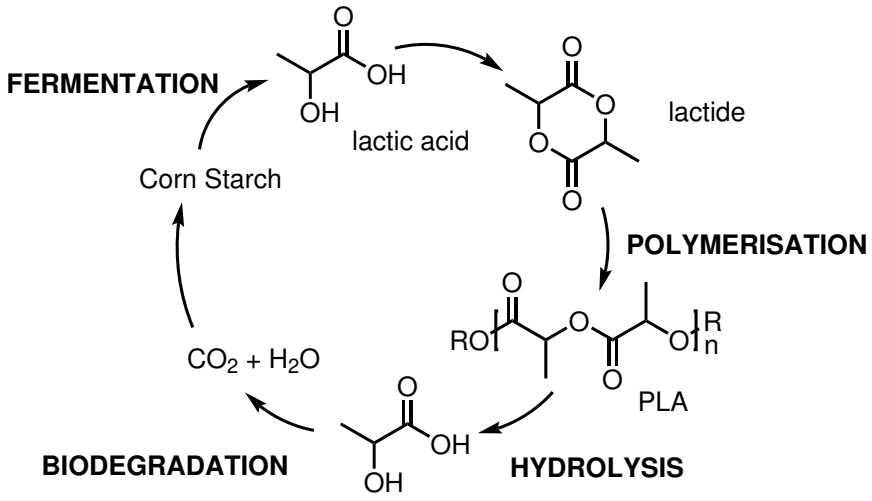

Scheme 1.1: Poly(lactide) life cycle, adapted from Williams and co-workers.[15]

Perhaps one of the most commercially available compostable polymers is poly(lactic acid), or PLA. Usage of the polymer is predicted to have a 50% growth increase within the next five years,[10] and it accounts for 24% of biopolymer production.[12] PLA is a renewable, thermoplastic polymer, which is compostable on an industrial scale and under enzymatic hydrolysis.[16] Interest in PLA largely stems from the potential to use this polymer in a versatile range of applications, including industrial packaging, microelectronics, fibres and, more importantly, in food packaging and *in vivo* biomedical applications such a sutures. Due to its favourable properties such as its strength and barrier properties, PLA has therefore been envisaged as a viable alternative to polyolefins.[12,15]

As the polymer is derived from lactic acid, the PLA that is produced is renewable with a distinct life cycle (Scheme 1.1, adapted from Platel *et al.*).[15] Lactic acid is a naturally occurring, optically-active α-hydroxy carboxyic acid which is itself often

produced within natural organisms and bacteria *via* the enzymatic fermentation of pyruvate in the absence of oxygen.[17] The fermentation process is currently used to produce over 90% of lactic acid from carbohydrate resources.[18] Consequently, when PLA undergoes post-use hydrolysis, lactic acid is produced which is non-toxic, thereby making it one of the most suitable biorenewable polymers for *in vivo* biomedical devices.

1.3 Polymerisation mechanisms of PLA

1.3.1 Polycondensation

PLA can be synthesised using on of two methods, starting from either lactic acid or lactide (LA). In the former, direct condensation of several lactic acid monomer units forms polymers referred to as poly(lactic acid); this step-growth process is known as polycondensation. As condensation reactions are in constant equilibrium, difficulty in manipulating the reaction toward the polymer (*i.e.* the need for constant removal of water to push the reaction towards the product), and the viscosity of the polymerisation medium have been cited as some of the downfalls to the polycondensation reaction.[18] PLA formed by this method can therefore suffer from low molecular weights (M_{n}), and a lack of dispersity control ($Đ_{\mathrm{M}} = M_{\mathrm{w}}/M_{\mathrm{n}}$) may result in non-optimal properties. This can cause the PLA to have significantly lower performance by altering its melting point (T_{m}) and glass transition temperatures (T_{g}), in addition to the polymers strength. Alternative routes to the polymer have therefore been investigated.

1.3.2 Ring-opening polymerisation

A secondary, chain-growth mechanism also exists, known as ring-opening polymerisation (ROP, Scheme 1.2) using LA, the cyclic dimer of lactic acid. The work herein concerns ROP of LA to form poly(lactide), which will be referred to throughout as PLA.

The ROP of LA was first demonstrated by Carothers *et al.* in 1932.[20] The cyclic ketone could be obtained by polycondensation of aqueous lactic acid, followed by a depolymerisation (backbiting) step to form the cyclic ketone; polymers formed

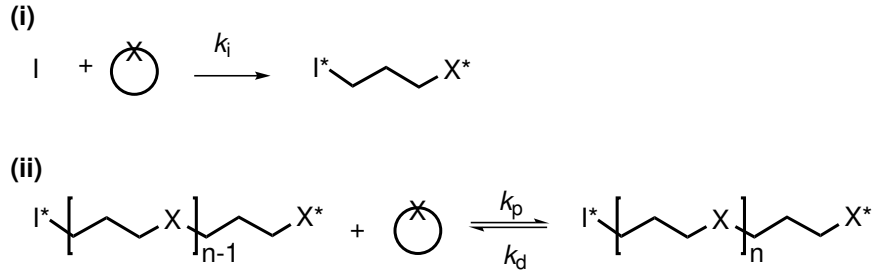

Scheme 1.2: General ROP of cyclic monomers, including the (i) initiation and (ii) propagation steps, adapted from Kamber *et al.*.[19]

this way are dubbed poly(lactide). The full synthesis is carried out at temperatures exceeding 200 °C and pressures below 100 mbar, surpressing the reverse reaction, which is thermodynamically favoured.[17,18] LA can equally be produced *via* an alkyl lactate intermediate,[21] or using zeolites. The latter's small pore size enables polycondensation to dimeric and trimeric oligomers, followed by instant cyclisation to lactide. This encourages shape-selectivity of the product, and reduces the quantity of oligomeric waste products that are seen with the two-step process described above.[22]

ROP is an equilibrium process which lies towards the macromolecular product, the polymerisability of the monomer is dependent on thermodynamic drive to form a polymer. This is a process best described by the Gibbs free energy (ΔG_p), which contains both enthalpic (ΔH_p) and entropic (ΔS_p) components (Equation 1.1).[23] Since the relief of ring strain of 4, 6 and 7 membered cyclic monomers is thermodynamically favoured (*e.g.* $\Delta H_\mathrm{LA} = -22.9$ kJ mol^{-1}, generating a negative ΔG_p), ROP has become the industrially preferred method to synthesise polymers such as PLA.[15,24] Industrial ROP is typically conducted in melt conditions with a $\mathrm{Sn(Oct)_2}$ catalyst at 140 - 180 °C for up to 5 hours, using a catalyst loading of 100-1000 ppm.[25]

$$\Delta G_p = \Delta H_p - T\Delta S_p \tag{1.1}$$

ROP offers far greater M_n and $Đ_\mathrm{M}$ control by comparison to polycondensation,[26] the latter of which is obtained when the rate of initiation (k_i) is greater than or equal to that of propagation (k_p).[23] The potential to obtain a "living" polymer-

isation reaction, where chain transfer and termination reactions are suppressed (therefore k_{tr} and k_t, respectively, are equal to zero),[23,27] results in an overall linear increase in molecular weight with conversion, which is described by simple first order kinetics.[19]

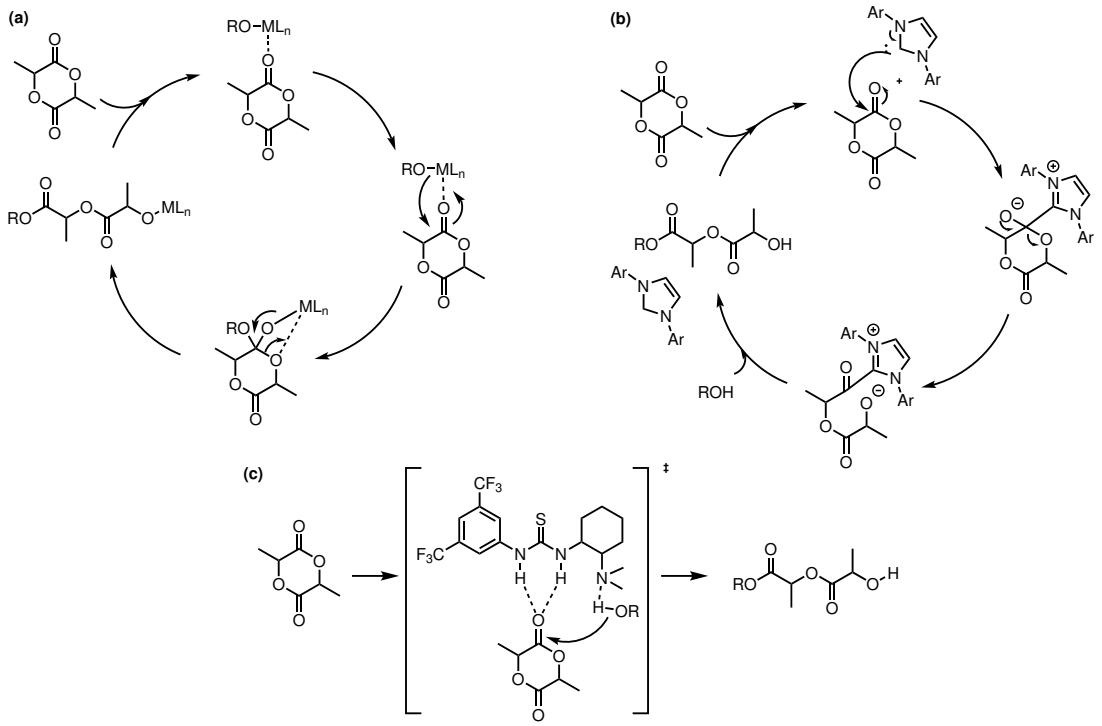

Scheme 1.3: Ring-opening polymerisation of poly(lactide), occuring *via* the (a) coordination-insertion mechanism, (b) activated monomer mechanism, or (c) bifunctional mechanism.[15,28]

ROP itself has many possible mechanisms, including coordination-insertion, covalent and anionic or cationic mechanisms, determined by the initiator used to catalyse the reaction. Amongst these, ROP will typically occur *via* the anionic coordination-insertion mechanism if a metal complex is used (Scheme 1.3a). This is typically seen with nucleophilic metal alkoxides such as Al(O^{i}Pr)$_3$, or tin(II) octoate (Sn(Oct)$_2$); the latter of which has been suggested to proceed *via* generation of a metal alkoxide *in situ* when used in conjunction with an alcohol initiator.[29] In this case, the metal will coordinate to the carbonyl oxygen, activating the carbonyl carbon to attack by the alkoxide. Insertion of the lactide into the metal alkoxide bond can then occur through the breakage of the C−O ether bond, *via* a four-membered transition state.[24]

ROP can also occur *via* an activated monomer mechanism, whereby abstraction of the monomer hydrogen generates an activated monomer anion. The latter is then able to add to the propagating chain through nucleophilic attack onto an alcohol group. This mechanism has been proposed for organocatalytic systems, such as with N-heterocyclic carbenes (Scheme 1.3b, adapted from Platel *et al.*).[15]

A bifunctional mechanism (Scheme 1.3c) has also been reported, whereby an electrophile and nucleophile work synergistically to activate both the monomer and the initiator.[27,30,31] For a more detailed discussion on this, please refer to Chapters 5 and 6.

The ROP of lactide can be conducted in both solvent and melt conditions (above the melting temperature of LA, 95 °C). The latter is environmentally favoured over the use of potentially toxic and otherwise harmful solvents, which are often used in huge excess and to a large economic cost.

1.4 Structure/property relationship of PLA

1.4.1 Lactide isomers and PLA microstructure

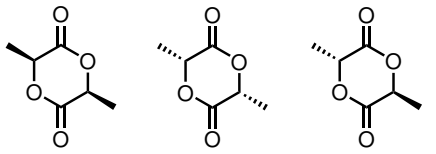

Scheme 1.4: Lactide conformers.

Each LA unit contains two stereocentres which can adopt either D*(R)*- or L*(S)*-chirality. When both chiral centres are *S*-configured, this is known as *L*-LA, whilst *R, R*-conformers are known as *D*-LA (although this is less common). An intermediate *meso*-lactide stereoisomer is formed when one of each chiral centre is present in the lactide unit (Scheme 1.4).

Once ring-opened, this can lead to a multitude of different tacticities (Scheme 1.5), and therefore even trace amounts of optical impurities can lead to varying crystallinity of the final polymer. This can lead to changes in both the rates

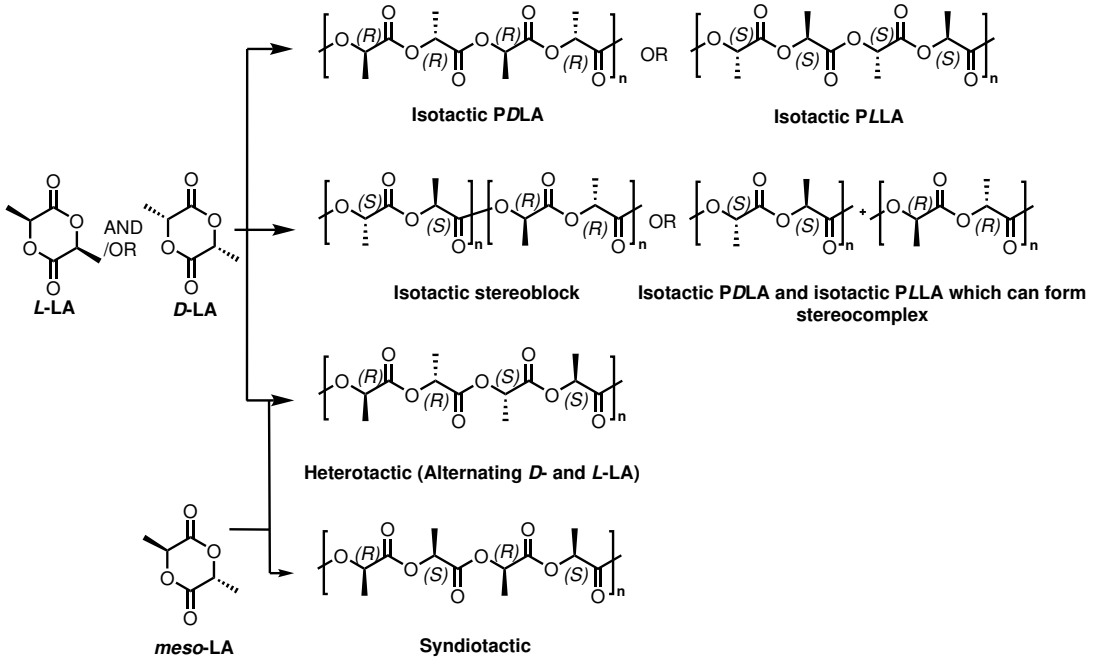

Scheme 1.5: Microstructures of PLA arising from different lactide stereoisomers, adapted from Dove and co-workers.[32]

of biodegradation and the physical properties such as the melt (T_{m}) and glass transition temperatures (T_{g}).[33]

Semicrystalline, isotactic PLA (P*L*LA or P*D*LA), for example, has a T_{m} of ∼180 °C, and T_{g} of 50 °C, whilst atactic PLA T_{g} of 60 °C, with no reported T_{m}.[32,34] Stereocomplexation of two low molecular weight homopolymeric forms of PLA can increase the T_{m} to 230 °C.

The tacticity of the polymer can be deconvoluted by analysis of ^{13}C and, more commonly, homonuclear decoupled (HND) ^{1}H nuclear magnetic resonance (NMR). These can identify the different splitting patterns of the methine and methyl hydrogens in different stereochemistries.[32] In HND ^{1}H NMR, the five overlapping quartets of the PLA methine proton can be decoupled to five singlets, each representative of one tetrad (sequence of four lactic acid units) combination: *sis*, *sii*, *iis*, *iii* or *isi*, where the four units are arranged either *iso* (*i*, meso) or *syndio* (*s*, racemic), to each other (Figure 1.1). If the tetrad were in *LLLL* configuration, this would correspond to the *iii* peak, for example. The tacticity is typically defined by the parameters P_{m} (probablity of isotactic enchainment, *i.e.* probability of

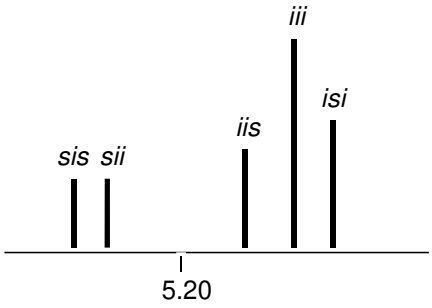

Figure 1.1: Scheme of homonuclear decoupled methine region of PLA in the ^{1}H NMR spectrum, highlighting the peaks and associated tetrads, adapted from Stanford and Dove.[32]

inserting a new isotactic diad) and P_{r} (probablity of heterotactic enchainment), which are based on Bernoullian statistics (Table 1.1). Integration of the signals relative to each other can then determine the polymer microstrucutre by calculating the P_{r} or P_{m}.[35–38]

Table 1.1: Tetrad probabilities, based on Bernoullian statistics.[38]

Tetrad	**Probability**
iii	$P_m^2 + P_r P_m/2$
iis	$P_r P_m/2$
sii	$P_r P_m/2$
sis	$P_r^2/2$
isi	$(P_r^2 + P_r P_m)/2$

1.4.2 Stereocontrolled ROP

Whilst there are multiple mechanisms for the ROP of LA, control of the stereochemistry can only proceed by one of two distinct pathways: Stereocontrolled ROP can be achieved by either the enantiomorphic site control (ESC), or by the chain-end control (CEC) mechanisms.[24]

In the former case, stereocontrol is imparted by the chirality of the metal centre in chiral metal complexes, which are some of the only known catalysts to influence stereochemistry *via* this method. It is thought that the chirality of the metal complex influences the stereochemistry of the bound monomer.

If an achiral metal complex is used, however, chain-end control is the most likely

route. In this case, the stereochemistry of the teminal unit bound to the metal in the propagating polymer chain influences the stereochemistry of the next inserted monomer.[32]

1.4.3 Effect of transesterification and epimerisation

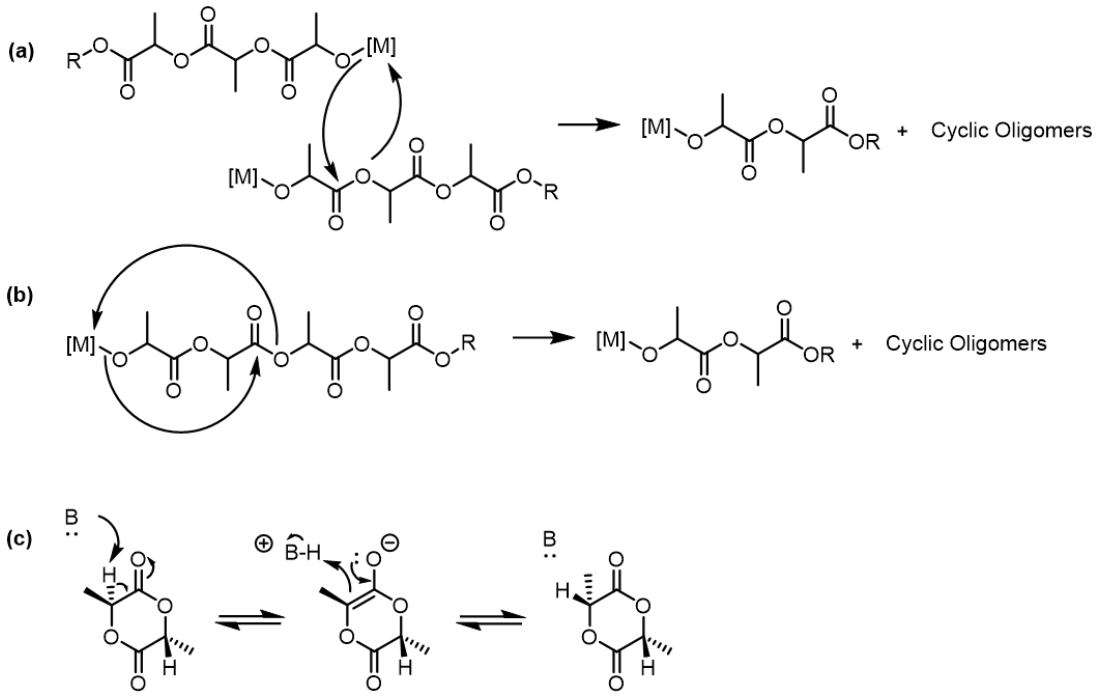

Scheme 1.6: (a) Intermolecular transesterification. (b) Intramolecular transesterification. (c) Epimerisation of lactide with a base.

The dispersity of a polymer is largely controlled by the need for k_p to be slower than k_i. However, it can also be broadened significantly through side reactions, including both inter- and intramolecular transesterification, and therefore the k_p should ideally be greater than the k_tr (rate of transesterification), also.[39] The dispersity of a polymer is important as it can have noticeable effect on the properties of a polymer, such as the melting and glass transition temperatures, and mechanical properties.[40–43]

Intermolecular transesterification (Scheme 1.6a) occurs between two discrete polymer chains, were the oxygen on the alkoxide group of one polymer chain attacks an internal ether group on a neighbouring chain, creating an uneven distribution of chain lengths, and thus increasing the dispersity. In contrast, intramolecular

reaction (Scheme 1.6b) – otherwise known as backbiting – is a slower process which takes place when the ester bridges are cleaved through attack by the alkoxide on the same polymer chain.[44]

Both processes become more likely at higher ROP temperatures, and result in the formation of not only a wider range of polymer chains, but also in the polymer degradation into side products such as both linear and cyclic oligomers.[43–45] Furthermore, as the ROP progresses, the concentration of the monomer decreases to the point where transesterification may become more important; It is therefore vital to obtain the optimum conditions to maximise the M_{n}, whilst avoiding any unwanted transesterifications.

In addition to this, the tacticity of PLA can vary significantly depending on the initiator used. If a strong base is used as an organocatalyst in ROP, for example, this can induce epimerisation of the lactide, whereby abstraction of the methine hydrogen by the base can result in scrambling of the chirality of the lactide. Consequently, the final tacticity of the polymer is randomised once the lactide is ring-opened, forming so-called "stereoerrors" in the polymer, leading to a decrease in the T_{m} of isotactic PLA (Scheme B.25 is an example of the ^{1}H NMR spectra of PLA with and without epimerisation).[46,47]

1.5 Current catalysts in the ROP of LA

Current catalytic investigations have mostly diverged into two paths: creation of biocompatible catalysts which can compete with the current industrial standard, $\mathrm{Sn(Oct)_2}$, and development of catalysts which can promote stereocontrolled ROP of *rac*-LA. The latter is due to the nature of LA as a chiral monomer with multiple tacticities of the final polymer – each with unique properties – so meticulous tailoring of the catalyst to favour one tacticity over another is necessary to control the final properties. An extensive discussion of specific catalysts pertinent to this research is covered within the relevant chapters, although some key recent discoveries are highlighted below (Scheme 1.7).

In terms of speed, both organocatalysts and metal complexes have been reported which provide excellent rates, converting quantative yields in seconds or minutes. Until recently, for example, a zinc guanidine complex was reportedly the fastest

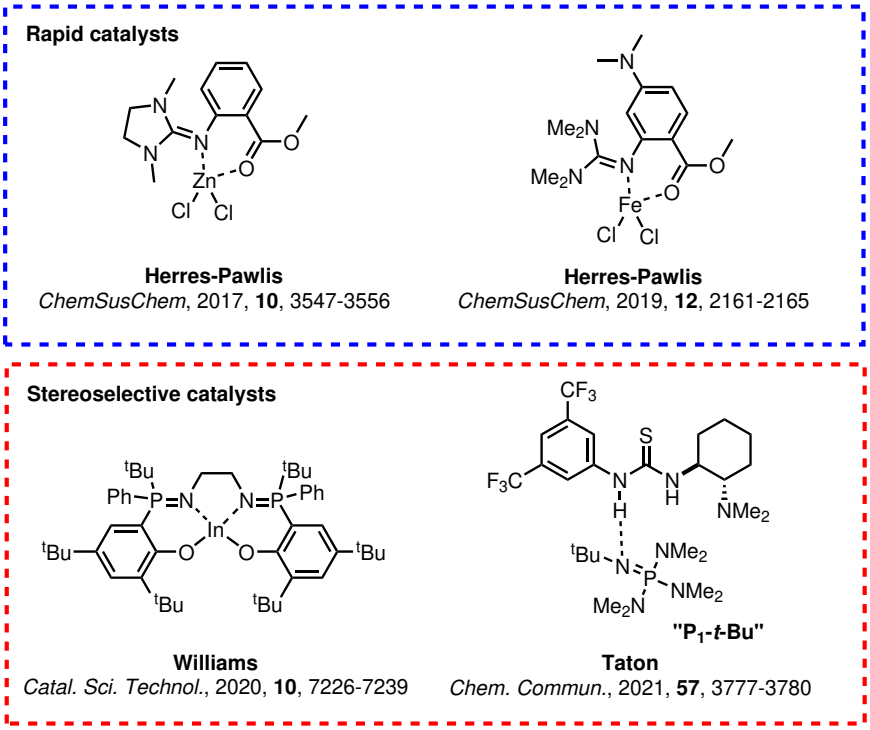

Scheme 1.7: Examples of highly active and selective ROP catalysts.

"robust catalyst" in the bulk (solvent-free) ROP of LA ($k_p = 1.26 \pm 0.06 \times 10^{-4}$ s^{-1}, 52% conversion, M_n 49 400 Da, [LA]:[Cat] = 500:1, 90 minutes at 150 °C, where Cat = catalyst).[48]

However, simply changing the metal can alter catalyst activity drastically. More recently, Herres-Pawlis and co-workers replaced the central zinc atom of a guanidine complex (bearing a similar ligand structure to the above catalyst) with iron, leading to a five-fold improvement in the rate, creating one of the most active metal complexes in the bulk (melt) ROP of LA.[49] In fact, the resulting iron complex was three orders of magnitude faster in the ROP of technical grade *rac*-LA than the previously reported fastest iron catalyst, with a k_{app} of $43.5 \pm 3.5 \times 10^{-4}$ s^{-1} and 0.13×10^{-4} s^{-1}, respectively. *In situ* Raman spectroscopy using recrystallised *L*-LA (for accurate comparison between reactions) determined that the iron complex exceeded the rate of $Sn(Oct)_2$ catalysed reactions under the same conditions (k_p(Fe) = 0.554 ± 0.02 L mol^{-1} s^{-1}, k_p(Sn) = 0.084 ± 0.02 L mol^{-1} s^{-1}, [LA]:[Cat] = 1 000:1, 150 °C, where k_p is determined by plotting k_{app} against catalyst concentration).

On the other hand, (thio)urea organocatalysts have enabled ultrafast ROP in seconds on combination with a strong base and this shall be examined later on in more detail (Chapters 5-6).[50–53] Their tailorable substituents and diverse choice of base has established them as highly competitive with metal complexes.

Imparting chirality into a thiourea bearing an internal amine has also recently enabled stereoselective ROP.[54] When used in conjunction with a phosphazene base (P_1-*t*-Bu), the P_m increased from just 0.57 with P_1-*t*-Bu alone, to 0.96, indicative of a highly isotactic polymer (*rac*-LA, 89%, 8 hours, M_n 23 000 Da, $Đ_M$ 1.08).

While this is an example of organocatalysed stereocontrolled ROP, the majority of catalysts focusing on this area extend primarily to metal complexes. Stereoselectivity can be imparted *via* CEC or ESC, depending on the structure of the complex. Recently, for example, Williams and co-workers developed an achiral indium complex bearing a phosphasalen ligand.[55] The catalyst was determined to adopt a *meso* structure and accomodated a CEC mechanism for stereocontrol according to experimental and computational investigations. At 25 °C in THF ([LA]:[Cat] = 500:1, [LA] = 1 mol L^{-1}), 90% of *rac*-LA was converted in 4.5 hours, yielding highly isotactic PLA (P_i 0.91, TOF = 100 h^{-1}). A comparison to other literature examples established it as not only one of the most isoselective catalysts, but one of the most rapid as well, balancing high activity with stereoselectivity.

Switchable catalysts are another method of achieving similar stereocontrol. Here, one conformation of the catalyst preferentially accommodates one monomer so that, in a one-pot mixture of two monomers, one monomer is consumed before the other, leading to distinct "blocks".[56,57] Application of a stimulus, external to the catalyst ("switch"), interconverts the catalyst between two distinct states (for example, geometrical connectivity or oxidation states) so that it can accommodate an alternative monomer. In the ROP of *rac*-LA, this can mean that defined stereoblocks are accessible through selective consumption of one conformation of LA over the other. The principle is more typically extended to the ring-opening copolymerisation (ROCOP) of lactones with alternative monomers (CO_2, epoxides) to form block copolymers.[58–60] This, however, is beyond the scope of the work herein and shall not be covered further.

In all cases, both homogeneous organo- and metal catalysts have been detailed, providing excellent, tailorable activities due to intelligent catalyst design. These must also be viewed critically, and the following sections shall look to discussing these and offering viable solutions.

1.6 Challenges with homogeneous catalysts

ROP usually uses homogeneous metal alkoxides and complexes based on metals such as Al, Ti, lanthanides and Sn; industrially, $Sn(Oct)_2$ is by far the most prevalent. Whilst this particular catalyst has been approved by the FDA, research has revealed that it is cytotoxic and can inhibit cell growth by 50%, even in low doses.[61,62] Purification of polymers to remove trace quantities of catalyst are costly and often it is impossible to remove all of the catalyst. The Sn content could be reduced to 5 ppm in the ROP of ϵ-CL, however, extremely low catalyst loadings were required to achieve this ([CL]:[$Sn(Oct)_2$]:[I] = 10 000:1:25), which does not always balance with high activities.[63] Indeed, in this particular example, reaction times of two to four days were necessary to achieve reasonable conversions at these loadings.

Consequently, many groups have looked into the use of benign metals such as zinc, calcium and magnesium,[64,65] however hydroxide functionalised complexes of these can be harmful due to their basicity.[15] A zinc proline complex was investigated for cytotoxicity by Parwe *et al.*, for example, finding that the catalyst had very little effect on cell growth.[62] Comparisons between equivalent ligands complexes to various benign metals found that reactivity progressed from the more electropositive metals to the least *e.g.* Mg>Zn>Sn,[24] while Dusselier and co-workers found that transesterification followed roughly the opposite, with Sn catalysts causing the most transesterification.[18]

Organocatalysts such as NHCs or thioureas have also been proposed as alternatives to metal catalysts, as it is widely regarded to have far lower toxicity than their metal counterparts. Despite this theory, research conducted by Nachtergael *et al.* has in fact shown that thioureas, for example, are also extremely cytotoxic.[66]

Aside from toxicity, many other issues exist with homogeneous catalysts, namely

in their recovery and reuse. As separation of homogeneous catalysts is almost impossible, these become trapped in the final polymer; the cost of purification is high and reduction of the metal content in the catalyst is often not sufficient to get below the required ppm for a polymer used in the biomedical sector. Loss of the catalyst in the polymer means that recycling of the former is not viable, and where costly metals are used, this can have not only cytotoxic consequences, but also economic ones. Despite trace amounts of catalyst being used for each ROP, the cumulative cost can be high. One further problem is potential for the trace metal to enable post-reaction transesterification and depolymerisations, resulting in broadening of dispersities.

Finally, homogeneous catalysts are typically used in batch processes, which are typically stop-start methods, and therefore costly and time-inefficient. Contrastingly, heterogeneous catalysts can been favoured because of their ability to be applied into flow reactors, enabling continuous syntheses to be carried out.

1.7 Heterogeneous catalysts for ROP

The immobilisation of active catalysts on inert supports has grown as a field in the last few decades, offering significant advantages over homogeneous catalysts.[67] One of the main drawbacks of homogeneous catalysis is their recyclability and reuse; typically the catalyst can be lost within the product and often separation of the two is costly or impossible. Deposition of the catalyst onto an insoluble, inert support by either ionic or covalent interactions to create a so-called "heterogeneous analogue" can therefore result in ease of separation of the catalyst from the final product.[68–70] Simple filtration of the catalyst from the reaction medium and washing allows products of high purity to be obtained.[71]

Since one of the draws to PLA is its potential to be used in biomedical applications, a reduction in the metal content in the final polymer is vital. This not only results in the recovery of the catalyst, but also allows for potential catalyst reuse.

Several other added benefits also exist, such as the overall cost of a catalytic system. Where expensive precious metals or complex, unsymmetrical ligand structures with lengthy synthetic pathways are used, recovery and reuse is vital to

ensure that these materials are not put to waste and lost in the reactions they enable. Furthermore, whilst many catalysts are only used in trace amounts and therefore the individual cost of each reaction is low, when scaled up, loss of the catalyst can have a significant impact on the overall cost of the process.

The immobilisation of catalysts has also been shown to improve their stability:[70] The immobilisation process of typically air and moisture sensitive reagents, such as those based on lewis acidic metals like $AlCl_3$ on polystyrene, has mediated the sensitivity and thus poisoning of these catalysts, allowing them to be used under atmospheric conditions.[72] This phenomenon can also be applied for toxic or odorous chemicals.

Some evidence has been presented for a slight alterations in the "microenvironment" around an immobilised reagent, altering in selectivity and reactivity.[73] Nevertheless, these can be mitigated to some extent by careful reagent design. Further, use of the inert support provides very little structural change of the catalyst itself, so these heterogenised catalysts can carry out the same reactions as their homogeneous counterparts. Excess reagents can also be used to drive reactions to completion with no added complications to the synthetic procedure.[74] The synthesis of these catalysts therefore does not change – an immobilisation step is merely required.

All of these characteristics enable heterogeneous catalysts to be applied in flow reactors,[75] where the catalyst can be implemented into a reactor column, with reagents flowing through the reactor in liquid or gaseous form. In this way, the catalyst is inherently separated from the reagents and a continuous synthesis generating high yields can be obtained.[76] This is far more beneficial to industry over batch syntheses, which typically employ a stop-start method and can therefore be very energy intensive processes.

Since immobilised catalysts for ROP are still relatively novel, characterisation of the catalyst remains limited to very few techniques, as solution-phase NMR spectroscopy is impossible.[77] Amongst these techniques, infra-red (IR) spectroscopy remains one of the predominant methods to identify characteristic bond vibrations within a complex, for example.[70] The shift in frequency of these vibrations, depending on substituent effects or complexation to a metal, can also

be monitored to indicate the success of a reaction. Whilst not quantitative, IR spectroscopy is a quick and accessible tool to monitor reactions and these can be extended to kinetic investigations through use *in situ* IR probe. Solid-state NMR is another possiblity, but the expense and lack of access to facilities often mean that this is not a widely-used method. Thermogravimetric analysis (TGA) and elemental analysis (EA) are additional tools to support the synthesis of a single-atom site catalyst; the latter can be used as a more quantitative tool to determine functional group loading on a resin.

The support is also frequently porous, leading to diffusion and mass transport limitations. Whilst this problem can be reduced by swelling the support in solvent prior to use, longer reaction times are generally necessary in comparison to homogeneous systems.

1.7.1 Heterogeneous catalysts in small molecule synthesis

Heterogeneous catalysis is typically associated with small molecule synthesis and transformation. This class of catalysts can itself vary widely, depending on both support and functional group choice, covering frameworks to nanoparticles on bulk supports. Metal-organic frameworks (MOFs), are some key examples of modifiable frameworks, while zeolites and silica are examples of acidic surfaces which can be utilised directly.[78–80] Other supports involve nanoparticles as semi-heterogeneous catalysts,[81,82] or catalysts supported on bulk materials such as SiO_2, Al_2O_3, TiO_2 or carbon-based supports such as activated carbon,[83,84] although these shall not be covered in the following discussion.

Instead, the focus shall be directed towards polymer-supported catalysts: bulk materials or polymers, which are typically functionalised with organic molecules or metal complexes, as single-site heterogeneous catalysts (SSHCs), with well-defined active sites.[67]

The design of various ligand architectures is a crucial benefit to site-isolated heterogeneous catalysts (SIHCs) over supported metals or nanoparticles. SIHCs are well-defined organometallic complexes, immobilised onto supports through covalently bound ligands.[86] The complexes can be immobilised in a "bottom-up" approach, where either anchoring of a pre-formed metal complex onto the support,

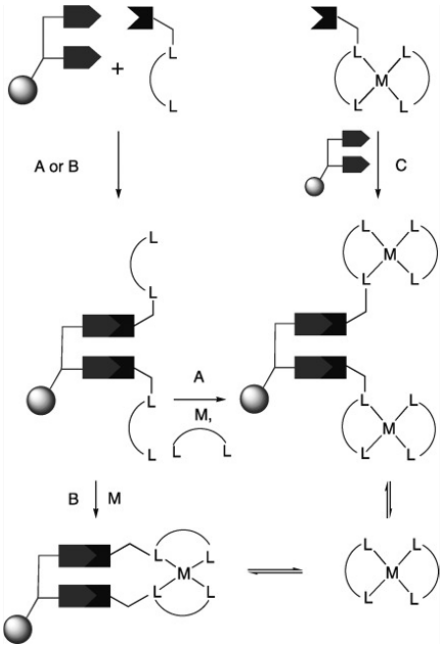

Scheme 1.8: Strategies for catalyst immobilisation on an insoluble support, from Jain *et al.*[85]

or build-up of the complex in a step-wise manner starting from immobilisation of the ligand, followed by metal complexation, can occur (Scheme 1.8).[85,87] The reagent can thus be covalently or ionically tethered to the support.[88] Although characterisation of the final complex and easy monitoring of reaction progress is limited with these types of system, this remains a very popular and easy method for the synthesis of immobilised reagents.

A large proportion of this class of catalyst feature polymeric supports, which have been extensively reviewed in the literature.[68,69,76,88] A urea functionalised ionic polymer based on imidazolium, formed by high temperature synthesis, was also used in the formation of carbonates from CO_2 (Sheme 1.9).[89] The final catalyst was reminiscent of a branched covalent-organic framework (COF), with ionic bonding between Br^- and the imidazolium cation linkers. Similarly, a semi-immobilised catalyst created out of a microporous polymer network (MPN) was reported, based on Lewis basic triarylphosphine backbones.[90] The latter formed a Frustrated Lewis Pair (FLP) with $B(C_6F_5)_3$ (BCF), allowing for cleavage of H_2 at room temperature.

Silica (SiO_2) supports have also been used extensively as both catalysts in their

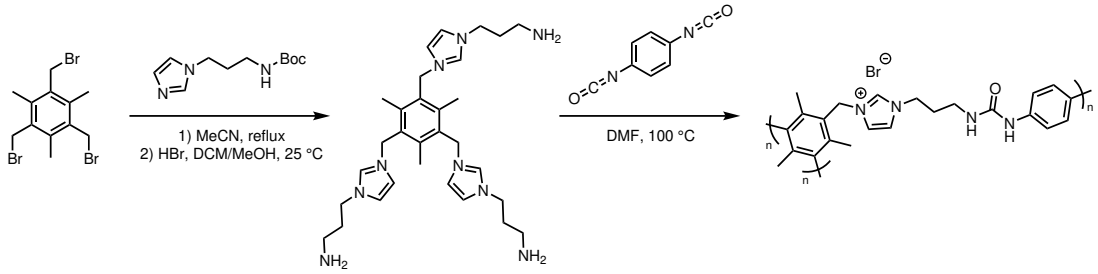

Scheme 1.9: Urea-functionalised COF based on imidazoleum, used in carbonate formation from CO_2.[89]

"raw" bulk format, or as functionalised catalysts. The hydroxy-functional groups on the SiO_2 surface serve as anchoring points for further modification such as metal complex or nanoparticle immobilisation. Accordingly, their versatility in structure spans a wide range of applications. When an amine was immobilised onto a SiO_2 surface, the resulting material was applied in CO_2 capture, encouraging the chemisorption of CO_2 onto the surface.[91] Alternatively, an iridium complex was built up onto the silica surface, generating a catalyst used in C−H borylation.[92] Despite its relative success – in part due to the low cost and high availability – SiO_2 as a support possesses two key issues: in order to get uniform and consistent activity, meticulous control over the micro and mesopores is necessary, while the inherent acidic nature of the support is also problematic, limiting its use in all types of catalysis. SiO_2 as a catalyst support shall be further explored in the following sections, focussing on its uses in polymerisation catalysis.

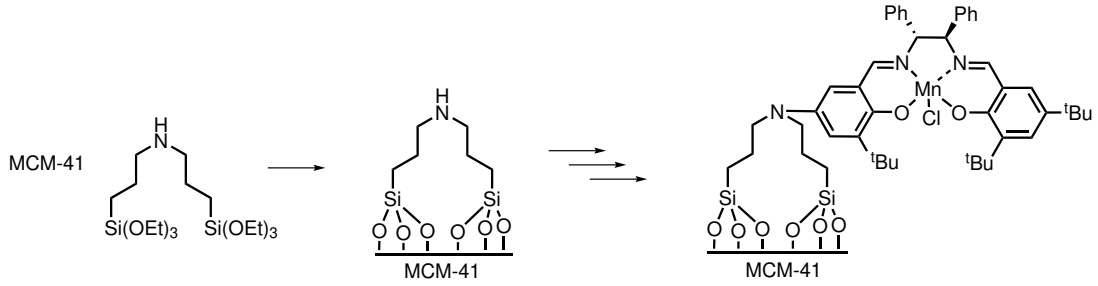

Scheme 1.10: Build up of a metal complex onto the MCM-41 support.[93]

MCM-41, a hierarchically porous silicate, has been functionalised with a manganese complex for use in asymmetric epoxidation.[93] Step-wise construction of the

complex was achieved by first reacting MCM-41 with bis[3-(trimethoxysilyl)propyl]amine, followed by anchoring a benzaldehyde derivative to the secondary amine, forming the base of the salen ligand. The final heterogeneous catalyst was synthesised by from the build-up of the salen ligand, followed by complexation of Mn(III) using traditional salen complexation methods (Scheme 1.10). Recovery of this catalyst was possible, although inductively-coupled plasma (ICP) revealed some leaching of the catalyst had occurred, however recycling the catalyst was possible in certain transformations and conditions.

There have been several reviews published summarising the use of immobilised salen ligands in small molecule organic synthesis,[76,85,94] demonstrating precedent to using these catalysts in polymer synthesis. Given the tendency to use salen catalysts in the ROP of cyclic esters (Chapter 3), immobilisation of these offers an extremely interesting avenue in the advancement of catalysis for ring-opening procedures.

In the previous example, a heterogenised salen catalyst was synthesised in a "bottom-up" approach. Alternatively, a "top-down" approach can be used, whereby a complex is synthesised first, bearing polymerisable functional groups on the ligand (Scheme 1.8). Cross-linking of the complex results in the formation of a self-polymerised porous matrix, similar to a traditional metal-organic framework.

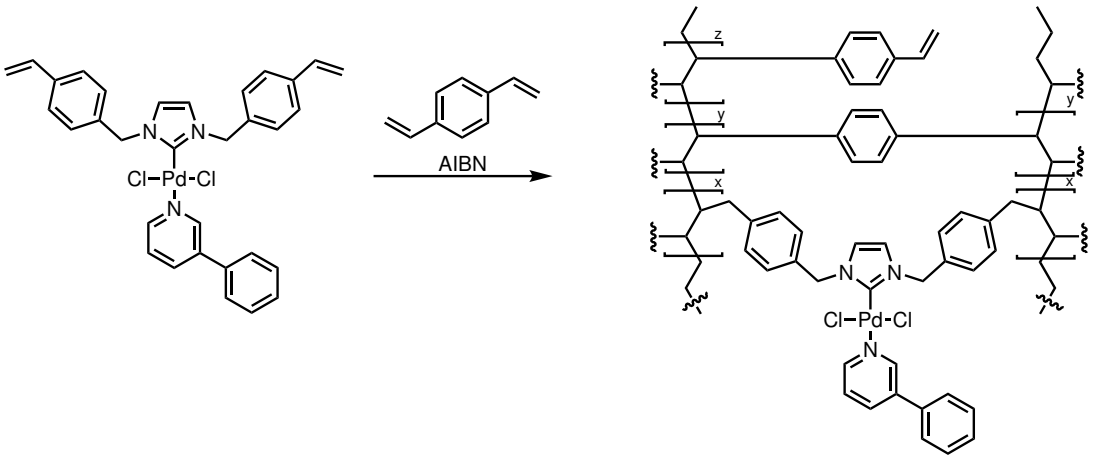

Scheme 1.11: Top down approach: a homogeneous complex with polymerisable substituents is initially synthesised, followed by radical polymerisation with AIBN to form a porous matrix bearing active catalytic sites.[95]

This approach was adopted by Majeed *et al.*, forming a Pd(II) based catalyst with a coordinated N-heterocyclic carbene (NHC) ligand bearing polymerisable alkene groups (Scheme 1.11).[95] Co-polymerisation with azobisisobutyronitrile (AIBN) and divinylbenzene (DVB) resulted in a cross-linked polymer framework made up of Pd(II) complex "nodes" and connecting DVB linkers. While its activity was comparable to that of the molecular analogue (*i.e.* the precursor to the cross-linked matrix), the heterogenised version was recycled up to four times with no loss of activity in the C−H acetoxylation of arenes. Another metal-organic framework based around a Zn(II) salen complex was also reported for CO_2 capture and conversion.[96] Similarly, more traditional salen ligands bearing carboxylate substituents on the phenoxy-moiety can also be used to make polymer matrices, through hydrothermal synthesis of the salen-metal complex to create a coordination polymer.[97–99]

In theory, forming the complex prior to anchoring it within a heterogeneous matrix would reduce leaching of the metal, as robust covalent bonds between the ligand and complex have already been achieved. Characterisation would also not be a problem, as rigorous reaction monitoring and X-ray crystallography and simple solution-phase NMR spectroscopy are available for accurately determining the structure of each intermediate, which is not the case with heterogeneous compounds.

However, the "top-down" approach presents the same difficulties as regular frameworks, including the complexity of the support framework, along with the difficulty in rigorously controlling pore size and uniformity. The presence of unwanted reactive sites (for example, acid sites in silica supports) and often harsh working conditions has also meant that monitoring reactions and elucidating catalyst activity has been challenging.[96] As an example, acidic sites in ROP of lactones cause unwanted side reactions, which can affect the final polymer properties. It is therefore of interest to investigate alternative, inert supports, which do not take part in side reactions, so that it is possible to study heterogeneous catalyst activity without external factors influencing the chemistry of the catalyst.

1.7.2 Poly(styrene) as an inert heterogeneous support

Instead, it is possible to use entirely inert supports as simple alternatives. The ability of these inert supports to swell can potentially minimise diffusion limitations seen with other supports.[69]

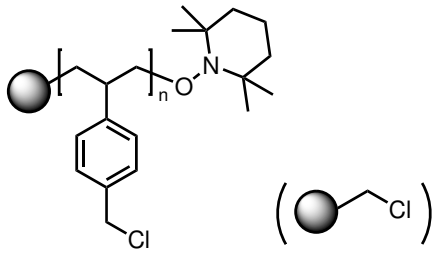

Scheme 1.12: General structure of crosslinked poly(styrene), and simplified format used throughout this report.

Interest in using polymer supports as a strategy for peptide synthesis gained momentum from the development of "Merrifield's resin" in the early 1960s.[100] Merrifield's resin is a chloromethylated polystyrene matrix, typically crosslinked with di(vinyl)benzene (DVB), making it insoluble.[69,74] The nature of the support, bearing pendant Cl-groups (Scheme 1.12), allows for further functionalisation or modification of the support, so that reagents can be grafted onto the support to impart activity onto it.[101] Using this resin, it is possible to undertake what is termed "Solid-Phase Peptide Synthesis" (SPPS), where the resin acts as an anchoring group, the functional group reacts with a substrate (in the case of peptide synthesis: an amino acid), tethering it to the resin, and allowing it to react with the next substrate. The resulting peptide can then be isolated through cleavage of the peptide-to-resin bond.[69]

A benefit of SPPS over using traditional synthetic techniques is the ability to use an excess of reagent to drive the reaction forward. As these are manageable heterogeneous supports, simple filtration to remove any unreacted substrate allows for excellent purification and the ability to synthesise well-defined peptide sequences.

It is also possible to exploit functionalised PS in other applications;[69] these can either tether the substrate to the resin or participate in a chemical process without the final product becoming attached to the surface. The tuneability of various PS

resins bearing either organic[102] or metal functionality has procured a multitude of different applications, including scavengers, transfer agents, or catalysts.[74,103,104] For example, the build up of ligand systems onto PS supports and subsequent complexation to metals has typically been explored for the synthesis of small organic molecules, such as in oxidation,[105] substitution[106] and halogenation reactions.[107] Resulting from their inherent insolubility is the ability to filter out and reuse the resins, as has been the practice with more traditional heterogeneous catalysts.

Inspired by SPPS, Solid-Phase Synthesis (SPS) and combinatorial chemistry quickly became a method of creating large libraries of organic compounds,[108] using Merrifield's resin or derivatives of this.[108,109] Frequently reported is the possibility to automate such SPS procedures – as is the practice with SPPS – which again would benefit the creation of these libraries, without extra purification.[69] However, use of resin based reagents remains more wasteful than traditional processes, as the resin is often not regenerated at the end. Scialdone and co-workers, for example, reported a phoxime resin as a reagent for the SPS of ureas, similar to the method used by Brase *et al.*[110–112] The phoxime resin acted as a transfer agent, moving the functional group immobilised on the resin to the final urea; reuse of the resin in the same process is therefore not possible.

While much research into the development of SPS and SPPS was conducted in the years following Merrifield's first report, the catalytic application was less well investigated until the turn of the century. Despite this, polymer-immobilised catalysts hold a lot of interest due to their versatility and modifiability.

In the following discussion, examples of the uses of polymer-immobilised catalysts in small molecule synthesis and polymerisation reactions shall be explored. Only some relevant examples shall be discussed below, however the area of functionalised PS is a growing area, with reviews covering the synthesis and applications of these reagents.[68,69,76,88,108]

As we have seen, heterogeneous catalysts can be built in a "top-down" or "bottom-up" approach, allowing for a myriad of organic and inorganic complexes to be anchored onto an inert surface (Scheme 1.8).[85] The tuneability of these systems has allowed more interesting characteristics to be introduced into the catalyst.

Magnetic properties can be embedded into the core of the catalyst to ease recovery of the catalyst: Reiser and co-workers, for example, synthesised a tri-substituted urea with an iron nanoparticle core into the PS-support.[104] Nanoparticles can also be accomodated on PS surfaces, such as the Au nanoparticles on PS used by Kaboudin *et al.* in alcohol oxidation.[84] Further, specific ligand architectures can induce chirality at the metal centre, such as an iridum Lewis acid complex reported by Larionov *et al.*.[103] This catalyst proved active in Friedel-Crafts alkylation, with >99% conversions reported, and 97% *ee* for the *R*-isomer.

Immobilised salen ligands have been an excellent example for both of these synthetic methods.[94] A cobalt salen complex was anchored onto PS and used in the [3+2] cycloaddition of azides to alkynes, with yields of up to 98% between 1-2 hours.[85] An immobilised Zn(II) salen catalyst was also reported for the CO_2 coupling with epoxides to produce cyclic carbonates.[96] Due to their success in small molecule organic synthesis, the extensive use of this class of ligand in ROP and synthetic ease, salen complexes immobilised onto PS supports have also been used in polymerisation reactions; this shall be discussed further in the next section.

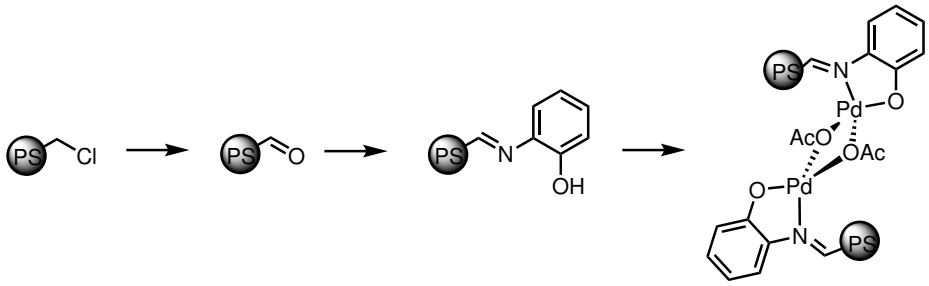

Scheme 1.13: Immobilised complex based on a half-salen ligand.[113]

Half-salen complexes, where there is only one {NO} ligand rather than an {ONNO}-coordination mode, are readily prepared through stepwise build up of the complex onto the PS support, starting with Merrifield's resin (Scheme 1.13).[113,114] Indeed, similar, stepwise synthetic strategy has been emplyed to create a library of immobilised ligands ranging from half-salen to imidazole ligands. These are able to complex a variety of metals, including Pd(II), Ru(II) and Co(II) for carbonylation reactions,[113,115] aerobic oxidations[71] and the synthesis of substituted ureas,[116] respectively. In 2014, for example, a PS-immobilised Pd(II) catalyst was used and recycled in the aminocarbonylation reaction at temperatures of 70 °C, with no

reported leaching of palladium and no decrease in activity.[115]

The variety of ligands, metals and synthetic methods to access these supported catalysts means that a great range of PS-immobilised catalysts are possible. While so far these have been discussed of in terms of small molecule synthesis, their applications are diverse, and it is possible to apply them into polymerisation reactions.

1.7.3 Immobilised catalysts in the ROP of cyclic esters

With regards to heterogeneous catalysts in polymerisations, a large proportion have been used to produce olefins,[78] which has been covered in several reviews.[88,117] One such example involved the anchoring of metallocenes for α-olefin polymerisations, onto an amine binding site on the PS, producing polymers between 80-180 kDa with high $Đ_M$ ($\sim$2).[117]

With regards to ROP, Chen and co-workers anchored a phosphazene onto coated Fe_3O_4 magnetic nanoparticles to use in the ROP of ϵ-caprolactone (ϵ-CL) and δ-valerolactone (δ-VL).[118] In 48 hours, 99% of ϵ-CL was converted in at 25 °C, while control reactions were unsuccessful (M_n 10 400 Da, $Đ_M$ 1.17, [CL]:[Cat]:[I] = 100:1:1). The catalyst could also be recovered and reused up to three times, with no observed decrease in activity (12 hours per cycle, [CL]:[Cat]:[I] = 25:1:3, [CL] = 1 mol L^{-1}, toluene). Despite the low dispersities and high conversions, the reactions were slow, and conducted in solution-phase, and remained untested in solvent free conditions.

Heterogeneous ROP and co-polymerisation reactions have become more common. Wang *et al.*, for example, reported a Cr(III) salen catalyst grafted onto a modified poly(aniline-co-*o*-aminophenol) (MPOAP), which co-polymerised cyclohexene oxide (CHO) and CO_2.[119] The heterogeneous catalyst obtained a $Đ_M$ of 1.08, with a M_n of 10.9 kDa (compared to $Đ_M$ 1.27, M_n of $\sim$ 7.0 kDa for the homogeneous analogue). Similarly, Tsang and co-workers co-polymerised CO_2 and propylene oxide using both SiO_2-supported and unsupported TBD (Scheme 1.14). Reaction at 150 °C and 50 bar CO_2 led to quantitative conversion in 24 hours, showing no decrease in activity on immobilisation of the organocatalyst.[120]

Deng and co-workers developed a heterogeneous ternary catalyst system based on

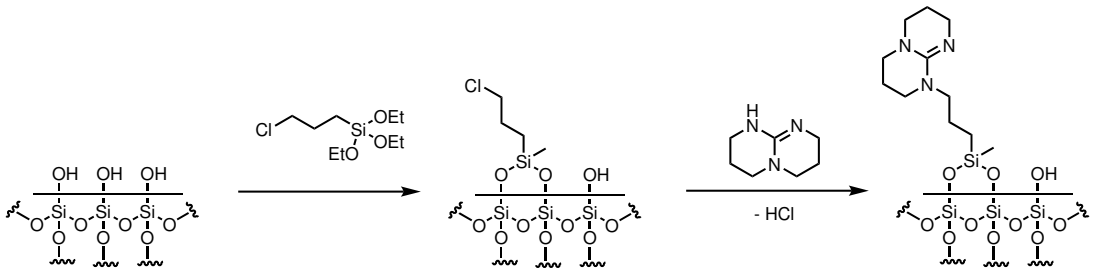

Scheme 1.14: Synthetic strategy to TBD immobilisation.[120]

Zinc glutarate (ZnGA), a cobalt (III) salen complex (SalenCo^{III}) and bis(triphenylphosphine)iminium chloride (PPNCl) for the ring-opening copolymerisation (ROCOP) of CO_2, epoxides and lactones.[121] While ZnGA was inactive in the ROP of *L*-LA, combination with SalenCo^{III} promoted ROCOP of the lactone along with CO_2 and propylene oxide (PO); the cooperation between the Co and Zn centres improved catalytic activity significantly. Molecular weights up to 700 000 Da were possible in the terpolymerisations with the heterogeneous catalyst, at [LA]:[PO]:[Zn]:[SalenCo^{III}]:[PPNCl] = 2 000:7 500:100:1:1 (1 MPa CO_2) in 17 hours ($Đ_M$ 1.01). However, no tests into the catalyst recovery or reuse in sequential cycles were carried out.

SiO_2-immobilised catalysts

With regards to ROP of cyclic esters, the majority of examples involve silica supported catalysts. In 2003, Jones and co-workers immobilised a zinc diimidate complexes onto two types of silica with varying pore sizes (SBA-15 has a pore diameter of 105 Å, and controlled pore glass, or CPG, has a diameter of 246 Å).[122] When used in the copolymerisation of CO_2 and CHO, these complexes demonstrated decent success, with M_n reaching 25 000 Da and broad $Đ_M$ over 1.31 (50 °C, with 6.9 bar pressure of CO_2), comparatively lower than the homogeneous complexes. It was rationalised that the presence of pores created diffusion limitations, thereby reducing the size of polymer, yet were necessary in order to prevent complex decomposition. When used in the solution-phase ROP of LA, it was again concluded that the catalytic activity was significantly lower than the homogeneous analogues first demonstrated by Coates and co-workers.[123] Both diffusion and mass transport limited the M_n of PLA to half the theoretical value, with a conversion of 59% when using SBA-15 (M_n 2400 Da, $Đ_M$ 1.09 at

45 °C in DCM over 24 hours) and 68% with CPG (M_n 2600 Da, $Đ_M$ 1.12 in the same conditions). The higher, more randomly distributed porosity of the CPG support allowed for slightly higher molecular weights over the one dimensional pore structure of SBA-15.

The ROP of lactones has mostly utilised heterogeneous catalysts whose vast majority are tethered onto porous silica (SiO_2) supports. For both LA and ϵ-CL, alkoxide catalysts grafted onto SiO_2 have been synthesised.[79,124–126] A Nd alkoxide on silica catalyst, for example, achieved 100% conversion of ϵ-CL in 30 minutes, with a degree of polymerisation of 9.8.[127] Similarly, the ROP of *L*-LA with a $Ti(O^iPr)_3/SiO_2$ catalyst was carried out over 12 hours at 70 °C.[128] Conversions of 74%, M_n up to 30 300 Da and $Đ_M$ of 1.20 were reported for the heterogeneous catalyst, whilst the homogeneous analogue reached only 66% conversion and 9 600 Da, with a broader dispersity. A tin(II) methoxide catalyst on silica was reported to have higher conversions of LA than the homogeneous version over 1 hour at 180 °C.[129] After 5 hours, the conversions stabilised, reaching 93% (32 000 Da, $Đ_M$ 1.85) compared to 92% (49 000 Da and $Đ_M$ 1.94) for the homogeneous catalyst. The difference in initial activity was attributed to the changing of the electronics of the active site once immobilised, thus creating different electronic environments between sites.

Although silica supports have been effective for the immobilisation of complexes, in many cases that the acidic sites in the silica support play a significant role in chain transfer and transesterification, thereby affecting the polymer properties.[129] An effort has been made to reduce this issue, with some reports of capping of the free silanol sites;[123] while reducing the potential for chain transfer reactions, the lack of silanol groups significantly diminished conversions to 48% compared to the uncapped supports, and increased dispersities due to lack of control (bimodal distributions were observed with $Đ_M$ up to 1.38).[123] The silica pore size has been proposed to prevent the polymer from backbiting, justifying the low dispersities obtained with this catalyst.[79]

The use of SiO_2-immobilised salen ligands in the ROP of lactide is much more sparse; as detailed previously, these have typically been used in small molecule organic synthesis or other polymerisation of other monomers. Most pertinently, Jones *et al.* tethered a Zn(II) half-salen complex to a silica support, and used the

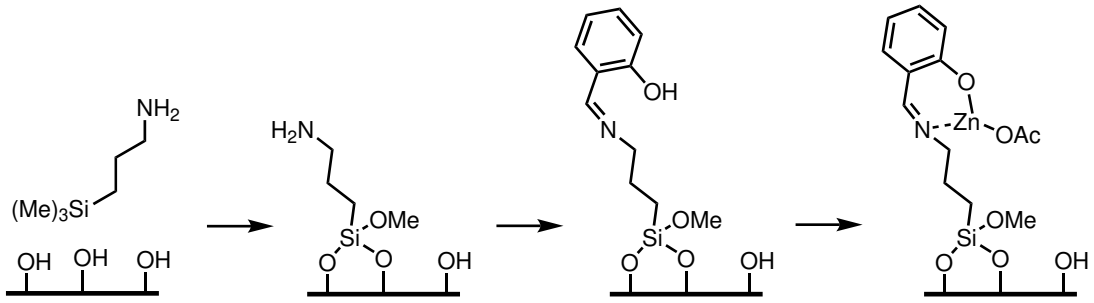

Scheme 1.15: Schematic of the build up of a 6-membered metallacycle, onto a silica support, adapted from Jones *et al.*[126]

catalyst in the ROP of *rac*-lactide in the melt, at 130 °C, with [LA]:[Cat] = 300:1 (Scheme 1.15).[126] Where the homogeneous catalyst achieved an 80% conversion, with M_n 41 200 Da and a broad dispersity ($Đ_M$ 1.43, P_r 0.5), the heterogeneous analogue achieved moderate molecular weights at similar conversions (M_n 19 000 Da), however the dispersity was far lower ($Đ_M$ 1.08), indicating that confinement of the complex within a pore had enabled an improvement in selectivity.[126,130]

PS-immobilised metal complexes

In contrast, there are only a few examples of PS-immobilised catalysts in ROP, most of which are used in solution-phase. Despite the precedent outlined throughout the previous sections, only a small number are metal based – the majority are grafted organocatalysts. PS-supported lithium catalysts, for example, were designed by Chisholm *et al.* to produce cyclic oligomers of PLA using *meso*-lactide in a solution of benzene (25 °C over 4 hours).[131,132] An order of reactivity of Li>Mg>Zn was found, with Li reaching 98% conversion to the cyclic oligomer, whilst Zn catalyst only converted 14% of the lactide to the cyclic oligomer.

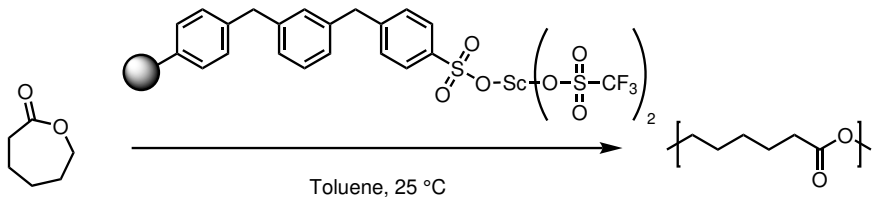

Scheme 1.16: PS-immobilised $Sc(OTf)_3$ used in the ROP of ϵ-CL.[133]

In 2009, Nagata and co-workers used a commercially available PS-immobilised

$Sc(OTf)_3$ in the ROP of ϵ-CL (Scheme 1.16).[133] Using an ethanol co-initiator in toluene at 25 °C, with a monomer:catalyst ratio of 40:1, dispersities remained low ($Đ_M$ 1.12 − 1.26) when using the heterogenised catalyst, despite the longer reaction times required to get similar conversions to the homogeneous catalysts (ca. 85−90%, M_n 6 200 Da). Reuse was also possible, with only a very slight drop in both conversion and M_n to 84% and 5 800 Da, respectively. The bulk ROP of ϵ-CL was also attempted, although dispersities increased despite shorter reaction timescales ($M_{n,SEC}$ 6 300 Da, $Đ_M$ 1.34, 98% conversion after 3 hours, 80 °C, [CL]:[Cat]:[I] = 40:1:1).

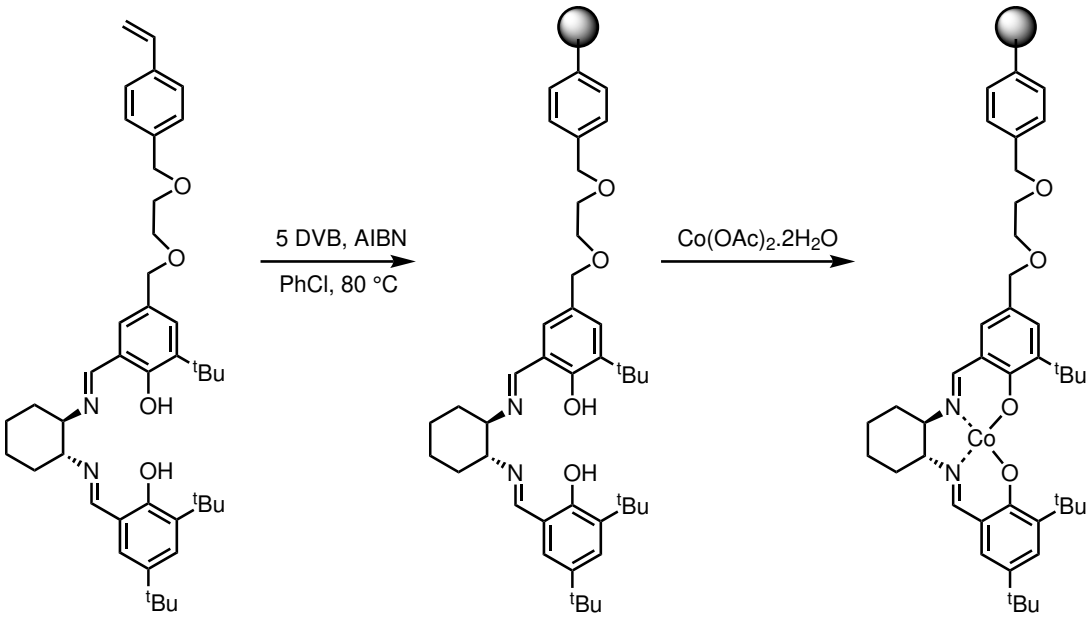

Scheme 1.17: "Top-down" approach towards an immobilised catalyst based on Jacobsen's ligand.[134]

Jones and co-workers have reported the only example of a metal-salen complex grafted onto a polymer resin for use in ROP (Scheme 1.17).[134] Whilst not PS-supported, this catalyst was synthesised similarly to the "top-down" approach: An unsymmetrical salen ligand based off the Jacobsen ligand bearing a chain with an alkene terminal group, substituted on one of the phenoxy- groups of the ligand, was reacted with DVB and AIBN to form an insoluble polymer matrix. Reaction with Co(II) acetate tetrahydrategenerated the salen complex-functionalised resin, which was used in the regioselective ROP of 1,2-epoxyhexane and methanol. Good activities were observed, however catalyst deactivation and leaching of the

metal restricted recycling. Thus far, this is seemingly the only example of an inert polymer-supported salen complex in a ROP procedure. Since many metal complexes on SiO_2 are reported, it is therefore surprising that this has not been explored before.

PS-immobilised organocatalysts

In contrast, organocatalysts grafted onto PS have received slightly more attention, albeit only as side notes in research which mostly concerned their homogeneous analogues. As such, less focus has been placed into exploiting their full capacity to be reused. A study by Shuklov *et al.* used PS-supported 1,8-diazabicyclo[5.4.0]undec-7-ene (PS-DBU) to epimerise *meso*-LA; whilst they showed it was possible, reuse was difficult as lactide oligomers deactivated the catalyst.[135]

Hedrick and co-workers briefly used PS-immobilised DMAP (4-(dimethylamino) pyridine) as an alternative to the homogeneous amidine.[136] After 70 hours at 35 °C, a DP (degree of polymerisation) of 25 was achieved, close to the DP 30 target and comparable activity to the homogeneous counterpart. Excellent ROP control was also achieved, with a $Đ_M$ of 1.08. No further studies were conducted beyond the observation that the catalyst could be removed by filtration; however, these results are evidence for the potential to use these catalysts more regularly.

Likewise, Dove *et al.* reported one ROP example using a PS-immobilised NHC.[137] The ROP reached 95% conversion after one hour at 20 °C ($Đ_M$ 1.52, [LA]:[Cat]:[I] = 200:1.5:1, [LA] = 0.16 mol^{-1} in THF). Comparable activity to the homogeneous NHCs was observed, albeit with slightly higher dispersities. Again, no emphasis was placed on exploring the use of these PS-supported catalysts further than using them as a tool to compare to the homogeneous catalysts.

More recently, Ren *et al.* used immobilised phosphazene catalysts in the solution-phase ROP of various lactones (Scheme 1.18). At a [M]:[Cat]:[I] ratio of 100:2:1, one immobilised phosphazene catalyst (PS-*t*-BuP_2) was recovered *via* filtration, and reused up to five times without any significant decrease in conversion for δ-VL after each cycle (cycle 1: 85% vs. cycle 5: 79%, 100 °C in toluene ($[VL]_0$ = 5 mol L^{-1} in toluene).[138] Later cycles were, however, left for 72 hours as

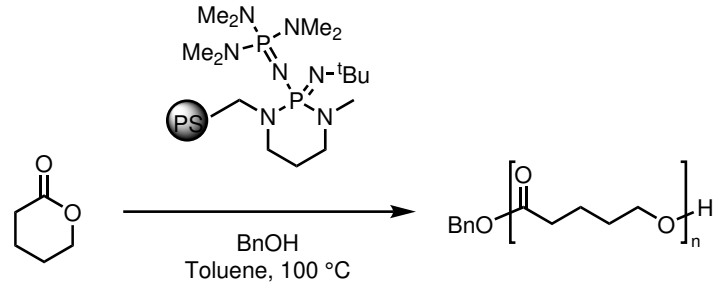

Scheme 1.18: PS-*t*-BuP_2 catalyst for the ROP of δ-VL.[138]

opposed to the original 48 hours, in order to achieve similar conversions to the earlier reuse cycles. Despite the increased timescale, M_n remained consistent, but dispersities dropped from 1.47 to 1.12. An alternative heterogeneous phosphazene (PS-CTPB) was later used for the ROP of other monomers, including *rac*-LA.[139] Conversions of both ϵ-CL, δ-VL and *rac*-LA reached greater than 95% conversion within 15 minutes at room temperature, and recycling of the catalysts was also possible. A cytotoxic assay proved low toxicity of the resulting polymer, further re-enforcing the benefits to alternative heterogeneous catalysts.

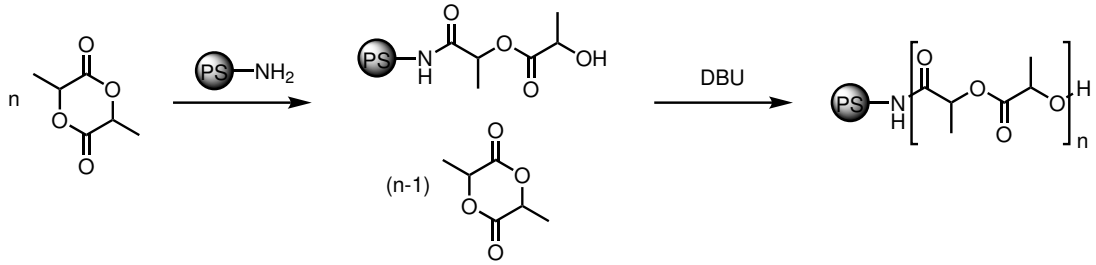

Scheme 1.19: Preparation of amide end-capped PLA to reduce polymer degradation rates. A PS-CH_2NH_2 is used to separate the final polymer from unreacted monomer to improve polymer purity.[140]

It is evident that only some reports exist where an inert PS-support has been used in the ROP of lactones, and often these are not as the catalyst, but initiators, followed by addition of a homogeneous base. Alba *et al.* used both supported and unsupported, "free" amines to initiate the ring-opening of the first unit of lactide at 60 °C for two hours (Scheme 1.19).[140] Subsequent addition of DBU to propagate the reaction afforded amide end-capped PLA, with slower degradation rates compared to the polyester. By using an PS-NH_2 initiator to ring-open LA, it was possible to remove residual unreacted LA at the end of ROP; the PLA would

grow off the PS-support, and removal of the LA could be achieved by filtration of the PS-supported PLA to provide pure, amine end-capped polymer. Various architectures, such as telechelic or star shaped polymers, were also possible using secondary or tertiary amines. It is therefore conceivable to use PS-DBU or another immobilised amine as a catalyst in the ROP of lactide.

Similarly, Wade and co-workers used phosphazene base catalysts in the ROP of cyclic esters, in conjunction with immobilised macroinitiators, to afford block copolymers.[141] When a hydroxyl-functionalised PS (PS-OH) was used as the macroinitiator, the polymerisation reached >99% conversion after 5 hours at room temperature in DCM ([LA]:[Cat]:[I] = 100:1:1, [LA] = 1 mol^{-1}), and SEC analysis indicated successful synthesis of the diblock copolymer. The ROP was well controlled, with molecular weights and dispersities of 20 000 Da and 1.07, respectively.

It is therefore of interest to combine the ROP of lactones with catalysts grafted on inert PS-supports, in order to exploit the versatility of these catalysts and their potential to avoid contamination of the polymer through reuse, and recycling opportunities.

1.8 Catalysis in continuous flow

Flow chemistry has been investigated extensively within the last 30 years, for small molecule synthesis and polymerisation. Implementation of reactions into a flow reactor set-up is viewed a means of process intensification, as scale-up is possible through a variety of means. In the first instance, the flow rate and operation time can be increased, while maintaining a constant residence time (τ_r, time that the reagent spends in the reactor). Alternatively, it is possible to align a series of identical reactors in parallel (either connected to one pump or each with their own individual pump) to obtain a higher volume of product per hour.

Many types of flow reactor exist, such as the continuous-stirred tank reactor (CSTR) or plug flow reactor (PFR); the focus shall be placed on the latter. In plug flow reactors, flow chemistry is the process by which the reagents (often in solution) are pumped through a narrow channel, typically a tubular reactor, to generate the products.

Typically, a PFR will consist of several parts: syringes containing the reagent and the catalyst are operated by a pump, pushing the reagent through narrow tubing. The streams of both syringes are combined through a mixing unit, then pumped through the main reactor. With reactions that experience a build up of pressure, a back-pressure regulator (BPR) is placed at the end of the reactor; BPRs also decrease solvent vapour pressure, so higher temperatures and more rigorous reaction conditions can be accessed compared to those possible with batch reactors. An additional quenching system can be implemented after the reactor, matching the flow rate of the quenching unit to the reaction flow rate enables precise control of the reaction time. In the case of heterogeneous reactions or photocatalysis, this set-up typically only utilises one syringe, with the reactor either containing the catalyst in a fixed-bed, or surrounded by a light source (in photochemical reactions, for example).[142]

In contrast to batch reactors, reactions in continuous flow display several advantages to overcome issues often found in batch processes. Microreactors (with channels of internal diameter, I.D., of <1 mm) have proved popular due to the ease of set-up and accessibility compared to larger continuous flow reactors; generally consisting of little more than PTFE or silicone tubing and a syringe pump.

It is worth noting flow patterns vary across the different reactor sizes. Turbulent and laminar flow patterns can be observed, where turbulent flow is akin to chaotic mixing, while laminar flow is described by parallel layers of fluid. These patterns are dependent on channel diameter (L), viscosity of the medium (η) and density (ρ), and flow velocity (υ); all defined by the Reynold's number, R_e (Equation 1.2).[143,144] Larger diameters tend to lean towards high R_e (>4000), and therefore display a turbulent flow pattern, whilst smaller diameters characterised by a laminar flow pattern, and low Reynolds numbers (<2200), particularly seen with microreactors. Importantly, mixing within laminar flow occurs through diffusion between the layers, which reduces concentration and temperature gradients. While this usually does not present a problem due to the short path length, meaning that diffusion throughout the medium is rapid as the reagent does not have far to travel, it highlights the importance of choosing the appropriate mixing unit, be it a T-mixer or Y-mixer or ball-mixing unit (Figure 7.3, Chapter 7). Implementation of mixing units which combine the two incoming streams

by chaotic mixing, for example, can also improve mass transfer, removing the dependency on diffusion in laminar flow.

$$R_e = \frac{\upsilon \rho L}{\eta} \tag{1.2}$$

Due to the narrow tubing diameter in comparison to batch reactors, high surface-to-volume ratios can be obtained, which are beneficial on multiple levels. Heat transfer is one of the aspects that is much improved compared to batch reactors; heat gradients across the reactor are much smaller in flow than in batch, allowing for uniform, heating and consequently uniform reactivity across the reaction medium. The temperature can thus be more precisely controlled and changed, and the same can be said for mass transfer.

The small channels and volumes used in flow reactors leads to an inherent, inbuilt safety regarding more hazardous chemicals. This, combined with the temperature control and use of BPRs enables a far greater range of reaction conditions to be tested, without compromising safety.[145] Improved mixing and temperature control also increase the reproducibility of reactions, that is otherwise unattainable in batch.

While a variety of different phases and mixed phases can be accommodated in flow reactors, this particular work shall focus on liquid-phase continuous flow, working towards liquid-solid phases for heterogeneous reactions, as these are the most relevant in the current work.

Aside from those coming from the inherent flow reactor design, other advantages include the higher precision and accuracy of the pump; the latter also enable high synthetic precision.[146] The ability to systematically alter reaction conditions readily, enabling rapid and continuous high-throughput screening, and optimisation of reaction conditions.[147] Inclusion of online (continuous sampling) or inline (connection of the analytical equipment in series to the reactor) monitoring with NMR, mass spectrometry or SEC (among others), further decreases the lag time between sampling and analysis.[148] In the case of online and inline monitoring, it is possible to get near-immediate information about the progress of a reaction, allowing for rapid change of conditions to obtain the desired result. Junkers

and co-workers, for example, recently developed an inline NMR to monitor the progress of the RAFT polymerisation of methyl acrylate,[149] while inclusion of an automated, programmable feedback loop between the syringe pump and the online SEC led to rapid optimisation of conditions for specific targeted molecular weights.[150]

Indeed, inclusion of a programmable feedback loop has become an interesting way of fully automating the flow process,[151] and has been used in the flow ROP of lactones in solution-phase.[52] Automated flow processes remove the need for a user to monitor the reaction themselves, and have therefore been highly regarded as the next goal in the development of a fully autonomous flow reactor. It is clear from the significant leaps in flow chemistry within just the last two decades that the advantages of this method greatly outweigh those of batch reactors, and are thus important to consider wherever possible.

A number of criteria must be considered prior to transferring a reaction into flow.[142,152] Aside from ease of flow chemistry, it is important to consider working volumes, reaction conditions including temperature and pressures of the reaction, and whether the benefits of flow chemistry will help the user manage these, or whether the batch process is all that is required. Although it is clear the density of information that can be obtained in a continuous flow reactor can be much higher if connected to in- or online equipment, it is necessary to consider whether this will be of any benefit to the reaction itself. Moving from a batch to flow system will come with added time needed to optimise the set-up, so it is vital these questions are addressed.

Polymerisation chemistry often suffers from the need to systematically alter reaction conditions and ratios of monomer to initiator to optimise the reaction, which in batch is a challenging process. Further, scale up of many polymerisations remains challenging, not least for the inherent increase in viscosity that accompanies high conversions, such that the reactions often are diffusion limited.[153] Flow chemistry addresses both of these challenges; scale-up is possible through a increased run times whilst maintaining a constant residence time (thus the scale at any one point in time is maintained), whilst the higher surface-to-volume ratios reduce the effect of mass transport limited polymerisations due to the viscosity.

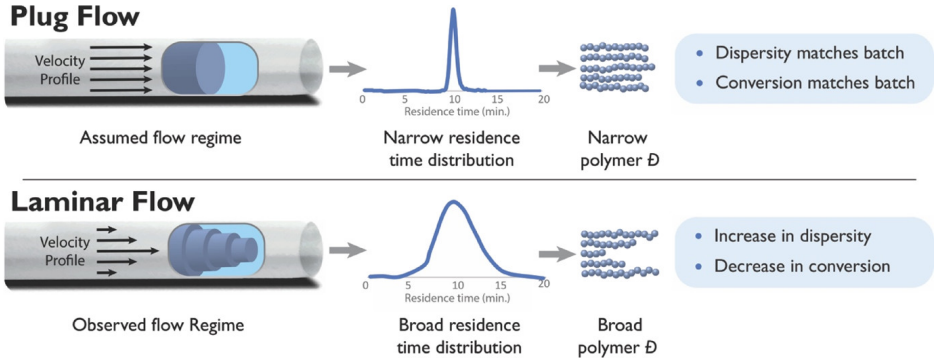

Figure 1.2: Plug (segmented) and laminar flow patterns leading to different molecular weight profiles, from Reis *et al.*[154]

Additionally, flow polymerisations offer an excellent method of precisely engineering the desired molecular weight distributions and dispersities; control over flow rates and residence times, as well as precisely controlling quenching methods allow for the reproducible, precise production of macromolecules.[155] Improved mixing and heat transfer, as well as the ability to precisely control flow patterns and residence time distributions has also had significant effect on the polymer properties. Switching from a purely liquid-phase system to a gas-liquid or liquid-liquid mix, can switch the flow pattern from laminar flow to segmented (droplet) flow. The droplets of co-solvent or gas break up the flow of reagent, reducing the parabolic gradient that occurs in laminar flow, and thus leading to a narrower dispersity (Figure 1.2). The parabolic gradient profile occurs in laminar flow due to the difference in friction between the centre and the walls of the tubular reactor, resulting in slower flow at the walls compared to the in the centre of the reactor. In turn, a larger distribution in residence time is observed, which can lead to a broader dispersity is the polymers forming by the walls of the reactor are left in the reactor longer than in the centre.[154]

Finally, aligning several reactors in sequence has been used to rapidly generate block copolymer libraries,[52] rather than the more tedious batch methods involving sequential addition (where the timings are dependent on manual addition and are therefore susceptible to human error) or one-pot reactions (which are harder to manipulate and monitor, and require the development of selective catalysts).

1.8.1 Homogeneous catalysis in flow polymerisations

While interest in moving from batch processes to continuous flow grew rapidly in the field of small molecule synthesis, it is only within the last decade that flow polymerisations have been considered. Most examples of polymerisations surround ATRP and RAFT polymerisations, such as those explored by Junkers and co-workers.[156] These are typically easy to apply to flow as they do not suffer from air or moisture sensitivity. In order to get high-throughput, however, higher concentrations are required, leading to challenges with viscosity and mixing; these can be overcome by rigorous optimisation of reaction conditions and modification of reactor engineering. In 2017, for example, glycerol was oligomerised with potassium carbonate catalyst, in a continuous flow stirred tank reactor.[157] Despite its high inherent viscosity, switching to a HPLC pump improved performance, and after optimisation of conditions, selective formation of cyclic oligomers was possible at 250 °C, with a flow rate of 1.3 mL min^{-1}.

ROP in flow, however, was first explored only in 2005 by Gao and co-workers, who polymerised the amino acid N-carboxyanhydride in a microreactor with a tertiary amine as the homogeneous catalyst (internal diameter, I.D., of <1 mm) to excellent results. The flow set-up yielded polymers with much lower dispersities than those observed in batch, as concentration gradients were minimised; $Đ_M$ of 1.17 were possible.[158]

Yet the first ROP in flow of a lactone was only reported a few years later,[159] despite the clear advantages that flow polymerisation offers. A relatively recent review on continuous flow ROP highlights how sparse this particular field is,[160] with most examples being dedicated to TBD, or enzyme promoted ROP.[161–165]

Some metal-catalysed flow ROP examples have been explored, using $Sn(OTf)_2$, a catalyst often used in the ROP of various lactones and carbonates. In 2015, the first example of a continuous flow ROP of ϵ-CL was carried out with $Sn(OTf)_2$ in a PTFE tubular microreactor.[166] After 40 minutes, 90% of the monomer was converted to polymer; contrastingly, only 82% had been converted in the batch test (80 °C, DP_{target} 10). An improvement in the dispersity was also observed. Thiol-functionalised PCL was also targeted using a thiol-terminated co-initiator ([CL]:[Cat]:[I] = 10:0.01:1, 99%, τ_r 180 minutes, $M_{n,NMR}$ 1 360 Da, $Đ_M$ 1.11).[167]

However, continuous flow ROP of lactones with TBD has presumably received more attention than other catalysts due to the speed at which the catalyst converts the monomer, by way of its pseudo-bifunctional mechanism. In 2016, TBD was used in the solution-phase ROP of ϵ-CL and δ-VL.[168] A typical microreactor set-up for a homogeneous reaction was adopted, involving two separate stock solutions (one of the monomer, the other containing the catalyst and co-initiator) combined with a T-mixing unit (Scheme 1.20). For ϵ-CL and δ-VL, dispersities of less than 1.09 were possible within one hour, and the precise control of reaction residence time and flow rate allowed for excellent control over targeted molecular weight distributions. However, quantitative conversion did not seem to be possible under the conditions tested (25 °C in toluene, [M] = 2 mol L^{-1}). An increased ROP control was achieved with the flow set-up, in contrast to the batch reactor, reaching apparent rate constants which were roughly double those of batch ROP (k_{app} 0.0062 min^{-1} and 0.00286 min^{-1}, respectively, for ϵ-CL, DP 100). The high surface-to-volume ratio possible in a flow reactor was cited as the reason for this drastic improvement, resulting in improved mass and heat transfer, and improved mixing. Aligning two reactors in sequence allowed for block copolymer synthesis within 20 minutes, maintaining low dispersities.

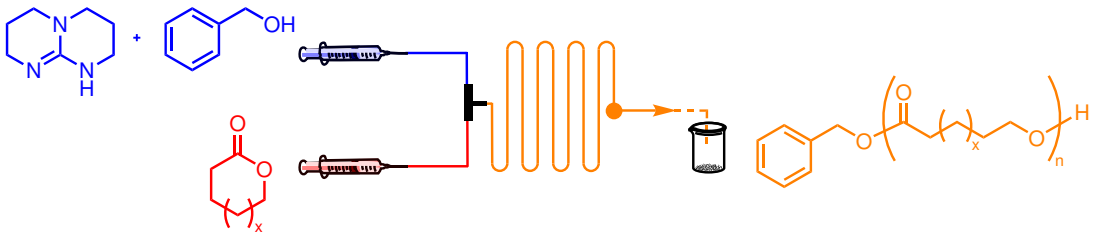

Scheme 1.20: Solution-phase ROP in flow of ϵ-CL and δ-VL with TBD in toluene, 25 °C.[168]

The mechanism of ROP of δ-VL by TBD was investigated using a gas-driven droplet flow reactor (*i.e.* a flow reactor with segmented flow disrupted by gas-droplets to prevent laminar flow).[169] The rate-limiting step was determined to be the association of the monomer to the the catalyst (*i.e.* monomer activation); this was followed by reaction of the monomer with the hydroxyl end group of the growing polymer chain. Using this type of reactor, too, led to extremely low and consistent dispersities, indicative of the highly controlled ROP.

Another example of a TBD catalysed ROP was reported in 2016, this time using lactide. Using catalyst loadings as low as 0.25 mol%, conversions of >95% were possible, maintaining decent dispersities of around 1.2.[170] At 30 °C, for example, it took 4 seconds (residence time, τ_r) to reach 99 % with a DP of 85 ($Đ_M$ 1.28). A high degree of control was needed with regards to residence time and flow rate in order to prevent further transesterification at higher conversions, and competing depolymerisations when the reaction reached thermodynamic control. End-group functionality was further introduced into the polymer, either by using macroinitiators to make a PEG-*b*-PLA block copolymer, or by using alkyne-functionalised initiators, for end-group click chemistry. These later experiments were, however, typically conducted at temperatures of −10 °C, reducing the overall practicality of the flow systems.

Alternative bases such as KO^{t}Bu and KHDMS (potassium bis(trimethylsilyl)amide) have also been used in the solution-phase ROP of lactide and other lactones, in a microreactor.[53] The combination of sterically hindered bases and excellent mixing efficiency and short residence times enabled the controlled ROP of *L*-LA, CL and VL within milliseconds, accessing high conversions and low dispersities. Using KO^{t}Bu, for example, 86% of LA was converted in 38 milliseconds, and mininal transesterification was reported (M_n 8 500 Da, $Đ_M$ 1.13, [LA] = 1 mol L^{-1} in THF, room temperature, DP_{target} 50). This was extended to the ROP of lactones with lower activities such as CL and VL, and as such the microreactor was adapted to accommodate the synthesis of block copolymers. Comparison of the flow reactions to the batch reactions under the same conditions highlighted just how much control was possible with microreactors: it was only possible to manually quench the after a minimum of 2 seconds, leading to broad dispersities.

More complex organocatalysts have also very recently been explored, building on this work the use of potassium salts as catalysts.[52] Using bifunctional ureas, generated from reaction of the latter with KOMe, an elegant catalyst switch system by matching the activities of the ureas to the monomers, was implemented to generate a library of over 100 block copolymers within minutes. This was achieved using the relative pK_as of the ureas; a highly active and basic urea was first matched with a lactone which was typically difficult to ring-open. Addition of a more acidic urea results in a proton transfer which ultimately quenched the

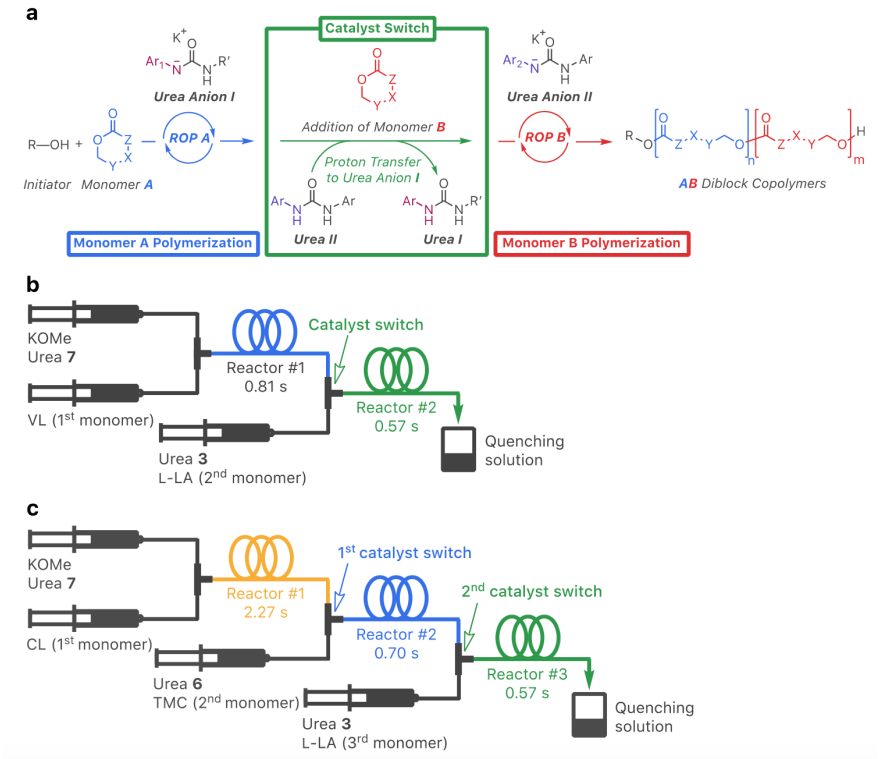

Figure 1.3: Schematic of the block copolymer synthesis through a sequential assembly of flow reactors, designed by Waymouth and co-workers,[52] showing a) Catalyst switch mechanism by transfer of a proton from the more acidic urea, followed b ythe reactor set-up for the synthesis of diblock (b) and triblock (c) copolymers.

first urea, and the new active urea was matched with a slightly more reactive monomer, generating an elegant way to block copolymer synthesis. Figure 1.3 illustrates the mechanism by which this was carried out, and the mechanism of proton transfer. In contrast, it was impossible to go the opposite way, reacting less active monomers, due to the acidities and activities of the ureas. The final di- and triblock (ABC) copolymers were shown to exhibit well controlled dispersities and molecular weights within one second residence time ($Đ_M$ 1.08-1.36). The highly active nature of these urea catalysts, coupled with a programme to fully automate the process allowed for the generation of several different copolymers in minutes.

1.8.2 Heterogeneous catalysis in flow: benefits and applications

When considering heterogeneous catalysis in flow, many advantages exist in addition to those that apply to homogeneous reactions. The most important, perhaps, is that the catalyst forms part of the main reactor as part of a packed-bed, and a stream of reagent is pumped through the catalyst, simultaneous producing product whilst separating the catalyst from the product; the in-built filtration system is therefore often a benefit of heterogeneous catalysts.[130,171] Although regeneration is often required prior to recycling of the catalyst, immobilisation of the latter within a packed-bed enables rapid and instantaneous separation of the catalyst from the reaction mixture, resulting in a polymer of much higher purity than in batch processes, where separation is only possible in further downstream processing by, for example, filtration. With regards to ROP, this is of interest due to the need to reduce the levels of cytotoxic trace metals in the polymer.[61] Design of the catalyst should, however, endeavour to avoid any leaching of the metal into the reaction medium, which would negate the benefit of flow to some degree.[68] Simultaneously, adoption of a fixed-bed reactor further reduces the amount of catalyst wasted throughout the various reuse cycles, as it is not lost systematically through the different purification steps in batch chemistry.[172]

Recycling and reuse, catalysis, reduction of derivatives (such as side reactions avoided by improved reaction control), as well as safer handling of chemicals that is inherent to flow chemistry are some of the principles of green chemistry outlined by Anastas and Warren, indicating that heterogeneous flow polymerisation is a highly desirable field.[173,174] Indeed, several reviews are available detailing the various benefits and numerous examples of heterogeneously catalysed small molecule synthesis in continuous flow.[143,172,175]

In one example, when a support was input into continuous flow, the catalyst itself could be generated first, with a reduction of reaction time by up to 40% compared to the batch synthesis.[176] Degradation of the support throughout the reaction was also reduced in the flow set-up, as magnetic stirring was no longer required. The ability of a catalyst to be produced *in situ*, followed by use of the catalyst without removing it from the reactor significantly reduces the amount

of purification steps required, offering another improvement in process chemistry, provided catalysts synthesis is reproducible and well studied prior to this.

Numerous methods of implementing the heterogeneous catalyst into the reactor have been explored, and these are highly dependent on the structure of the catalyst. Supported catalysts can either be input into a flow set-up through monoliths,[177] immobilised in a packed-bed within the tubular reactor,[75,178] or coated onto the reactor wall.[143,172] Most pertinent to this work are those catalysed by polystyrene-immobilised metal or organocatalysts, which have consistently been optioned as excellent, readily synthesised catalysts for flow synthesis.[69] On example is the simple immobilisation of of a highly active PS-amine catalyst into a packed-bed column for use in the Robinson annulation reaction, yielding excellent results, and demonstrating that it could be reused up to 10 times.

1.8.3 Heterogeneous catalysis in flow ROP

Enzyme catalysed ROP of lactones, such as ϵ-CL, have been just as prevalent in continuous flow as metal and organocatalysed ROP. The first example of an enzyme catalysed ROP was carried out through immobilisation of the enzyme on a solid-support, implemented into a packed-bed microreactor, for the polymerisation of ϵ-CL.[159]

In 2012, continuous polymerisation of ϵ-CL was achieved by immobilising a lipase into a packed-bed reactor (PBR).[161] Lowering the flow rate and thereby increasing the residence time of the monomer in the reactor, it was possible to convert 98% in 12 minutes, although dispersities were high ($Đ_M$ 2.1).

The controlled ROP of ϵ-CL by Novoenzyme435 was performed in a tubular flow reactor, producing thiol-end-functionalised telechelic PCL, with high end group fidelity.[163] A residence time of 5 minutes at 60 °C yielded PCL in 97% conversion with a 98% end-group fidelity, and controlled polymerisation was demonstrated through the consistency between theoretical and obtained number average molecular weights (M_n 3 500 Da, $Đ_M$ 1.17). Comparison of the kinetic semi-logarithmic plots of the flow and batch reactions demonstrated the improved rates obtained when using a flow reactor, due to the improved mass and heat transfer possible in these systems. Aligning two flow reactors in sequence allowed

for block copolymer synthesis, yielding PVP-*b*-PCL or PCL-*b*-PVP blocks (where PVP is poly(*N*-vinylpyrrolidone, $Đ_M$ 1.10). Similarly, thiol-functionalised PVL (poly(δ-valerolactone)) and PVL-*b*-PCL block copolymers (and *vice versa*) were synthesised using a lipase immobilised in a tubular reactor (>95% conversion to the block copolymers, $Đ_M$ 1.12-1.24).[162]

In supercritical CO_2 with a DCM co-solvent, solubility of the polymer was improved, thereby avoiding polymer (PCL) precipitation on the Novoenzyme beads (Scheme 1.21). Modest dispersities were observed ($Đ_M$ 1.3-1.6), however it was possible to reuse the enzyme up to six times, with negligible decrease in activity.[164]

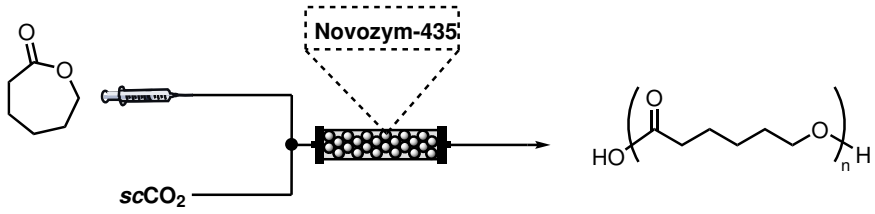

Scheme 1.21: Heterogeneous ROP of ϵ-CL in flow reactor with a supercritical CO_2 and DCM co-solvent system. A fixed-bed reactor was used for the catalyst, packed with Novoenzyme beads.[164]

A combination of the same enzyme and TBD were extended to the copolymerisation of other ϵ-CL with lactones and cyclic carbonates. While *L*-LA could not be polymerised by the enzyme at room temperature, reaction in flow with TBD yielded 95% conversion in 10 seconds ($Đ_M$ 1.05).[165] In one reactor, Novoenzyme435 was immobilised in a packed-bed, and a single mixed-feed of monomer and co-initiator (BnOH) were injected in continuous flow through the heterogeneous catalyst. In the other, two feeds – one containing a solution of TBD and BnOH and the other containing a solution of monomer – were connected to one tubular reactor. Sequential assembly of these two reactors allowed for the successful copolymer synthesis of diblocks and triblocks. Comparison of the flow set-up to a batch reactor demonstrated that the batch reactor required longer to polymerise the copolymers; dispersities also tended to be slightly higher in batch.

Aside from enzymatic ROP of lactones, the majority of heterogeneously catalysed ROP in continuous flow occurred in the late 1990s, with only initial studies having

been the focus. These examples all involved immobilised metal complexes, with no investigation into the flow polymerisation using immobilised organocatalysts which were shown to have decent activity in batch ROP.

Hamaide and co-workers built on previous work developing SiO_2-grafted aluminium alkoxides for the oligomerisation of ϵ-CL,[179,180] and implementing these into a plug flow reactor.[179,181] Excess alcohol co-initiator was added to encourage exchange between the active polymer chain growing from the Al centres, leading to low dispersities and controlled oligomers – similar to the concept used in immortal polymerisation. An intermediate SiO_2 particle size was chosen to avoid large pressure drops across the packed-bed, while a T-mixer was used to mix the incoming streams of monomer and co-initiator solution. Issues with the benzyl alcohol co-initiator were observed, as they tended to graft to the polar silica surface if the residence time was not precisely controlled; a problem which would be best avoided through immobilisation on an inert surface. Despite these drawbacks, it was possible to control the molecular weight distribution (MWD) based on the flow rates.

The same procedure was applied to SiO_2 or Al_2O_3-immobilised zirconium and Rare Earth metal alkoxides.[182] Improved activities were observed with the Rare Earth metals, with SiO_2-grafted yttrium oligomerising ϵ-CL within five minutes at 50 °C (100% conversion); Silica overwhelmingly improved activity compared to alumina, the latter only providing quantitative conversion of the monomer in 5 hours (grafted Nd). These solid-supports allowed the catalysts to be packed into a plug flow reactor. While initial investigations into MWD dependence of residence time were carried out as in the previous example, no further experiments were conducted. Catalyst recycling and reuse was also not explored, although it was mentioned that regeneration of the catalyst column could be achieved through washing with alcohol to regenerate the catalyst.

1.9 Summary

Although there has been a lot of research developing catalysts for the ring-opening polymerisation of lactones, specifically focussing on lactide, most of these have addressed one of two problems: either the targeting of stereocontrolled ROP,

or attempts at replacing expensive or toxic metals with cheaper, abundant alternatives without toxicity concerns, or replacing these entirely by switching to organocatalysts.

In order to fully move past these often repetitive motions of catalyst development followed by testing under conditions which are potentially not industrially relevant, it is important to consider the requirements which would be needed in future, which would legitimately help progress to replacing the industrial catalysts. It is also necessary to consider the future of polymerisation engineering, in order to better optimise not only the catalyst, but the process itself. Whilst acknowledging that several extensive hurdles exist within process intensification, lab scale progress must be pushed further than what it remains to be currently, to bridge the gap between lab-to-pilot scale chemistry.

Throughout the introduction, both homogeneous and heterogeneous catalysts are highlighted, as well as the development of flow chemistry for polymerisations. Overall, it is clear that heterogeneous catalysts offer several advantages over homogeneous catalysts that could be beneficial to polymerisation processes. Some difficulties still exist in the understanding of what happens at the surface level, due to limitations in and availability of analytical tools. Despite these limitations, heterogenised catalysts are more readily separated from reaction media, and the potential to reuse these either directly or once re-activated, is a significant advantage.

Flow chemistry is also beneficial with regards to polymerisations. Meticulous control over the reaction conditions is significantly improved compared to batch processes, including both in mass and heat transfer, enabling narrow polymer molecular weight distributions.

References

[1] *Nat Commun*, 2018, **9**, 2157.

[2] R. Geyer, J. R. Jambeck and K. L. Law, *Sci Adv*, 2017, **3**, 1–5.

[3] A. A. de Souza Machado, W. Kloas, C. Zarfl, S. Hempel and M. C. Rillig, *Glob Change Biol*, 2018, **24**, 1405–1416.

[4] *A European Strategy for Plastics in a Circular Economy*, European Comission, Communication from the Comission to the European Parliament, the Council, the European Economic and Social Committee and the Committee of Regions, Document 52018DC0028, 2018.

[5] C. Romera-Castillo, M. Pinto, T. M. Langer, X. A. Álvarez-Salgado and G. J. Herndl, *Nat Commun*, 2018, **9**, 1430.

[6] K. Law and R. C. Thompson, *Science*, 2014, **345**, 144–145.

[7] *UN Sustainable Development Goals*, https://sdgs.un.org/goals, Accessed: 06/2021.

[8] *The Ellen MacArthur Foundation*, https://www.newplasticseconomy.org, Accessed: 06/2021.

[9] *Pathway to a Healthy Planet for All EU Action Plan: 'Towards Zero Pollution for Air, Water and Soil'*, European Comission, Communication from the Comission to the European Parliament, the Council, the European Economic and Social Committee and the Committee of Regions, Document 52021DC0400, 2019.

[10] *PlasticsEurope*, http://www.plasticseurope.org/en/resources/market-data, Accessed: 06/2021.

[11] *On the reduction of the impact of certain plastic products on the environment*, European Parliament, Directive, Document 32019L0904, 2019.

[12] T. P. Haider, C. Völker, J. Kramm, K. Landfester and F. R. Wurm, *Angew Chem Int Edit*, 2019, **58**, 50–62.

[13] M. F. Cosate de Andrade, P. M. Souza, O. Cavalett and A. R. Morales, *J Polym Environ*, 2016, **24**, 372–384.

[14] Y. Zhu, C. Romain and C. K. Williams, *Nature*, 2016, **540**, 354–362.

[15] R. Platel, L. Hodgson and C. Williams, *Polym Rev*, 2008, **48**, 11–63.

[16] S. Lambert and M. Wagner, *Chem Soc Rev*, 2017, **46**, 6855–6871.

[17] A. Södergård and M. Stolt, *Prog Polym Sci*, 2002, **27**, 1123–1163.

[18] M. Dusselier, P. Van Wouwe, A. Dewaele, E. Makshina and B. F. Sels, *Energy Environ Sci*, 2013, **6**, 1415–1442.

[19] N. E. Kamber, W. Jeong, R. M. Waymouth, R. C. Pratt, B. G. Lohmeijer and J. L. Hedrick, *Chem Rev*, 2007, **107**, 5813–5840.

[20] W. H. Carothers, G. L. Borough and F. J. Natta, *J Am Chem Soc*, 1932, **54**, 761–772.

[21] D. W. Hwang, J.-S. Chang, Y. K. Hwang, U.-H. Lee and H. Gwak, *Recovery method of highly pure lactic acid and alkyl lactate*, 2012, US Patent 2012/142945.

[22] M. Dusselier, P. Van Wouwe, A. Dewaele, P. A. Jacobs and B. F. Sels, *Science*, 2015, **349**, 78–80.

[23] A. Duda and A. Kowalski, in *Handbook of Ring-Opening Polymerization*, ed. P. Dubois, O. Coulembier and J.-M. Raquez, Wiley-VCH, Germany, 2009, ch. 1, pp. 1–52.

[24] O. Dechy-Cabaret, B. Martin-Vaca and D. Bourissou, in *Handbook of Ring-Opening Polymerization*, ed. P. Dubois, O. Coulembier and J.-M. Raquez, Wiley-VCH, Germany, 2009, ch. 10, pp. 255–286.

[25] T. Maharana, B. Mohanty and Y. S. Negi, *Melt-solid polycondensation of lactic acid and its biodegradability*, 2009.

[26] P. J. Flory, *J Am Chem Soc*, 1940, **62**, 1561–1565.

[27] M. L. Di Lorenzo and R. Androsch, in *Advances in Polymer Science*, Springer, Switzerland, 2018, ch. 279, pp. 67–118.

[28] A. P. Dove, R. C. Pratt, B. G. G. Lohmeijer, R. M. Waymouth and J. L. Hedrick, *J Am Chem Soc*, 2005, **127**, 13798–13799.

[29] A. Kowalski, A. Duda and S. Penczek, *Macromolecules*, 2000, **33**, 7359–7370.

[30] M. K. Kiesewetter, E. J. Shin, J. L. Hedrick and R. M. Waymouth, *Macromolecules*, 2010, **43**, 2093–2107.

[31] X. Zhang, G. O. Jones, J. L. Hedrick and R. M. Waymouth, *Nat Chem*, 2016, **8**, 1047–1053.

[32] M. J. Stanford and A. P. Dove, *Chem Soc Rev*, 2010, **39**, 486–494.

[33] S. Inkinen, M. Hakkarainen, A. C. Albertsson and A. Södergård, *Biomacromolecules*, 2011, **12**, 523–532.

[34] C. L. Wanamaker, M. J. Bluemle, L. M. Pitet, L. E. O'Leary, W. B. Tolman and M. A. Hillmyer, *Biomacromolecules*, 2009, **10**, 2904–2911.

[35] B. M. Chamberlain, M. Cheng, D. R. Moore, T. M. Ovitt, E. B. Lobkovsky and G. W. Coates, *J Am Chem Soc*, 2001, **123**, 3229–3238.

[36] M. Cheng, A. B. Attygalle, E. B. Lobkovsky and G. W. Coates, *J Am Chem Soc*, 1999, **121**, 11583–11584.

[37] K. A. M. Thakur, R. T. Kean, E. S. Hall, J. J. Kolstad and E. J. Munson, *Macromolecules*, 1998, **31**, 1487–1494.

[38] M. H. Chisholm, S. S. Iyer and M. E. Matison, *Chem Commun*, 1997, 1999.

[39] P. Dubois, O. Coulembier and J.-M. Raquez, *Handbook of ring-opening polymerization*, 2009, p. 408.

[40] D. T. Gentekos, L. N. Dupuis and B. P. Fors, *J Am Chem Soc*, 2016, **138**, 1848–1851.

[41] K. Benabdillah, M. Boustta and J. Coudane, *Polym from Renew Resour*, 2000, **764**, 200–220.

[42] S. J. Li, S. J. Xie, Y. C. Li, H. J. Qian and Z. Y. Lu, *Phys Rev E*, 2016, **93**, 1–10.

[43] E. Castro-Aguirre, F. Iñiguez-Franco, H. Samsudin, X. Fang and R. Auras, *Adv Drug Deliver Rev*, 2016, **107**, 333–366.

[44] T. Endo, in *Handbook of Ring-Opening Polymerization*, ed. P. Dubois, O. Coulembier and J.-M. Raquez, Wiley-VCH, Germany, 2009, ch. 2, pp. 53–62.

[45] I. C. McNeill and H. A. Leiper, *Polym Degrad Stabil*, 1985, **11**, 267–285.

[46] J. B. Zhu and E. Y. Chen, *J Am Chem Soc*, 2015, **137**, 12506–12509.

[47] R. C. Pratt, B. G. Lohmeijer, D. A. Long, P. N. Lundberg, A. P. Dove, H. Li, C. G. Wade, R. M. Waymouth and J. L. Hedrick, *Macromolecules*, 2006, **39**, 7863–7871.

[48] P. M. Schäfer, M. Fuchs, A. Ohligschläger, R. Rittinghaus, P. McKeown, E. Akin, M. Schmidt, A. Hoffmann, M. A. Liauw, M. D. Jones and S. Herres-Pawlis, *ChemSusChem*, 2017, **10**, 3547–3556.

[49] R. D. Rittinghaus, P. M. Schäfer, P. Albrecht, C. Conrads, A. Hoffmann, A. N. Ksiazkiewicz, O. Bienemann, A. Pich and S. Herres-Pawlis, *ChemSusChem*, 2019, **12**, 2161–2165.

[50] B. Lin and R. M. Waymouth, *J Am Chem Soc*, 2017, **139**, 1645–1652.

[51] B. Lin and R. M. Waymouth, *Macromolecules*, 2018, **51**, 2932–2938.

[52] B. Lin, J. L. Hedrick, N. H. Park and R. M. Waymouth, *J Am Chem Soc*, 2019, **141**, 8921–8927.

[53] B. Lin, C. N. Jadrich, V. E. Pane, P. L. Arrechea, T. Erdmann, C. Dausse, J. L. Hedrick, N. H. Park and R. M. Waymouth, *Macromolecules*, 2020, **53**, 9000–9007.

[54] M. S. Zaky, A.-L. Wirotius, O. Coulembier, G. Guichard and D. Taton, *Chem Commun*, 2021, **57**, 3777–3780.

[55] N. Yuntawattana, T. M. McGuire, C. B. Durr, A. Buchard and C. K. Williams, *Catal Sci Technol*, 2020, **10**, 7226–7239.

[56] S. M. Guillaume, E. Kirillov, Y. Sarazin and J. F. Carpentier, *Chem - Eur J*, 2015, **21**, 7988–8003.

[57] E. Stirling, Y. Champouret and M. Visseaux, *Catalytic metal-based systems for controlled statistical copolymerisation of lactide with a lactone*, 2018.

[58] C. Romain, Y. Zhu, P. Dingwall, S. Paul, H. S. Rzepa, A. Buchard and C. K. Williams, *J Am Chem Soc*, 2016, **138**, 4120–4131.

[59] C. Romain, J. A. Garden, G. Trott, A. Buchard, A. J. White and C. K. Williams, *Chem - Eur J*, 2017, **23**, 7367–7376.

[60] G. S. Sulley, G. L. Gregory, T. T. Chen, L. Peña Carrodeguas, G. Trott, A. Santmarti, K. Y. Lee, N. J. Terrill and C. K. Williams, *J Am Chem Soc*, 2020, **142**, 4378.

[61] M. C. Tanzi, P. Verderio, M. G. Lampugnani, M. Resnati, E. Dejana and E. Sturani, *J Mater Sci-Mater M*, 1994, **5**, 393–396.

[62] S. P. Parwe, S. D. Warkad, M. V. Mane, P. S. Shedage and B. Garnaik, *Polymer*, 2017, **111**, 244–251.

[63] A. Stjerndahl, A. Finne-Wistrand, A. C. Albertsson, C. M. Bäckesjö and U. Lindgren, *J Biomed Mater Res A*, 2008, **87**, 1086–1091.

[64] B. J. O'Keefe, M. A. Hillmyer and W. B. Tolman, *J Chem Soc, Dalton Trans*, 2001, 2215–2224.

[65] C. K. Williams, L. E. Breyfogle, S. K. Choi, W. Nam, V. G. Young, M. A. Hillmyer and W. B. Tolman, *J Am Chem Soc*, 2003, **125**, 11350–11359.

[66] A. Nachtergael, O. Coulembier, P. Dubois, M. Helvenstein, P. Duez, B. Blankert and L. Mespouille, *Biomacromolecules*, 2015, **16**, 507–514.

[67] A. M. P. Salvo, F. Giacalone and M. Gruttadauria, *Molecules*, 2016, **21**, 1288.

[68] Y. Chauvin, D. Commereuc and F. Dawans, *Prog Polym Sci*, 1977, **5**, 95–226.

[69] A. Kirschning, H. Monenschein and R. Wittenberg, *Angew Chem Int Edit*, 2001, **40**, 650–679.

[70] X. Cui, W. Li, P. Ryabchuk, K. Junge and M. Beller, *Nat Catal*, 2018, **1**, 385–397.

[71] S. M. Islam, K. Ghosh, R. A. Molla, A. S. Roy, N. Salam and M. A. Iqubal, *J Organomet Chem*, 2014, **774**, 61–69.

[72] D. C. Neckers, D. A. Kooistra and G. W. Green, *J Am Chem Soc*, 1972, **94**, 9284–9285.

[73] P. Hodge, *Chem Soc Rev*, 1997, **26**, 417–424.

[74] G. L. Thomas, C. Böhner, M. Ladlow and D. R. Spring, *Tetrahedron*, 2005, **61**, 12153–12159.

[75] S. Cañellas, C. Ayats, A. H. Henseler and M. A. Pericàs, *ACS Catal*, 2017, **7**, 1383–1391.

[76] N. E. Leadbeater and M. Marco, *Chem Rev*, 2002, **102**, 3217–3274.

[77] A. R. Vaino and K. D. Janda, *J Comb Chem*, 2000, **2**, 579–596.

[78] R. J. Comito, K. J. Fritzsching, B. J. Sundell, K. Schmidt-Rohr and M. DincĂ, *J Am Chem Soc*, 2016, **138**, 10232–10237.

[79] T. M. Abdel-Fattah and T. J. Pinnavaia, *Chem Commun*, 1996, 665.

[80] C. M. A. Parlett, K. Wilson and A. F. Lee, *Chem Soc Rev*, 2013, **42**, 3876–93.

[81] A. Schätz, O. Reiser and W. J. Stark, *Chem - Eur J*, 2010, **16**, 8950–8967.

[82] W. Long, C. S. Gill, S. Choi and C. W. Jones, *Dalton Trans*, 2010, **39**, 1470–1472.

[83] L. Stadler, M. Homafar, A. Hartl, S. Najafishirtari, M. Colombo, R. Zboril, P. Martin, M. B. Gawande, J. Zhi and O. Reiser, *ACS Sustain Chem Eng*, 2019, **7**, 2388–2399.

[84] B. Kaboudin, H. Khanmohammadi and F. Kazemi, *Appl Surf Sci*, 2017, **425**, 400–406.

[85] S. Jain and O. Reiser, *ChemSusChem*, 2008, **1**, 534–541.

[86] J. Liu, *ACS Catal*, 2017, **7**, 34–59.

[87] S. Hübner, J. G. de Vries and V. Farina, *Adv Synth Catal*, 2016, **358**, 3–25.

[88] G. G. Hlatky, *Chem Rev*, 2000, **100**, 1347–1376.

[89] M. A. Ziaee, Y. Tang, H. Zhong, D. Tian and R. Wang, *ACS Sustain Chem Eng*, 2019, **7**, 2380–2387.

[90] M. Trunk, J. Teichert and A. Thomas, *J Am Chem Soc*, 2017, **139**, 3615–3618.

[91] J. J. Lee, C.-J. Yoo, C.-H. Chen, S. E. Hayes, C. Sievers and C. W. Jones, *Langmuir*, 2018, **34**, 12279–12292.

[92] F. Wu, Y. Feng and C. W. Jones, *ACS Catal*, 2014, **4**, 1365–1375.

[93] D. Zhao, J. Zhao, S. Zhao and W. Wang, *J Inorg Organomet Polym*, 2007, **17**, 653–659.

[94] C. Baleizão and H. Garcia, *Chem Rev*, 2006, **106**, 3987–4043.

[95] M. H. Majeed, P. Shayesteh, L. R. Wallenberg, A. R. Persson, N. Johansson, L. Ye, J. Schnadt and O. F. Wendt, *Chem - Eur J*, 2017, **23**, 8457–8465.

[96] S. Bhunia, R. A. Molla, V. Kumari, S. M. Islam and A. Bhaumik, *Chem Commun*, 2015, **51**, 15732–15735.

[97] L. N. Hao, Y. Lu, Z. Z. He, Z. J. Liu and E. Wang, *Inorg Chem Commun*, 2015, **55**, 88–91.

[98] L. Hao, Y. Lu, Z. He, Q. Lan and E. Wang, *J Coord Chem*, 2015, **68**, 2682–2690.

[99] H. Jiang, L. Jiawei, Y. Ren and C. Qi, *Dalton Trans*, 2017, **46**, 7821–7832.

[100] R. B. Merrifield, *J Am Chem Soc*, 1963, **85**, 2149–2154.

[101] J. Lu and P. H. Toy, *Chem Rev*, 2009, **109**, 815–838.

[102] T.-K. Lee, S.-J. Ryoo, J.-W. Byun, S.-M. Lee and Y.-S. Lee, *J Comb Chem*, 2005, **7**, 170–173.

[103] V. A. Larionov, T. Cruchter, T. Mietke and E. Meggers, *Organometallics*, 2017, **36**, 1457–1460.

[104] Q. M. Kainz, M. Zeltner, M. Rossier, W. J. Stark and O. Reiser, *Chem - Eur J*, 2013, **19**, 10038–10045.

[105] J. M. Fréchet, M. Jean Farrall and G. Darling, *Reactive Polymers, Ion Exchangers, Sorbents*, 1982, **1**, 27–34.

[106] W. Xu, R. Mohan and M. M. Morrissey, *Tetrahedron Lett*, 1997, **38**, 7337–7340.

[107] M. Zupan and A. Pollak, *J Chem Soc Chem Commun*, 1975, 715–716.

[108] N. Kann, *Molecules*, 2010, **15**, 6306–6331.

[109] C. Schuerch and J. M. Fréchet, *J Am Chem Soc*, 1971, **93**, 492–496.

[110] M. A. Scialdone, S. W. Shuey, P. Soper, Y. Hamuro and D. M. Burns, *J Org Chem*, 1998, **63**, 4802–4807.

[111] S. Bräse, S. Dahmen and M. Pfefferkorn, *J Comb Chem*, 2000, **2**, 710–715.

[112] Y. Hamuro, W. J. Marshall and M. a. Scialdone, *J Comb Chem*, 1999, **1**, 163–172.

[113] S. M. Islam, K. Ghosh, A. S. Roy and R. A. Molla, *RSC Adv*, 2014, **4**, 38986–38999.

[114] T. Erkenez and M. Tümer, *Arabi J Chem*, 2019, **12**, 2618–2631.

[115] S. M. Islam, R. A. Molla, A. S. Roy, K. Ghosh, P. W. N. M. van Leeuwen, K. Vrieze, M. M. Salberg and D. X. West, *RSC Adv*, 2014, **4**, 26181–26192.

[116] S. M. Islam, K. Ghosh, A. S. Roy, R. A. Molla, N. Salam, T. Chatterjee and M. A. Iqubal, *J Organomet Chem*, 2014, **772**, 152–160.

[117] S. B. Roscoe, C. Gong, J. M. J. Frechet and J. F. Walzer, *J Polym Sci Pol Chem*, 2000, **38**, 2979–2992.

[118] Y. Chen, W. Xiao, J. Zhang, M. Bu, X. Zhang, A. Chen, J. Xu and C. Lei, *J Polym Sci*, 2020, **58**, 3411–3418.

[119] J. Wang, X. Shan, S. Shan, H. Su, S. Wu and Q. Jia, *Catal Commun*, 2015, **59**, 116–121.

[120] K. M. K. Yu, I. Curcic, J. Gabriel, H. Morganstewart and S. C. Tsang, *J Phys Chem A*, 2010, **114**, 3863–3872.

[121] X. Li, R. Duan, C. Hu, X. Pang and M. Deng, *Polym Chem*, 2021, **12**, 1700–1706.

[122] K. Yu and C. W. Jones, *Organometallics*, 2003, **22**, 2571–2580.

[123] K. Yu and C. W. Jones, *J Catal*, 2004, **222**, 558–564.

[124] J. H. Khan, F. Schue and G. A. George, *Polym Int*, 2009, **58**, 296–301.

[125] M. D. Jones, M. G. Davidson, C. G. Keir, A. J. Wooles, M. F. Mahon and D. C. Apperley, *Dalton Trans*, 2008, 3655–3657.

[126] M. D. Jones, M. G. Davidson, C. G. Keir, L. M. Hughes, M. F. Mahon and D. C. Apperley, *Eur J Inorg Chem*, 2009, **2009**, 635–642.

[127] K. Tortosa, T. Hamaide, C. Boisson and R. Spitz, *Macromol Chem Phys*, 2001, **3**, 1156–1160.

[128] E. Kim, E. W. Shin, I. K. Yoo and J. S. Chung, *J Mol Catal A-Chem*, 2009, **298**, 36–39.

[129] E. J. Lee, K. M. Lee, J. Jang, E. Kim, J. S. Chung, Y. Do, S. C. Yoon and S. Y. Park, *J Mol Catal A-Chem*, 2014, **385**, 68–72.

[130] M. Jones, in *Heterogenized Homogeneous Catalysts for Fine Chemicals Production*, ed. P. Barbaro and F. Liguori, Springer, Switzerland, 2010, ch. 11, pp. 385–412.

[131] M. H. Chisholm, J. C. Gallucci and H. Yin, *P Natl Acad Sci USA*, 2006, **103**, 15315–20.

[132] M. H. Chisholm, *J Organomet Chem*, 2008, **693**, 808–818.

[133] M. Oshimura, A. Takasu and K. Nagata, *Macromolecules*, 2009, **42**, 3086–3091.

[134] Y. Feng, M. E. Lydon and C. W. Jones, *ChemCatChem*, 2013, **5**, 3636–3643.

[135] I. A. Shuklov, H. Jiao, J. Schulze, W. Tietz, K. Kühlein and A. Börner, *Tetrahedron Lett*, 2011, **52**, 1027–1030.

[136] F. Nederberg, E. F. Connor, M. Möller, T. Glauser and J. L. Hedrick, *Angew Chem Int Edit*, 2001, **40**, 2712–2715.

[137] A. P. Dove, R. C. Pratt, B. G. Lohmeijer, D. A. Culkin, E. C. Hagberg, G. W. Nyce, R. M. Waymouth and J. L. Hedrick, *Polymer*, 2006, **47**, 4018–4025.

[138] C. Ren, X. Zhu, N. Zhao, Y. Shen, L. Chen, S. Liu and Z. Li, *Eur Pol J*, 2019, **119**, 130–135.

[139] C. Ren, X. Zhu, N. Zhao, S. Fang and Z. Li, *Polymer*, 2020, **204**, 122797.

[140] A. Alba, O. T. du Boullay, B. Martin-Vaca and D. Bourissou, *Polym Chem*, 2015, **6**, 989–997.

[141] L. Zhang, F. Nederberg, R. C. Pratt, R. M. Waymouth, J. L. Hedrick and C. G. Wade, *Macromolecules*, 2007, **40**, 4154–4158.

[142] M. B. Plutschack, B. Pieber, K. Gilmore and P. H. Seeberger, *Chem Rev*, 2017, **117**, 11796–11893.

[143] A. Tanimu, S. Jaenicke and K. Alhooshani, *Chem Eng J*, 2017, **327**, 792–821.

[144] M. Seo, Z. Nie, S. Xu, M. Mok, P. C. Lewis, R. Graham and E. Kumacheva, *Langmuir*, 2005, **21**, 11614–11622.

[145] C. Wiles and P. Watts, *Eur J Org Chem*, 2008, **2008**, 1655–1671.

[146] S. A. M. W. van den Broek, R. Becker, K. Koch and P. J. Nieuwland, *Micromachines*, 2012, **3**, 244–254.

[147] D. K. B. Mohamed, X. Yu, J. Li and J. Wu, *Tetrahedron Lett*, 2016, **57**, 3965–3977.

[148] M. V. Gomez and A. De La Hoz, *Beilstein J of Organic Chemistry*, 2017, **13**, 285–300.

[149] M. Rubens, J. Van Herck and T. Junkers, *ACS Macro Lett*, 2019, **8**, 1437–1441.

[150] M. Rubens and T. Junkers, *Polym Chem*, 2019, 6315–6323.

[151] M. Rubens, J. H. Vrijsen, J. Laun and T. Junkers, *Angew Chem Int Edit*, 2019, **58**, 3183–3187.

[152] R. L. Hartman, J. P. McMullen and K. F. Jensen, *Deciding whether to go with the flow: Evaluating the merits of flow reactors for synthesis*, 2011, http://doi.wiley.com/10.1002/anie.201004637.

[153] T. Junkers, *J Flow Chem*, 2017, **7**, 106–110.

[154] M. H. Reis, T. P. Varner and F. A. Leibfarth, *Macromolecules*, 2019, **52**, 3551–3557.

[155] T. Junkers, *Macromol Chem Phys*, 2017, **218**, 1600421.

[156] F. Lauterbach, M. Rubens, V. Abetz and T. Junkers, *Angew Chem Int Edit*, 2018, **57**, 14260–14264.

[157] N. Galy, R. Nguyen, P. Blach, S. Sambou, D. Luart and C. Len, *J Ind Eng Chem*, 2017, **51**, 312–318.

[158] T. Honda, M. Miyazaki, H. Nakamura and H. Maeda, *Lab Chip*, 2005, **5**, 812–818.

[159] S. Kundu, A. S. Bhangale, W. E. Wallace, K. M. Flynn, C. M. Guttman, R. A. Gross and K. L. Beers, *J Am Chem Soc*, 2011, **133**, 6006–6011.

[160] X. Hu, N. Zhu, Z. Fang and K. Guo, *React Chem Eng*, 2017, **2**, 20–26.

[161] M. J. Zhang, E. Z. Su, J. P. Lin and D. Z. Wei, *Chem Biochem Eng Q*, 2012, **26**, 1–6.

[162] N. Zhu, W. Huang, X. Hu, Y. Liu, Z. Fang and K. Guo, *Macromol Rapid Comm*, 2018, **39**, 1700807.

[163] N. Zhu, W. Huang, X. Hu, Y. Liu, Z. Fang and K. Guo, *Chem Eng J*, 2018, **333**, 43–48.

[164] J. G. Veneral, D. de Oliveira, S. R. Ferreira and J. V. Oliveira, *Chem Eng Sci*, 2018, **175**, 139–147.

[165] W. Huang, N. Zhu, Y. Liu, J. Wang, J. Zhong, Q. Sun, T. Sun, X. Hu, Z. Fang and K. Guo, *Chem Eng J*, 2019, **356**, 592–597.

[166] N. Zhu, Z. Zhang, W. Feng, Y. Zeng, Z. Li, Z. Fang, K. Zhang, Z. Li and K. Guo, *RSC Adv*, 2015, **5**, 31554–31557.

[167] N. Zhu, Y. Liu, W. Feng, W. Huang, Z. Zhang, X. Hu, Z. Fang, Z. Li and K. Guo, *Eur Pol J*, 2016, **80**, 234–239.

[168] N. Zhu, W. Feng, X. Hu, Z. Zhang, Z. Fang, K. Zhang, Z. Li and K. Guo, *Polymer*, 2016, **84**, 391–397.

[169] S. Lu and K. Wang, *React Chem Eng*, 2019, **4**, 1189–1194.

[170] S. A. Van Den Berg, H. Zuilhof and T. Wennekes, *Macromolecules*, 2016, **49**, 2054–2062.

[171] A. R. Bogdan, B. P. Mason, K. T. Sylvester and D. T. McQuade, *Angew Chem Int Edit*, 2007, **46**, 1698–1701.

[172] R. Munirathinam, J. Huskens and W. Verboom, *Adv Synth Catal*, 2015, **357**, 1093–1123.

[173] P. T. Anastas and J. C. Warner, *Green Chemistry: Theory and Practice*, Oxford University Press, New York, 1998, p. 30.

[174] J. Yue, *Catal Today*, 2018, **308**, 3–19.

[175] I. Rossetti, *Catal Today*, 2018, **308**, 20–31.

[176] P. H. de Oliveira, B. M. Bruno, R. A. Leão, L. S. Miranda, R. A. San Gil, R. O. de Souza and F. G. Finelli, *ChemCatChem*, 2019, **11**, 5553–5561.

[177] Y. Xiao, M. Zheng, Z. Liu, J. Shi, F. Huang and X. Luo, *ACS Sustain Chem Eng*, 2019, **7**, 2056–2063.

[178] Y. Chu, N. Corrigan, C. Wu, C. Boyer and J. Xu, *ACS Sustain Chem Eng*, 2018, **6**, 15245–15253.

[179] T. Hamaide, C. Palix, J. L. Freysz, V. Jacquier, R. Spitz and A. Guyot, *Polym Bull*, 1996, **37**, 313–320.

[180] C. Miola, F. Delolme, I. Zanella-Cléon, G. Dessalces and T. Hamaide, *Polym Bull*, 1998, **40**, 541–548.

[181] E. Pollet, T. Hamaide, M. Tayakout-Fayolle and C. Jallut, *Polym Int*, 2004, **53**, 550–556.

[182] C. Miola-Delaite, E. Colomb, E. Pollet and T. Hamaide, *Macromol Symp*, 2000, **153**, 275–286.

Chapter 2

Aims of the Thesis Work

In the following paragraphs, the aims of each chapter are outlined, which tie together in the hope of developing active and stable heterogeneous catalysts for the ROP of LA (and other lactones), working towards the future application of these catalysts into continuous flow. The thesis aims to work towards a robust continuous flow reactor for the ROP of cyclic esters, using heterogeneous catalysts. In order to do this, several developmental steps are required, including preliminary solution-phase ROP tests in a flow reactor and extensive catalyst development, with both commercially available and synthesised immobilised catalysts. Both organocatalysts and metal catalysts aim to be tested, to have an excellent understanding of what is available for potential use in a continuous flow reactor. Due to the extensive scope of this project, it is necessary to start looking at heterogeneous catalyst development, followed by initial reactor development; the next Chapters therefore follow this structure.

To begin, Chapters 3 and 4 aim to explore immobilised metal complexes for melt ROP. In particular, the focus was placed on the immobilisation of simple half-salen, 5-membered metallacycles onto inert supports such as PS. These supports are notably robust, inert supports, with an excellent track record in combinatorial chemistry, and not complicated by acidic sites on the surface as SiO_2 surfaces are. In terms of the ligand choice: previous literature noted that salen and half-salen ligands are robust, readily-synthesised and tailorable ligand frameworks and many examples of successful ROP catalysts built off these skeletons exist. In

particular, immobilised zinc half-salen complexes provided PLA of comparable dispersity and molecular weights to the homogeneous analogues.[1] With this in mind, it is of interest to explore how immobilisation of this class of catalyst affects ROP activity, and if they can be recovered and reused in ROP. As such, the work described in Chapter 3 aims to develop a PS-immobilised metal-based catalyst in a bottom-up approach, starting from immobilisation of a simple, half-salen ligand, followed by complexation to a metal. Once successful catalysts have been identified in Chapter 3, Chapter 4 aims to explore the monomer selectivity of the catalysts, to identify whether the immobilised catalysts have any in-built monomer selectivity, and whether block copolymers could be accessed, which could tailor the polymer properties.

In addition to metal-based catalysts, it is important to also identify any immobilised organocatalysts which could be competitive with the current homogeneous ROP catalysts. Organocatalysts have been shown to be highly active in the ROP, however no example of immobilised bases used in the ROP of LA in melt conditions has yet been reported, to the best of our knowledge. Therefore it is necessary to screen several commercially available, immobilised organocatalysts and compare these to their homogeneous counterparts, to evaluate their catalytic activity. This work is therefore the focus of Chapter 5, which concerns the melt ROP of LA. The Chapter also explores the modification of the base acitivity upon combination with (thio)ureas to form bifunctional cataysts, to see if an improvement is possible under melt conditions as seen in solution-phase homogeneous work. In a similar vein, bifunctional catalysts have previously been formed between (thio)ureas and stronger bases such as KOEt and KOMe, pioneered by Waymouth and co-workers.[2,3] Chapter 6 aims to try and harness the same level of activity – which would enable rapid reactions in a flow reactor – using the immobilised (thio)ureas, combined with KOEt and used in solution-phase ROP.

The final two chapters shift the focus from catalyst development to application of catalysts into flow reactors. Chapter 7 describes work carried out in the Polymer Reaction Design group at Monash University, supervised by Professor Tanja Junkers. It aims to input simple homogeneous organocatalysts into a microreactor, to develop a catalytic system in continuous flow ROP. The simple microreactor set-up is only suitable for solution-phase ROP, however, due to the

increased pressure which cannot be handled by syringe pumps and commercially available syringes. Thus, the focus of this chapter is directed towards solution-phase ROP as a proof-of-concept. Although the reactor is a simple design and homogeneous catalysts in solution are used, the chapter emphasises the difficulties faced when applying a highly water and air-sensitive anionic procedure into continuous flow. These are essential to understand prior to the application of the immobilised catalysts into flow, and are necessary to highlight the value of flow to polymerisations. A rigorous optimisation procedure is detailed, followed by attempts to develop further applications for the polymers produced in flow, in the form of data encryption.

The final Chapter (Chapter 8) details the initial developments of a much more complex continuous flow system to accommodate the immobilised catalysts developed in the previous chapters.

References

[1] M. D. Jones, M. G. Davidson, C. G. Keir, L. M. Hughes, M. F. Mahon and D. C. Apperley, *Eur J Inorg Chem*, 2009, **2009**, 635–642.

[2] B. Lin and R. M. Waymouth, *J Am Chem Soc*, 2017, **139**, 1645–1652.

[3] B. Lin, J. L. Hedrick, N. H. Park and R. M. Waymouth, *J Am Chem Soc*, 2019, **141**, 8921–8927.

Chapter 3

Immobilised Metal Complexes

3.1 Introduction

Whilst some catalyst development has addressed some of the requirements to improve the ROP of lactones (specifically lactide), concerns about their toxicity and accumulation in the environment remain.[1] Most of these attempts have also not considered catalyst stability in water, oxygen and towards impurities in the monomer source, nor catalyst recovery. Throughout the following chapters, it shall be made clear that even simple, commercially available catalysts pose a difficulty in obtaining controlled ROP of LA. Further to this, despite the development of several elegant catalytic systems, such as the bifunctional organocatalysts developed by Waymouth and co-workers (explored in Chapter 6), several limitations still exist.[2,3] Namely, whilst the synthesis of these catalysts proceeds through a simple route, they themselves are often highly air and moisture sensitive and are therefore difficult to manipulate outside of an air sensitive environment. These catalysts have the added disadvantage that their activities are matched with specific lactones; whilst this can be exploited in incredibly elegant chemistry (such as their copolymer synthesis whereby they can add different monomers/catalysts of increasing acidity), this is limited practically by the need to match each monomer to a specific catalyst, and therefore is not practical on a much larger, industrial scale.[3]

$Sn(Oct)_2$ as an industrial catalyst, and requirements for biocompatible alternative catalysts

The scope of ROP initiators ranges from metal complexes to organocatalysts, the latter of which shall be discussed in later Chapters. Of these, metal complexes, and more specifically metal alkoxides, have typically been favoured for the efficient ROP control.[4] Industrial production of PLA instead makes use of the homoleptic metal catalyst, $Sn(Oct)_2$, a Sn(II) based catalyst with two 2-ethylhexanoate associated ligands, which is relatively air and moisture stable and a liquid, making it ideal for handling on an industrial scale. This catalyst can attain high molecular weight P*L*LA ($\sim 10^5$ Da), in the presence of an alcohol co-initiator, and can be used in the melt at high temperatures (typically 180 °C).[5,6]

At the end of the 20th century, Penczek and co-workers suggested that the likely mechanistic route involves the $Sn(Oct)_2$ pre-catalyst reacting with an alcoholic co-initiator to produce the tin(II) alkoxide active catalyst, $Sn(OR)_2$, *in situ*.[7,8] The alkoxide then coordinates to the lactide to initiate polymerisation, resulting in a living polymerisation; the activity of a catalyst is optimal when fast exchange between the alcohol and alkoxide species is possible.[6]

Other simple alkoxides ionically coordinated to aluminium or group 1 alkali metals such as lithium and sodium also have shown high ROP activity, with polymers reaching molecular weights of 40 000 Da. Despite the success of $Sn(Oct)_2$, in the majority of cases concerning homoleptic metal alkoxides the stronger nucleophilicity of the ionically bound alkoxy-group compared to covalently bound analogues can result in significant amount of epimerisation, leading to atactic PLA.[4,9–12] Further to this, despite having been FDA approved, the industrial $Sn(Oct)_2$ has come into question regarding its toxicity, with reports suggesting that it leads to cell depletion and death.[13,14]

A strong effort has therefore focused instead on the design of typically heteroleptic metal catalysts to enable (primarily) stereocontrolled ROP. In 2002, Feijen and co-workers outlined some key requirements that were necessary in the design of new catalysts to address the challenges in PLA synthesis:[14]

1. Ligands must be commercially available or synthesised through a simple,

cost effective route.

2. Catalyst synthesis must also be easy, and must result in a high yield.
3. The catalyst must be able to withstand industrial conditions, *i.e.* above 130 °C, solvent-free (melt) conditions.
4. The ROP should reach a high conversion, with a high M_n.
5. It should ideally be possible to use the catalyst with other monomers, to make other interesting polymers with alternative properties.

These requirements are catalyst specific, with the ultimate aim of optimising the properties of lactide. These include a high M_n which increases linearly with conversion, a low $Đ_M$, with low levels of transesterification, epimerisation and hydrolysis side reactions.[15] The reaction should also display a fast initiation rate compared to propagation rate.[4] Although a huge scope of catalysts have been studied in the last few decades to optimise these properties, a full understanding of how a catalyst can influence the reactivity and subsequent structure-property relationship of PLA is necessary to develop PLA as a competitive alternative plastic.

To satisfy these criteria, metal complexes comprising of sterically bulky ligands encompassing a Lewis acidic metal have been tested, which can activate the carbonyl group on the lactone to increase the $\delta+$ charge on the carbon.[16] Such catalysts are usually made up of a metal bound to both a ligand (often chelating) and an initiating group, such that they adopt the form [L_nM-X], where X is the initiating group.[17] An in-depth discussion of homogeneous metal-ligand complexes is beyond the scope of this report, although a review is available.[12] It is nevertheless necessary to discuss the most important developments, and those which are pertinent to this report in ROP catalysis.

Aluminium catalysts: effect of ligand structure

Historically, many of the most successful and ground breaking catalysts were based on an Al metal centre coordinated to ligand systems including salen, salan, salalen, Schiff base, β-diiminates, among others. A large subset of these catalysts have involved salen ligands bound to metals such as aluminium and various

lanthanides; these have been shown to initiate the fast and stereocontrolled ROP of lactide (Scheme 3.1). These ligands are often symmetrical, chelating complexes derived from the Schiff base motif, such that they contain sp^2-hybridised nitrogen donors. Salen ligands and their derivatives (salan and salalen, for example) are favoured due to their ease of synthesis, tuneability and stability, thereby making them ideal candidates for the complexes used in ROP.

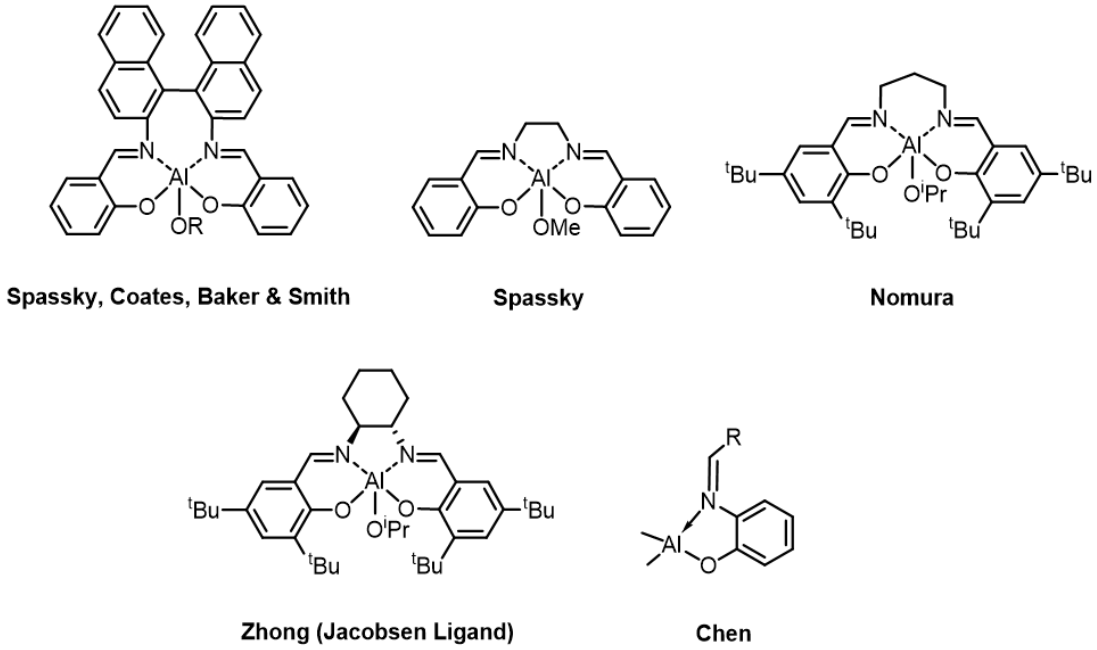

Scheme 3.1: Salen-Aluminium complexes used in ROP. Chen reported improved activity with 5-membered metallacycles over 6-membered half-salen complexes.[18]

Spassky and co-workers discovered the first example of enantiomorphic site controlled ROP on *rac*-lactide to produce stereoblock PLA at high conversions by selectively polymerising *D*-lactide at conversions below 50% (70 °C in toluene, [Cat]:[LA] = 1:100). The reported catalyst contained a central Al(III) atom coordinated to a chiral {ONNO}-salen ligand and a methoxy intiating group, depicted in Scheme 3.1.[19] Furthermore, catalysts coordinated to the Jacobsen ligand have been used by many groups to polymerise *rac*-lactide, such as Zhong *et al.*[20] In this case, the chiral catalyst showed selectivity towards *L*-LA to produce isotactic stereoblock PLA, at 85% conversion in the melt.

It was soon demonstrated that more structurally simple achiral ligands could also be used to produce isotactic PLA from *rac*-lactide.[21] A new aluminium

salen catalyst by Spassky and co-workers with a simple C2 linker was reported to show increased activity than the original chiral binapthyl catalyst they reported in 1993, whilst also reducing transesterification reactions.

Changing the substituents on a ligand can greatly influence both the activity of a catalyst and the final stereochemistry of the polymer.[22] The catalytic activity of achiral aluminium complexes was improved by addition of sterically encumbered substituents to the *ortho* and *para* positions.[10,23] At 70 °C in toluene ([LA]:[Cat]:[BnOH] = 100:1:1), replacing the hydrogens in these positions with Ph-substituents increased the isotacticity of the final polymer whilst retaining high molecular weights (M_n=10.2–14.1 $\times 10^3$ Da) and dispersity ($Đ_M = 1.0-1.2$). When the *ortho* and *para* substituents were changed to ^{t}Bu groups, however, the activity dropped significantly due to their electron donating capacity, reaching only 95% after 14 hours, yet isoselectivity was improved.[10]

Electron withdrawing substituents on the phenoxide component of the ligand have been shown to improve the activity of aluminium complexes, such as Cl or Br atoms.[12] This is thought to be due to a change in the electronics and therefore coordination of the ligand to the metal, resulting in knock-on effects in monomer coordination.[24] In 2006, a study by White and co-workers on the stereoelectronic effects of aluminium salen complexes revealed an electronic factor played a role in polymerisation rates, where the dichloro- substituted phenoxy donor component of the salen ligands at the *ortho* and *para* positions increased the rates by 3 times.[25] Increasing the length and flexibility of the linker in the ligand backbone from C2 to C3 could also greatly influence the activity of a complex, leading to an even higher degree of isotacticity, increased molecular weights (M_n 20.0 $\times 10^{-3}$ Da) and activity.[10,25]

Most recently, Tolman and co-workers built an aluminium complex using a salen ligand analogue.[26] The typical phenoxy- group of the salen ligand architecture was replaced with an indolide group bound to the Schiff base *via* the 2-position, creating a 5-membered chelate ring {NNNN}-donor analogue ("L^2AlOBn"). A second indolide-imine ligand was also formed by attaching the indolide to the Schiff base *via* the 7-position, creating a 6-membered chelate ring ("L^7AlOBn", Scheme 3.2A). From their previous work, X-ray crystallography and NMR studies pointed to solution-phase ligand fluxionality between inequivalent and equivalent

indolides on either side of the tetradentate ligand (Scheme 3.2B). Melt reactions at [LA]:[I] = 300:1 (135 °C) for both L^7AlOBn and L^2AlOBn reached >93% conversion of *rac*-LA within 30 minutes with $M_{n,SEC}$ close to the $M_{n,Theo}$ of 44 000 Da. It was noticeable that the 5-membered chelate ring produced far higher dispersities ($Đ_M$ 1.74, P_m 0.58) compared to the 7-membered metallacycle ($Đ_M$ 1.11, P_m 0.64), although neither catalyst were stereoselective to induce a polymer with a discernable T_m.

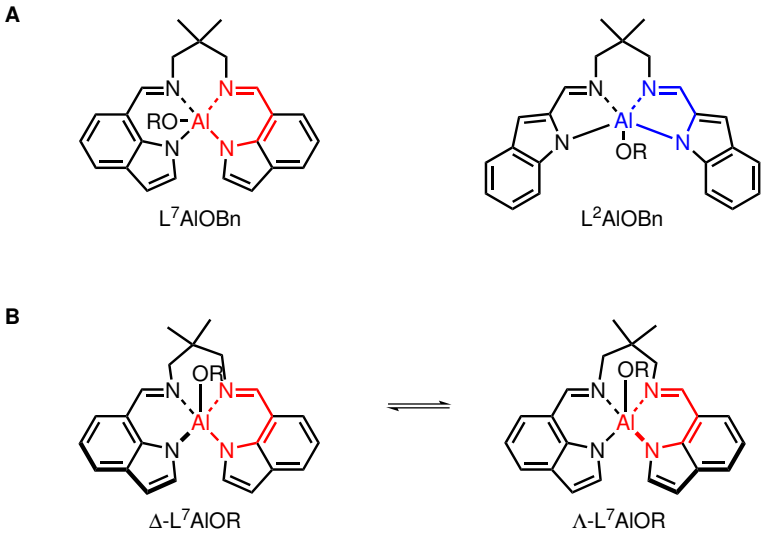

Scheme 3.2: (A) Aluminium complexes based on indoline-imine ligands, bearing 5- and 6-membered chelate rings, (B) Ligand fluxionality determined by ^{1}H VT-NMR spectroscopy.[26]

Whilst most salen-ligands form 6-membered metallacycles once coordinated to a metal, Chen and co-workers recently demonstrated that changing the ring size of the chelate ring could also have a positive effect on the catalytic activity in the ROP of lactones (Scheme 3.1).[18] In their work, 5- and 6-membered metal-containing rings were synthesised and coordinated to aluminium centres, with varying substituents on the Schiff base ligands. They proposed that the smaller angle of the 5-membered rings caused the complex to pucker, providing greater space around the metal centre as the ligand would sit slightly below the plane of the metal. Access of the monomer would occur more readily due to the reduced steric repulsion, and therefore an improved reaction rate. When ROP of caprolactone (ϵ-CL) was conducted in toluene (2 mol L^{-1}), the rate was improved by 2-3 times using the 5-membered ring equivalent, with $Đ_M$ of 1.73, in comparison

to 1.17 with the 6-membered ring.

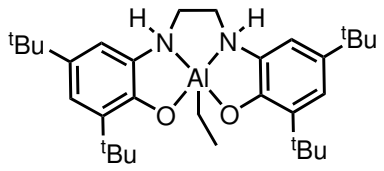

Dalton Tras., 2018, **47**, 10410-10414

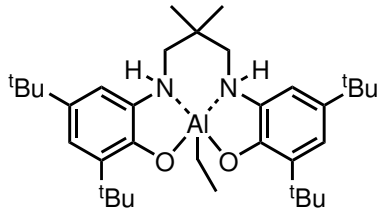

ACS Catal., 2019, **9**, 7912-7920

Scheme 3.3: Catam-ligand backbone towards stereoselective ROP of *rac*-LA. The more rigid tethering group (right) leads to a strong heterotactic bias.[27,28]

Further adding to the structure-activity relationship between catalyst design and activity in ROP of lactide, Romain and co-workers developed Al complexes bearing catam (catechol-amine) ligands; the latter comprising of two, rigid aminophenoxy groups tethered by an adjustable linker (Scheme 3.3).[27,28] The N−H moiety in this case differs from a traditional salen/salan ligand in that it is connected directly to the aryl group, and is available for H−bonding in order to increase activity through non-covalent interactions (NCIs). The secondary amine hydrogen on the activity of the complex was shown to play an important role: the activity of a deuterated analogue of the complex was almost half that of the original complex under the same conditions (2.52×10^{-4} s^{-1} and 4.75×10^{-4} s^{-1}, respectively). Substituting methyl groups onto the N-donor atoms to create tertiary amines rendered the complex inactive, further emphasising the importance of the N−H moiety for NCIs, in accordance with Merkhodavandi and co-workers' observations using indium catalysts.[29] Reacting the ligand under organocatalytic conditions with a mixture of sparteine and isopropyl alcohol (IPA) increased the activity compared to both the ligand alone, and a control experiment of a salen derivative combined with sparteine and IPA. Altering the ligand backbone from an ethyl group to a more rigid structure also caused a change in selectivity, switching from isotactic to heterotactic bias. This is attributed to the decrease in flexibility, reducing the catalysts ability to reorganise into the pseudo-octahedral transition state required to adopt (*e.g.*) a site control mechanism.[30]

In THF at room temperature, one preactivated Al-catam catalyst could reach 91% conversion of *rac*-lactide in 90 minutes, with excellent heteroselectivity ([LA]:[^{i}PA]:[Cat] = 100:0:1, [LA] = 1 mol L^{-1}, $Đ_M$ 1.3, P_r 0.91).[28] Catalyst load-

ings as low as 0.1 mol% were also possible, as well as in a variety of solvents at different temperatures. Whilst these catalysts were predominantly tested in solution, limited testing in the melt revealed excellent activity albeit slightly higher dispersities, and stereoselectivity was lost at higher temperatures (4 hours, 77%, 4 900 Da, $Đ_M$ 1.6; conditions: [LA]:[BnOH]:[Cat] = 1 000:9:1, 130 °C, TOF = 11 600 h^{-1}).

The last decade has seen a myriad of ligands and metals tested. While some of these studies have attempted to elucidate the precise structure-activity profile for efficient ROP, they have only shed some light onto the subject, and a detailed understanding of optimum catalyst design is yet to be discovered.

Despite the great advances that have been made using aluminium based catalysts, and the relative abundace of the latter, its toxicity remains a concern,[31] particularly in cases where these plastics are used in food packaging – a key market for PLA; accumulation of the aluminium and potential transmission into the body has been reported as neurotoxic. Al complexes have also typically been used in solution-phase and whilst some testing has indicated high activity in the melt, extensive studies using industrial conditions is limited. In order to address these concerns, other metal centres must be considered.

Biocompatible metals: Zinc, Magnesium and Iron catalysts

Following the requirements for an alternative biocompatible metal catalyst operable under harsh industrial conditions (T > 130 °C), attention has turned to inexpensive, non-toxic metals, preferably in high abundance. Of these, a multitude of papers have been released in recent years, spanning from group 1 alkali and alkaline Earth metals, through to transition metals ranging from Ni(II) and Zn(II) to Zr(IV) and Hf(IV), as well as various lanthanides.[4,15,32] The most relevant cases shall be discussed below.

One of the elements that encompasses nearly all the requirements is Zn(II); both cheap and colourless, it has the added benefit of being non-toxic.[33] Typically enveloped in a bulky multidentate ligand, its high Lewis acidity also makes it an ideal candidate in the ROP of lactones, where the carbonyl group associates to the metal centre in a coordination-insertion mechanism. To prevent ligand

exchanges due to the kinetic lability of Zn(II) complexes, these are typically encased in multidentate, bulky ligands. While often used in CO_2/epoxide co-polymerisations, several examples of Zn catalysts exist for the ROP of LA.[13,34–37]

Since simple Zn(II) salts appeared to yield slow and uncontrolled ROP,[38] Zn(II) alkoxides based around ligands such as β-diketiminate,[39] or Schiff base ligands[40] have overtaken salts as catalysts that can provide controlled ROP.

Catalysts bearing a bulky β-diiminate (BDI) or diketiminate ligand coordinated to biocompatible metals such as Zn(II), Ca(II) or Mg(II) have been reported in the literature regularly in the last few years.[39,41–43] Chamberlain *et al.* reported Mg(II) and Zn(II) alkoxide coordinated to a BDI ligand scaffold, suggesting that the steric bulk would encourage a chain-end control mechanism to enable stereocontrolled ROP.[39] Complexes were synthesised in a two-step procedure *via* zinc amide intermediates, in toluene at 80 °C. Addition of isopropanol to the zinc amide resulted in the formation of the dimeric zinc BDI complexes with two bridging O^{i}Pr species, whilst reaction of the amide with methyl lactate generated a monomeric Zn(II) species with a $-$OCH(Me)CO_2Me initiating ligand. Alternative initiating species were introduced by direct reaction of the BDI ligand with $ZnEt_2$ or deprotonation of the ligand, following complexation to $Zn(OAc)_2$, yielding an OAc-bridged Zn(II) dimeric catalyst. Reaction in DCM at 20 °C revealed that only the O^{i}Pr bridged dimer and the Zn(BDI)$-$OCH(Me)CO_2Me catalysts displayed good activity, each reaching >95% in 20 minutes, with good dispersities ($Đ_M$ 1.10-1.14, respectively, [LA] = 0.4 mol L^{-1}). Contrastingly, the $-$Et and $-$OAc groups were slow to initiate ROP, as these had to react with the acidic impurities in the monomer feed to produce the active initiating species. Broad dispersities ($Đ_M$ >1.83) and differing $M_{n,SEC}$ *versus* $M_{n,Theo}$ were observed as a result, highlighting the importance of using the appropriate initiating group.

Another common motif within the ligand systems typically used are the {ONNN}-tetradentate motifs, such as those developed by Kol an co-workers for the improved stereocontrolled ROP of *rac*-lactide.[44] Several new precursors were created, based on Hillmyer/Tolman's {ONN}-ligand, displaying a bipyrrolidine motif with two donating N-atoms, coordinated to a Zn(II) centre (Scheme 3.4). Treatment with benzyl alcohol generated the active catalyst. Polymerisations were run in DCM, using a monomer to initiator ratio of 300:1, leading to near quantitative

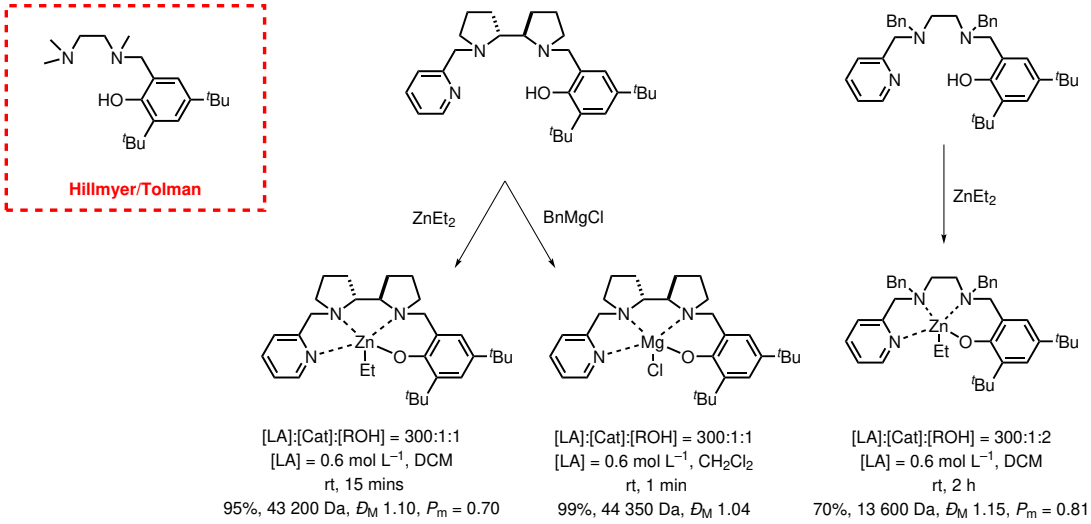

Scheme 3.4: Complexes based on {ONNO}-ligand backbones, developed by Kol and co-workers.[44,45]

conversion of *rac*-LA in 15 minutes (room temperature, [LA] = 0.6 mol L^{-1}, $Đ_M$ 1.10, P_m 0.70). By altering the ligand structure, to contain benzyl (Bn) groups off the N-donor atoms, isoselectivity improved to P_m 0.81. A Mg(II) analogue of the bipyrrolidine-based ligand was prepared (Scheme 3.4). Under the same conditions, conversions improved drastically compared to the original Zn(II) catalysts, yielding >99% conversion in one minute, with low dispersity ($Đ_M$ 1.04) and $M_{n,SEC}$ of 266 000 Da could be reached after 6 minutes ($Đ_M$ 1.07, [LA]:[Cat]:[I] = 4 300:1:2). This catalyst was able to make precise diblocks formed by sequential addition of *D*-LA to *L*-LA with up to 500 equivalents of each isomer, maintaining excellent control ($M_{n,SEC}$ 177 000 Da, $Đ_M$ 1.11). Stereoblocks of 8 alternating isomer blocks were also possible, with melting temperatures above 211 °C.

Similarly, Jones and co-workers developed a series of Mg(II) and Zn(II) complexes of {ONN}-tridentate ligands which were active at 180 °C in the ROP of *L*-LA, at industrial monomer:catalyst:initiator ([M]:[Cat]:[I]) ratios of 10 000:1:100.[46] These were able to reach conversions of up to 83 % in 5 minutes at lower temperatures of 130 °C, with well controlled dispersities ($Đ_M$ 1.04-1.14). At 180 °C, the same catalyst reached 90% conversion in 3 minutes, although dispersities broadened to 1.47. The Zn(II) catalysts reached TOF values exceeding 100 000 h^{-1}, with low epimerisation and producing colourless PLA. Mg(II) analogues

tended to cause transesterification of the polymer chain, and lower activity under certain conditions compared to their Zn(II) analogues.

To date, Herres-Pawlis and co-workers have pioneered work producing some of the most active and stable zinc catalysts in the melt ROP of lactide.[40,47–50] The catalysts commonly make use of neutral N-donor guanidine ligand scaffolds, which are able to stablise the complex towards air, water and impurities in the monomer feed *via* their strong donor capabilities.[48] Mechanistic insight from DFT calculations revealed that the high nucleophicity of the ligand allows it to act as the initiating group in ROP.[51]

In a recent example, complexation of the Zn atom to neutral N,O guanidine ligands, these catalysts demonstrated excellent activity in the ROP of technical grade *rac*-LA, with rate constants (k_p) up to 9.5×10^{-2} s^{-1} M^{-1}. M_n values of up to 49 500 Da are achieved in 90 minutes at 150 °C ([M]:[I] = 500:1, $Đ_M$ 1.39).[40] Conversions, however, stagnated around 52%, compared to the $Sn(Oct)_2$ control reaction which reached 90%, M_n 114 700 Da ($Đ_M$ 2.0). When the ratio was decreased to 100:1, however, 90% of the monomer had been consumed in 30 minutes. The effect of the halide donor atom was determined; whilst both bromido and chlorido complexes were equally fast, however the bromido complexes produced PLA with higher molar masses.

Notably, Herres-Pawlis and co-workers developed Fe(II) catalysts building on a similar guanidine motif, discussed in Chaper 1.[52] Fe(II) catalysts are typically not considered for industrial use owing to their air and moisture sensitivity, which makes complex synthesis and use challenging; coordinated to a guanidine ligand, however, reportedly overcomes these issues, however challenges with polymer colouring from the catalyst remain.

It is also possible to exploit intermetallic cooperativity in bimetallic catalysts to increase activity and selectivity. In 2003, Williams *et al.* synthesised a dizinc alkoxide complex, achieved *via* a two bridging mononuclear Zn(II) complexes.[53] ROP of lactide proceeded successfully in DCM at room temperature at a variety of [M]:[Cat] ratios ([LA] = 1 mol L^{-1}). At a ratio of 1500:1, 93% conversion was reached after 18 minutes (130 kDa, $Đ_M$ 1.34).

Such dinuclear catalysts were further developed by Williams and co-workers using

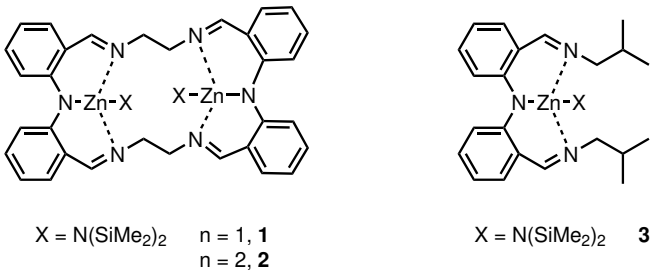

Scheme 3.5: Dinuclear complexes developed by Williams and co-workers.[54]

macrocyclic systems with varying lengths of bridging alkyl chains, coordinated to either $Zn(HDMS)_2$.[54] Results from the ROP of *rac*-lactide indicated that the activity of the HDMS complexes was at least three times that of the mononuclear analogue, indicative of cooperativity between the two Zn(II) centres. Using a catalyst loading of 0.1 mol%, macrocycle **2** reached 73% conversion in 30 seconds, compared to 78% in 1.3 hours (TOF = 45 000 h^{-1} and 14 300 h^{-1}, respectively). The $M_{n,SEC}$ observed for the HDMS complexes were much higher than the theoretical values (135 000 Da compared to 57 000 Da for complex **2**), suggesting that only some of the centres participated in the ROP. Adjusting the rates to accommodate this revealed that both macrocycles were faster than the mononuclear complex **3**. The rate also increased with a shorter proximity of the Zn(II) centres; the shorter bridging alkyl chain of macrocycle **1** resulted in a rate that was 1.5 times that of macrocycle **2**.

$$\text{Reaction rate } (\nu) = -\frac{\mathrm{d[M]}}{dt} = \frac{\mathrm{d[P]}}{dt} = \frac{k_2[\mathrm{Cat}][\mathrm{M}]}{K_\mathrm{M} + [\mathrm{M}]} \tag{3.1}$$

$$K_\mathrm{M} = \frac{k_{-1}}{k_1} = \frac{1}{K_{eq}} \tag{3.2}$$

Unusually, kinetic analysis revealed that the ROP was zeroth order in monomer, as opposed to first order kinetics typically observed. An induction period was also visible at low conversions (up to 20%), which was rationalised using Michaelis-Menten kinetics, based on the report by Tolman and co-workers (Equations 3.1-3.2).[55,56] The fast zeroth order kinetics occur once all the Zn(II) sites are occupied, reaching saturation, thereby rendering the ROP independent of monomer concen-

tration. Saturation kinetics are reached at high monomer concentrations, when the pre-equilibrium Michaelis constant (K_M) is much smaller than the [LA]. The rate determining step is instead related to the reversible binding of the lactide to the metal and the intrinsic productivity of the metal centre (described by K_M); these are themselves affected by the steric bulk of the HDMS ligand and the fast initiation and propagation rates. When the co-ligands were switched for O^{i}Pr groups, the ROP reverted back to first order kinetics in monomer, highlighting the effect of sterics on K_M. The higher activities of the HMDS catalysts compared to their O^{i}Pr analogues were rationalised using single-crystal XRD analysis of the catalyst structure. The steric bulk of the HMDS groups created a folded ligand structure, improving access of the lactide to the coordination sites, and reducing the distance between the Zn(II) atoms to enhance cooperativity. In contrast, O^{i}Pr containing catalysts were planar.

3.2 Aims

Significant catalyst developments have been carried out, yet, with the exception of a select few, most of these have been tested in solution-phase ROP, rather than in the absence of solvent. As a result of this decreased stability (and often disregard for metal toxicity when the focus is on stereoselective catalysts), several catalysts cannot be applied in an industrial setting.

It is therefore of interest to develop robust, biocompatible catalysts as a replacement of the current industrial standard $Sn(Oct)_2$ using a heterogeneous alternative. Use of such a catalyst could prevent the metal from being incorporated into the polymer, thereby producing polymers of high purity and increased atom efficiency. Moreover, solid catalysts offer possibilities for the catalyst to be recycled, thus decreasing the cost of the process further.[57–61]

Herein, we report a series of single-site metal complexes immobilised onto PS, and their application for the bulk polymerisation of *L*-lactide. The use of PLA as a model substrate in these studies has enabled the optimisation of ROP and comparison of these catalysts to the homogeneous catalysts. Industrial conditions were targeted, with a final aim of M_n of 50 000 Da. Particular focus has been placed on the metal leaching into the polymers, and catalyst recovery and reuse

are also explored.

3.3 Results and discussion

Synthesis and characterisation

A series of ligands and their complexes were immobilised onto poly(styrene) beads (PS), as depicted in Scheme 3.6. The complexes were synthesised in a simple 3-step pathway, in a procedure adapted from the literature.[18,62,63] Commercial PS-CH_2Cl, or "Merrifield's resin", readily underwent a Kornblum oxidation of the chlorine functional group to form aldehyde PS-CHO. A new, sharp absorption band at 1697 cm^{-1} in the IR spectrum was consistent with an aldehyde carbonyl stretch (Figure 3.1). A small peak at 2746 cm^{-1} corresponded to the aldehyde C−H stretching vibration,[63] and the disappearance of the C−Cl stretch at 673 cm^{-1} further confirmed the conversion to the aldehyde. Calculations based on elemental analysis of PS-CHO (Appendix B.1) indicated quantitative conversion to the aldehyde.

The aldehyde was condensed with 2-aminophenol to yield the immobilised Schiff base, **PS-HL^{H}**. The intensity of the carbonyl peak was significantly reduced in the spectrum of **PS-HL^{H}**, indicating incomplete conversion. At least partial formation of the ligand was confirmed by the presence of a hydroxyl vibration at 3381 cm^{-1}; the aromatic C−N stretch was also observed at 1285 cm^{-1}. Imine C=N stretches have been reported at 1627 cm^{-1}, consistent with the new peak seen in the IR spectrum of **PS-HL^{H}** 1624 cm^{-1}.[64] **PS-CHO** was also condensed with two other amines: 2,4-di-*tert*-butyl-6-(methylamino)phenol, 2,4-dichloro-6-aminophenol, to create ligands **PS-HL^{tBu}** and **PS-HL^{Cl}**, respectively. Imine stretches at 1623 cm^{-1} appeared in all ligands, as well as a C−O vibration at 1247 cm^{-1}. Elemental analysis of the ligands confirmed successful conversion to the imine (>75%).

Complexation of all ligands was achieved *via* reflux with the appropriate metal acetate source, as is typical of a Salen ligand complexation, yielding to similar structures to the 5-membered cycles reported in literature.[18,27] A variety of metals were complexed to **PS-HL^{H}**; disappearance of the –OH group at 3381 cm^{-1}

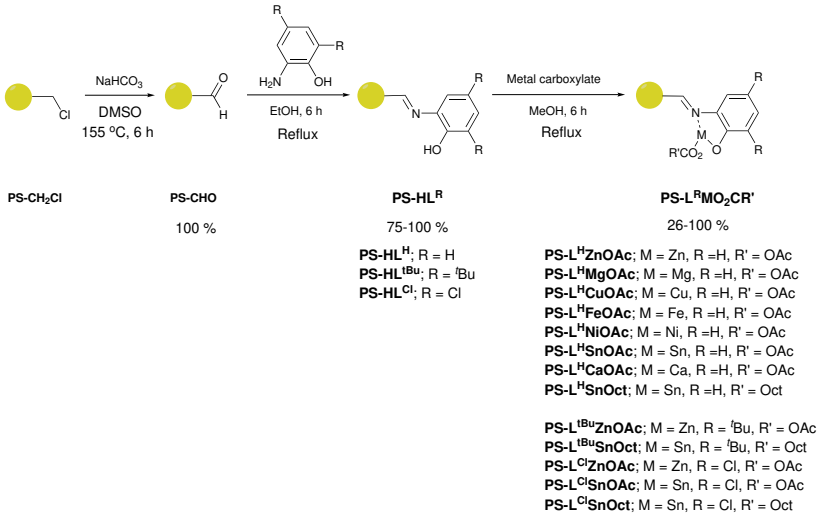

Scheme 3.6: Synthetic route to the immobilised imine complexes with the chemical notation **PS-L^{R}MO$_2$CR'**, where M = metal, O_2CR' = carboxylate (OAc = acetate; Oct = 2-ethylhexanoate) and L^{R} = ligand.

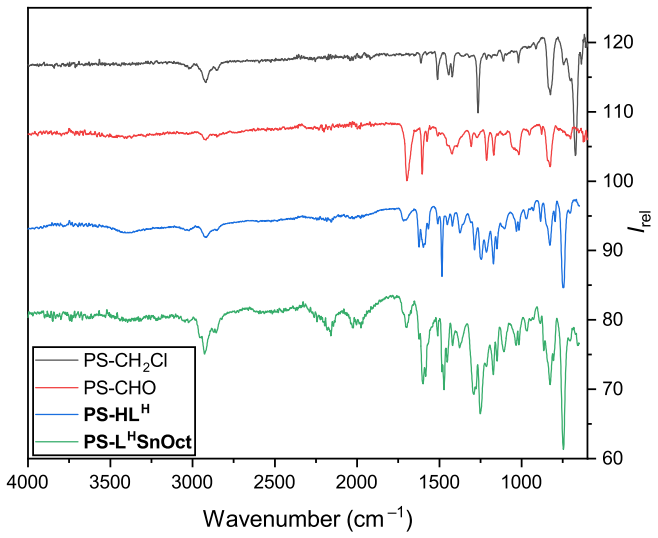

Figure 3.1: IR spectra of the PS-CH_2Cl starting material (black), PS-CHO (red), the immobilised ligand **PS-HL^{H}** (blue) and the complex **PS-L^{H}SnOct** (green).

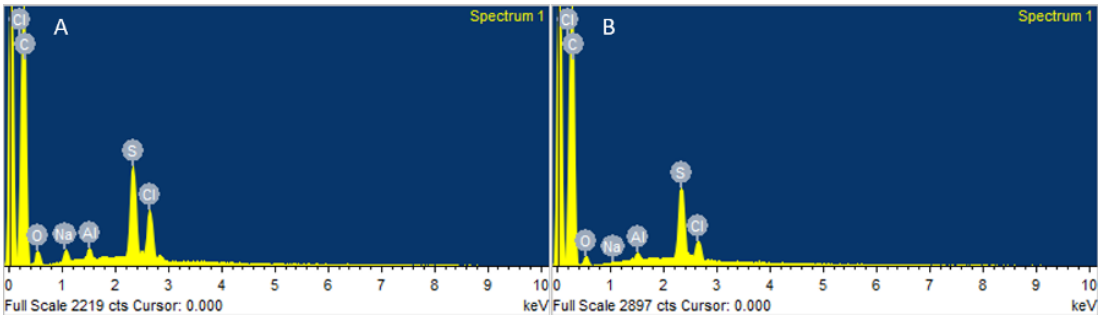

Figure 3.2: Energy Dispersive X-ray (EDX) spectra of (A) PS-CHO, (B) **PS-HL^{H}**.

indicated deprotonation of the hydroxyl group followed by covalent complexation to the metal, whilst the C=N group shifted from 1624 to 1604 cm^{-1}.[64,65] The acetate methyl C−H, $COO^{-}{}_{asymm}$ and C=O vibrations appeared at 1453, 1574 and 1698 cm^{-1}, respectively.[66]

Morphological composition of the samples at each stage was obtained using Scanning Electron Microscopy (SEM) and Energy Dispersive X-ray Spectroscopy (EDX). Triplicate EDX measurements of the samples showed some Cl in **PS-CHO**, suggesting either incomplete conversion to the aldehyde, or residual salt deposits (along with the presence of Na) on the surface from the work up (Figure 3.2). EDX spectra also confirmed the presence of Zn and Sn in **PS-L^{H}ZnOAc** and **PS-L^{H}SnOct**, respectively (Figure B.42). SEM imaging of the parent chlorinated resin revealed a highly porous matrix with pores of up to 5 μm (Figure 3.3A). The porosity decreased gradually after each functionalisation step, with the pore sizes appearing visibly smaller as they were coated by the complex (Figure 3.3C). Further surface area analysis by Brunauer-Emmet-Teller (BET), using N_2 sorption at 77.3 K, was carried out to investigate the porosity of **PS-L^{H}ZnOAc** and **PS-L^{H}SnOct** (Figure B.44). Low relative pressures (P/P_0) of nitrogen surface adsorption implied that the pore sizes were too large to be effectively measured by BET.

Thermogravimetric analysis (TGA) of **PS-HL^{H}** and its complexes (**PS-L^{H}ZnOAc** and **PS-L^{H}SnOct**) revealed that the ligand and complexes possessed similar major degradation temperatures (300-380 °C, Figures 3.4, B.45). However, the first derivative of the TGA trace revealed that the ligand underwent two

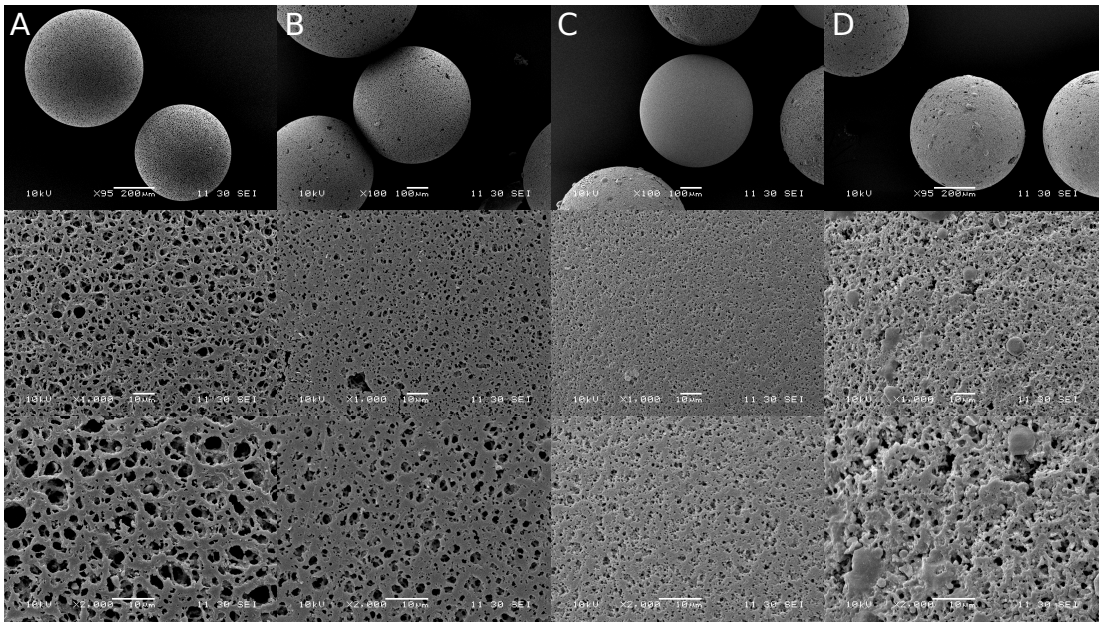

Figure 3.3: SEM images of (A) PS-CH_2Cl, (B) PS-CHO, (C) **PS-HL^{H}** and (D) **PS-L^{H}SnOct** at $\sim$ $\times$100 (top), $\times$1000 (middle) and $\times$2000 (bottom) magnification.

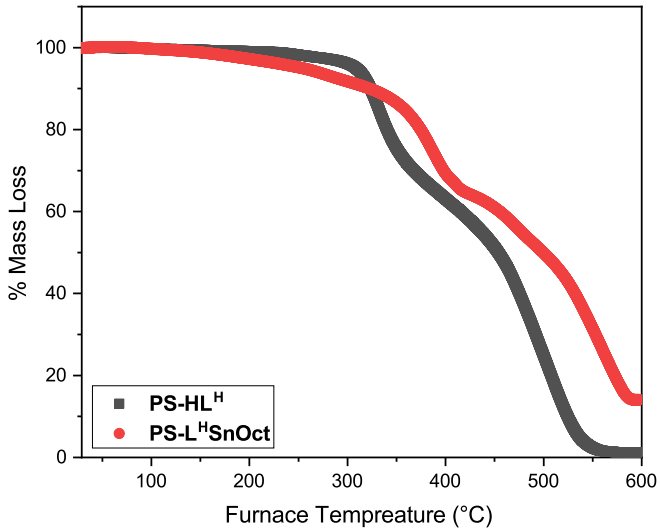

Figure 3.4: Thermogravimetric analysis (TGA) of ligand **PS-HL^{H}** (grey) and its metal complex, **PS-L^{H}SnOct** (red).

distinct degradation steps at 332 and 509 °C with weights approximately corresponding to the degradation of ligand followed by poly(styrene), respectively (Table B.1). The complexes had far more convoluted degradation pathways; **PS-L^{H}SnOct** displayed weight losses occurring at 280, 388 and 562 °C, in line with the more intricate architecture of the complex. The % mass loss of the complex revealed that some residue remained even at high temperatures, potentially due to the presence of inorganics, including the metals found in the complexes (Sn or Zn).

Polymerisation studies

ROP of *L*-LA

To begin, the immobilised metal complexes were employed in the ring-opening polymerisation (ROP) of *L*-LA, which was conducted in the melt at 130 °C, with [LA]:[Cat]:[I] = 50:1:1, using *p*-methylbenzyl alcohol as co-initiator (I). Initial investigations into the activity of the catalysts focused on complexes of imine **PS-HL^{H}**, coordinated to a metal acetate (**PS-L^{H}MOAc**, entries 1-6, Table 3.1). Conversions for successful catalysts were all similar in the 24 hour reaction window, as all catalysts were given sufficient time to reach "full" conversion; a conversion of >90% was deemed quantitative due to both NMR detection limits and the maximum conversion possible in a reversible ROP equilibrium, which states that there will always be some residual monomer left over as ROP to the polymer becomes thermodynamically unfavourable at high conversions. Over 24 hours, clear differences between metal centres were seen, although further studies to elucidate catalytic activity were explored subsequently (*vide infra*). **PS-L^{H}ZnOAc** was by far the most promising catalyst, giving high conversion (84%) into PLA with controlled molecular weight close to the theoretical value (M_{n} 6 450 and 6 050 Da, respectively), and narrow dispersity ($Đ_{M}$ 1.23, entry 1, Table 3.1). The immobilised 5-membered metallacycle compared favourably with its 6-membered half-salen equivalent (40% conversion was achieved with a Zn/SiO_2 catalyst prepared by Jones *et al.*, under similar conditions: [LA]:[Cat]:[I] = 300:1:1 in the melt at 130 °C, 24 hours).[67]

The effect of the carboxylate ligand was then studied. **PS-L^{H}SnOct** was formed by reacting **PS-HL^{H}** with $Sn(Oct)_2$. While **PS-L^{H}SnOAc** was inactive (entry

Table 3.1: Polymerisation data from the ROP of *L*-LA with **PS-L^{H}MO$_2$CR'** catalysts and control reactions, using [LA]:[Cat]:[I] = 50:1:1 (as a standard ROP procedure throughout the thesis to enable extraction of $M_{n,NMR}$ data) in the melt at 130 °C for 24 hours.

Entry	Catalyst	Conv. (%)[a]	$M_{n,Theo}$[b]	$M_{n,NMR}$[a]	$M_{n,SEC}$[c]	$M_{w,SEC}$[c]	$Đ_M$[c]
1	**PS-L^{H}ZnOAc**	84	6050	5800	6450	6600	1.23
2	**PS-L^{H}MgOAc**	30	2150	1350	1150	1200	1.05
3	**PS-L^{H}CuOAc**	7	500	-	-	-	-
4	**PS-L^{H}NiOAc**	6	450	500	-	-	-
5	**PS-L^{H}SnOAc**	8	600	550	-	-	-
6	**PS-L^{H}CaOAc**	30	2150	950	1750	1950	1.11
7	**PS-L^{H}SnOct**	93	6700	3150	5900	8800	1.49
8	**PS-HL^{H}**	7	500	450	-	-	-
9	PS-CHO	7	500	450	-	-	-
10	PS-CH_2Cl	4	300	-	-	-	-
11[d]	$Sn(Oct)_2$	94	6800	1550	8750	15350	1.76
12	$Zn(OAc)_2 \cdot 2\,H_2O$	94	6800	5600	3000	5200	1.73

[a] Determined from the ^{1}H NMR spectrum.
[b] Theoretical M_n = ([LA]/[I]) × (144 × equiv. LA) × (conv./100).
[c] As determined by SEC (THF) using RI methods, relative to poly(styrene) standards (multiplied by a factor of 0.58, rounded to the nearest 50).[68]
[d] Reaction quenched after 6 hours.

5, Table 3.1), switching the acetate to a 2-ethylhexanoate (Oct) ligand increased the conversion to 93% (M_n 5 900 Da, $Đ_M$ 1.49, entry 7, Table 3.1). The well-studied mechanism of homogeneous $Sn(Oct)_2$ involves an initiation step where the pre-catalyst carboxylate exchanges with the 4-MeBnO$^-$ co-initiator to generate an active metal alkoxide *in situ*.[7] From these results, it is suggested that the rate of this exchange affects the rate and success of ROP. Our attempts to transpose these results to Zn catalysts were unfortunately limited due to difficulties in synthesising a pure $Zn(Oct)_2$ precursor from $ZnEt_2$.

A control reaction with homogeneous $Sn(Oct)_2$ reached high conversion after 24 hours, but with narrower dispersities attained by the heterogeneous **PS-L^{H}SnOct** ($Đ_M$ 1.49 compared to 1.76, entries 7 and 11, Table 3.1). $Sn(Oct)_2$ can participate in further transesterification once complete conversion is reached, thus increasing the range of M_n and $Đ_M$.[6] The same was observed for **PS-L^{H}ZnOAc** and its precursor, $Zn(OAc)_2 \cdot H_2O$ (entries 1 and 12, Table 3.1) indicating that immobilisation generally leads to improved ROP control. Both **PS-L^{H}ZnOAc** and **PS-L^{H}SnOct** produced white polymers (Figure 3.5), with no evidence of

Figure 3.5: Polymers made using (A) **PS-L$^{\mathbf{H}}$ZnOAc** (6 450 Da, [LA]:[Cat]:[I] = 50:1:1), (B) **PS-L$^{\mathbf{H}}$SnOct** (5 900 Da, [LA]:[Cat]:[I] = 50:1:1), (C) **PS-L$^{\mathbf{H}}$SnOct** (35 250 Da, [LA]:[Cat]:[I] = 200:1:4), (D) $Sn(Oct)_2$ (24 000 Da, [LA]:[Cat]:[I] = 200:1:4).

lactide epimerisation in the proton NMR (Figure B.10) – both added benefits of the immobilised catalysts.

Polymers produced with **PS-L$^{\mathbf{H}}$SnOct** resulted in a melting point of 175 °C (Figure 4.14A), close to that of fully isotactic P*L*LA (T_m 180 °C),[69,70] whilst the polymer produced with $Sn(Oct)_2$ resulted in a larger decrease to T_m 171 °C (Figure 4.14B); this is indicative of a greater degree of epimerisation in PLA produced with $Sn(Oct)_2$. No activity was seen in control reactions with any of the immobilised ligands or precursors (entries 8-10, Table 3.1).

A Sheldon test was carried out to investigate the heterogeneity of the catalysts.[71] **PS-L$^{\mathbf{H}}$SnOct** was removed after 45 minutes (62% conversion), and when compared to a reaction performed with a solid catalyst present throughout the time course, the filtrate experiment showed a much smaller level of conversion after removal of the catalyst (72% and 94% after 2.5 hours, respectively, see Figure 3.7). Given that several forms of homogeneous Sn(II) are known to catalyse this reaction, the lack of a major increase in conversion likely indicates that either

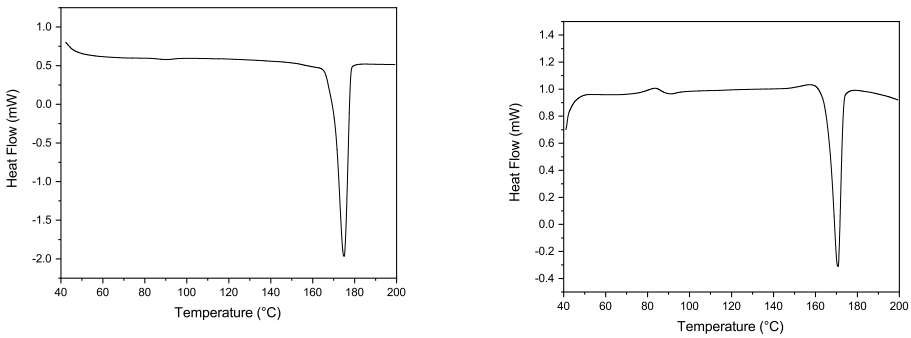

(a) **PS-L$^{\mathbf{H}}$SnOct**

(b) Sn(Oct)$_2$

.

Figure 3.6: DSC trace of PLA formed by (a) **PS-L$^{\mathbf{H}}$SnOct** (90%, M_{n} 35 250 Da, $Đ_{\mathrm{M}}$ 1.27, T_{m} 175 °C), and (b) Sn(Oct)$_2$ (90%, M_{n} 24 000 Da, $Đ_{\mathrm{M}}$ 1.88, T_{m} 171 °C). Conditions: [LA]:[Cat]:[I] = 400:1:1, 24 hours in the melt at 130 °C.

the species leached from the catalyst are inactive, or that only limited leaching occurs. However, in both scenarios, the lack of major increases in conversion confirm catalysis to be truly heterogeneous. Following these promising preliminary results, **PS-L$^{\mathbf{H}}$ZnOAc** and **PS-L$^{\mathbf{H}}$SnOct** were taken forward for further studies.

Effect of altering the ligand

The ligand backbone of these two successful catalysts was modified in order to optimise their activity. In the first instance, a reduced form of the Schiff base tether of ligand **PS-HL$^{\mathbf{H}}$**, **PS-HL$^{\mathbf{H}}_{\mathbf{red}}$**, was formed, featuring a secondary amine (Scheme 9.3-9.4). It was thought that increasing the flexibility of the linker would improve access of the lactide to the active centre of the catalyst, by allowing the catalyst to adopt the optimal geometry of the coordination sphere – an observation which has previously been reported in the literature.[18,27] Results from a 24-hour screen (Table 3.2) showed the opposite, with activity decreasing dramatically. In fact, reduction of ligand **PS-HL$^{\mathbf{H}}$** to **PS-HL$^{\mathbf{H}}_{\mathbf{red}}$** caused large drops in conversion and M_{n} (down to 500 Da), although low dispersities were still achieved ($Đ_{\mathrm{M}}$ 1.08-1.53). A maximum of 75% (Zn) and 22% conversion (Sn) for the unsubstituted amine **PS-L$^{\mathbf{H}}_{\mathbf{red}}$MOR'** complexes were observed, after 24 hours (M = Zn or Sn, R' = OAc or Oct). The same was observed with the complexed

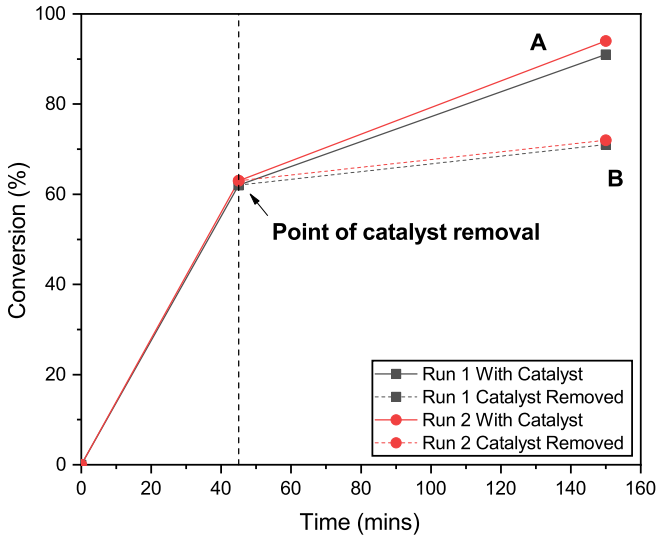

Figure 3.7: Sheldon test for heterogeneity: the catalyst was removed after 45 minutes (62% conversion, [LA]:[Cat]:[I] = 50:1:1 in the melt at 130 °C for 2.5 hours) and the batch without catalyst led to lower conversion (72%), whilst the remaining batch reached 94% conversion (M_n 6 750 Da, $Đ_M$ 1.13).

PS-HL$^{tBu}_{red}$ ligand.

In the second instance, ligand **PS-HL^{H}** was modified at positions *ortho* and *para* to the phenolic donor, to vary the electron density on the metal: Ligands **PS-HL^{tBu}** and **PS-HL^{Cl}** were synthesised to increase and decrease the electron donating ability of the ligand, respectively (Scheme 3.6). Increasing the steric bulk of the ligands using electron donating ^{t}Bu groups to make ligand **PS-HL^{tBu}**, caused a decrease in conversion within 24 hours for both **PS-L^{tBu}ZnOAc** (84 to 23%) and **PS-L^{tBu}SnOct** (93 to 69%, entries 1 and 8, Table 3.2). This is consistent with work by White and co-workers on salen ligands, who suggested that the larger substituents could block access of the monomer to the metal, resulting in a decrease in activity.[25] The increase in electron density on the metal resulting from the inductive effect of the ^{t}Bu groups could also have contributed to the decrease in conversion. This was made more evident when substituting **PS-HL^{H}** with smaller, electron withdrawing Cl groups to form **PS-HL^{Cl}**. **PS-L^{Cl}SnOct** required only 55 minutes to reach completion, as determined by *in situ* Attenuated Total Reflectance Fourier Transform Infra-Red (ATR-FT-IR) spectroscopy

Table 3.2: Polymerisation data from the ROP of *L*-LA with **PS-L^{R}MOR'** and **PS-L$^{R}_{red}$MOR'** catalysts (R = H, ^{t}Bu, Cl, R' = OAc, Oct) and control reactions, using [LA]:[Cat]:[I] = 50:1:1 in the melt at 130 °C for 24 hours.

Entry	Catalyst	Conv. (%)[a]	$M_{n,Theo}$[b]	$M_{n,NMR}$[b]	$M_{n,SEC}$[c]	$M_{w,SEC}$[c]	$Đ_M$[c]
1	**PS-L^{tBu}ZnOAc**	23	1650	850	1000	1200	1.16
2	**PS-L^{H}ZnOAc**	84	6050	5800	6450	6600	1.23
3	**PS-L^{Cl}ZnOAc**	87	6300	4300	4550	6100	1.33
4	**PS-L$^{H}_{red}$ZnOAc**	75	5400	3850	5100	7850	1.53
5	**PS-L$^{tBu}_{red}$ZnOAc**	45	3250	1100	3200	4000	1.24
6	**PS-L^{Cl}SnOct**	96	6900	5100	6271	9200	1.47
7	**PS-L^{H}SnOct**	93	6700	3150	5900	8800	1.49
8	**PS-L^{tBu}SnOct**	69	4950	1400	6200	7050	1.48
9[d]	**PS-L^{Cl}SnOct**	94	6750	1350	5700	6550	1.15
10	**PS-L$^{H}_{red}$SnOct**	22	1600	900	550	650	1.14
11	**PS-L$^{tBu}_{red}$SnOct**	21	1500	850	500	550	1.08

[a] Determined from the ^{1}H NMR spectrum.
[b] Theoretical M_n = ([LA]/[I]) × (144 × equiv. LA) × (conv./100).
[c] As determined by SEC (THF) using RI methods, relative to poly(styrene) standards (multiplied by a factor of 0.58, rounded to the nearest 50).[68]
[d] Result obtained after 2.5 hours.

(entry 9, Table 3.2, *vide infra*). Comparatively, the unsubstituted complex (**PS-L^{H}SnOct**) required 2.3 hours. The same increase in conversion over 24 hours was observed when using **PS-L^{Cl}SnOAc** instead of **PS-L^{H}SnOAc**: substitution of the ligand with Cl groups increased the conversion from only 8% to 96% (entry 6, Table 3.2). Substituting the ligand with electron withdrawing groups seemingly reduces the electron density on the metal, increasing its Lewis acidity and thus facilitating activation and coordination of the lactide to the metal centre.

In situ ATR-FT-IR kinetics

Kinetic analysis of **PS-L^{H}ZnOAc**, **PS-L^{H}SnOct** and **PS-L^{Cl}SnOct** was conducted by monitoring the ether stretches of the lactide and PLA by *in situ* ATR-FT-IR at 1240 and 1185 cm^{-1}, respectively, during ROP catalysis (Figure 3.8). A calibration using different concentration ratios of PLA and LA was used to directly convert the peak areas to concentration to get quantitative data (Figure B.4-B.5).[46] For each of the three catalysts, the catalyst loading was quartered to a [LA]:[Cat]:[I] ratio of 200:1:4, to reduce mechanical interference of the catalyst with the IR probe (by reducing the risk of the catalyst blocking the probe).

Whilst a control reaction using Sn(Oct)$_2$ reached full conversion within 7 minutes,

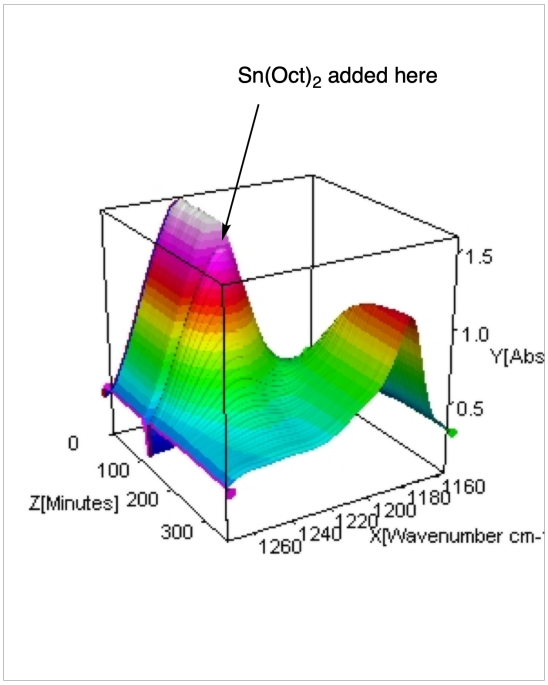

Figure 3.8: Ether stretch of the LA (left, 1240 cm^{-1}) and PLA (right, 1185 cm^{-1}) in the *in situ* Attenuated Total Reflectance Infra-Red (ATR-FT-IR) spectrum. Collated spectra collected from the ROP of *L*-LA using $Sn(Oct)_2$. Conditions: [LA]:[Cat]:[I] = 200:1:4. 130 °C, 55 minutes.

Table 3.3: Polymerisation data from the *in situ* ATR-FT-IR monitored ROP of *L*-LA with **PS-L^{H}MO$_2$CR'** catalysts, using [LA]:[Cat]:[I] = 200:1:4 in the melt at 130 °C.

Entry	Catalyst	Time (h)	Conv. (%)[a]	$M_{n,Theo}$[b]	$M_{n,NMR}$[a]	$M_{n,SEC}$[c]	$Đ_M$[c]	k_{obs} ($\times 10^{-4}$ s^{-1})[d]	$k_{obs,Sn(Oct)_2}/k_{obs,Cat}$	TON	TOF (h^{-1})
1	**PS-L^{H}ZnOAc**	6	89	6400	6100	7050	1.15	1.38	113	170	28.4
2	**PS-L^{H}SnOct**	2.3	87	6250	6300	7300	1.17	6.44	24	174	75.6
3	**PS-L^{Cl}SnOct**	0.8	83	6000	5800	5650	1.05	8.72	18	166	181.0
4	$Sn(Oct)_2$	0.12	89	6400	2450	6750	1.21	155	1	144	1231.7

[a] Determined from the ^{1}H NMR spectrum.
[b] Theoretical M_n = ([LA]/[I]) × (144 × equiv. LA) × (conv./100).
[c] As determined by SEC (THF) using RI methods, relative to poly(styrene) standards (multiplied by a factor of 0.58, rounded to the nearest 50).[68]
[d] Determined from *in situ* ATR-FT-IR kinetics.

the heterogeneous catalysts displayed excellent rates: **PS-L^{Cl}SnOct** and **PS-L^{H}SnOct** only took 55 minutes and 2.3 hours to reach completion, respectively (Figure 3.9), while **PS-L^{H}ZnOAc** was complete within 6 hours (Figure 3.10). Turnover frequencies (TOF) of up to 181 h^{-1} were possible with the heterogeneous catalysts (entry 3, Table 3.3). A comparison of the substituent effect

confirmed that reaction kinetics improve with electron withdrawing groups *ortho* and *para* to the phenoxy group: the Cl-substituted complex, **PS-L$^{\mathbf{Cl}}$SnOct**, was complete within 55 minutes (Figure 3.9B), while the ^{t}Bu substituted complex, **PS-L$^{\mathbf{tBu}}$SnOct**, had only reached 69% conversion after 24 hours (entry 6, Table 3.2).

In contrast to $Sn(Oct)_2$, where the full data set could be used to determine the k_{obs} from the first-order, semi-logarithmic plot, the kinetic data from the Sn-based catalysts was harder to determine. The full data-sets did not agree with either zeroth or second order kinetics, so ROP was assumed to proceed *via* first-order dependence on monomer (as is common with metal catalysts). Data was therefore collected at the steepest part of the S-curve of the conversion against time plots (analysed segment shown in grey, Figure 3.9A), after the observed induction period (for **PS-L$^{\mathbf{H}}$SnOct**, for example, this occurred at 20% conversion). Data was only collected until approximately 80% conversion had been reached, to avoid discrepancies in analysis due to viscosity-induced diffusion limitations, which could interfere with the probe. Whilst trendlines have been added to the data in the semi-logarithmic plots to indicate where the k_{obs} was obtained from, the full data set has been included in the semi-logarithmic plots to highlight deviation from first-order kinetics (Figure 3.9B). As mentioned, the acquired data deviated from the first-order kinetics towards the end due to viscosity, and an induction period was also seen. The latter could be attributed to both mass transfer limitations through the bulk to the active sites, and potentially to the exchange between the initiator and the carboxylate pre-catalyst. Further studies are required for an in-depth investigation into the rate of this exchange (*e.g.* by changing the co-ligand further, or creating the active catalyst prior to addition of monomer, to avoid this delay), or to identify whether this induction period was real or due to the assumption of first-order kinetics, which could ignore more complex kinetics.

A comparison of the k_{obs} relative to that of $Sn(Oct)_2$ revealed that **PS-L$^{\mathbf{Cl}}$SnOct** was 18 times slower than the industrial catalyst, while **PS-L$^{\mathbf{H}}$ZnOAc** was approximately 113 times slower, at the same [M]:[Cat]:[I] ratio (Table 3.3, Scheme 3.7). These results were shown to be reproducible across different batches of catalyst; two separate batches of **PS-L$^{\mathbf{H}}$SnOct** produced k_{obs} values of 6.44×10^{-4}

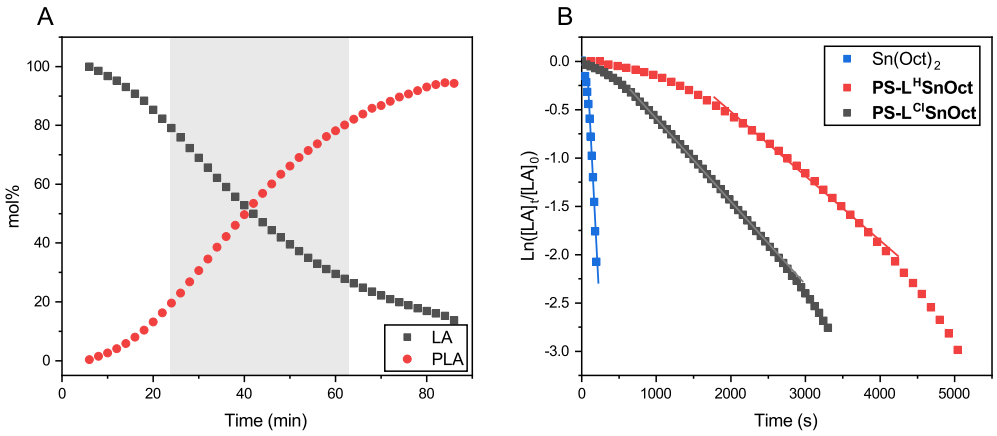

Figure 3.9: (A) Conversion of lactide to PLA over time for **PS-L$^{\mathbf{H}}$SnOct**, 2.3 hours in the melt, [LA]:[Cat]:[I] = 200:1:4, 130 °C. (B) Semi-logarithmic plot of the concentration of lactide, [LA], monitored by *in situ* ATR-FT-IR using **PS-L$^{\mathbf{X}}$SnOct**, where X = H or Cl.

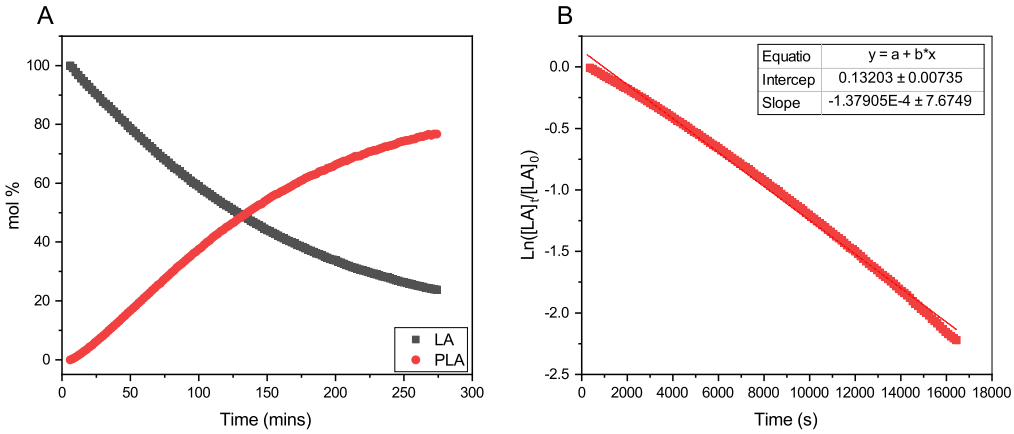

Figure 3.10: (A) Conversion of lactide to PLA over time for **PS-L$^{\mathbf{H}}$ZnOAc**, 6 hours in the melt, [LA]:[Cat]:[I] = 200:1:4, 130 °C (89%, M_{n} 6 100 Da, $Đ_{\mathrm{M}}$ 1.15). (B) Semi-logarithmic plot of the concentration of lactide, [LA], monitored by *in situ* ATR-FT-IR using **PS-L$^{\mathbf{H}}$ZnOAc**.

s^{-1} and 6.10×10^{-4} s^{-1}. Further, when the concentration of **PS-L$^{\mathbf{H}}$SnOct** was halved ([LA]:[Cat]:[I] = 400:1:8), the rate also halved, dropping to 3.49×10^{-4} s^{-1} (Figure 3.11), demonstrating that all of the active centres participate in ROP.

Subsequent studies with copolymers, using an alternative *in situ* monitoring set-up (see Chapter 4), did not display the same increase in k_{obs} seen in Figure 3.11, suggesting that this change in rate was a product of technical error at high monomer conversion.

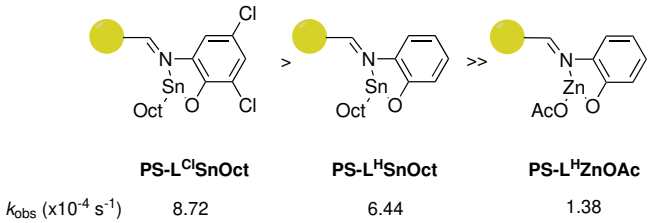

Scheme 3.7: Order of reactivity of the three successful catalysts according to *in situ* ATR-FT-IR kinetic analysis: **PS-L^{Cl}SnOct** (left), **PS-L^{H}SnOct** (middle), **PS-L^{H}ZnOAc** (right).

Analysis of the Matrix-Assisted Laser Desorption-Time of Flight (MALDI-ToF) spectra of the catalysts revealed that all produced major series of MeBnO$^-$/H$^+$end-capped PLA (Figure 3.12, Figures B.35-B.38), with some transesterification. The transesterification was more apparent in PLA made using **PS-L^{H}ZnOAc** than with **PS-L^{H}SnOct**, while **PS-L^{Cl}SnOct** displays the best polymerisation control, with minimal transesterification and no evidence of cyclic species (Figure 3.12). A comparison of the MALDI-ToF spectra and SEC traces of **PS-L^{H}SnOct** produced PLA after 2.5 and 24 hours revealed that the dispersity increases drastically with longer reaction time, once the monomer is fully consumed (Figures B.36, B.30). In the MALDI-ToF spectra, after 24 hours, the major series shifts to a lower molecular weight, and oligomers and minor series at higher M_n are now present, indicating that the catalyst can take part in side reactions at longer timescales.

As heterogeneous catalysts can be physically removed from the polymer, any potential side reactions can be suppressed without destroying the catalyst. Contrastingly, this problem cannot be remedied without destroying the catalyst when homogeneous catalysts are used, such as Sn(Oct)$_2$. The dispersity for the latter was already slightly higher than with heterogeneous catalysts, despite the shorter timescale during *in situ* ATR-FT-IR monitored ROP, suggesting Sn(Oct)$_2$ was already participating in transesterification reactions ($Đ_M$ 1.21, entry 4, Table 3.3). It is therefore evident that the ability to remove the heterogeneous catalysts from

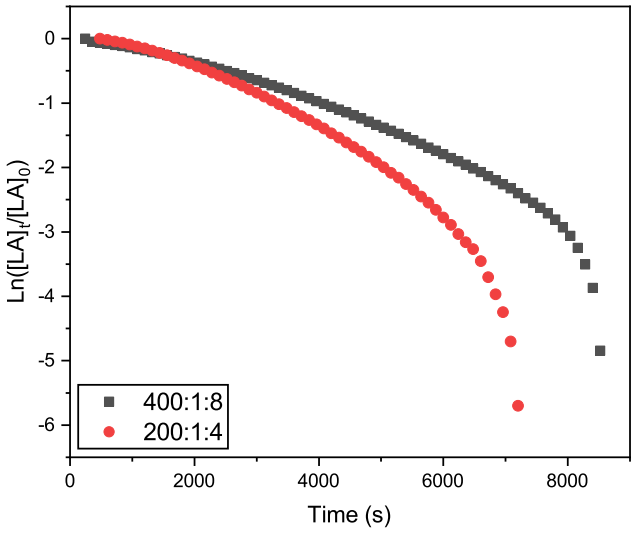

Figure 3.11: Semi-logarithmic plot of the concentration of lactide, [LA], monitored by *in situ* ATR-FT-IR using a new batch of **PS-L$^{\mathbf{H}}$SnOct**. Conditions: 130 °C in the melt. Red trace: [LA]:[Cat]:[I] = 200:1:4, k_{obs} 6.10×10^{-4} s^{-1} (90%, M_n 6 700 Da, $Đ_M$ 1.08). Grey trace: 400:1:8, k_{obs} 3.49×10^{-4} s^{-1} (87%, M_n 6 800 Da, $Đ_M$ 1.07). Kinetics measured using the same method as previously discussed, obtaining the k_{obs} from the slope of the steepest point of the S-curve (after the initiation period).

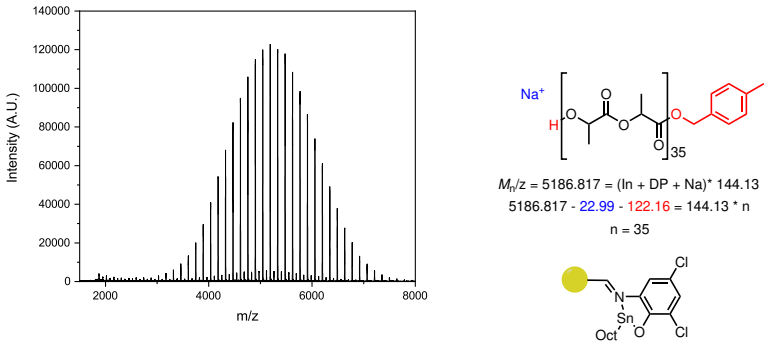

Figure 3.12: MALDI-ToF spectrum of PLA from **PS-L$^{\mathbf{Cl}}$SnOct**, showing a major series ($MeBnO^-/H^+$ end capped, Degree of Polymerisation (DP) ~35) and a minor transesterification series. Conditions: [LA]:[Cat]:[I] = 50:1:1, 55 minutes in the melt at 130 °C.

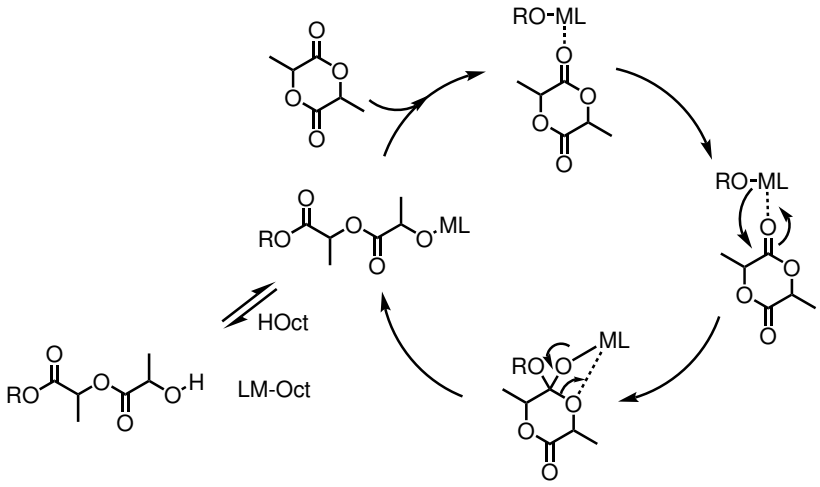

Scheme 3.8: Coordination-insertion mechanism for the ROP of *L*-LA, showing the dynamic exchange between the coordinated and free PLA. The exchange can be promoted by any protonating quenching agent, such as 2-ethylhexanoic acid (HOct).

the polymer is a huge benefit of these catalysts: recovery of the catalysts allows for both greater control over the M_n whilst also creating the potential to reuse them.

Recovery and reuse

Both the polymer end groups and the effect of the carboxylate ligand on reaction rates were highly suggestive of a coordination-insertion mechanism. In this mechanism, the PLA chain grows from the Lewis acidic metal centre, and participates in a dynamic exchange with the carboxylate, to yield the free PLA chain (Scheme 3.8). It is hypothesised that the equilibrium can be driven towards the free polymer upon addition of a protic solvent (with acid, for example), which would then regenerate the pre-catalyst (*vide infra*).

In all reactions, quenching the reaction was carried out with technical grade *n*-hexane to precipitate the free PLA, then re-dissolving the free polymer in dichloromethane (DCM) to filter out the catalyst. IR spectra were obtained of all recovered catalysts once the reaction had been quenched and compared to the original catalyst. The spectra of all the recovered catalysts contained peaks corresponding to the lactone C=O and C−O at 1755 and 1089 cm^{-1}, respectively

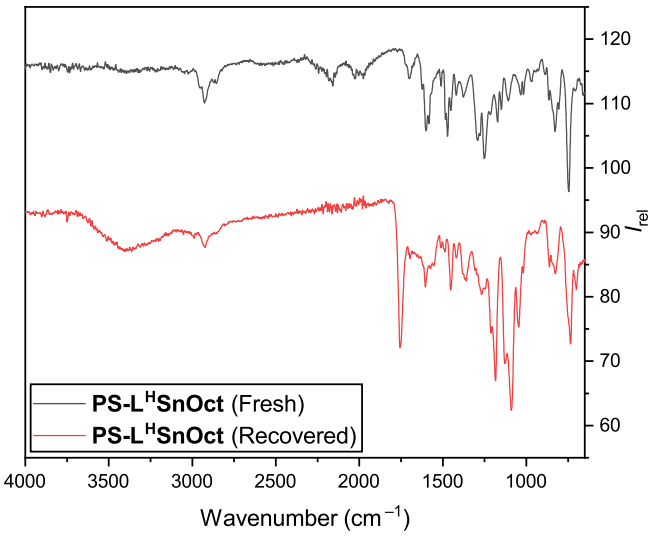

Figure 3.13: IR (ATR) spectra of **PS-L^{H}SnOct** prior to ROP (top), and once recovered and dried *in vacuo* (bottom).

(Figure 3.13). This suggested that not all the PLA had been released from the active centres and supported the importance of the dynamic exchange process.

To investigate the efficiency of the dynamic exchange, a reuse study was performed with several of the recovered catalysts (Figure 3.14). In all cases, recycling of the catalysts was carried out by quenching the reaction as described above, then drying the catalyst prior to reuse. Each reuse was accompanied by a significant drop in conversion: reuse of **PS-L^{H}ZnOAc**, for example, caused a drop from 84 to 33% (M_n 2 750 Da, $Đ_M$ 1.25, entries 1-2, Table A.1). A more in depth reuse study of **PS-L^{H}SnOct** was carried out over 7 reuse cycles; the same drop in conversion was observed throughout each cycle, stabilising out after the fourth cycle (Figures 3.15, B.12). The decrease in conversion can be either due to leaching of the metal, or from blocking of the active centres by the unreleased PLA, while the decline in conversion that occurred in the seventh cycle was attributed to the loss of catalyst mass through the various reuse procedures (Table 3.4). Potential deactivation of the catalyst could also occur during the work up procedure: water impurities in the technical grade *n*-hexane could protonate the chain-end of polymer, thereby releasing the free PLA from the metal centre.

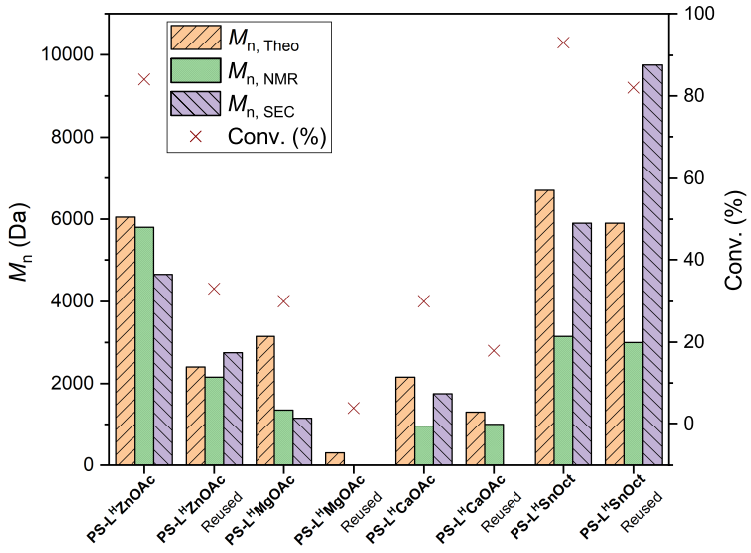

Figure 3.14: Recycling study of **PS-L^{H}MOR'**, where M = Zn, Mg, Ca and Sn and R' = OAc or Oct. Conditions: [LA]:[Cat]:[I] = 50:1:1, 24 hours in the melt at 130 °C.

However, this likely generated a Metal-OH species, which are inactive in ROP, in line with the decrease in conversion over time. Further catalyst regeneration studies using acid in place of *n*-hexane (to quench the reaction) could potentially regenerate the active catalyst immediately and therefore improve the conversions in subsequent reuse cycles.

Potential metal leaching was investigated by EDX, ^{119}Sn NMR spectroscopy and

Table 3.4: Mass balance of **PS-L^{H}SnOct** over the 7 reuse cycles. Initial mass of catalyst: 71.2 mg. Conditions: [LA]:[Cat]:[I] = 50:1:1 in the melt at 130 °C, 1 g LA scale. Decrease in mass during the last two measurements was due to loss of the catalyst during transfers between vessels, due to the catalyst breaking up during ROP.

Use #	Mass of Recovered Catalyst (mg)
1	71.8
2	99.5
3	99.8
4	100.2
5	96.9
6	92.8
7	78.4

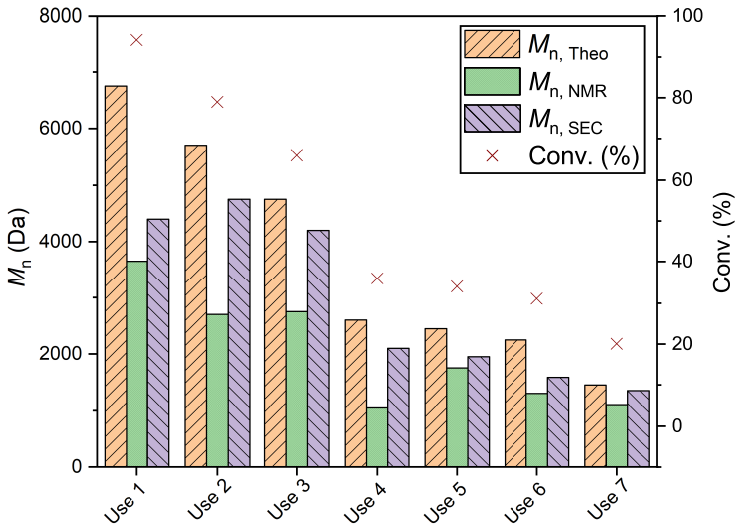

Figure 3.15: Polymerisation data from the ROP of *L*-LA with **PS-L^{H}SnOct** over 7 reuse cycles. Conditions: [LA]:[Cat]:[I] = 50:1:1 in the melt at 130 °C over 2.3 hours.

Inductively Coupled Plasma-Optical Emission Spectrometry (ICP-OES). ^{119}Sn NMR spectroscopy was not sensitive enough to detect any Sn between 2000 and −2000 ppm, even at higher numbers of scans, nor in PLA samples produced from $Sn(Oct)_2$ with a [LA]:[Cat]:[I] = 50:1:1 (Figure B.13). However, Sn was detected in PLA produced with $Sn(Oct)_2$ by EDX (Figure 3.16 A), yet no Sn was visible in PLA produced by the heterogeneous catalysts (Figure 3.16B). This indicated that the decrease in conversion was unlikely to have been caused entirely by leaching of the metal into the PLA during reaction. In fact, EDX of the recovered catalyst still showed a distribution of Sn across the catalyst surface (Figure 3.16C).

ICP-OES was used as a more quantitative tool to analyse the metal content of polymers before any purification was carried out (Table 3.5). PLA synthesised using $Sn(Oct)_2$ contained 5573 ppm of Sn, similar to the theoretical maximum value ([LA]:[Cat]:[I]=50:1:1, entry 4, Table 3.5). PLA made with the heterogeneous catalysts, on the other hand, contained significantly less metal content, of the same order of magnitude than polymers made using homogeneous systems and purified by classical methods involving dissolution and precipitation.[72,73] The

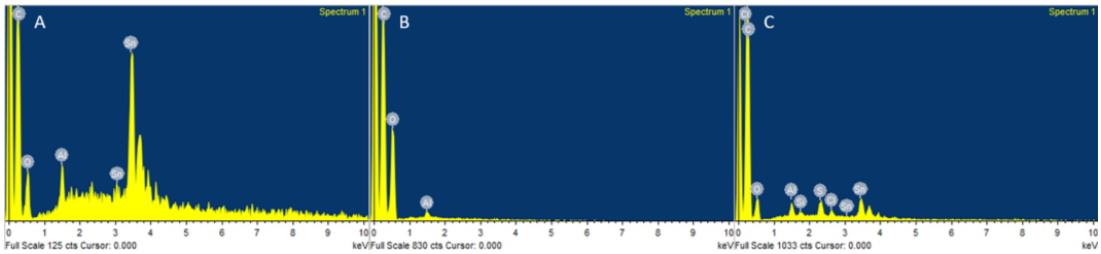

Figure 3.16: Energy Dispersive X-ray spectra of (A) PLA produced by $Sn(Oct)_2$, showing the high Sn content in the polymer, (B) PLA from **PS-L^{H}SnOct**, showing no evidence of Sn leaching, and (C) Recovered **PS-L^{H}SnOct** catalyst, with Sn still present in the catalyst.

Table 3.5: Inductively coupled plasma-optical emission spectrometry (ICP-OES) results of unpurified PLA from catalysts at different monomer:catalyst ratios.

Entry	**Catalyst**	**[LA]:[Cat]:[I]**	**Theoretical Maximum metal ppm**	**Experimental metal ppm residue in unpurified polymer**
1	**PS-L^{H}ZnOAc**	50:1:1	17200	385.5
2	**PS-L^{H}SnOct**	50:1:1	16551	1410.0
3	**PS-L^{H}SnOct**	400:1:1	2060	335.0
4	$Sn(Oct)_2$	400:1:1	4100	5573.0

experimental metal content of **PS-L^{H}ZnOAc** was 385.5 ppm – a fraction of the theoretical maximum value calculated if 100% of the metal had leached into the polymer ([LA]:[Cat]:[I]=50:1:1, entry 1, Table 3.5).

The same was observed for **PS-L^{H}SnOct**, although the metal leaching was slightly higher with this catalyst (335 ppm, [LA]:[Cat]:[I]=400:1:1, entry 3, Table 3.5). These findings could explain the slight increase in conversion observed in the supernatant during the Sheldon test. Since it has been shown to be practically impossible to entirely remove metal compounds from PLA, the observation that the metal content in the final unpurified polymer is of the same order of magnitude as in purified polymers made with homogeneous catalysts already, indicates that a major achievement has been made with the immobilised catalysts. These results suggest that purification of these polymers would result in a polymer of excellent purity, whose metal content would be far less than that of polymer formed by classical methods. In addition, there is obvious potential

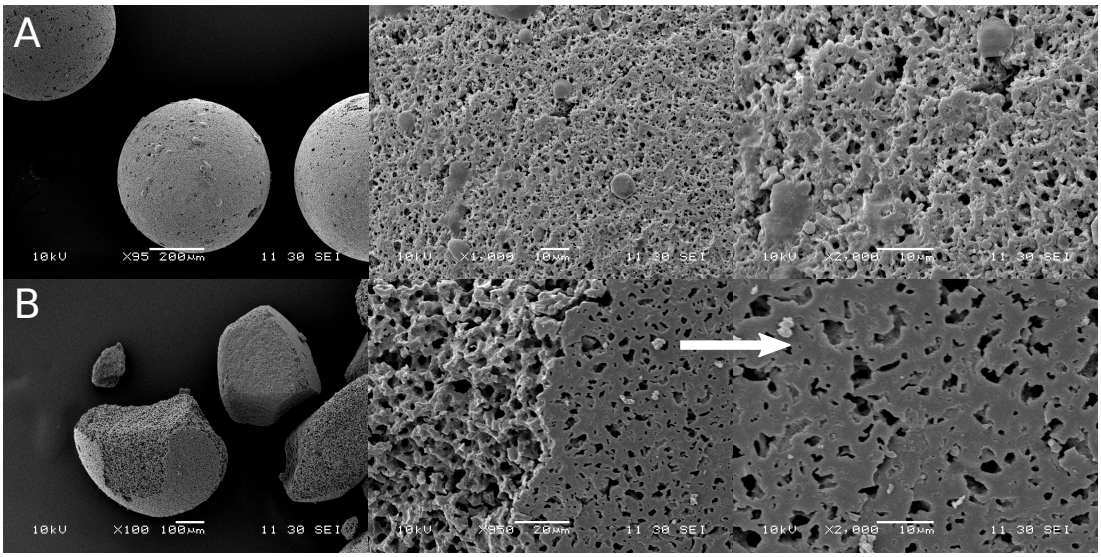

Figure 3.17: SEM images of (A) Fresh **PS-L^{H}SnOct**, (B) recovered **PS-L^{H}SnOct** post-ROP, at ×100 (left), ×1000 (centre) and ×2000 (right) magnification.

for further ligand design to strengthen ligand-metal interactions and to suppress any metal leaching altogether.

A gradual increase in weight of catalyst over reuse cycles (Table 3.4), further indicated that the PLA growing from the metal was increasing the mass of the catalyst. The decrease in mass after the fourth use was attributed to the degradation of the catalyst beads and subsequent loss of material during the recovery process. SEM imaging of the fresh and recovered catalyst showed that the catalyst was breaking up due to the mechanical stirring during reaction, exposing the unfunctionalised interior of the catalyst (Figure 3.17).

It was evident that the interior of the fresh catalyst could not be accessed by the PLA, as the interior remained highly porous, contrary to the exterior; the latter seemed to become blocked by PLA (Figure 3.17B). A similar observation has been reported in the literature using SiO_2-supported catalysts.[74] Evidence from both SEM imaging and ICP-OES could partially explain the decrease in conversion over the various reuses. To maximise the conversion to PLA during each reuse cycle, regeneration of the pre-catalyst was attempted by quenching with either acetic acid or benzoic acid and dissolving the polymer in DCM. Both attempts were unsuccessful, as the acid tended to cause depolymerisation, evidenced by the

lactic acid peaks in the ^{1}H NMR (Figure B.14). Washing the recovered catalyst in DCM over 72 hours recovered some more PLA, suggesting that polymer was still trapped on the catalyst surface. It would therefore be of interest to test a less porous catalyst in future studies, and investigate new methods of washing such as sonication or agitation.

Catalyst scope

Table 3.6: Polymerisation data from the ROP of *L*-LA with **PS-L$^{\mathbf{H}}$SnOct** at different monomer ratios, in the melt at 130 °C.

Entry	[LA]:[Cat]:[I]	Time (h)	Conv. (%)[a]	$M_{n,Theo}$[b]	$M_{n,SEC}$[c]	$M_{w,SEC}$[c]	$Đ_M$[c]	TON	TOF (h^{-1})
1	100:1:1	2.5	86	12400	11100	12850	1.16	86	34.4
2	200:1:1	2.5	86	24800	23700	28300	1.19	172	68.6
3	300:1:1	2.5	40	17300	19600	21200	1.08	60	24.0
4	300:1:1	6	72	41500	25300	27900	1.10	215	35.9
5	400:1:1	6	38	21900	18800	20350	1.08	152	25.3
6	400:2:1	6	69	39800	28200	32700	1.16	138	23.0
7	400:1:1	24	90	51900	35250	44750	1.27	360	15.0
8[d]	400:1:1	24	90	51900	24000	45200	1.88	179	7.5

[a] Determined from the ^{1}H NMR spectrum.
[b] Theoretical M_n = ([LA]/[I]) × (144 × equiv. LA) × (conv./100).
[c] As determined by SEC (THF) using RI methods, relative to poly(styrene) standards (multiplied by a factor of 0.58, rounded to the nearest 50).[68]
[d] Entry 8 used $Sn(Oct)_2$ as the catalyst in a control reaction, to directly compare to entry 7.

To demonstrate the versatility of the catalysts, **PS-L$^{\mathbf{H}}$SnOct** and **PS-L$^{\mathbf{H}}$ZnOAc** were used in the solution-phase was attempted in THF at room temperature and toluene at 80 °C over 24 hours. The polymerisations in THF were unsuccessful, presumably due to the coordinating oxygen which blocked the access of lactide to the metal (entries 1-2, Table A.2). Polymerisation in toluene, however, proceeded with good conversions for **PS-L$^{\mathbf{H}}$SnOct**, and improved dispersity compared to the industrial standard (entries 3-5, Table A.2).

Table 3.7: Polymerisation data from the ROP of *L*-LA with **PS-L$^{\mathbf{H}}$SnOct** over 24 hours, using [LA]:[I] = 400:1.

Entry	[LA]:[Cat]	ppm	Temp (°C)	Conv. (%)[a]	$M_{n,Theo}$[b]	$M_{n,SEC}$[c]	$M_{w,SEC}$[c]	$Đ_M$[c]	TON	TOF (h^{-1})
1	$400{:}6 \times 10^{-3}$	15	130	0	0	-	-	-	-	-
2	$400{:}6 \times 10^{-3}$	15	180	41	23650	17750	18900	1.07	19451	810.4
3	400:0.25	625	130	52	39800	15950	18750	1.18	841	35.0
4	400:0.5	1250	130	69	30000	31350	39800	1.13	558	23.3

[a] Determined from the ^{1}H NMR spectrum.
[b] Theoretical M_n = ([LA]/[I]) × (144 × equiv. LA) × (conv./100).
[c] As determined by SEC (THF) using RI methods, relative to poly(styrene) standards (multiplied by a factor of 0.58, rounded to the nearest 50).[68]

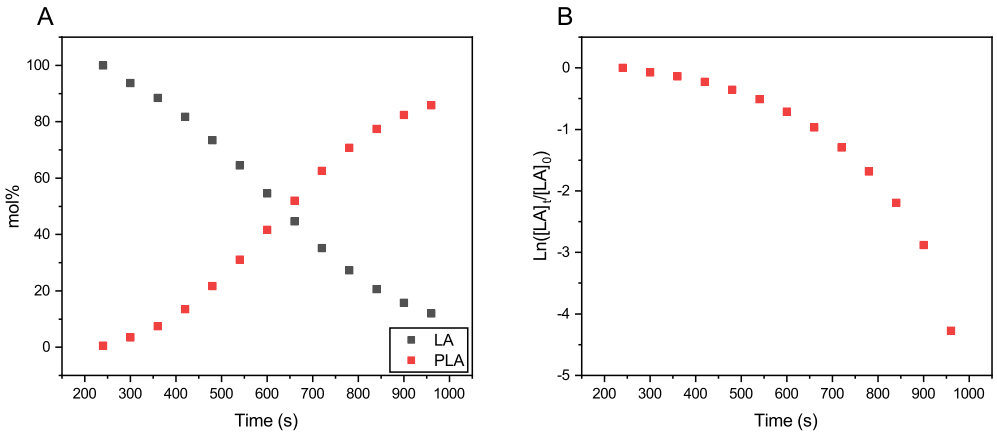

Figure 3.18: (A) Conversion over time for **PS-L$^{\mathbf{H}}$SnOct**, 20 minutes in the melt, [LA]:[Cat]:[I] = 200:1:4, 180 °C (89%, $M_{\mathrm{n,SEC}}$ 7 500 Da, $M_{\mathrm{n,Theo}}$ 6 400 Da, $Đ_{\mathrm{M}}$ 1.25). (B) Semi-logarithmic plot of [LA], monitored by *in situ* ATR-FT-IR using **PS-L$^{\mathbf{H}}$SnOct** (k_{obs} 1.25×10^{-3} s^{-1}). k_{obs} obtained from the slope of the steepest point of the S-curve (after the initiation period).

The industrial relevance of the heterogeneous catalysts was then explored by altering the monomer to catalyst ratios up to 400:1:1 (Table 3.6). Whilst longer reaction times were required to achieve higher conversions comparable to the 50:1:1 system, it was possible to target higher molecular weights up to M_{n} 35 250 Da ($Đ_{\mathrm{M}}$ 1.27, entry 7, Table 3.6). A control using Sn(Oct)$_2$ showed that even at these low loadings of catalyst ([LA]:[Cat]:[I] = 400:1:1), the homogeneous catalyst produced a polymer of lower M_{n} and higher dispersity (M_{n} 24 000, $Đ_{\mathrm{M}}$ 1.88, entry 8, Table 3.6). Catalyst loadings down to 15 ppm of metal were possible ([LA]:[I] = 400:1), although higher temperatures or longer timescales were required to reach modest conversions (69% conversion at 1250 ppm catalyst, M_{n} 31 350 Da, $Đ_{\mathrm{M}}$ 1.13, entry 5, Table 3.7).

When the temperature was increased to 180 °C, a TOF of 810 h^{-1} was achieved with 15 ppm of metal using **PS-L$^{\mathbf{H}}$SnOct** (41% conversion, entry 2, Table 3.7). **PS-L$^{\mathbf{H}}$SnOct** showed impressive activity when a [LA]:[Cat]:[I] ratio of 200:1:4 was used at 180 °C, reaching full conversion within 20 minutes and displaying excellent M_{n} and $Đ_{\mathrm{M}}$ control (k_{obs} 1.25×10^{-3} s^{-1}, M_{n} 7 500 Da, $Đ_{\mathrm{M}}$ 1.25, Figure 3.18), comparing well with Sn(Oct)$_2$ under the same conditions (k_{obs} 6.67×10^{-3}

s^{-1}, M_n 8 250 Da, $Đ_M$ 1.53, Figure 3.19).

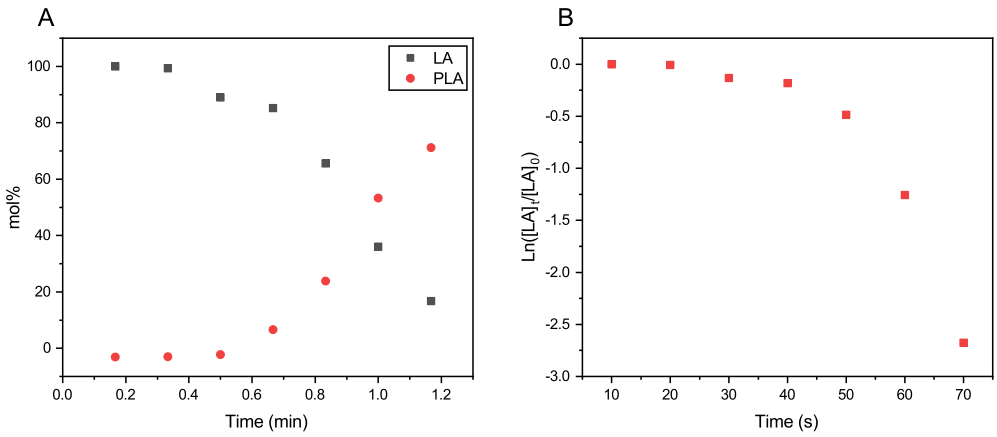

Figure 3.19: (A) Conversion over time for $Sn(Oct)_2$, 3 minutes in the melt, [LA]:[Cat]:[I] = 200:1:4, 180 °C (96%, $M_{n,SEC}$ 8 250 Da, $M_{n,Theo}$ 6 900 Da, $Đ_M$ 1.53). (B) Semi-logarithmic plot of [LA], monitored by *in situ* ATR-FT-IR using $Sn(Oct)_2$ (k_{obs} 6.67×10^{-3} s^{-1}). k_{obs} obtained from the slope of the steepest point of the S-curve (after the initiation period).

3.4 Conclusions and future work

Several highly efficient heterogeneous catalysts based on Sn(II) and Zn(II) were synthesised and employed in the ROP of *L*-LA, with **PS-L^{Cl}SnOct** displaying the best rate and control. It was noted that both changing the carboxylate ligand from the acetate to 2-ethylhexanoate, and employing electron withdrawing groups on the catalyst (such as Cl-substituents *ortho* and *para* to the phenoxy donor) improved the reaction rate of ROP drastically in comparison to H- or ^{t}Bu-substituted ligands; although all immobilised catalysts produced white polymers of high purity.

Catalyst loading as low as 15 ppm metal and TOF values of up to 810 h^{-1} could be achieved. Although polymerisation rates were slower than homogeneous industrial standard $Sn(Oct)_2$, these catalysts were shown to reproducibly deliver excellent control under a wide range of reaction conditions, providing an improvement to the sparse number of known heterogeneous systems for ROP.

The ability to use these catalysts in the melt and at industrially relevant ratios and temperatures is beneficial for industrial applications compared to other heterogeneous examples. Most significantly, ICP-OES showed that metal content in the final unpurified polymers was of the same order of magnitude as in purified polymers made with homogeneous catalysts. Recovery and reuse were possible, and these results suggest that the potential for achieving heterogeneous polymerisation with these systems is real.

Some work concerning catalyst scope under different conditions has already been explored thus far, yet the common factor has been the use of *L*-LA throughout. To emphasise catalyst viability, investigation into the potential use of the catalyst in the ROP of other lactones is necessary, and is the topic of subsequent studies (Chapter 4).

Separately, one benefit to heterogeneous catalysts is their application into flow reactors. The catalyst can be immobilised into a packed-bed, and the reaction mixture (typically consisting of monomer, initiator and solvent) can be pumped through the packed-bed reactor, such that the catalyst is immediately separated from the reaction mix. PS-supported catalyst beads have already been used in small molecule synthesis in flow,[75] while homogeneous flow ROP has also been discussed in the literature, so it is reasonable to couple these two to generate heterogeneous ROP in flow. Initial reactor development towards this goal is therefore the topic of discussions in Chapter 8.

Finally, the full mechanism of loss of activity is not yet fully understood, and hence improving the overall reusability of the catalyst towards an even greener process should be the topic of future work in the area.

References

[1] A. Nachtergael, O. Coulembier, P. Dubois, M. Helvenstein, P. Duez, B. Blankert and L. Mespouille, *Biomacromolecules*, 2015, **16**, 507–514.

[2] X. Zhang, G. O. Jones, J. L. Hedrick and R. M. Waymouth, *Nat Chem*, 2016, **8**, 1047–1053.

[3] B. Lin, J. L. Hedrick, N. H. Park and R. M. Waymouth, *J Am Chem Soc*, 2019, **141**, 8921–8927.

[4] B. J. O'Keefe, M. A. Hillmyer and W. B. Tolman, *J Chem Soc, Dalton Trans*, 2001, 2215–2224.

[5] S. P. Parwe, S. D. Warkad, M. V. Mane, P. S. Shedage and B. Garnaik, *Polymer*, 2017, **111**, 244–251.

[6] O. Dechy-Cabaret, B. Martin-Vaca and D. Bourissou, in *Handbook of Ring-Opening Polymerization*, ed. P. Dubois, O. Coulembier and J.-M. Raquez, Wiley-VCH, Germany, 2009, ch. 10, pp. 255–286.

[7] A. Kowalski, A. Duda and S. Penczek, *Macromolecules*, 2000, **33**, 7359–7370.

[8] A. Kowalski, J. Libiszowski, T. Biela, M. Cypryk, A. Duda and S. Penczek, *Macromolecules*, 2005, **38**, 8170–8176.

[9] J. E. Kasperczyk, *Macromolecules*, 1995, **28**, 3937–3939.

[10] N. Nomura, R. Ishii, M. Akakura and K. Aoi, *J Am Chem Soc*, 2002, **124**, 5938–5939.

[11] S. Penczek, A. Duda and J. Libiszowski, *Macromol Symp*, 1998, **128**, 241–254.

[12] M. L. Di Lorenzo and R. Androsch, in *Advances in Polymer Science*, Springer, Switzerland, 2018, ch. 279, pp. 67–118.

[13] A. Stjerndahl, A. Finne-Wistrand, A. C. Albertsson, C. M. Bäckesjö and U. Lindgren, *J Biomed Mater Res A*, 2008, **87**, 1086–1091.

[14] Z. Zhong, P. J. Dijkstra and J. Feijen, *Angew Chem Int Edit*, 2002, **41**, 4510–4513.

[15] R. Platel, L. Hodgson and C. Williams, *Polym Rev*, 2008, **48**, 11–63.

[16] H.-Y. Chen, J. Zhang, C.-C. Lin, J. H. Reibenspies and S. A. Miller, *Green Chemistry*, 2007, **9**, 1038.

[17] G. W. Coates, *Chem Rev*, 2000, **100**, 1223–1252.

[18] C.-L. Lee, Y.-F. Lin, M.-T. Jiang, W.-Y. Lu, J. K. Vandavasi, L.-F. Wang, Y.-C. Lai, M. Y. Chiang and H.-Y. Chen, *Organometallics*, 2017, **36**, 1936–1945.

[19] A. Le Borgne, V. Vincens, M. Jouglard and N. Spassky, *Makromol. Chem., Macromol. Symp.*, 1993, **73**, 37–46.

[20] Z. Zhong, P. J. Dijkstra and J. Feijen, *J Am Chem Soc*, 2003, **125**, 11291–11298.

[21] A. Bhaw-Luximon, D. Jhurry and N. Spassky, *Polym Bull*, 2000, **44**, 31–38.

[22] J. Belleney, M. Wisniewski and A. Le Borgne, *Eur Pol J*, 2004, **40**, 523–530.

[23] Z. Tang, X. Chen, Y. Yang, X. Pang, J. Sun, X. Zhang and X. Jing, *J Polym Sci Pol Chem*, 2004, **42**, 5974–5982.

[24] H. Y. Chen, W. Y. Lu, Y. J. Chen, S. C. N. Hsu, S. W. Ou, W. T. Peng, N. Y. Jheng, Y. C. Lai, B. S. Wu, H. Chung, Y. Chen and T. C. Huang, *J Polym Sci Pol Chem*, 2013, **51**, 327–333.

[25] P. Hormnirun, E. L. Marshall, V. C. Gibson, R. I. Pugh and A. J. P. White, *P Natl Acad Sci USA*, 2006, **103**, 15343–15348.

[26] A. M. Luke, A. Peterson, S. Chiniforoush, M. Mandal, Y. Popowski, H. Sajjad, C. J. Bouchey, D. Y. Shopov, B. J. Graziano, L. J. Yao, C. J. Cramer, T. M. Reineke and W. B. Tolman, *Macromolecules*, 2020, **53**, 1809–1818.

[27] S. Gesslbauer, H. Cheek, A. J. P. White and C. Romain, *Dalton Trans*, 2018, **47**, 10410–10414.

[28] S. Gesslbauer, R. Savela, Y. Chen, A. J. White and C. Romain, *ACS Catal*, 2019, **9**, 7912–7920.

[29] K. M. Osten, D. C. Aluthge, B. O. Patrick and P. Mehrkhodavandi, *Inorg Chem*, 2014, **53**, 9897–9906.

[30] D. E. Stasiw, M. Mandal, B. D. Neisen, L. A. Mitchell, C. J. Cramer and W. B. Tolman, *Inorg Chem*, 2017, **56**, 725–728.

[31] S. V. Verstraeten, L. Aimo and P. I. Oteiza, *Arch Toxicol*, 2008, **82**, 789–802.

[32] J. Byers, D. C. K. A. Biernesser, A. B. and J. A. Kehl, in *Synthesis, Structure and Properties of Poly(lactic acid)*, ed. M. Di Lorenzo and R. Androsch, Springer, Cham, 2017, ch. 3, pp. 74–97.

[33] S. Inkinen, M. Hakkarainen, A. C. Albertsson and A. Södergård, *Biomacromolecules*, 2011, **12**, 523–532.

[34] C. Romain, M. S. Bennington, A. J. White, C. K. Williams and S. Brooker, *Inorg Chem*, 2015, **54**, 11842–11851.

[35] C. Romain, J. A. Garden, G. Trott, A. Buchard, A. J. White and C. K. Williams, *Chem - Eur J*, 2017, **23**, 7367–7376.

[36] S. Paul, Y. Zhu, C. Romain, R. Brooks, P. K. Saini and C. K. Williams, *Chem Commun*, 2015, **51**, 6459–6479.

[37] S. Farah, D. G. Anderson and R. Langer, *Adv Drug Deliver Rev*, 2016, **107**, 367–392.

[38] D. J. Darensbourg and O. Karroonnirun, *Inorg Chem*, 2010, **49**, 2360–2371.

[39] B. M. Chamberlain, M. Cheng, D. R. Moore, T. M. Ovitt, E. B. Lobkovsky and G. W. Coates, *J Am Chem Soc*, 2001, **123**, 3229–3238.

[40] P. M. Schäfer, M. Fuchs, A. Ohligschläger, R. Rittinghaus, P. McKeown, E. Akin, M. Schmidt, A. Hoffmann, M. A. Liauw, M. D. Jones and S. Herres-Pawlis, *ChemSusChem*, 2017, **10**, 3547–3556.

[41] M. H. Chisholm, J. Gallucci and K. Phomphrai, *Inorg Chem*, 2002, **41**, 2785–2794.

[42] M. H. Chisholm, J. Gallucci and K. Phomphrai, *Chem Commun*, 2003, **9**, 48–49.

[43] C. N. Ayala, M. H. Chisholm, J. C. Gallucci and C. Krempner, *Dalton Trans*, 2009, 9237.

[44] T. Rosen, Y. Popowski, I. Goldberg and M. Kol, *Chem - Eur J*, 2016, **22**, 11533–11536.

[45] T. Rosen, I. Goldberg, V. Venditto and M. Kol, *J Am Chem Soc*, 2016, **138**, 12041–12044.

[46] P. McKeown, S. N. McCormick, M. F. Mahon and M. D. Jones, *Polym Chem*, 2018, **9**, 5339–5347.

[47] M. P. Coles and P. B. Hitchcock, *Eur J Inorg Chem*, 2004, **2004**, 2662–2672.

[48] I. Dos Santos Vieira and S. Herres-Pawlis, *Eur J Inorg Chem*, 2012, **2012**, 765–774.

[49] A. Metz, P. McKeown, B. Esser, C. Gohlke, K. Kröckert, L. Laurini, M. Scheckenbach, S. N. McCormick, M. Oswald, A. Hoffmann, M. D. Jones and S. Herres-Pawlis, *Eur J Inorg Chem*, 2017, **2017**, 5557–5570.

[50] P. M. Schäfer, P. McKeown, M. Fuchs, R. D. Rittinghaus, A. Hermann, J. Henkel, S. Seidel, C. Roitzheim, A. N. Ksiazkiewicz, A. Hoffmann, A. Pich, M. D. Jones and S. Herres-Pawlis, *Dalton Trans*, 2019, **48**, 6071–6082.

[51] J. Börner, I. Dos Santos Vieira, A. Pawlis, A. Döring, D. Kuckling and S. Herres-Pawlis, *Chem - Eur J*, 2011, **17**, 4507–4512.

[52] R. D. Rittinghaus, P. M. Schäfer, P. Albrecht, C. Conrads, A. Hoffmann, A. N. Ksiazkiewicz, O. Bienemann, A. Pich and S. Herres-Pawlis, *ChemSusChem*, 2019, **12**, 2161–2165.

[53] C. K. Williams, L. E. Breyfogle, S. K. Choi, W. Nam, V. G. Young, M. A. Hillmyer and W. B. Tolman, *J Am Chem Soc*, 2003, **125**, 11350–11359.

[54] A. Thevenon, C. Romain, M. S. Bennington, A. J. P. White, H. J. Davidson, S. Brooker and C. K. Williams, *Angew Chem Int Edit*, 2016, **55**, 8680–8685.

[55] K. Ding, M. O. Miranda, B. Moscato-Goodpaster, N. Ajellal, L. E. Breyfogle, E. D. Hermes, C. P. Schaller, S. E. Roe, C. J. Cramer, M. A. Hillmyer and W. B. Tolman, *Macromolecules*, 2012, **45**, 5387–5396.

[56] M. Normand, V. Dorcet, E. Kirillov and J. F. Carpentier, *Organometallics*, 2013, **32**, 1694–1709.

[57] S. M. Islam, K. Ghosh, R. A. Molla, A. S. Roy, N. Salam and M. A. Iqubal, *J Organomet Chem*, 2014, **774**, 61–69.

[58] Y. Chauvin, D. Commereuc and F. Dawans, *Prog Polym Sci*, 1977, **5**, 95–226.

[59] A. Kirschning, H. Monenschein and R. Wittenberg, *Angew Chem Int Edit*, 2001, **40**, 650–679.

[60] X. Cui, W. Li, P. Ryabchuk, K. Junge and M. Beller, *Nat Catal*, 2018, **1**, 385–397.

[61] S. Hübner, J. G. de Vries and V. Farina, *Adv Synth Catal*, 2016, **358**, 3–25.

[62] S. M. Islam, K. Ghosh, A. S. Roy and R. A. Molla, *RSC Adv*, 2014, **4**, 38986–38999.

[63] C. Schuerch and J. M. Fréchet, *J Am Chem Soc*, 1971, **93**, 492–496.

[64] S. Jain and O. Reiser, *ChemSusChem*, 2008, **1**, 534–541.

[65] G. G. Mohamed, M. M. Omar and A. M. Hindy, *Spectrochim Acta A*, 2005, **62**, 1140–1150.

[66] R. A. Taylor and H. A. Ellis, *Spectrochim Acta A*, 2007, **68**, 99–107.

[67] M. D. Jones, M. G. Davidson, C. G. Keir, L. M. Hughes, M. F. Mahon and D. C. Apperley, *Eur J Inorg Chem*, 2009, **2009**, 635–642.

[68] J. Baran, A. Duda, A. Kowalski, R. Szymanski and S. Penczek, *Macromol Rapid Comm*, 1997, **18**, 325–333.

[69] M. J. Stanford and A. P. Dove, *Chem Soc Rev*, 2010, **39**, 486–494.

[70] H. Tsuji, *Macromol Biosci*, 2005, **5**, 569–597.

[71] H. E. Lempers and R. A. Sheldon, *J Catal*, 1998, **175**, 62–69.

[72] A.-c. Albertsson and I. K. Varma, *Biomacromolecules*, 2003, **4**, 1466–1486.

[73] G. Schwach, J. Coudane, R. Engel and M. Vert, *Polym Bull*, 1996, **37**, 771–776.

[74] E. J. Lee, K. M. Lee, J. Jang, E. Kim, J. S. Chung, Y. Do, S. C. Yoon and S. Y. Park, *J Mol Catal A-Chem*, 2014, **385**, 68–72.

[75] S. Cañellas, C. Ayats, A. H. Henseler and M. A. Pericàs, *ACS Catal*, 2017, **7**, 1383–1391.

Chapter 4

Alternative Polymer Architectures

4.1 Introduction

Although PLA remains a key, commercially available biodegradable polymer, ROP has also extended to other lactones, including ϵ-caprolactone (ϵ-CL), ϵ-decalactone (ϵ-DL), δ-decalactone (δ-DL), δ-valerolactone (δ-VL) and γ-butyro lactone (γ-BL).[1] The ROP of lactones is dependent on the relative size of the ring and the associated ring strain.[2,3] The 6- and 7-membered lactones pertinent to this study include *rac*- and *L*-LA, ϵ-CL and ϵ-DL, and shall be discussed in more detail.

The ROP of ϵ-CL, in particular, has been extensively studied, with organocatalytic[4–6] and metal-catalysed polymerisations reported.[7–14] Many of the metal based catalysts which have been used employ ligands with a Schiff base motif, similar to the heterogeneous catalysts developed in Chapter 3. Catalysts of this type shall be used in the following studies. Notably, the 5-membered Al containing metallacycle – which the **PS-L$^{\mathbf{X}}$MO$_{\mathbf{2}}$CR** catalysts were derived from – was first applied to the ROP of ϵ-CL.[10] The 5-membered ring displayed superior reactivity to its 6-membered counterpart, such that high conversions and molecular weights of poly(caprolactone) (PCL) were accessible (90%, M_{n} 41 600 Da, $Đ_{\mathrm{M}}$ 1.29).

More recently, both PCL and a PCL−*b*−PLA block copolymer were prepared with $Sn(Oct)_2$, without the need for anhydrous reagents and solvents. Polymerisation either in a vacuum oven, or addition of titanium isopropoxide, removed residual water, such that DP of up to 500 (PCL) were obtained, although moderate dispersities were observed (ca. 1.5) and analysis of transesterification levels by MALDI-ToF mass spectrometry were absent from this study.[15] Loadings of $Sn(Oct)_2$ as low as [CL]:[Cat] = 10 000:1 could also be used to achieve low metal content PCL (5 ppm).[16] This was only the case once the PCL has been thrice purified, and 99% conversion was only obtained after 72 hours, indicating that the **PS-L$^{\mathbf{X}}$MO$_\mathbf{2}$CR** heterogeneous catalysts could provide several benefits over traditional homogeneous options.

Some more examples of heterogeneous catalysts in the ROP of ϵ-CL exist, although most were, once again, dependent on silica or porous supports.[17–24] This opens up a new avenue for the heterogeneous catalysts, which shall be discussed in the following sections.

Although less extensively studied, solution-phase ROP of ϵ-DL reached M_n up to 26 400 Da with low dispersities (<1.18) using a lanthanum catalyst (>80% conversion, [DL] = 1.5 mol L^{-1}, 30 °C).[25] Melt ROP was also possible with $Sn(Oct)_2$ or TBD, the latter converting 80% of the monomer in 360 hours at 110 °C (M_n 40 500 Da, $Đ_\mathrm{M}$ 1.21, [DL]:[Cat]:[I] = 600:1:3).[26] To the best of our knowledge, there have been no reported heterogeneous catalysts for the ROP of ϵ-DL so far.

Polymer properties can be modified, through blends,[27] composites and copolymers to enable improved processing ability. Copolymerisation has proved one of the most diverse ways of imparting different properties onto a given polymer. Combination of two or more different lactones (or indeed one lactone with another class of monomer – although this is beyond the scope of this research) can modify the properties of each homopolymer significantly. PLA, for example – a brittle polymer with a T_m of about 180 °C – can be copolymerised with PCL (a polymer with a T_m of 60 °C and a T_g below room temperature) to improve the toughness of the final diblock polymer. Variations of the molecular weight and relative lengths of each block can then determine the crystallinity of the polymer.[28]

Addition of a third block to the AB diblock copolymer can further alter both the physical properties or microphase behaviour of the polymer, to access a large library of different structural architectures, to suit the particular application.[29] Triblocks can take ABA or ABC forms, where a second block of monomer A, or a third monomer (C) is added to the AB copolymer.

The ABA triblock copolymers are a class of thermoplastic elastomer (TPE), with a wide range of applications due to their high processability and superior thermal properties and flexibility.[30] These triblocks contain two separate and immiscible blocks, where the central "B" segment of the linear ABA copolymer is typically made of a soft, amorphous polymer with low T_g, and crystalline PLA can be used as the external hard "A" segments with high T_g.[31–33] Altering the core segment can improve the polymer properties and biodegradability. For example, alternative sustainable monomers, such as the lactones discussed above, have been utilised in an effort to move away from petrochemically-derived triblock TPEs. These have also seen improved plastic degradation at end-of-life through hydrolysis of the ester linkages.[34–36]

Both ϵ-CL and ϵ-DL have regularly been used as monomers in the block copolymerisation with a variety of monomers such as CO_2 and cyclic carbonates.[35,37,38] Copolymerisation of these monomers has also been achieved with lactones, as this increases the thermal properties and flexibility of the resulting polymer, with the ϵ-CL or ϵ-DL blocks acting as the "soft" midblock segment.[32,39–44]

PLA−PCL−PLA triblocks, for example, showed improved degradation rates compared to homopolymers.[40] The midblock also altered mechanical properties, with improved tensile properties obtained when a PCL−*co*−PDL midblock was sandwiched between the two PLA segments.[32] Rosen *et al.* utilised a Mg-based complex with a tetradentate ligand to access complex microstructures ranging from diblocks of PCL−*b*−PLA to multiblock copolymers such as P*D*LA−*b*−P*L*LA−*b*−PCL−*b*−P*L*LA−*b*−P*D*LA, in minutes.[45] Melting temperatures (T_m) over 200 °C were possible, due to varying the microphase separation between blocks. PCL could be swapped with PϵDL to obtain similar results.[46]

Similar improvements to PLA properties were observed though the incorporation of ϵ-DL into TPEs; PDL acts as a "toughening" agent, with excellent polymer

elongation properties due to the amorphous and flexible nature of the central segment.[25,26,47–49] The PLA T_m of 168 °C could be maintained upon copolymerisation to PLA−*b*−PDL−*b*−PLA, yet the triblock increased the % strain-at-break almost 280 fold, due to the central PDL segment.[26]

Preparations of these copolymers can be carried out through a one-pot method, where all monomers are added into the reaction mixture at the start of reaction. In order to prevent scrambling of the monomers during ROP (likely resulting in amorphous polymers which don't exploit the properties of either homopolymer) and to achieve well-defined blocks, this method is reliant on highly selective catalysts, which preferentially polymerise one monomer over another. Catalysts can be designed to promote the selective consumption of one monomer over another, such as with switchable catalysts,[37,50,51] or dinuclear or dual catalysts.[48,52–55]

Alternatively, copolymerisation can occur through a sequential addition method, where the ROP of one monomer to form the first block precedes the ROP of the second monomer; the latter is only added in once the ROP of the first monomer is complete, such that distinct blocks can be synthesised.[35,56,57] This method can be applied to the majority of catalysts, regardless of their lack of selectivity, as long as they promote a living polymerisation and is commonly used to prepare TPEs. For a more in depth discussion concerning both synthetic strategies for the ROP of lactones, the reader is directed to a recent review complied by Diaz and Mehrkhodavandi.[57]

4.2 Aims

In the following sections, the synthesis homopolymers from alternative lactones and linear di- and triblock (both ABA and ABC structures) copolymers shall be explored, to investigate the scope of the heterogeneous catalysts developed in Chapter 3: **PS-L^{H}SnOct** and **PS-L^{H}ZnOAc**.

In the first instance, homopolymers of various lactones were synthesised to evaluate which polymers were accessible and determine whether the catalysts displayed any selectivity towards any one monomer. Following this, copolymers were synthesised through sequential polymerisation to obtain copolymers with distinct blocks. Triblocks were shown to be accessible through simple addition of another

monomer in the sequential process. Similarly, altering the initiator to a diol enabled the synthesis of an ABA triblock similar to the TPE structure reported in literature.

One-pot reactions (where both monomers are added into the reaction mixture simultaneously) were subsequently tested. Analysis of relative monomer rates in these one-pot reactions further evaluated catalyst selectivity. Finally, analysis of the polymer microstructure was investigated through SEC, ^{1}H, ^{13}C{^{1}H} and ^{1}H Diffusion-Ordered Spectrospopy (DOSY) NMR spectroscopy and DSC thermograms.

4.3 Results and discussion

Catalyst scope: alternative homopolymers

Table 4.1: Homonuclear Decoupled ^{1}H NMR ($CDCl_3$, 500 MHz) of PLA produced by **PS-L^{H}SnOct**. Conditions: [M]:[Cat]:[I] = 50:1:1, 2.5 h in the melt at 130 °C (PS-L^{H}ZnOAc: 6 hours). Probability of heterotactic enchainment calculated by $P_r = \sqrt{2 \times isi}$.[58]

Entry	Catalyst	P_r
1	**PS-L^{H}ZnOAc**	0.53
2	**PS-L^{H}SnOct**	0.59
3	$Sn(Oct)_2$	0.61
4	$Zn(OAc)_2 \cdot 2H_2O$	0.51

The ROP of *rac*-LA and other lactones (Scheme 4.1), commonly used in literature,[25,26,49,59] was carried out to demonstrate the monomer scope of the catalysts (Table 4.1). Neither catalyst showed any isotactic bias when using *rac*-LA, with P_r (probability of racemic enchainment) around 0.50, characteristic of an atactic polymer (Figure B.11, Table 4.1).[60]

When using less sterically hindered lactones such as ϵ-caprolactone (ϵ-CL), high conversions were achieved when using the optimised times from the *L*-LA study in Chapter 3 (up to 91%, entries 5-8, Table 4.2). Larger lactones such as ϵ-decalactone (ϵ-DL) struggled to reach high conversions within the *L*-LA optimised times (entries 9-12, Table 4.2). However, high conversions were still possible after 24 hours (entries 10 and 12, Table 4.2), and it is tentatively proposed that

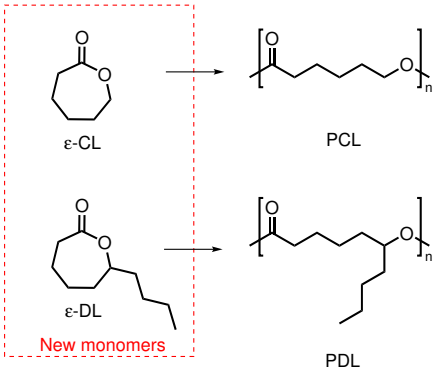

Scheme 4.1: Alternative monomers ϵ-caprolactone (ϵ-CL) and ϵ-decalactone (ϵ-DL), and their polymers that form through ROP.

the secondary alkoxide (less nucleophilic compared to ϵ-CL) resulted in a slower propagation rate. ϵ-DL was used without any purification prior to ROP, further proving the robustness of the heterogeneous catalysts.

Copolymers

Diblock copolymers *via* sequential addition

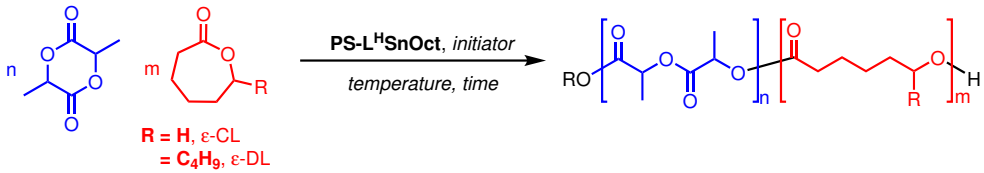

Scheme 4.2: General scheme for the synthesis of diblock copolymers.

Due to the success of the catalyst in comparison to the Zn-based catalyst, all subsequent reactions were carried out using **PS-L$^{\mathbf{H}}$SnOct**. The focus was placed on exploring alternative polymers, specifically copolymers involving combinations of the monomers tested in the previous section (Scheme 4.2). Diblock copolymers were therefore synthesised through sequential polymerisation, whereby one monomer is polymerised prior to the addition of the second monomer, to get distinct and well-defined blocks. Sampling of the reaction mixture after the first block had been allowed to polymerise (prior to the addition of the second monomer) enabled analysis of the polymer by NMR spectroscopy and SEC to extract conversions and molecular weights of the homopolymer (labelled "Block

Table 4.2: Polymerisation data from the ROP of other cyclic lactones with **PS-L^{H}ZnOAc** and **PS-L^{H}SnOct** and control reactions, using optimised times from the lactide study. Conditions: [M]:[Cat]:[I] = 50:1:1 in the melt at 130 °C (M = monomer).

Entry	Catalyst	M	Time (h)	Conv. (%)[a]	$M_{n,Theo}$[b]	$M_{n,SEC}$[c]	$M_{w,SEC}$[c]	$Đ_M$[c]
1	**PS-L^{H}ZnOAc**	*rac*-LA	6	89	6400	6100	10200	1.67
2	**PS-L^{H}SnOct**	*rac*-LA	2.5	91	6550	5450	6950	1.28
3	$Sn(Oct)_2$	*rac*-LA	10 mins	90	6500	6450	7850	1.22
4	$Zn(OAc)_2 \cdot 2H_2O$	*rac*-LA	24	84	6050	2800	4550	1.63
5	**PS-L^{H}ZnOAc**	ϵ-CL	6	91	5200	6300	9400	1.49
6	**PS-L^{H}SnOct**	ϵ-CL	2.5	89	5100	5350	7350	1.38
7	$Sn(Oct)_2$	ϵ-CL	10 mins	77	4400	5350	6150	1.15
8	$Zn(OAc)_2 \cdot 2H_2O$	ϵ-CL	24	94	5350	3400	4800	1.42
9	**PS-L^{H}ZnOAc**	ϵ-DL	6	36	2050	2950	3500	1.18
10	**PS-L^{H}ZnOAc**	ϵ-DL	24	46	1550	4050	4600	1.13
11	**PS-L^{H}SnOct**	ϵ-DL	2.5	0	-	-	-	-
12	**PS-L^{H}SnOct**	ϵ-DL	24	74	2100	6300	7100	1.12
13	$Sn(Oct)_2$	ϵ-DL	10 mins	8	450	-	-	-
14	$Sn(Oct)_2$	ϵ-DL	24	92	5250	8400	11450	1.36
15	$Zn(OAc)_2 \cdot 2H_2O$	ϵ-DL	24	64	5450	3500	4050	1.15

[a] Determined from the ^{1}H NMR spectrum.
[b] Theoretical $M_n = ([M]/[I]) \times (MW_M \times \text{equiv. M}) \times (\text{conv.}/100)$.
[c] As determined by SEC (THF) using RI methods, relative to poly(styrene) standards (rounded to the nearest 50). Molecular weights multiplied by the respective correction factor for the polymer: PLA values multiplied by a factor of 0.58,[61] PCL by 0.56.[4]

1" in the Tables of results). More in depth structural analysis was also carried out, and the results are discussed further on.

Initially, addition of a second batch of 50 equivalents of *L*-LA to the polymerisation mixture of *L*-LA, **PS-L^{H}SnOct** and 4-methylbenzyl alcohol (in a 50:1:1 ratio, respectively) demonstrated the living ROP of *L*-LA (entry 1, Table 4.3). After 2.5 hours, 79% of the first 50 equivalents of monomer had been polymerised, yielding a polymer of 5 100 Da, $Đ_M$ 1.25 ($M_{n,Theo}$ 5 700 Da). Once the second batch of *L*-LA had been added and polymerised for a further 2.5 hours, a similar conversion was calculated from the ^{1}H NMR spectrum, and the $M_{n,SEC}$ had increased linearly to 9 850 Da ($Đ_M$ 1.22, entry 1, Table 4.3, Figure 4.1). This indicated that the sequential copolymerisation in the melt would be possible, so other monomers were introduced.

The sequential copolymerisation of *L*-LA then ϵ-CL was not initially possible in the melt (130 °C) at [LA]:[CL]:[Cat]:[I] = 50:50:1:1, or even at lower ratios of *L*-LA; the molten LA would solidify as it was converted into PLA, resulting

Table 4.3: Polymerisation data from sequential copolymerisation reactions with **PS-L^{H}SnOct**. General conditions: In the melt at 130 °C (M = monomer).

Entry	Polymer[a]	[M_1]:[M_2]:Cat]:[I]	Time (h)	Temp. (°C)	Conv. M_1/M_2 (%)[b]	Block 1		Diblock Copolymer		
						$M_{n,Theo}$[c]	$M_{n,SEC}$ [$Đ_M$][d]	$M_{n,Theo}$[e]	$M_{n,SEC}$ [$Đ_M$][d]	Content M_2 in Polymer (%)[f]
1	PLA_{50}–*b*–PLA_{50}	50:50:1:1	5	130	79/78[g]	5700	5100 [1.25]	11300	9850 [1.22]	N/A [50]
2	PLA_{50}–*b*–PCL_{50}	50:50:1:1	5	130	96/12	6900	5850 [1.15]	7600	10850 [1.36]	12 [50]
3	PLA_{25}–*b*–PCL_{100}	25:100:1:1	5	130	91/3	6550	n.d.	6800	n.d.	11 [80]
4[h]	PLA_{50}–*b*–PCL_{50}	50:50:1:1	48	80	42/1	3050	1750 [1.21]	3100	3950 [1.18]	2 [50]
5[i]	PLA_{50}–*b*–PCL_{50}	50:50:1:1	2.8	180	91/86	6550	4200 [1.78]	11450	10250 [1.78]	52 [50]
6	PCL_{50}–*b*–PLA_{50}	50:50:1:1	5	130	98/80	5600	5600 [1.69]	11350	19100 [1.63]	55 [50]
7	PCL_{50}–*b*–PLA_{100}	50:100:1:1	5	130	96/83	5500	4200 [1.50]	17450	15100 [1.40]	54 [67]
8	PCL_{100}–*b*–PLA_{25}	100:25:1:1	5	130	88/81	10050	10200 [1.36]	12950	21050 [1.47]	52 [20]
9	PDL_{50}–*b*–PLA_{50}	50:50:1:1	26.5	130	92/90	7850	n.d.	14300	14400 [1.25]	51 [50]

[a] Polymer notation in the format of "Monomer 1-Monomer 2", where M_1 = Monomer 1 and M_2 = Monomer 2.

[b] Determined from the ^{1}H NMR spectrum. Conversion reported after each respective block has been polymerised.

[c] Theoretical M_n of first block = ([M_1]/[I]) × (MW_{M1} × equiv. M_1) × (conv. M_1/100).

[d] As determined by SEC (THF) using RI methods, relative to poly(styrene) standards (rounded to the nearest 50). Molecular weights of first block multiplied by the respective correction factor for the polymer: PLA values multiplied by a factor of 0.58, PCL by 0.56.[4,62]

[e] Theoretical M_n of copolymer = [([M_1]/[I]) × (MW_{M1} × equiv. M_1) × (conv. M_1/100)] + [([M_2]/[I]) × (MW_{M2} × equiv. M_2) × (conv. M_2/100)].

[f] Calculated from the ratio of polymer units in the crude product. In brackets are the expected % content values for M_2 based on 100% conversion, assuming 100% inclusion of both monomers in the polymer.

[g] Conversion of M_2 calculated based on the assumption that M_1 is 100% converted.

[h] Solution-phase, 80 °C, 48 hours total (24 hours per monomer), [LA] = [CL] = 0.69 mol L^{-1} in toluene.

[i] 180 °C, 4 hours total (20 mins for LA, then 2.5 hours for CL).

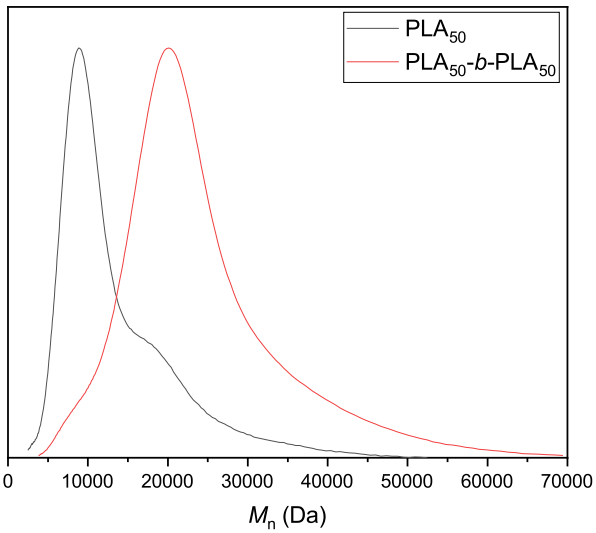

Figure 4.1: SEC traces from the living ROP of *L*-LA to form $PLA_{50}-b-PLA_{50}$. Conditions: $[LA_1]$:$[LA_2]$:[Cat]:[I] = 50:50:1:1; Block 1: $M_{n,SEC}$ 5 100 Da [$Đ_M$ 1.25]; Final polymer: $M_{n,SEC}$ 9 850 Da [$Đ_M$ 1.22] (entry 1, Table 4.3).

in a deposit of ϵ-CL on top of the layer of PLA, the former unable to access the catalyst trapped in the PLA matrix (entries 2-3, Table 4.3, Figure 4.2). Increasing the temperature in the melt to 180 °C enabled the polymerisation of both monomers successfully, keeping the PLA matrix molten enough to allow the second monomer access to the catalyst (entry 5, Table 4.3). Conversions of *L*-LA and ϵ-CL reached 91% and 86% respectively, with $M_{n,SEC}$ increasing from 4 200 Da ($Đ_M$ 1.78) after the first block, to 10 250 Da ($Đ_M$ 1.78) upon polymerisation of the second block (Figure 4.3).

Polymerisation of the PCL block first, followed by the PLA block was possible at 130 °C. $[M_1]$:$[M_2]$:[Cat]:[I] feed ratios of 50:50:1:1, 50:100:1:1 and 100:25:1:1 (where M_1 = ϵ-CL, M_2 = *L*-LA) were all carried out successfully (entries 6-8, Table 4.3, Figure 4.4). At 50:50:1:1, 98% of ϵ-CL and 80% were obtained, with an increase in molecular weight from 4 200 to 15 100 Da, while the $M_{n,SEC}$ increased from 10 200 to 21 050 Da at 100:25:1:1, somewhat higher than the predicted molecular weight ($M_{n,Theo}$ 12 950 Da, entry 8, Table 4.3). The % content of the second monomer (LA) was calculated as 52% in comparison to the

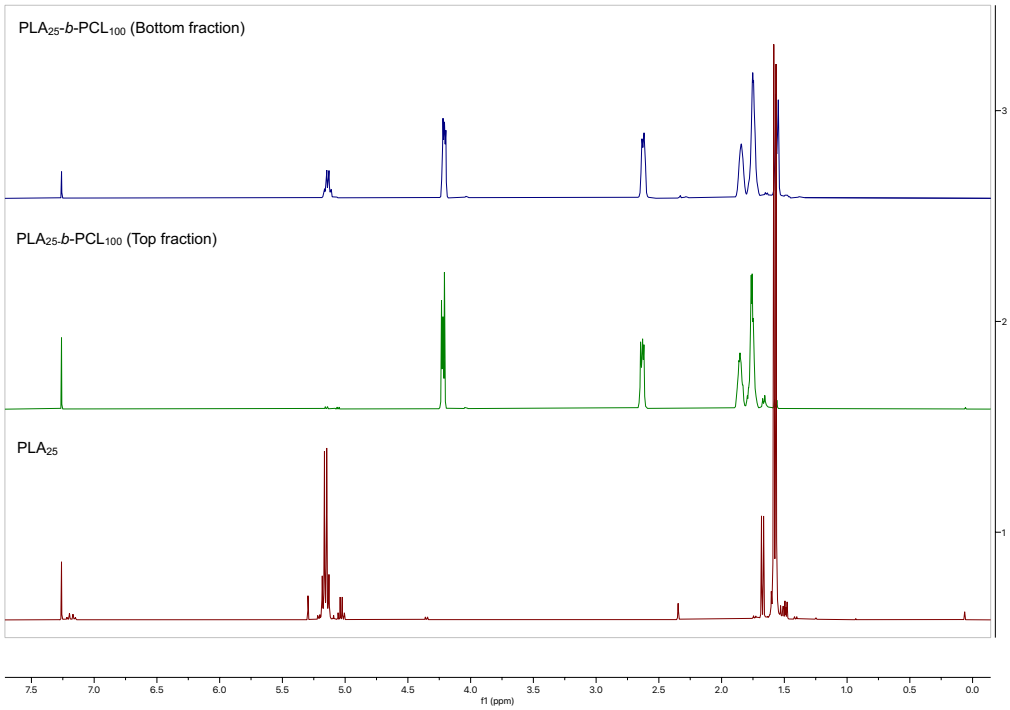

Figure 4.2: ^{1}H NMR spectra of the sequential ROP to PLA$_{25}-b-$PCL$_{100}$ in the melt at 130 °C ([LA]:[CL]:[Cat]:[I] = 25:100:1:1). Block 1 (PLA$_{25}$, red) solidifies as it polymerises. Addition of CL to create the second block is unsuccessful, forming a top fraction (green), on top of the solid PLA (blue).

expected content of 20%. This suggested that some CL has not been incorporated in the copolymer and potentially some PCL homopolymer remained, altering the observed $M_{\mathrm{n,SEC}}$.

Alternative copolymers were also possible, by replacing ϵ-CL with ϵ-DL as the first monomer enabled the formation of a PDL-*b*-PLA block copolymer, although longer reaction times were required for polymerisation of the first block based on results from earlier homopolymerisation work. Nevertheless, 92 and 91% conversion were obtained for the first and second block, respectively, reaching a final $M_{\mathrm{n,SEC}}$ of 14 400 Da ($M_{\mathrm{n,Theo}}$ 14 300 Da, $Đ_{\mathrm{M}}$ 1.25, entry 9, Table 4.3).

The sequential copolymerisation process was expanded to triblock copolymers, using one of two methods: Addition of a third block, following the same method as the previous copolymers was possible, although the monomer addition or-

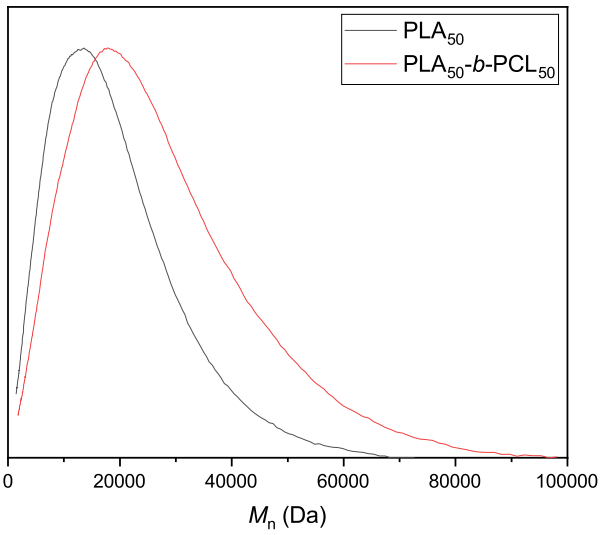

Figure 4.3: SEC traces for the synthesis of $PLA_{50}-b-PLA_{50}$. Conditions: [LA]:[CL]:[Cat]:[I] = 50:50:1:1, 3 hours at 180 °C. Block 1: $M_{n,SEC}$ 4 200 Da [$Đ_M$ 1.78]; Copolymer: $M_{n,SEC}$ 10 250 Da [$Đ_M$ 1.78] (entry 5, Table 4.3).

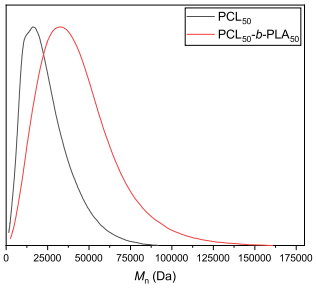

(a) [CL]:[LA]:[Cat]:[I] = 50:50:1:1

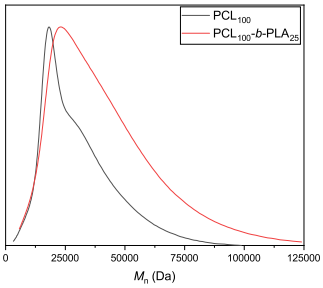

(b) [CL]:[LA]:[Cat]:[I] = 100:25:1:1

Figure 4.4: SEC traces for the synthesis of PCL−b−PCL copolymers at different ratios. (a) Block 1: $M_{n,SEC}$ 5 600 Da [$Đ_M$ 1.69]; Copolymer: $M_{n,SEC}$ 19 100 Da [$Đ_M$ 1.63] (entry 6, Table 4.3). (b) Block 1: $M_{n,SEC}$ 10 200 Da [$Đ_M$ 1.36]; Copolymer: $M_{n,SEC}$ 21 050 Da [$Đ_M$ 1.47] (entry 8, Table 4.3).

der was important to prevent previous issues of solidifying polymer. Thus a $PDL_{50}-b-PCL_{50}-b-PLA_{50}$ was synthesised, with conversions of 93, 98 and 84% for each respective block, with a final $M_{n,SEC}$ of 21 200 Da ($Đ_M$ 1.33, entry 3, Table 4.4).

Table 4.4: Polymerisation data from sequential copolymerisation reactions with **PS-L^{H}SnOct**. General conditions: In the melt at 130 °C, 5 hours (M = monomer).

Entry	Polymer[a]	$[M_1]$:$[M_2]$:$[M_3]$:[Cat]:[I]	Initiator	Block 1			Block 2			Block 3		Copolymer			
				Conv. (%)[b]	$M_{n,Theo}$[c]	$M_{n,SEC}$ [$Đ_M$][d]	Conv. (%)[b]	$M_{n,Theo}$[e]	$M_{n,SEC}$ [$Đ_M$][d]	Conv. (%)[b]	$M_{n,Theo}$[c]	$M_{n,Theo}$[e]	$M_{n,SEC}$ [$Đ_M$][d]	M_2/M_3 Content (%)[f]	
1	PLA_{25}–*b*–PCL_{25}–*o*–PCL_{25}–*b*–PLA_{25}	50:50:0:1:1	1,2-dimethoxybenzene	98	5600	4300 [1.19]	87	6250	-	-	-	11850	15100 [1.19]	53/- [50/50]	
2	PLA_{25}–*b*–PCL_{50}–*o*–PCL_{50}–*b*–PLA_{25}	100:50:0:1:1	1,2-dimethoxybenzene	92	10500	11050 [1.50]	90	6500	-	-	-	17000	30050 [1.33]	67/- [67/33]	
3[g]	PDL_{50}–*b*–PCL_{50}–*b*–PLA_{50}	50:50:50:1:1	4-Methylbenzyl alcohol	93	7900	7150 [1.22]	98	5600	16150 [1.41]	84	6050	19550[h]	21200 [1.33]	36/31 [33/33]	

[a] Polymer notation in the format of "Monomer 1-Monomer 2", where M_1 = Monomer 1 and M_2 = Monomer 2.
[b] Determined from the ^{1}H NMR spectrum.
[c] Theoretical M_n = ($[M_1]/[I]$) × (MW_{M1} × equiv. M_1) × (conv. $M_1/100$).
[d] As determined by SEC (THF) using RI methods, relative to poly(styrene) standards (rounded to the nearest 50). Molecular weights of first PCL block multiplied by the correction factor of 0.56.[62]
[e] Theoretical M_n = [($[M_1]/[I]$) × (MW_{M1} × equiv. M_1) × (conv. $M_1/100$)] + [($[M_2]/[I]$) × (MW_{M2} × equiv. M_2) × (conv. $M_2/100$)].
[f] Calculated from the ratio of polymer units in the crude product. In brackets are the expected % content values for M_2/M_3 based on 100% conversion, assuming 100% inclusion of all monomers in the polymer.
[g] Time = 26 hours.
[h] Theoretical M_n = [($[M_1]/[I]$) × (MW_{M1} × equiv. M_1) × (conv. $M_1/100$)] + [($[M_2]/[I]$) × (MW_{M2} × equiv. M_2) × (conv. $M_2/100$) + [($[M_2]/[I]$) × (MW_{M3} × equiv. M_3) × (conv. $M_3/100$)].

Alternatively, a diol could be used as the initiator, with two branches of polymer growing simultaneously from the initiator; the latter would become the centre of the polymer, rather than the end group (denoted as $-o-$ in Table 4.4), forming an ABA thermoplastic elastomer. This way, a triblock involving only two monomers was possible, such that a central core of PCL, flanked by two PLA end blocks was synthesised when ϵ-CL was polymerised as the first monomer, followed by addition of *L*-LA (entries 1-2, Table 4.4). Both methods yielded polymers of high conversion and $M_{\mathrm{n,SEC}}$ up to 30 050 Da, with narrow dispersities ($Đ_{\mathrm{M}}$<1.33, Figure 4.5).

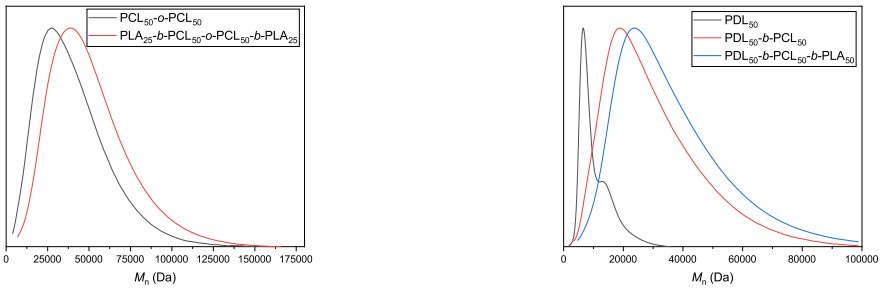

(a) $\mathrm{PLA_{25}}-b-\mathrm{PCL_{100}}-b-\mathrm{PLA_{25}}$ (b) $\mathrm{PDL_{50}}-b-\mathrm{PCL_{50}}-b-\mathrm{PLA_{50}}$

Figure 4.5: SEC traces for the synthesis of triblock copolymer. (a) Initiator: 1,4-dimethoxybenzene, [CL]:[LA]:[Cat]:[I] = 100:50:1:1; Block 1: $M_{\mathrm{n,SEC}}$ 11 050 Da [$Đ_{\mathrm{M}}$ 1.50]; Copolymer: $M_{\mathrm{n,SEC}}$ 30 050 Da [$Đ_{\mathrm{M}}$ 1.33] (entry 2, Table 4.4). (b) Initiator: 4-MeBnOH; Block 1: $M_{\mathrm{n,SEC}}$ 7 150 Da [$Đ_{\mathrm{M}}$ 1.22]; Block 2: $M_{\mathrm{n,SEC}}$ 16 150 Da [$Đ_{\mathrm{M}}$ 1.41]; Copolymer: $M_{\mathrm{n,SEC}}$ 21 200 Da [$Đ_{\mathrm{M}}$ 1.33] (entry 3, Table 4.4).

Copolymerisation kinetics of one-pot reactions

So far, only sequential polymerisation had been explored to access block copolymers. However, one-pot copolymerisations, where both monomers are added in simultaneously at the start of reaction, are also of interest, specifically in cases where the catalyst is selective and polymerises one preferred monomer prior to the the second, yielding a block copolymer. Earlier work covering the ROP of *rac*-LA showed that **PS-L$^{\mathbf{H}}$SnOct** was not selective towards any one lactide isomer, however it was not yet known if the catalyst had any preference towards specific lactones. For the following reactions, therefore, both monomers were added together in a one-pot approach. *L*-LA was defined as $\mathrm{M_1}$, while ϵ-CL or

Table 4.5: Polymerisation data from *in situ* ATR-FT-IR monitored one-pot co-polymerisation reactions with **PS-L^{H}SnOct**. Conditions: Melt at 130 °C.

Entry	Polymer[a]	[M_1]:[M_2]:[Cat]:[I]	Time (h)	Conv. M_1/M_2 (%)[b]	Content M_2 in Polymer (%)[c]	$M_{n,Theo}$[d]	$M_{n,SEC}$ [$Đ_M$][e]
1[f]	PCL_{50}−PLA_{50}	50:50:1:1	3	92/88	52 [50]	11600	19600 [1.92]
2	PCL_{50}−PLA_{50}	50:50:0.25:1	3	98/44	31 [50]	9550	17750 [1.90]
3	PCL_{50}−PLA_{50}	50:50:1:1	5	95/79	45 [50]	11350	15050 [2.28]
4	PDL_{50}−PLA_{50}	50:50:1:1	24	96/61	39 [50]	12100	11150 [1.99]

[a] Polymer notation in the format of "Monomer 1 − Monomer 2", where M_1 = Monomer 1 (*L*-LA) and M_2 = Monomer 2 (ϵ-CL or ϵ-DL).
[b] Determined from the ^{1}H NMR spectrum.
[c] Calculated from the ratio of polymer units in the crude product. In brackets are the expected % content values for M_2 based on 100% conversion, assuming 100% inclusion of both monomers in the polymer.
[d] Theoretical $M_n = [([M_1]/[I]) \times (MW_{M1} \times \text{equiv. } M_1) \times (\text{conv. } M_1/100)] + [([M_2]/[I]) \times (MW_{M2} \times \text{equiv. } M_2) \times (\text{conv. } M_2/100)]$.
[e] As determined by SEC (THF) using RI methods, relative to poly(styrene) standards (rounded to the nearest 50).
[f] Small scale one-pot, test reaction outside of the *in situ* ATR-FT-IR.

ϵ-DL was denoted as M_2 in the results tables. The $-b-$ notation between blocks was not included, as further investigations into the nature of these polymers were required to determine whether discrete blocks had been formed (see below).

A preliminary one-pot copolymerisation test of ϵ-CL and *L*-LA was carried out, using a [LA]:[CL]:[Cat]:[I] feed ratio of 50:50:1:1, in the melt at 130 °C (entry 1, Table 4.5). High conversions of both monomers were observed (92% and 88% for *L*-LA and ϵ-CL, respectively), reaching a total molecular weight of 19 600 Da after 3 hours. While the $M_{n,SEC}$ of the one-pot reaction was similar to that of the equivalent sequential copolymerisation reaction ($M_{n,SEC}$ 19 100 Da, $Đ_M$ 1.63, entry 6, Table 4.3), the dispersity had increased to 1.92, suggesting less control was possible in the one-pot reactions.

Subsequent one-pot copolymerisations were conducted on a larger scale, monitored by *in situ* ATR-FT-IR to obtain information about the relative observed rate constants of each monomer (entries 2-4, Table 4.5). The areas under the peaks at 1766, 1750, 1735, 1723 cm^{-1} (corresponding to LA, PLA, PCL and ϵ-CL, respectively) were monitored over time (Figures 4.6 and B.6); similarly positioned peaks were monitored for the ϵ-DL/*L*-LA one-pot copolymerisation (Figure B.7), determined through addition of one monomer, followed by the other to get accurate peak positions. Although comparable results could be obtained this way with a consistent method, quantitative data with 100% accuracy was not possible due to the potential overlap of two nearby peaks, which could skew results – this could be seen in Figure 4.7, where conversion of PLA continued to increase slowly after 70 minutes, while LA had been entirely consumed by the 70 minute mark. Nevertheless, the consistent method allowed for direct comparison between the samples tested herein, with kinetic data collected as described in

the previous chapter (*i.e.*, up to 80% conversion to avoid errors in measurement from viscosity, assumed first-order). To monitor the reactions effectively, both monomers were heated together with the initiator until the reaction temperature had stabilised, and all the lactide had melted to a homogenous mixture. The catalyst was then introduced under a flow of argon, allowing precise monitoring of the reaction and avoiding reaction of the monomers with the catalyst before all the lactide had melted fully.

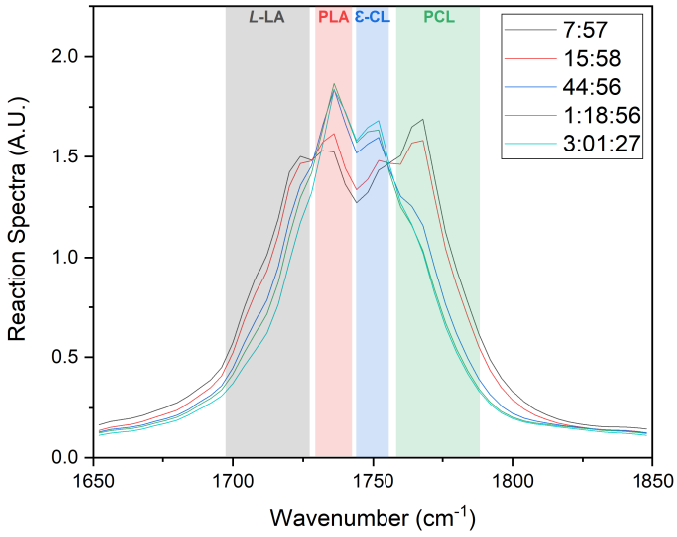

Figure 4.6: C=O region of selected IR spectra from the *in situ* ATR-FT-IR monitored one-pot copolymerisation of ϵ-CL and *L*-LA ([LA]:[CL]:[Cat]:[I] = 50:50:0.25:1, melt, 130 °C). Kinetic analysis carried out by monitoring the area beneath the LA (grey), PLA (red), PCL (blue) and CL (green) peaks at 1766, 1750, 1735, 1723 cm^{-1}, respectively. Legend refers to time during reaction.

A [LA]:[CL]:[Cat]:[I] feed ratio of 50:50:0.25:1 was conducted for direct comparison to work described in Chapter 3. Conversion of *L*-LA reached 98%, however only 44% of ϵ-CL was converted within the allotted time. The final polymer reached $M_{n,SEC}$ 17 750 Da, with a similar dispersity to the test reaction ($Đ_M$ 1.90, entry 2, Table 4.5).

In previous ATR-FT-IR monitored ROP, a [LA]:[Cat]:[I] of 50:0.25:1 was used (effectively quartering the amount of catalyst, relative to the standard ROP procedure), to minimise the catalyst interference with the probe. For copolymerisation

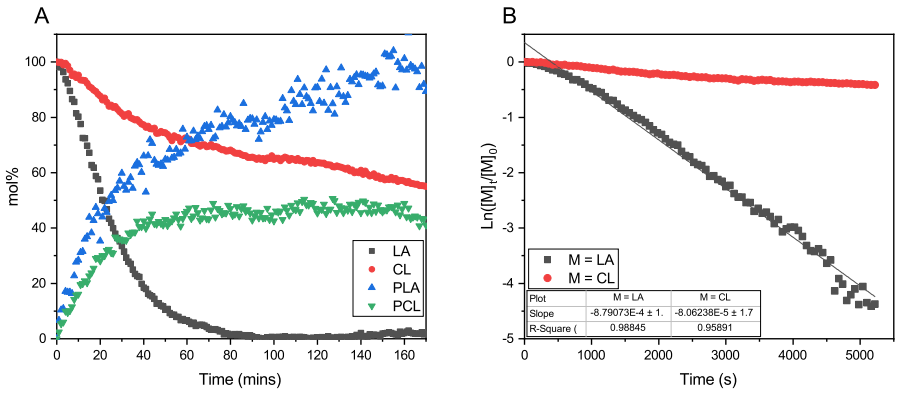

Figure 4.7: (A) Conversion of *L*-LA to PLA and ϵ-CL to PCL over time ([LA]:[CL]:][Cat]:[I] = 50:50:0.25:1, 130 °C, one-pot copolymerisation in the melt, 3 hours). (B) Semi-logarithmic plot of [LA] and [CL], monitored by *in situ* ATR-FT-IR using **PS-L$^{\mathbf{H}}$SnOct** (entry 1, Table 4.6).

reactions, however, the doubled amount of monomer meant that original ratios of catalyst would not interfere with the probe to the same extent, so one-pot co-polymerisations of *L*-LA with ϵ-CL or ϵ-DL at 50:50:1:1 were also tested (entries 3-4, Table 4.5). Both copolymerisations were successful, attaining high conversions of *L*-LA (>95%) and good conversions of the second monomer (>61%). The lower conversion of ϵ-CL in comparison to the homopolymerisation of this monomer could be explained by the solidifying reaction mixture as the LA was polymerised, preventing effective access of ϵ-CL to the catalyst. $M_{\mathrm{n,SEC}}$ of the final copolymers were in line with the predicted molecular weights ($M_{\mathrm{n,Theo}}$).

Reaction kinetics were assessed through calibration of the monomer and polymer peaks to external sampling obtained at the beginning and end of reaction. Due to the solvent-free nature of the reactions, the polymer matrix would solidify at high conversions and magnetic stirring was not sufficient to overcome this, leading to "pockets" of unreacted monomer or areas with a higher concentration of polymer. As such, data obtained at higher conversions was unreliable and this was particularly evident when reactions were left for extended periods of time (Figures B.8-B.9). Reaction kinetics were therefore obtained from the first portion of the data, where consumption of both monomers was still visible, having not reached high enough conversions to interfere with the probe monitoring.

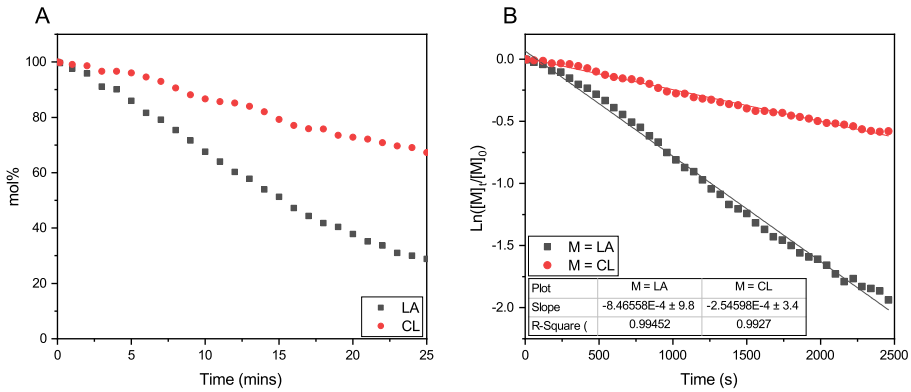

Figure 4.8: (A) Conversion of *L*-LA to PLA and ϵ-CL to PCL over time ([LA]:[CL]:][Cat]:[I] = 50:50:1:1, 130 °C, one-pot copolymerisation in the melt, 5 hours). (B) Semi-logarithmic plot of [LA] and [CL], monitored by *in situ* ATR-FT-IR using **PS-L$^{\mathbf{H}}$SnOct** (entry 2, Table 4.6).

All reactions were first order with respect to each monomer, evidenced through linear semi-logarithmic plots (Figures 4.7-4.9). The k_{obs} were determined as 8.47×10^{-4} s^{-1} and 2.55×10^{-4} s^{-1} for *L*-LA and ϵ-CL, respectively (50:50:1:1, entry 2, Table 4.6). For the *L*-LA and ϵ-DL copolymerisation, the k_{obs} were determined as 7.88×10^{-4} s^{-1} and 0.25×10^{-4} s^{-1}, respectively, with ϵ-DL consumed marginally slower than ϵ-CL (entries 2 and 3, Table 4.6). An experimental order of reactivity of *L*-LA > ϵ-CL > ϵ-DL, in agreement with with the thermodynamics of ring-opening, and the resulting order of reactivity of monomers in the literature.[32]

Although it was immediately clear that both monomers were consumed from the start of reaction – suggesting that the catalyst showed no preference for one monomer over another – the kinetics of each monomer varied significantly. The k_{obs} of *L*-LA and ϵ-CL varied as ratios and monomers were changed: *L*-LA went from being only 3 times as rapid as ϵ-CL to 11 times greater, upon quartering the amount of catalyst (entries 1-2, Table 4.6), potentially caused by a large increase in catalyst affinity for LA at low concentrations. Similarly, in the *L*-LA homopolymerisation, the k_{obs} of *L*-LA was found to be 6.44×10^{-4} s^{-1} (Chapter 3), changing to 8.79×10^{-4} s^{-1} during a copolymerisation with ϵ-CL, under the same conditions ([LA]:[CL]:[Cat]:[I] = 50:50:0.25:1, entry 1, Table 4.6).

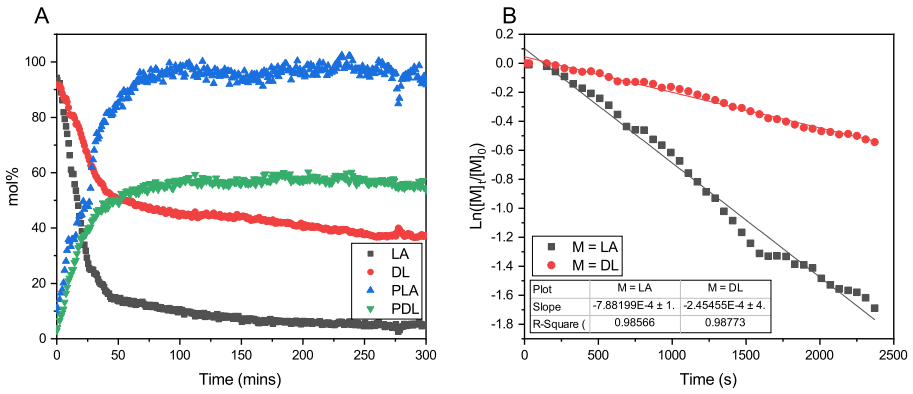

Figure 4.9: (A) Conversion of *L*-LA to PLA and ϵ-DL to PCL over time ([LA]:[DL]:][Cat]:[I] = 50:50:1:1, 130 °C, one-pot copolymerisation in the melt, 24 hours). (B) Semi-logarithmic plot of [LA] and [DL], monitored by *in situ* ATR-FT-IR using **PS-L$^{\mathbf{H}}$SnOct** (entry 3, Table 4.6).

Table 4.6: Observed rate constants for one-pot copolymerisation reactions with **PS-L$^{\mathbf{H}}$SnOct**, conducted in the melt at 130 °C. Constants obtained *via in situ* ATR-FT-IR.

Entry	Polymer[a]	$[M_1]$:$[M_2]$:[Cat]:[I]	k_{obs} M_1 ($\times 10^{-4}$ s^{-1})	k_{obs} M_2 ($\times 10^{-4}$ s^{-1})	k_{obs} M_1/M_2
1	PLA_{50}–PCL_{50}	50:50:0.25:1	8.79	0.86	11
2	PLA_{50}–PCL_{50}	50:50:1:1	8.47	2.55	3
3	PLA_{50}–PDL_{50}	50:50:1:1	7.88	2.58	3

[a] Polymer notation in the format of "Monomer 1 – Monomer 2", where M_1 = Monomer 1 (*L*-LA) and M_2 = Monomer 2 (ϵ-CL or ϵ-DL).

The slight disparity in k_{obs} between the homo- and copolymerisations could stem from several factors. With the homopolymerisations, the original ATR-FT-IR method (whereby the catalyst was added to the mixture before the lactide was melted) was sufficient, as the 0.25 equivalents of catalyst did not catalyse the initial reaction at such a rate that it was impossible to analyse. However, the original method could be subjected to slight changes in peak intensity while the lactide was melting as the reaction mixture reached temperature, thereby altering the results and causing a potential error in measurement during the initial stages of reaction. Nevertheless, the original ATR-FT-IR method was conducted in transmission mode. The change in peak intensity is more likely in absorption mode, where the intensity of the peak is directly related to the concentration (or effective concentration, mol%) by way of the Beer-Lambert law, so this reasoning

for changes in k_{obs} is unlikely.

Second and more likely, it was observed that on combination with the two different monomers (ϵ-CL or ϵ-DL), the observed rate constant for *L*-LA also varies, so it is not unreasonable to suggest that the rate constant fluctuates based on external factors. This could also explain the changes in kinetics of ϵ-CL between the 50:50:0.25:1 and 50:50:1:1 reactions (entries 1 and 2, Table 4.6), and the varying *L*-LA k_{obs} between different copolymerisations. Indeed, previous research has indicated that the rate constant for one monomer will change when the monomer is incorporated into a random or tapered copolymer.[63]

So far, only crude information about the polymer microstructure had been gathered from the kinetics: as no preference for one monomer over another was observed (*i.e.* simultaneous consumption of both monomers occurred), a diblock copolymer (AAA−BBB) was unlikely. Yet, a high $M_{n,SEC}$ and varying k_{obs} hinted towards the synthesis of one single copolymer (either tapered, alternating or random), rather than two separate homopolymers of shorter M_n. In order to gain more information about the structure, further investigation of the polymer properties were necessary.

Polymer characterisation

Table 4.7: Diffusion coefficients of copolymers (D_{poly}) and $CDCl_3$ (reference solvent, D_{sol}), determined through ^{1}H DOSY NMR spectroscopy.

Entry	Polymer	D_{sol} ($\times 10^{-5}$ cm^2 s^{-1})	D_{poly} ($\times 10^{-6}$ cm^2 s^{-1})
1	PLA_{50}−*b*−PCL_{50}	1.54	3.28
2	PCL_{50}−*b*−PLA_{50}	2.00	0.88
3	PCL_{50}−*b*−PLA_{100}	2.04	2.71
4	PCL_{100}−*b*−PLA_{25}	1.80	0.53
5	PDL_{50}−*b*−PLA_{50}	2.18	1.97
6	PCL_{50}−PLA_{50} (one-pot)	2.05	2.27
7	PDL_{50}−PLA_{50} (one-pot)	2.10	1.21
8	PLA_{25}−*b*−PCL_{25}−*o*−PCL_{25}−*b*−PLA_{25}	1.91	0.01
9	PLA_{25}−*b*−PCL_{50}−*o*−PCL_{50}−*b*−PLA_{25}	1.87	0.57
10	PDL_{50}−*b*−PCL_{50}−*b*−PLA_{50}	2.18	2.22

SEC data from sequential polymerisations showed an increase in M_n after the polymerisation of the first monomer to the final copolymer, hinting toward the formation of a single copolymer. In contrast, sampling of the one-pot reactions in the melt was not possible, and while *in situ* ATR-FT-IR pointed toward the

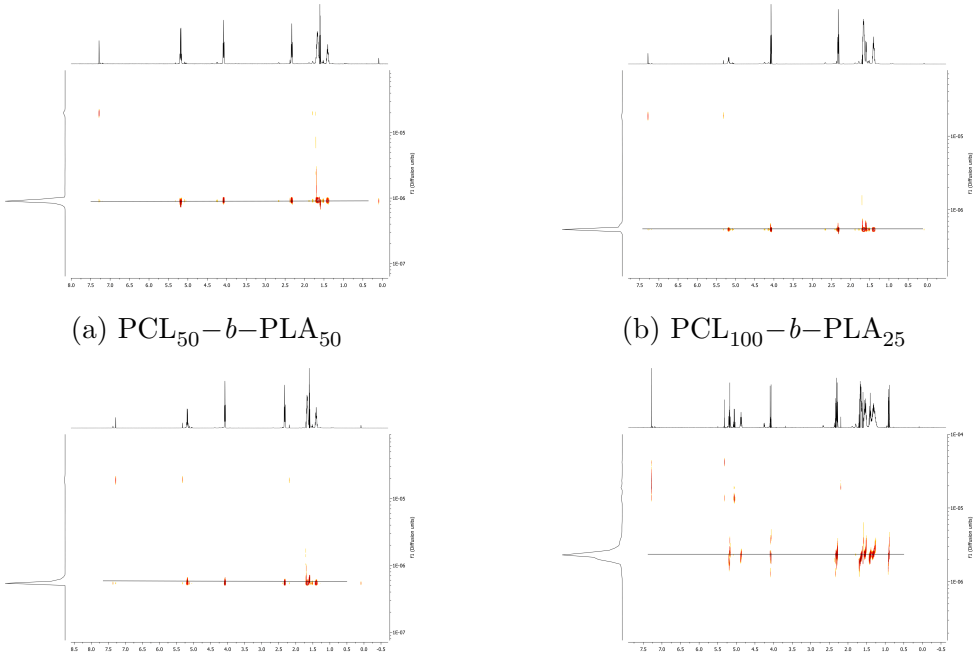

(a) $PCL_{50}-b-PLA_{50}$ (b) $PCL_{100}-b-PLA_{25}$

(c) $PLA_{25}-b-PCL_{100}-b-PLA_{25}$ (d) $PDL_{50}-b-PCL_{50}-b-PLA_{50}$

Figure 4.10: ^{1}H DOSY NMR spectra in $CDCl_3$ for the di- (a-b), and triblock (c-d) copolymerisations. Diffusion constants found in Table 4.7.

simultaneous incorporation of both monomers into one polymer, more in depth analysis was required to determine the microstructure of the final polymer.

^{1}H DOSY NMR spectra were collected for all copolymers. While a quantitative method was not applied to the ^{1}H DOSY NMR spectra (so direct comparison was not possible between samples) analysis of both components of the polymer revealed that they both possessed the same diffusion coefficient. This supported the theory that one copolymer had formed rather than two separate homopolymers (Table 4.7).

Despite the similarity in molecular weights of *L*-LA and ϵ-CL, particularly when in equal equivalents to one another (entries 1-2, Table 4.7, Figure 4.10A), ^{1}H DOSY NMR spectra of polymers produced from different [LA]:[CL] ratios also showed the PLA and PCL components diffusing at the same rate (entries 3-4, Table 4.7, Figure 4.10B). Both observations were applied to the formation of triblock copolymers (entries 8-10, Table 4.7, Figures 4.10C-4.10D), and one-pot copolymerisations (entries 7-10, Table 4.7, Figures B.22-B.24).

Although ^{1}H DOSY NMR analysis supported the formation of copolymers, no information about the microstructure of these copolymers was available from this technique. While sequential polymerisations were likely to take the form of block copolymers (either distinct blocks or tapered copolymers), one-pot copolymers could have a block, tapered, or random microstructure. Increasing the number of scans in the ^{1}H NMR to 128 scans enabled elucidation of peaks between the homopolymer and monomer signals; the quartets pertaining to the PLA and *L*-LA methine protons typically appear at 5.19 ppm and 5.04 ppm, whilst "intermediate" peaks centred at 5.10 ppm.

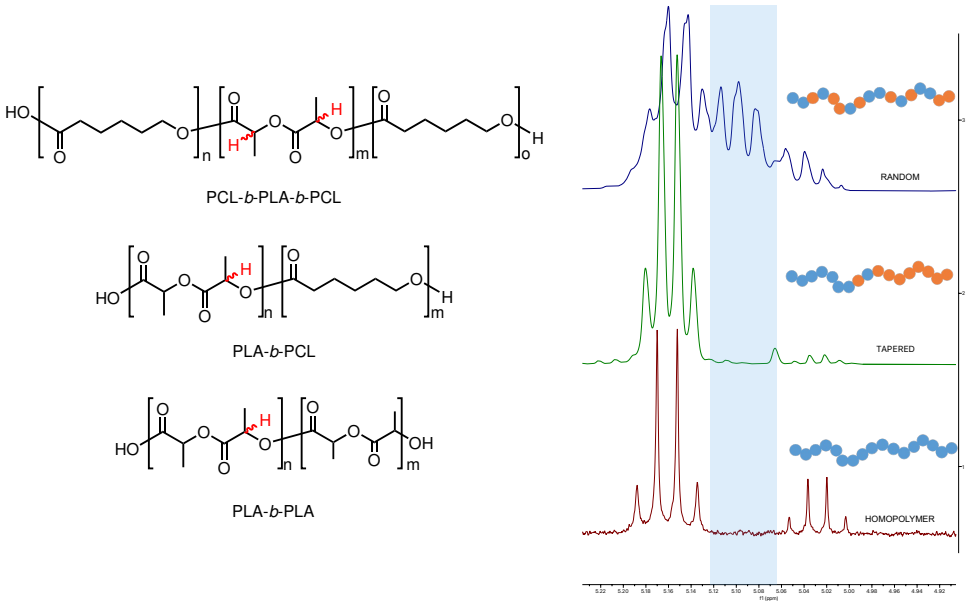

Figure 4.11: Methine region of the ^{1}H NMR spectra of crude PLA quartet (5.16 ppm, LA quartet at 5.03 ppm) and copolymers showing the different microstructures pertaining to homopolymers, tapered (gradient) and random copolymers.

These new peaks appear when the methine proton of the LA unit was in a different environment, next to a different monomer unit. Introduction of this second monomer would create a different environment for the methine proton in the *L*-LA unit connecting the PLA and PCL or PDL blocks, such that the signal would likely shift upfield, leading to a "scrambling" (shifting) of the PLA methine signal (Figure 4.11). In cases where many methine PLA protons were next to units of the second monomer in the polymer chain, these intermediate, shifted signals would increase in intensity, as in cases of random or alternating copolymers.

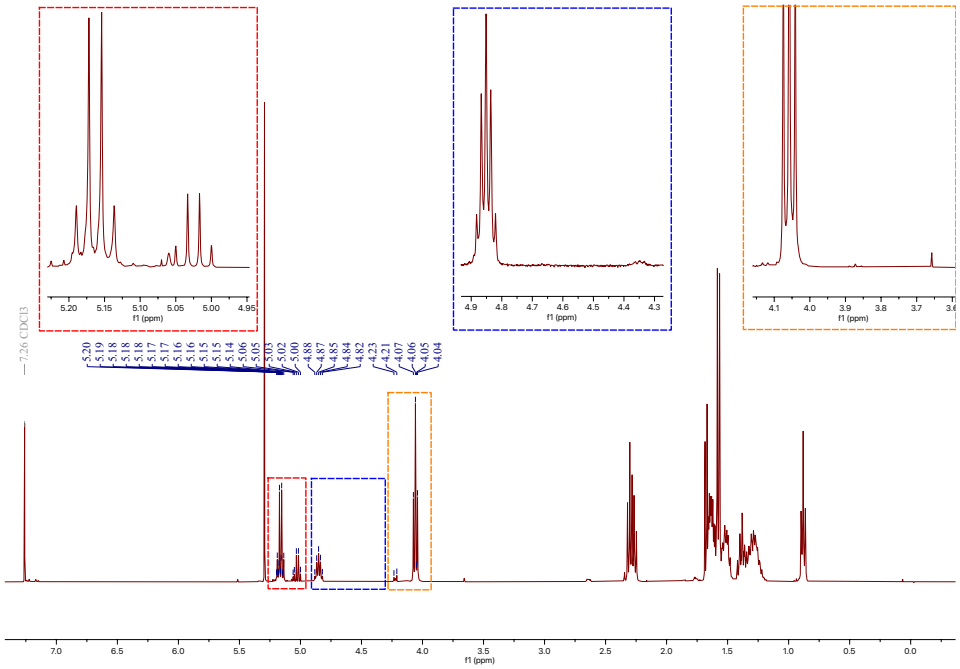

(a) ^{1}H NMR (128 scans)

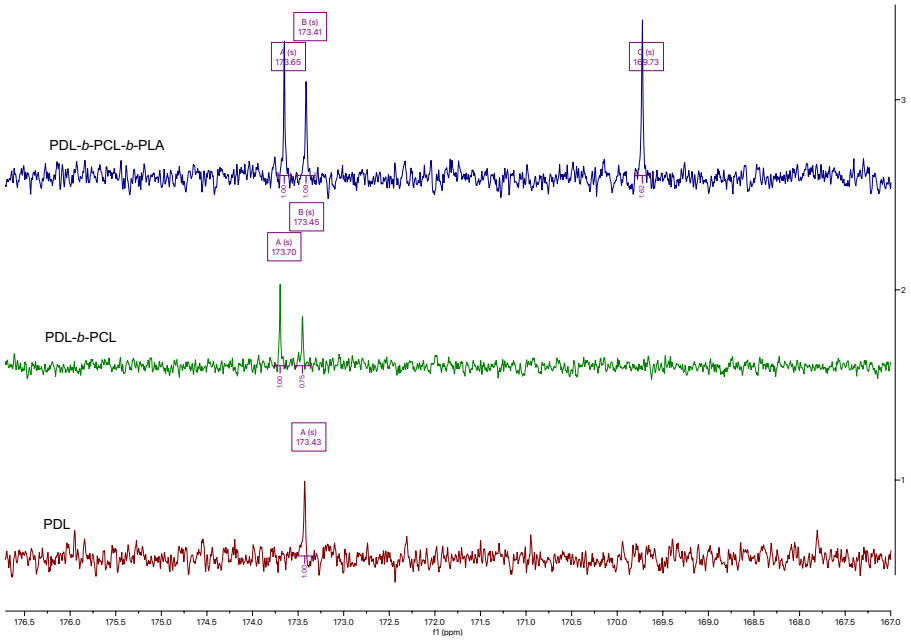

(b) ^{13}C{^{1}H} NMR

Figure 4.12: NMR spectra in $CDCl_3$ of the sequential copolymerisation to $PDL_{50}-b-PCL_{50}-b-PLA_{50}$ (entry 3, Table 4.4).

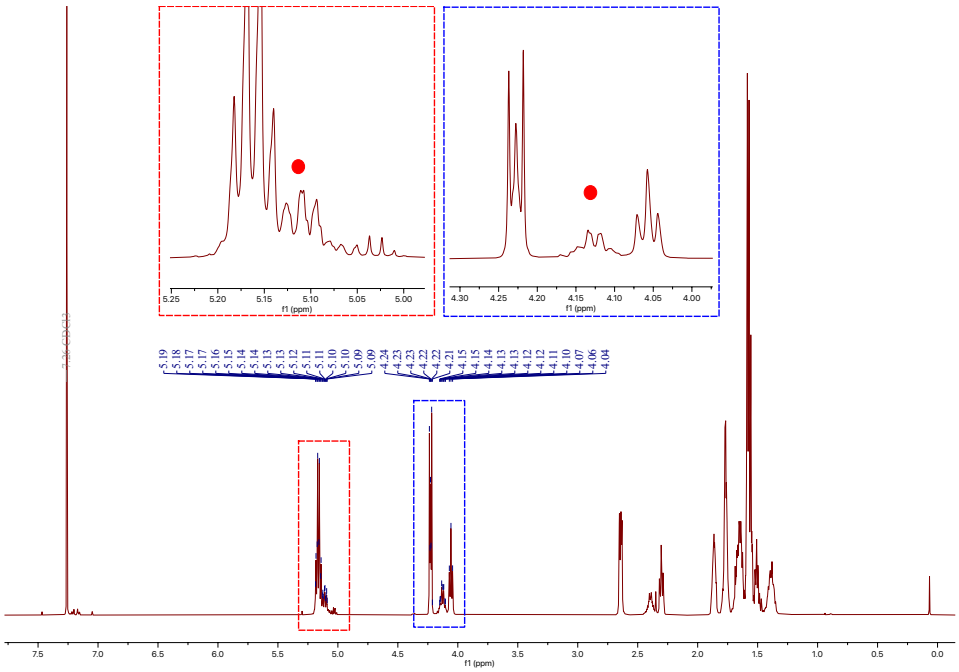

(a) ^{1}H NMR (128 scans)

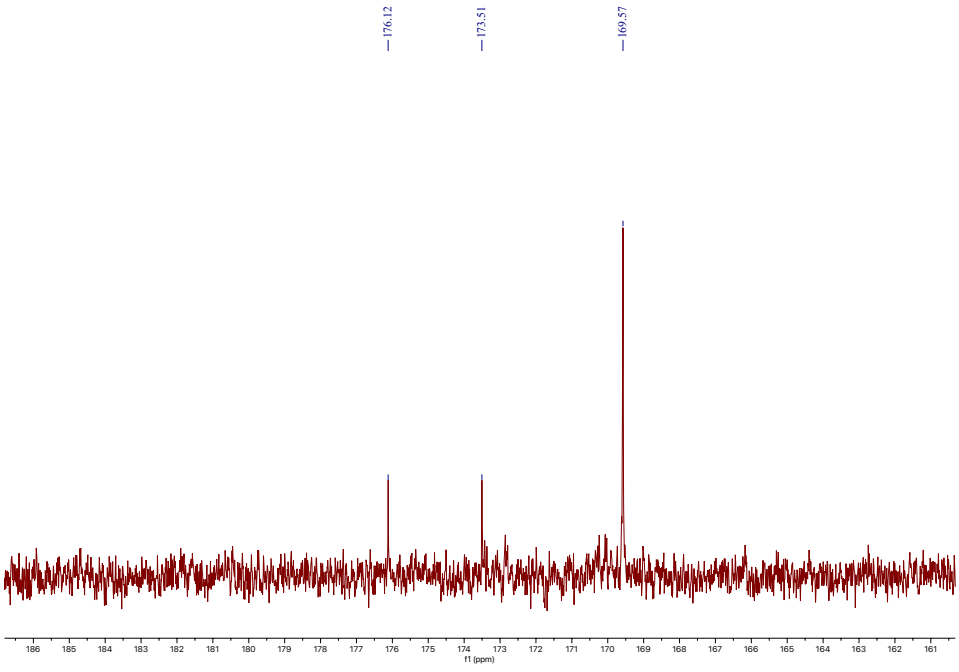

(b) ^{13}C{^{1}H} NMR

Figure 4.13: NMR spectra in $CDCl_3$ of one-pot copolymerisation of *L*-LA and ϵ-CL (entry 1, Table 4.6).

These signals were more prominent in samples produced through one-pot reactions (Figure 4.13A), whilst they were absent in homopolymers and only slightly visible in polymers produced through sequential polymerisation (Figure 4.12A). As such, coupled with SEC data, samples produced through sequential polymerisation were likely block copolymers with some tapering between blocks (where a gradient of monomers occurred in between the two blocks). In contrast, one-pot copolymers were likely statistical (random monomer distribution, AABBABABBBAB), supported by the simultaneous monomer consumption at different rates, observed through *in situ* ATR-FT-IR, and in agreement with previous observations in the literature.[26]

This conclusion was supported by $^{13}C\{^{1}H\}$ NMR: presence of multiple peaks corresponding to the carbonyl C was likely due to the different environments of the carbon atom in different microstructures. In sequential copolymers, such as the $PDL_{50}-b-PCL_{50}-b-PLA_{50}$ triblock, only three carbon environments were observed at 173.65, 173.41 and 169.73 ppm, corresponding to the PCL, PDL and PLA blocks, respectively.[26] The addition of a new block would add another distinct environment (Figure 4.12B).

In contrast, one-pot copolymers displayed multiple carbonyl carbon peaks in the ^{13}C NMR spectra, at 176.65, 173.64 and 169.71 ppm, when only two different environments were expected for a block copolymer (Figure 4.13B). Coupled with the scrambling of the methine proton in the ^{1}H NMR spectrum, this was suggestive of several different carbon environments occurring in a random or alternating copolymer.

Finally, DSC thermograms were obtained to confirm the microstructure of the different polymers (Figure 4.14). The P*L*LA homopolymer was highly crystalline, with a sharp melting temperature (T_m) at 159 °C (entry 1, Table 4.8). The melting temperature increased when PLA was combined with PCL to form the sequential $PCL_{50}-b-PLA_{50}$ copolymer (165 °C, entry 2, Table 4.8), in line with reports in literature.[26,28] The $PLA_{50}-b-PCL_{50}-o-PCL_{50}-b-PLA_{50}$ triblock lowered the T_m to 153 °C, likely due to the decreased crystallinity observed in symmetrical copolymers.[45] A glass transition temperature (T_g) was observed at 54 °C (entry 3, Table 4.8). In contrast, the one-pot copolymer of PLA and PCL was totally amorphous, with no discernable T_g or T_m in the temperature

range tested (20-200 °C, entry 4, Table 4.8). The T_g of an amorphous PLA/PCL copolymer has been found to be −15 °C,[64] so subsequent DSC thermograms should cover a wider temperature range to confirm the phase behaviours of these copolymers.

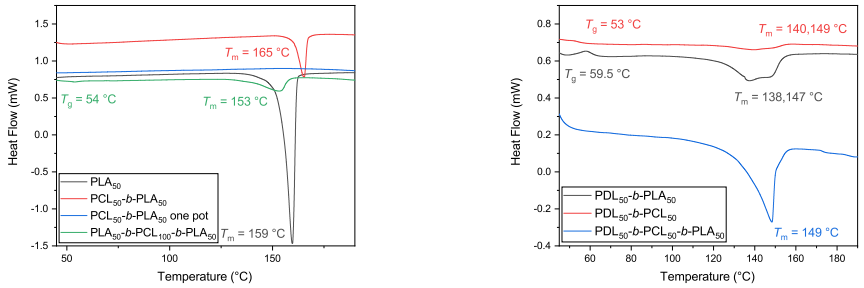

(a) PLA-PCL (b) PDL

Figure 4.14: DSC thermograms of the second heating cycle for polymers containing combinations of PLA, PCL and PDL (20 °C/min).

Two T_m at 138 and 147 °C were observed when *L*-LA was copolymerised with ϵ-DL – the latter being is a "soft" block due to its amorphous nature in the homopolymer.[26] Combination of PLA with PDL significantly decreased the T_m, and the two temperatures were likely due to the two segments of varying crystallinity (entry 5, Table 4.8). Similar results were observed in the diblock of PDL$_{50}$−*b*−PCL$_{50}$ (entry 6, Table 4.8). Addition of a PLA end-segment to form the PDL$_{50}$−*b*−PCL$_{50}$−*b*−PLA$_{50}$ triblock increased the crystallinity of the polymer, with a T_m of 149 °C (entry 5, Table 4.8).

Table 4.8: Glass transition (T_g) and melting (T_m) temperatures for the copolymerisation of lactones with **PS-L^{H}SnOct**, obtained from the second heat cycle (10 °C/min) of the DSC thermogram. Reactions conducted in the melt at 130 °C).

Entry	Polymer	Polymerisation Method	T_g (°C)	T_m (°C)
1	PLA$_{50}$	N/A	-	159
2	PCL$_{50}$−PLA$_{50}$	Sequential	-	165
3	PLA$_{25}$−*b*−PCL$_{50}$−*o*−PCL$_{50}$−*b*−PLA$_{25}$	Sequential	54	153
4	PCL$_{50}$−PLA$_{50}$	One-Pot	-	-
5	PDL$_{50}$−*b*−PLA$_{50}$	Sequential	59.5	138, 147
6	PDL$_{50}$−*b*−PLA$_{50}$	Sequential	53	140, 149
7	PDL$_{50}$−*b*−PCL$_{50}$−*b*−PLA$_{50}$	Sequential	-	149

4.4 Conclusions and future work

Although **PS-L^{H}SnOct** did not show any preference for one isomer of LA over another in the ROP of *rac*-LA, the catalyst was shown to tolerate several lactone substrates, including ϵ-CL and ϵ-DL. This allowed the synthesis of block copolymers, confirmed as single polymeric structures by ^{1}H DOSY NMR spectroscopy and increase in the M_{n} upon monomer addition by SEC monitoring.

One-pot reactions are possible through simultaneous addition of both monomers into the reaction. *In situ* ATR-FT-IR of these one-pot copolymerisations revealed an order of reactivity of the monomers as *L*-LA > ϵ-CL > ϵ-DL, consistent with literature.[65] Simultaneous consumption of both monomers at significantly different rates in the reaction mixture led to the formation of random copolymers, confirmed through inspection of the ^{1}H, ^{13}C{^{1}H} NMR spectra. The amorphous morphology of the copolymer was further evidence of the random microstructure of the copolymer formed by the one-pot method.

Therefore, depending on the desired properties, various microstructures can be synthesised with the heterogeneous catalyst. If distinct blocks were targeted, for example in the synthesis of ABA triblock TPEs, the one-pot method did not provide the required selectivity, unlike the sequential polymerisation method, which provided different triblocks depending on the initiator used.

Following from this, it is conceivable that more complex structures such as star or branched copolymers could be accessed easily by changing the initiator. Similarly, addition of further blocks could be investigated further to identify how these would change the properties. Finally, more in-depth analysis of the current polymers are required to investigate their properties fully.

The use of alternative copolymer architectures (star or branched copolymers) could negate some of the disadvantages afforded by linear block copolymers which display low crystallinity and therefore higher viscosity.[30] Similarly, metal catalysts based on Schiff base motifs have been used successfully in the the copolymerisation of LA with alternative monomers such as cyclic carbonates and epoxides. The application of **PS-L^{H}SnOct** to the copolymerisation of other monomers is also of interest when looking at the catalyst scope of this class of heterogeneous catalysts.

More pertinent to this work, development of alternative ligand structures could be carried out, such as the tri- or tetradentate ligands applied by Kol and co-workers,[56,66] to achieve both stereoselective lactide ROP and successful one-pot block copolymerisation.

References

[1] A. M. Goldys and D. J. Dixon, *Macromolecules*, 2014, **47**, 1277–1284.

[2] X. Zhang, M. Fevre, G. O. Jones and R. M. Waymouth, *Chem Rev*, 2018, **118**, 839–885.

[3] A. Duda and A. Kowalski, in *Handbook of Ring-Opening Polymerization*, ed. P. Dubois, O. Coulembier and J.-M. Raquez, Wiley-VCH, Germany, 2009, ch. 1, pp. 1–52.

[4] G. Gontard, A. Amgoune and D. Bourissou, *J Polym Sci Pol Chem*, 2016, **54**, 3253–3256.

[5] A. Kowalski, J. Libiszowski, T. Biela, M. Cypryk, A. Duda and S. Penczek, *Macromolecules*, 2005, **38**, 8170–8176.

[6] T. K. Sen, S. C. Sau, A. Mukherjee, A. Modak, S. K. Mandal and D. Koley, *Chem Commun*, 2011, **47**, 11972–11974.

[7] R. M. Slattery, A. E. Stahl, K. R. Brereton, A. L. Rheingold, D. B. Green and J. M. Fritsch, *J Polym Sci Pol Chem*, 2019, **57**, 48–59.

[8] W. M. Stevels, M. J. K. Ankone, P. J. Dijkstra and J. Feijen, *Macromolecules*, 1996, **29**, 8296–8303.

[9] C.-h. Huang, F.-c. Wang, B.-t. Ko, T.-l. Yu and C.-c. Lin, *Macromolecules*, 2001, **34**, 356–361.

[10] C.-L. Lee, Y.-F. Lin, M.-T. Jiang, W.-Y. Lu, J. K. Vandavasi, L.-F. Wang, Y.-C. Lai, M. Y. Chiang and H.-Y. Chen, *Organometallics*, 2017, **36**, 1936–1945.

[11] H. Y. Chen, W. Y. Lu, Y. J. Chen, S. C. N. Hsu, S. W. Ou, W. T. Peng,

N. Y. Jheng, Y. C. Lai, B. S. Wu, H. Chung, Y. Chen and T. C. Huang, *J Polym Sci Pol Chem*, 2013, **51**, 327–333.

[12] S. M. Kirk, G. Kociok-Kohn and M. D. Jones, *Organometallics*, 2016, **35**, 3837–3843.

[13] A. Kowalski, A. Duda and S. Penczek, *Macromolecules*, 2000, **33**, 7359–7370.

[14] Y.-T. Huang, W.-C. Wang, C.-P. Hsu, W.-Y. Lu, W.-J. Chuang, M. Y. Chiang, Y.-C. Lai and H.-Y. Chen, *Polym Chem*, 2016, **7**, 4367–4377.

[15] S. Atta, J. Cohen, J. Kohn and A. J. Gormley, *Polym Chem*, 2021, **12**, 159–164.

[16] A. Stjerndahl, A. Finne-Wistrand, A. C. Albertsson, C. M. Bäckesjö and U. Lindgren, *J Biomed Mater Res A*, 2008, **87**, 1086–1091.

[17] E. Martin, P. Dubois and R. Jérôme, *Macromolecules*, 2003, **36**, 7094–7099.

[18] B. C. Wilson and C. W. Jones, *Macromolecules*, 2004, **37**, 9709–9714.

[19] N. Wanna, T. Kraithong, T. Khamnaen, P. Phiriyawirut, S. Charoenchaidet and J. Tantirungrotechai, *Catal Commun*, 2014, **45**, 118–123.

[20] W. Long, C. S. Gill, S. Choi and C. W. Jones, *Dalton Trans*, 2010, **39**, 1470–1472.

[21] C. Miola, T. Hamaide and R. Spitz, *Polymer*, 1997, **38**, 5667–5676.

[22] C. Miola, F. Delolme, I. Zanella-Cléon, G. Dessalces and T. Hamaide, *Polym Bull*, 1998, **40**, 541–548.

[23] M. Tarnacka, A. Dzienia, P. Maksym, A. Talik, A. Zi, R. Bielas, K. Kaminski and M. Paluch, *Macromolecules*, 2018, **51**, 4588–4597.

[24] M. Oshimura, A. Takasu and K. Nagata, *Macromolecules*, 2009, **42**, 3086–3091.

[25] J.-o. Lin, W. Chen, Z. Shen and J. Ling, *Macromolecules*, 2013, **46**, 7769–7776.

[26] P. Olsén, T. Borke, K. Odelius and A.-c. Albertsson, *Biomacromolecules*, 2013, **14**, 2883–2890.

[27] K. M. Van De Voorde, J. K. Pokorski and L. T. Korley, *Macromolecules*, 2020, **53**, 5047–5055.

[28] L. Peponi, I. Navarro-Baena, J. E. Báez, J. M. Kenny and A. Marcos-Fernández, *Polymer*, 2012, **53**, 4561–4568.

[29] F. S. Bates, M. A. Hillmyer, T. P. Lodge, C. M. Bates, K. T. Delaney and G. H. Fredrickson, *Multiblock polymers: Panacea or Pandora's box?*, 2012.

[30] J. Zhang, T. Li, A. M. Mannion, D. K. Schneiderman, M. A. Hillmyer and F. S. Bates, *ACS Macro Lett*, 2016, **5**, 407–412.

[31] A. Watts, N. Kurokawa and M. A. Hillmyer, *Biomacromolecules*, 2017, **18**, 1845–1854.

[32] D. K. Schneiderman, E. M. Hill, M. T. Martello and M. A. Hillmyer, *Polym Chem*, 2015, **6**, 3641–3651.

[33] D. K. Schneiderman and M. A. Hillmyer, *Macromolecules*, 2016, **49**, 2419–2428.

[34] G. L. Gregory, G. S. Sulley, L. P. Carrodeguas, T. T. Chen, A. Santmarti, N. J. Terrill, K. Y. Lee and C. K. Williams, *Chem Sci*, 2020, **11**, 6567–6581.

[35] L. P. Carrodeguas, T. T. Chen, G. L. Gregory, G. S. Sulley and C. K. Williams, *Green Chem*, 2020, **22**, 8298–8307.

[36] G. X. De Hoe, M. T. Zumstein, B. J. Tiegs, J. P. Brutman, K. McNeill, M. Sander, G. W. Coates and M. A. Hillmyer, *J Am Chem Soc*, 2018, **140**, 963–973.

[37] G. S. Sulley, G. L. Gregory, T. T. Chen, L. Peña Carrodeguas, G. Trott, A. Santmarti, K. Y. Lee, N. J. Terrill and C. K. Williams, *J Am Chem Soc*, 2020, **142**, 4378.

[38] S. Paul, Y. Zhu, C. Romain, R. Brooks, P. K. Saini and C. K. Williams, *Chem Commun*, 2015, **51**, 6459–6479.

[39] X. Deng, Z. Zhu, C. Xiong and L. Zhang, *J Polym Sci Pol Chem*, 1997, **35**, 703–708.

[40] M.-H. Huang, S. Li and M. Vert, *Polymer*, 2004, **45**, 8675–8681.

[41] M. K. Kang, Y. Jung and S. H. Kim, *Macromol Res*, 2013, **21**, 1036–1041.

[42] Q. Song, Y. Xia, S. Hu, J. Zhao and G. Zhang, *Polymer*, 2016, **102**, 248–255.

[43] B. H. Tan, J. K. Muiruri, Z. Li and C. He, *ACS Sustain Chem Eng*, 2016, **4**, 5370–5391.

[44] R. Feng, S. Jie, P. Braunstein and B. Li, *J Polym Sci*, 2020, **58**, 2108–2115.

[45] T. Rosen, I. Goldberg, W. Navarra, V. Venditto and M. Kol, *Angew Chem Int Edit*, 2018, **57**, 7191–7195.

[46] T. Rosen, I. Goldberg, V. Venditto and M. Kol, *J Am Chem Soc*, 2016, **138**, 12041–12044.

[47] M. T. Martello, D. K. Schneiderman and M. A. Hillmyer, *ACS Sustain Chem Eng*, 2014, **2**, 2519–2526.

[48] S. Thongkham, J. Monot, B. Martin-Vaca and D. Bourissou, *Macromolecules*, 2019, **52**, 8103–8113.

[49] S. Lee, K. Lee, J. Jang, J. Sun, W. Jin, G.-j. Kim, Y.-w. Kim and J. Shin, *Polymer*, 2017, **112**, 306–317.

[50] C. Chen, Z. Bai, Y. Cui, Y. Cong, X. Pan and J. Wu, *Macromolecules*, 2018, **51**, 6800–6809.

[51] C. Romain, Y. Zhu, P. Dingwall, S. Paul, H. S. Rzepa, A. Buchard and C. K. Williams, *J Am Chem Soc*, 2016, **138**, 4120–4131.

[52] P. K. Saini, C. Romain and C. K. Williams, *Chem Commun*, 2014, **50**, 4164.

[53] T. K. Saha, V. Ramkumar and D. Chakraborty, *Inorg Chem*, 2011, **50**, 2720–2722.

[54] N. E. Clayman, L. S. Morris, A. M. Lapointe, I. Keresztes, R. M. Waymouth and G. W. Coates, *Chem Commun*, 2019, **55**, 6914–6917.

[55] S. Naumann, P. B. V. Scholten, J. A. Wilson and A. P. Dove, *J Am Chem Soc*, 2015, **137**, 14439–14445.

[56] T. Rosen, Y. Popowski, I. Goldberg and M. Kol, *Chem - Eur J*, 2016, **22**, 11533–11536.

[57] C. Diaz and P. Mehrkhodavandi, *Polym Chem*, 2021, **12**, 783–806.

[58] B. M. Chamberlain, M. Cheng, D. R. Moore, T. M. Ovitt, E. B. Lobkovsky and G. W. Coates, *J Am Chem Soc*, 2001, **123**, 3229–3238.

[59] M. T. Martello, A. Burns and M. Hillmyer, *ACS Macro Lett*, 2012, **1**, 131–135.

[60] P. McKeown, S. N. McCormick, M. F. Mahon and M. D. Jones, *Polym Chem*, 2018, **9**, 5339–5347.

[61] J. Baran, A. Duda, A. Kowalski, R. Szymanski and S. Penczek, *Macromol Rapid Comm*, 1997, **18**, 325–333.

[62] M. Save, M. Schappacher and A. Soum, *Macromol Chem Phys*, 2002, **203**, 889–899.

[63] G. L. Gregory, G. Kociok-Köhn and A. Buchard, *Polym Chem*, 2017, **8**, 2093–2104.

[64] D. W. Grijpma, G. J. Zondervan and A. J. Pennings, *Polym Bull*, 1991, **25**, 327–333.

[65] O. Dechy-Cabaret, B. Martin-Vaca and D. Bourissou, in *Handbook of Ring-Opening Polymerization*, ed. P. Dubois, O. Coulembier and J.-M. Raquez, Wiley-VCH, Germany, 2009, ch. 10, pp. 255–286.

[66] I. D'Auria, M. C. D'Alterio, C. Tedesco and C. Pellecchia, *RSC Adv*, 2019, **9**, 32771–32779.

Chapter 5

Organocatalysis in Melt Conditions

5.1 Introduction

Simple organocatalysts

Homogeneous catalysts are known to be difficult to separate from the reaction mixtures. With polymers, the catalyst will become trapped in the final product causing metal residue impurities, with the added drawback that recovery of the catalyst is impossible. These residues can then promote side reactions over the course of the lifetime of the polymer, leading to degradation of the polymer properties. In addition, the toxicity of both the ligand and metal of the residual catalyst are brought into question.[1] When considering PLA as a polymer for use in the biomedical sector, it is important to either reduce the metal content in the final polymer, or find alternative biocompatible catalysts.

Although metal complexes have been exhaustively studied in the ROP of LA, several organocatalysts have also demonstrated excellent activity in ROP, and are summarised in many reviews.[2] Many benefits exist for using the latter over metal based catalysts, in particular their moisture tolerance, making them easy to handle without the possibility of degradation.[3] Their substrate tolerance is an added advantage, therefore they can be used with a multitude of different monomers.

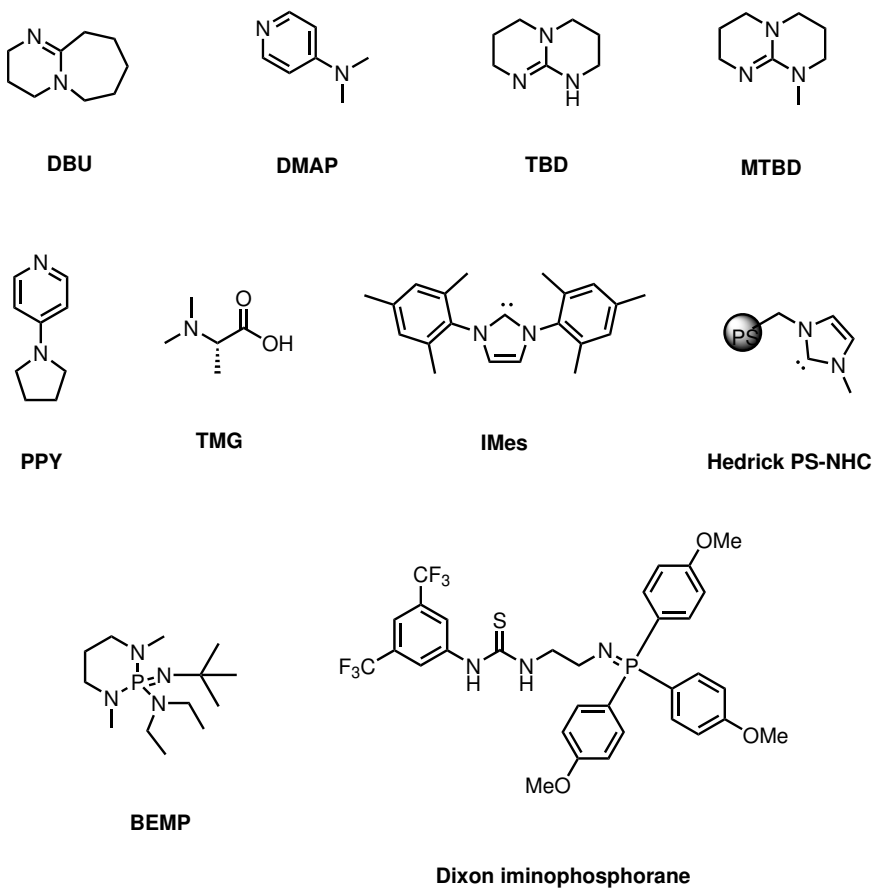

Scheme 5.1: Various bases used in the ROP of lactide.

Thus the more simple organocatalysts can generally fall into one of two "sub-groups": the nitrogen-based nucleophiles such as various amine bases and ureas, and the carbon-based nucleophiles, covering N-heterocyclic carbenes (NHCs),[4] organic acids and iminophosphoranes and phosphazines (Scheme 5.1).[5–8]

More relevant to the work described herein are the N-containing nucleophilic organocatalysts. The first example of the ROP of lactide with an organocatalyst was published by Hedrick and co-workers in 2001. In this work, 4-(dimethylamino)pyridine (DMAP) and 4-pyrrolidinopyridine (PPY) – two pyridine-based organocatalysts – were used in dichloromethane (DCM) at 35 °C.[9,10] Using an ethanol co-initiator, reaction times of over 24 hours were required to reach near quantitative conversion, reaching a degree of polymerisation of 29 after 60 hours ([LA]:[DMAP]:[EtOH] = 30:1:1, $Đ_M$ of 1.13). Molecular weights could be controlled by varying the catalyst loading, and when left to stir for up to 96 hours,

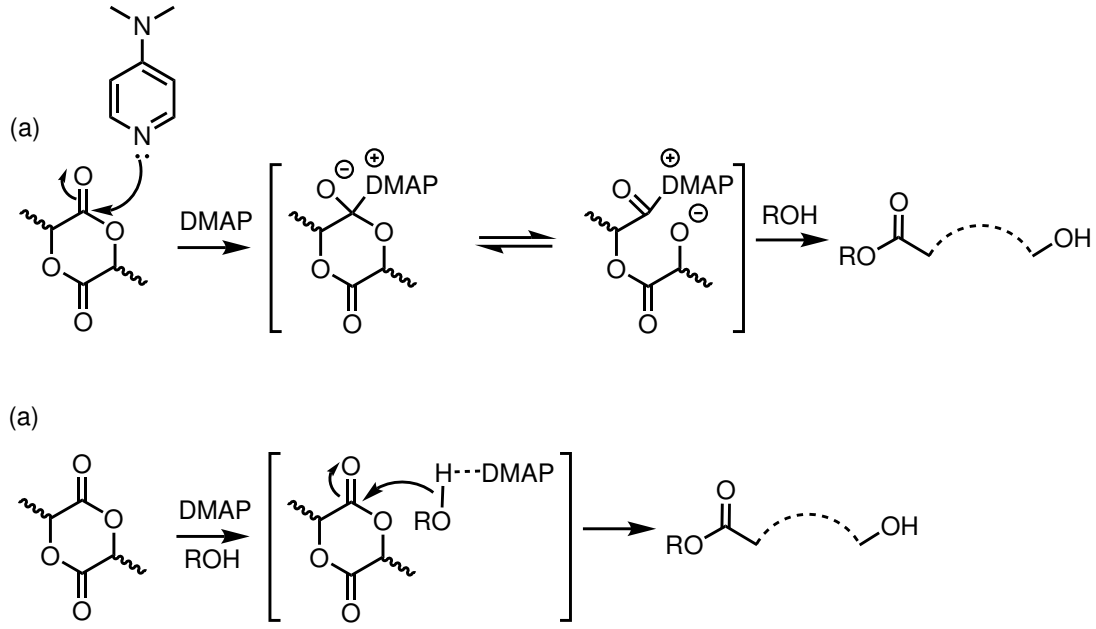

Scheme 5.2: Schematic representation of the (a) activated monomer mechanism undertaken by many organocatalysts, and (b) the alcoholic activation proposed to be the preferred route when using DMAP, adapted from Bourrissou and co-workers.[11]

the dispersity did not increase, indicating that transesterification was not present in the reaction. Increasing the amine loading led to a living polymerisation with quantitative yields and a low dispersities; when a [LA]:[DMAP]:[EtOH] ratio of 30:2:1 was used, the reaction time almost halved to 36 hours (DP = 29, $Đ_M$ 1.13). Melt ROP at 135 °C was complete within 20 minutes at a ratio of 100:4:1, and dispersities remained low ($Đ_M$ of 1.19). Similar results were obtained with PPY, albeit rates seemed marginally quicker; in solution-phase, it took 20 hours to reach 98% conversion at [LA]:[PPY]:[EtOH] = 30:2:1 ($Đ_M$ of 1.10), whilst melt conditions produced PLA within 20 minutes. A DFT study by Bourissou and co-workers indicated that DMAP showed a preference for the alcohol activation mechanism (activation of the co-initiator) over traditional monomer activation (direct nucleophilic activation of the lactone carbonyl) that is known for most organocatalysts (Scheme 5.2).[11]

The use of DMAP as a ROP catalyst initiated the investigation of many other simple organic "superbases" (extremely strong bases; the following examples have pK_a over 11 in THF):[12,13] 1,5,7-triazabicyclo[4.4.0]dec-5-ene (TBD), 7-Methyl-

1,5,7-triazabicyclo[4.4.0]dec-5-ene (MTBD) and 1,8-diazabicyclo[5.4.0]undec-7-ene (DBU).[14] In contrast to both DMAP and PPY, these use guanidine and amidine motifs.

At room temperature, DBU resulted in over 98% conversion ([LA]:[Cat] = 500:1, [LA] = 0.7 mol L^{-1} in chloroform), although transesterification was pronounced.[15] Whilst DBU adopts the same type of alcohol activation mechanism as DMAP, DBU ($^{DMSO}pK_a$ 12) is a notably stronger base than DMAP ($^{DMSO}pK_a$ 9.2).[16,17] Consequently, DBU is a stronger base leading to large amounts of both transesterification and epimerisation of the PLA, resulting in a significantly broader $Đ_M$ than that produced by DMAP. Despite the high activity of DBU, the latter did not show high monomer tolerance, and was inefficient at catalysing the ROP of smaller lactones such as δ-valerolactone (VL) without a thiourea additive (*vide infra*).[18,19]

Typically organocatalytic ROP has been carried out in the presence of solvent, however a solvent-free, "green" process was reported using DBU, TBD or MTBD as catalyst and 1,3-butanediol initiator in the preparation of short chain PLA (M_n<4 400 Da). Using DBU, 97% conversion was reached after three hours in the melt at 130 °C, and a low dispersity was maintained ($Đ_M$ 1.21).[5] DBU has also been used as a chain-extension catalyst (*i.e.* sequential addition of monomer units) in solution-phase ROP, following the ring-opening of the first lactone unit by a primary amine.[20]

With a similar pK_a to those of the NHCs (between 17-26),[21] TBD demonstrated a higher catalytic activity in the ROP of lactide in DCM compared to the other amine bases, as reported by Hedrick and co-workers.[18] 95% conversion was attained in one minute in DCM using [LA]:[Cat] = 500:1 (M_n 63 000 Da, $Đ_M$ 1.11). However, TBD, a stronger base than both DBU and DMAP ($^{H2O}pK_a$ 15),[22] and has only recently been shown to produce isotactic PLA in the ROP of *rac*-LA under cryogenic conditions (P_m = 0.88, −75 °C).[23] At more reasonable temperatures, however, it was noted to cause significantly more transesterification than the weaker superbases.[24] Leaving a reaction mixture unquenched also resulted in broadening of the dispersity.[21]

TBD has been widely used in the ROP of other lactones such as δ-decalactone

(δ-DL), δ-valerolactone (δ-VL) and ϵ-caprolactone (ϵ-CL), due to its high rates of polymerisation and stability at higher temperatures used in bulk polymerisations, although ROP of β-butyrolactone (β-BL) was unsuccessful.[21,25] Indeed block copolymers such as PLA-*b*-PDL-*b*-PLA triblocks were formed in the melt due to the selectivity of the catalyst, which showed preference for one monomer over another, demonstrating the versatility of this particular catalyst. Further to this, TBD has been found to catalyse the ROP of cyclic esters through a bifunctional activation mechanism. Where most organocatalysts have been known to solely activate either the monomer or the co-initiator, the structure of TBD, and the positioning of two of the three nitrogen atoms within the bicyclic structure allow it to hydrogen bond to both the monomer and the co-initiator.[14]

A methylated version of TBD, MTBD, showed lower activity, reaching near quantitative conversion in 30 minutes compared to the 20 second reaction TBD underwent under the same conditions (DCM, 1 mol% catalyst, [LA]:[I] = 100:1).[21]

Phosphazenes are another class of neutral organic base, which can, in contrast to the bases described above, be categorised as carbon-based nucleophiles.[7] Commercially available phosphazenes, including BEMP, have shown excellent activity in living ROP of cyclic esters, reaching 97% conversion after 66 hours ([*rac*-LA]:[Cat]:[I] = 100:1:1 in toluene, M_n 15 000 Da, $Đ_M$ 1.05).[8] However, only the ROP of of δ-VL was carried out in solvent-free conditions, the ROP of *L*- and *rac*-LA was carried out at room temperature in toluene. At low temperature (−75 °C), the phosphazene (P_2-*t*-Bu) was shown to be stereoselective in the ROP of *rac*-LA, reaching quantitative conversion after 180 minutes with a [LA]:[I] ratio of 100:1 and 1 mol% catalyst (M_n 27 200 Da, $Đ_M$ 1.11, P_i 0.95).[26]

NHCs have also been extensively studied in the ROP of cyclic carbonates,[27] epoxides[28] and, more relevantly, lactones.[29,30] The high activities of these catalysts have frequently been demonstrated in the synthesis of small molecules. NHCs were first used in the solution-phase living ROP in THF at room temperature (25 °C), reaching quantitative conversion after 2 hours ([LA] = 1 mol L^{-1}).[31] Varying the monomer-to-initiator ratio did not affect the dispersity, which remained consistently low, indicative of good polymerisation control, although transesterification increased at higher conversions ($Đ_M$ between 1.08-1.15 using benzyl alcohol as the co-initiator, I, up to [LA]:[Cat]:[I] = 200:1.5:1). It was proposed that the

likely mechanism went *via* an anionic activated monomer route, whereby protonation of the NHC by the alcohol initiator creates an anionic alkoxide, which is then free to activate the monomer.

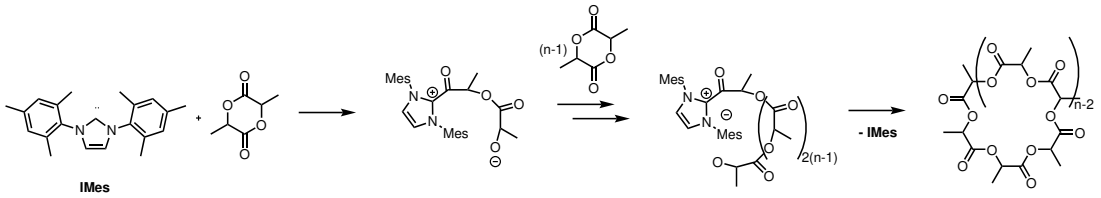

Scheme 5.3: Zwitterionic mechanism towards cyclic PLA with NHC catalysts, proposed by Waymouth and co-workers.[4,32]

The stereoelectronics of the NHC were shown to influence ROP activity and control.[29,33] By varying the substituents and heteroatom within the ring, it was evident that less sterically bulky NHCs were more active in the ROP of LA. Saturated NHC backbones demonstrated similar activity compared to their unsaturated counterparts, however they could be synthesised *in situ* (15 minutes in THF at 20 °C using a KO^{t}Bu initiator, [LA]:[Cat]:[I] = 200:1.5:1, [LA] = 0.16 mol L^{-1}, >85% conversion, $Đ_M$ 1.18-1.25). Importantly, the same study also highlighted the importance of solid-supported catalysts as a way to drive progress in the field; their only example of a PS-supported NHC resulted in a less controlled ROP ($Đ_M$ 1.52 after one hour), suggesting that there is significant room for improvement in this field.[33] By exploiting the structure of the NHCs, it was possible to promote zwitterionic ROP to produce exclusively cyclic PLA (Scheme 5.3).[4,32]

Despite their success and ability to modify these, NHCs are highly air sensitive, deactivating rapidly if in contact with water, making them hard to both store and manipulate, particularly on an industrial scale. This is perhaps why immobilisation of catalysts onto a solid support has been mentioned as the way forward with these catalysts,[29,33] otherwise other more stable catalysts are preferred.

For many years organocatalytic ROP was dominated by the likes of Hedrick, Waymouth, Dove and others, who propelled research around "superbases" and NHCs forward, as described above. Recently, however, research has branched into other classes of organocatalyst.

Many organocatalysts have not been applied to the ROP in solvent-free conditions, leaving a large amount of scope to improve these processes. As an example, the bulk ROP of cyclic carbonates at 70 °C was recently achieved using trimethyl glycine (TMG).[34] Along with its low toxicity, TMG is reportedly readily available and bio-derived. Its zwitterionic nature comprising of an carboxylate anion and ammonium cation, which simultaneously activate the alcohol (*via* H-bonding to the anion) and carbonyl group of the cyclic carbonate (*via* H-bonding to the cation). Conversions between 74 and 89% were attained depending on the initiator used, with consistently low dispersities ($Đ_M$ 1.13-1.23), and a variety of different architectures possible. These results suggest that there is potential to extend these types of system to cyclic esters.

Bifuctional organocatalysts

It is clear that simple organocatalysts have been used successfully in ROP procedures, with activities often matching those of organometallic catalysts. However, even with the most successful of these, problems do still arise. Strong "superbases" such as TBD and DBU are prime examples of this: despite its high activity, TBD lends itself to undesirable side reactions at high conversions, including transesterification, due to its high basicity. Further, several of these simple organocatalysts have limited monomer scope, and are unable to catalyse the ring-opening of smaller or larger lactones.

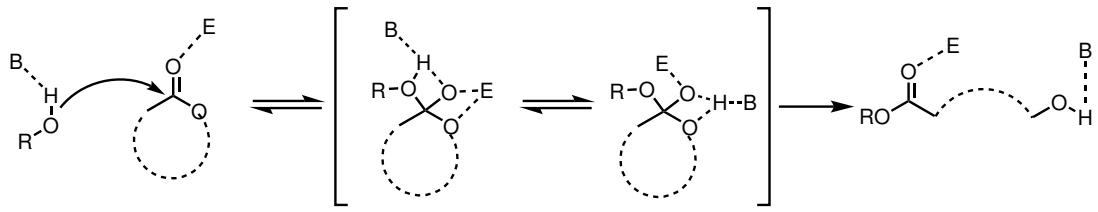

Scheme 5.4: General mechanism of bifunctional activation of both the monomer by an electrophile (E) and initiator or chain end by a base (B).[2]

Bifunctional catalytic systems have been explored in order to increase the control in ROP by exploiting dual activation of both the monomer (by an electrophile) and of the co-initiator (by a nucleophile, Scheme 1.3).[6,35] For this reason, interest in bifunctional catalysis has recently overtaken simple organocatalysis.

Comprising of two opposing functionalities, which activate the monomer and co-initiator (or the growing polymer) separately and simultaneously (Scheme 5.4), bifunctional catalysts can therefore display significantly higher activity and selectivity than their monofunctional counterparts through synergistic, cooperative effects.[6,19]

There have been numerous examples of bifunctional ROP catalysts have been explored over the past decade, including Lewis pairs,[36] and amine/Lewis acid (of the form MX_n) combinations.[19] A list of the bifunctional catalysts described in Chapters 5 and 6 can be found at the end of the introduction in Chapter 6. These dual catalysts can either be intra- or extramolecular, where the two functional groups are either tethered together within the same molecule, or are two separate components, respectively. TBD, while classified as a simple, commercially available nucleophile, is an example of the former, as mechanistic studies have shown that it operates through dual activation.

Often, research has focused on combination of a nucleophilic bases such as DBU, DMAP or phosphines with a metal-based Lewis acid such as $Al(O^iPr)_3$, the earliest example occurring in 1997.[37] Combination of DMAP or an NHC with classic Lewis acids such as $MgCl_2$, $SnCl_2$ and $AlCl_3$ was explored to evaluate the effects of both components on the ROP of PDL (ω-pentadecalactone).[19] When used independently, neither $MgCl_2$ nor the NHC initiated ROP. When an NHC-adduct of $MgCl_2$ was used, a high activity was observed after 6 hours, using ranges of [PDL]:[$MgCl_2$]:[BnOH] up to 200:1:1 in toluene ([M] = 1 mol L^{-1}, 110 °C). Dispersities were significantly higher than typical organometallic or organocatalysts ($Đ_M$ 1.80-2.50); thermal dissociation of the NHC from the Lewis acid provided the dual activation of the chain end and the carbonyl group of the monomer. Similar results were obtained when the two components were added separately to the reaction medium, rather than as a preformed adduct. When the Lewis acids were combined with less nucleophilic bases such as DMAP (in comparison with the NHC), a similar dual activation was seen. Heavier Mg halides displayed higher polymerisation rates than $MgCl_2$, regardless of base used, resulting in an order of reactivity of $MgI_2 > MgBr_2 > MgCl_2$; larger differences between the bases were thought to be partly due to the complexation of the free base to the Lewis acid, reducting the concentration of "active" catalyst. Combination of the

MgI_2 with DMAP or DBU – more robust and available bases – immediately improved their activity in ROP: within two hours, 95% conversion of both PDL and CL was possible compared to its relatively low monomer monomer tolerance without the use of MgI_2.

Excellent activity was also attained when using the $Zn(C_6F_5)_2$/DBU Lewis pair in the ROP of PDL, with no transesterification ($M_n > 100$ kDa).[36] Defined block copolymers with CL and LA were possible, yet little research was conducted into the application of these catalysts in the homopolymerization of LA. The high dispersities of PPDL were another disadvantage to the Lewis pair.

Some of the more successful bifunctional catayst have been derived from Brønsted acids and bases, containing a H-bond donor and acceptor functionality. Bibal and co-workers, for example, reported the use of phenols substituted with electron-withdrawing groups (H-bond donors) coupled with simple tertiary amines as the H-bond acceptor. Transesterification was not observed, and the polymerisations appeared well controlled, with low dispersities ($Đ_M$ <1.09) and M_n close to the theoretical value. No evaluation of the activity of the individual components was performed ([LA] = 0.7 mol L^{-1} in CH_2Cl_2, 20 °C, 24 h).[35]

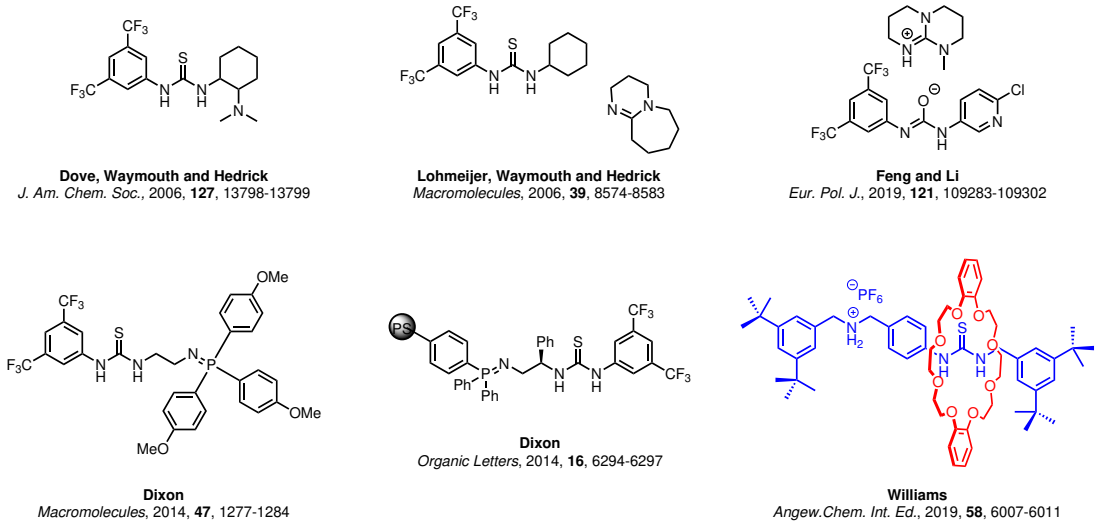

Scheme 5.5: Examples of varying (thio)urea structures throughout literature.

Perhaps the most well known of these H-bonding systems are the ureas (U) and thioureas (TU, Scheme 5.5). Recent developments in U and TU bifunctional systems offer an interesting insight into the future of controlled ROP by organocata-

lysts. Two component systems comprising of a thiourea or urea (denoted herein as "(T)U") and an amine (either intramolecular or extragenous) enable simultaneous activation of the alcohol co-initiator and monomer through H-bonding *via* the amine proton and the (T)U secondary amine, respectively (Scheme 5.6). ROP was shown to proceed *via* the bifunctional activation of the monomer through H-bonding of the N−H groups of the lactide carbonyl, with simultaneous activation of the co-initiating alcohol through H-bonding to amine.[38] Attack of the C=O by the alcohol was identified as the initiating stage of nucleophilic ROP, followed by chain extension with other units of monomer.

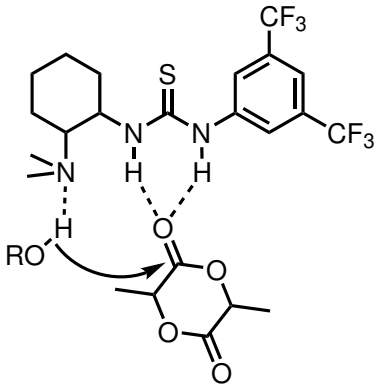

Scheme 5.6: TU/amine bifunctional activation mechanism.[15]

Selectivity is imparted through the preferential H-bonding of the monomer carbonyl over that of the growing polymer chain. These reactions have only been performed in solution-phase, using non-polar solvents to avoid competitive H-bonding and quenching of the catalyst, and enabling good contact between the two co-catalysts. A summary of the results from the various (thio)urea/base combinations that shall be discussed in Chapters 5-6 can be found in Table 6.1.

Williams, Beer and co-workers developed an isoselective [2]rotaxane catalyst comprising of a macrocycle encompassing an axle.[39] The latter was made up of an ammonium cation and a TU or triazole terminal group. When used on their own, the rotaxanes were inactive in the ROP of LA. Once combined with a base, deprotonation of the rotaxane ammonium generated the active catalyst. Extensive NMR studies showed deprotonation of the ammonium created macrocycle fluxionality along the axle, as it was no longer held in place through H-bonding to the cation. The catalysts therefore displayed high stereoselectivity, up to P_i =

0.8 (80% conversion in 96 hours at room temperature, [LA] = 1 mol L^{-1} in THF, M_n 5 800 Da, $Đ_M$ 1.08), compared to $P_i = 0.56$ when the rotaxane was not added. Altering the terminal group by replacing the TU with a weaker H-bonding triazole reduced stereoselectivity (P_i 0.66), as did using a sterically hindered TU (P_i 0.73). The catalysts were suggested to proceed *via* a chain-end control mechanism, resulting in catalyst with comparable isoselectivities to those of many metal based catalysts and complex, chiral organocatalysts.

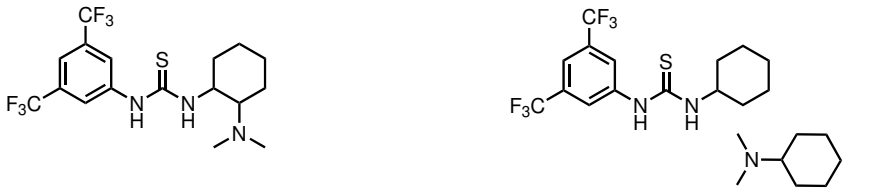

$[LA]_0$ = 0.7 mol L^{-1} ($CDCl_3$), [LA]/[I] = 100:1
25 °C, 24 h
51 % ($M_n/Đ_M$ *not detected*)

$[LA]_0$ = 0.7 mol L^{-1} ($CDCl_3$), [LA]/[I] = 100:1
25 °C, 72 h
98 %, M_n 17 800 Da, $Đ_M$ 1.09

Scheme 5.7: Literature examples of discrete and paired TU/amine systems.[15,38]

TUs have also been coupled with amines to produce dual functionality; the amine can either be directly connected to the TU or be added into the reaction as an exogenous entity (Scheme 5.7). Control experiments using either the TU or the amine demonstrated that both components were necessary to get the dual activation of the monomer and initiator, thus promoting ROP.[15] The TU moiety has been reported to have a higher affinity (through intermolecular recognition) for the lactone ester over the ester of the growing polymer chain, resulting in the low levels of transesterification observed with these catalysts.[15,40]

Varying the TU structure has also been studied by substituting the phenyl ring on their thiourea systems with electron withdrawing groups.[41] One study emphasised the importance of (T)U flexibility of the second substituent: some flexibility was required to allow optimal cooperation between the Lewis acid and base co-catalysts, whilst too much flexibility could create an unwanted adduct, neutralising both components, although this issue is likely more problematic when the amine is tethered to the (T)U.[15] Placing the latter at the 3- and 5-positions of the phenyl ring promoted catalytic activity by enhancing the acidity of the TU, thus

promoting electrophilic activation of the monomer. It was possible to reach 98% conversion over 72 hours with an M_n 17 800 Da ($Đ_M$ 1.09), using $NCyMe_2$ as the co-initiator.[15] Replacing the sulfur atom with an oxygen, creating a urea, resulted in slightly lower activity due to solubility issues, although the structure of the urea was not varied to investigate whether this changed with substituent. Indeed, later research indicated preference towards the urea for better stereocontrol and speed.[42]

Varying the tertiary amine also had significant effects on the catalytic activity. When DMAP was used in conjunction with the TU, conversions reached 94% over 48 hours ([LA] = 0.7 mol L^{-1}, $CDCl_3$, 25 °C) with a high degree of stereocontrol (M_n 23 000 Da, $Đ_M$ 1.06); absence of the TU yielded poor results.[15] Both discrete and paired catalyst systems have been reported with the amine attached to the TU or separated, and both have been shown to provide low dispersities (<1.08).[24] Furthermore, TU combination with strong bases such as DBU and TBD have been shown to improve the monomer tolerance of these bases (*e.g.* functionalised carbonates), whilst also mitigating their tendency to transesterify the polymers. A monomer preference of LA>VL>CL was found for TU/DBU systems, with 95% of the first monomer consumed before the second, opening up a route to well defined block copolymers.[18]

Similarly, Dixon and co-workers synthesised a TU with a tethered electron withdrawing group on one side and a phosphine based group on the other. The iminophosphorane was used in the ROP of various lactones: 99% conversion of LA was achieved in under an hour for [LA]:[Cat]:[I] ratios of up to 500:1:1, and excellent dispersities.[43] Heterogeneous analogues through immobilisation of the iminophosphorane onto a PS-support were also reported, however these were only applied to the nitro-Mannich reaction.[44] Nevertheless, this is precedent for the immobilisation of ureas onto an inert PS-support, to be used in ROP procedures.

Notably, a pyridyl-urea catalyst was combined with MTBD to create a bifunctional catalyst which was used in the bulk polymerisation of various lactones.[45] At a ratio of [VL]:[U]:[MTBD] = 200:1:1, 99% conversion of δ-VL to PVL was attained after 10 minutes at room temperature. Similar results were achieved in combination with TBD, although when the pyridyl-urea catalyst was combined with DBU, only 47% conversion was possible. NMR studies revealed that

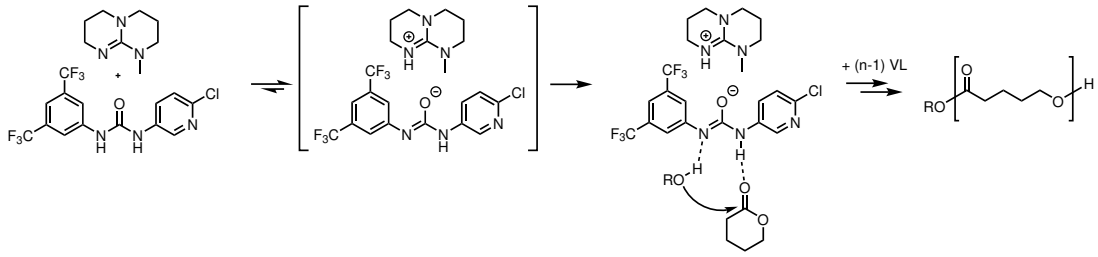

Scheme 5.8: Proposed zwitterionic mechanism of pyridyl-urea cataysts for the ROP of valerolactone (VL), when used in conjunction with MTBD.[45]

the mechanism likely proceeded *via* a zwitterion formed through protonation of MTDB, generating an anionic urea (Scheme 5.8). The pyridyl component of the urea was also shown to affect the activity of the catalyst: when electron donating groups were substituted onto the pyridyl ring, only 77% conversion was reached, while sterically bulky groups did not affect activity. Location of the N-atom *meta* to the tethering carbon atom within the ring was also key to maximising activity. To our knowledge, this is one of the very few bifunctional catalysts used in solvent-free ROP.

Although this research focused on amine-based bifunctional (thio)ureas, interest in the latter has exploded in recent years. Recently, for example, (T)Us have also been used in conjunction with other bases phosphazenes,[46] iminophosphoranes[47] and NHCs[41] tethered to the (T)U structure, building on the success of these bases seen earlier. Yuan *et al.* designed a thiourea using a similar skeleton framework as the Dove/Waymouth catalysts,[38] replacing the tethered amine with a tethered ^{t}BuP$_2$ phosphazene.[46] In 10 hours, the catalyst demonstrated controlled ROP of *rac*-LA (99%, M_{n} 3 900 Da, $Đ_{\mathrm{M}}$ 1.12), yielding PLA with a slight isoselective bias (P_{m} 0.70, [LA]:[Cat]:[I] = 50:0.25:1, [LA] = 1 mol L^{-1} in CH_2Cl_2 at room temperature). Similarly results were observed when a tethered iminophosphorane was used.[47] Extensive reviews of other combinations of (thio)urea and bases is available,[48,49] although the relevant catalysts have been covered.

5.2 Aims

The aim to create immobilised catalysts is part of an overall effort to implement this class of catalyst into flow reactors for continuous production of polymer of

high purity. The following chapter shall explore the implementation of similar bifunctional systems to those discussed above, into solvent-free ROP, using heterogeneous versions of both the amine and the urea.

Initially, efforts towards immobilising the amine component of these bifunctional systems is described, including a study exploring control reactions omitting the use of urea (U) co-catalyst or solvent. Commercially available heterogeneous amines were tested in the solvent-free ROP of *L*-LA, with a focus on the monitoring of the reaction kinetics and the stereoselectivity of these bases. Their activities were subsequently compared to those of the homogeneous analogues to gain a greater understanding of the effect of the support on the catalytic activity.

Once a good understanding was obtained, the attention will then turn towards immobilising the U component of the ideal co-catalyst system. Systematic investigations of the various combinations of heterogeneous U with homogeneous or heterogeneous amine (and the same again with homogeneous U) were carried out, enabling the development of the optimal heterogeneous co-catalyst system.

5.3 Results and discussion

Commercial immobilised amines

Simple amine-polystyrene resins

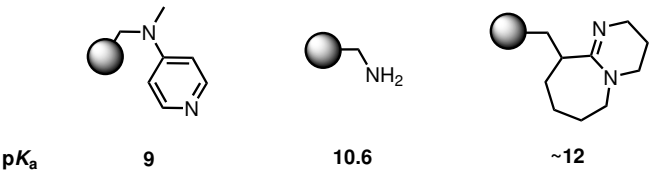

Scheme 5.9: The three different amine bases and the pK_as of their homogeneous counterparts: 4-Dimethylaminopyridine (DMAP, left), (Aminomethyl)polystyrene (middle) and 1,8-Diazabicyclo(5.4.0)undec-7-ene (DBU, right).

Three commercially available immobilised organocatalysts, of varying basicity, were purchased for use in the ROP of *L*-lactide (Scheme 5.9). Of these, 4-Dimethylaminopyridine (DMAP) and 1,8-Diazabicyclo(5.4.0)undec-7-ene (DBU) have previously been successful as homogeneous catalysts for the same process,

obtaining quantitative conversions and low $Đ_M$. Heterogenised DBU on PS has previously also been used as immobilised bases for *meso*-lactide epimerisation in EtOAc at room temperature, although no information was given about its efficacy as a ROP catalyst.[50]

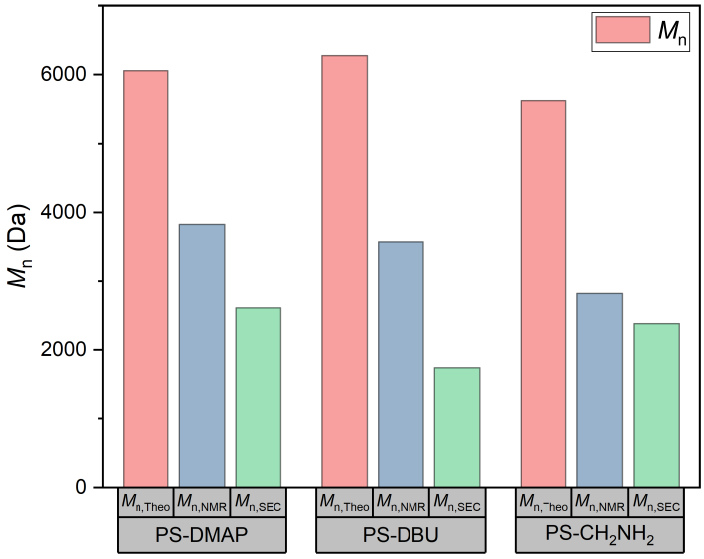

Figure 5.1: Results from ROP of *L*-LA with PS-DBU, PS-DMAP and PS-CH_2NH_2. Conditions: [LA]:[Cat]:[I] = 50:1:1, 130 °C, 24 hours in the melt.

From initial screening in the melt at 130 °C over 24 hours ([LA]:[Cat]:[I]= 50:1:1), it was evident whilst both DMAP and DBU produced PLA in relatively high conversions (∼85%), the dispersities were higher than seen with the metal complexes ($Đ_M$ 1.37-2.24, Table 5.1, Figure 5.1). Control reactions omitting the catalyst and initiator did not produce any PLA ([LA]:[Cat]:[I] = 50:0:1 and 50:0:0). Use of DMAP and DBU also resulted in high amounts of epimerisation, evidenced by the scrambling of the methine signal pertaining to the PLA quartet at 5.18 ppm, which was modest for PS-CH_2NH_2. A comparison of the ^{1}H NMR spectra of the crude PLA formed using PS-CH_2NH_2 and PS-DMAP is highlighted in Figure B.25. Although the $^{DMSO}pK_a$ of DMAP is 9.6,[17] immobilisation of the base may alter the basicity somewhat; the pK_a is potentially increased on immobilisation, leading to significant amounts of epimerisation of the starting monomer, *L*-lactide, although other factors including the rate of exchange with the alcoholic

Table 5.1: Polymerisation data from the ROP of *L*-LA with PS-DBU, PS-DMAP and PS-CH_2NH_2. Conditions: [LA]:[Cat]:[I] = 50:1:1, 130 °C, 24 hours in the melt (Figure 5.1).

Entry	Catalyst	Conv. (%)[a]	$M_{n,Theo}$[b]	$M_{n,NMR}$[a]	$M_{n,SEC}$[c]	$Đ_M$[c]
1	PS-DMAP	84	6050	3800	2600	2.24
2	PS-DBU	87	6250	3550	1740	1.40
3	PS-CH_2NH_2	78	5600	2800	2400	1.37

[a] Determined from the ^{1}H NMR spectrum.
[b] Theoretical M_n= ([LA]/[I]) × (144 × equiv. LA) × (conv./100).
[c] As determined by SEC (THF) using RI methods, relative to poly(styrene) standards (multiplied by a factor of 0.58, rounded to the nearest 50).[51]

initiator could also affect the activity. In theory, both PS-DMAP and PS-DBU would modify the tacticity during the ROP of *rac*-lactide, resulting in a lack of stereocontrol.

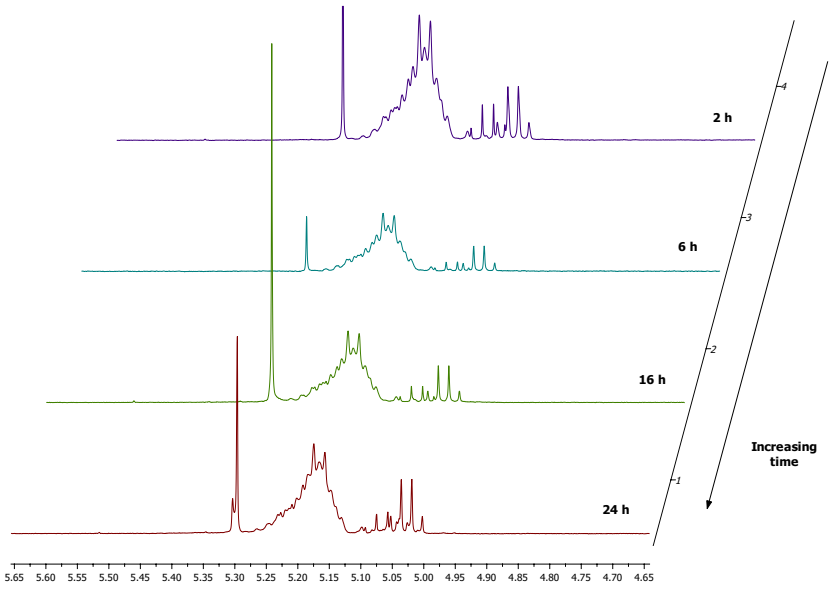

Figure 5.2: ^{1}H NMR spectra ($CDCl_3$, 400 MHz) of the methine region of PLA produced within 2, 6, 16 and 24 hours (top to bottom), with high levels of epimerised product, even at shorter ROP timescales, with PS-DBU.

Following this, the ROP of *L*-lactide using PS-DBU was carried out at 2, 6 and 16 hours to monitor epimerisation and polymerisation over time (Figure 5.2). Although high activity was retained at shorter times, epimerisation was still prominent, indicating that epimerisation was occurring simultaneously to

propagation, rather than occurring once ROP was complete, and a by-product of catalyst residue within the final polymer matrix. ROP control was poor, with erratic fluctuation of the M_n and $Đ_M$.

MALDI-ToF Mass Spectrometry analysis of all the polymers produced with each organocatalyst revealed that the PLA was capped with H^+ and $MeBnO^-$ and a sodium cation, as expected. Some transesterification was observed in all cases, however a series corresponding to cyclic PLA was also observed with PS-DBU (Table 5.2, Figures B.39-B.41).

Table 5.2: MALDI-ToF Mass Spectrometry analysis summary of the PLA produced with the immobilised amine bases in the melt ([LA]:[Cat]:[I] = 50:1:1, 130 °C, 24 hours).

Catalyst	**Series**	**Repeat Unit (g/mol)**	M_n	End Groups	**n (number of units)**
PS-DMAP	1_{Major}	144.11	1295.78	$MeBnO^-/H^-/Na^+$	8
PS-DMAP	2_{Minor}	72.11	1223.42	$MeBnO^-/H^-/Na^+$	7.5
PS-CH_2NH_2	1_{Major}	144.11	1728.39	$MeBnO^-/H^-/Na^+$	11
PS-CH_2NH_2	2_{Minor}	72.11	1800.64	$MeBnO^-/H^-/Na^+$	11.5
PS-DBU	1_{Major}	144.11	1007.16	$MeBnO^-/H^-/Na^+$	6
PS-DBU	2_{Minor}	72.11	1079.26	$MeBnO^-/H^-/Na^+$	6.5
PS-DBU	2_{Cyclic}	-	1029.19	$MeBnO^-/H^-/Na^+$	6

In contrast to PS-DMAP and PS-DBU, PS-CH_2NH_2 produced PLA with little to no epimerisation in good conversions, with higher M_n. Further to this, the dispersity using PS-CH_2NH_2 was lower in comparison to the $Đ_M$ obtained when using PS-DMAP or PS-DBU ($Đ_M$ 1.37 compared to 2.24 with PS-DMAP).

For all amine catalysts, it was observed that the theoretical molecular weight ($M_{n,Theo}$) was double the value obtained by ^{1}H NMR spectroscopy. This suggested that either double the initiator had not been added to the reaction or that both the alcohol and the amine were initiating polymerisation (entries 1-3, Table 5.3). It was therefore necessary to ensure that the integrals of the PLA and initiator peaks were quantitative and gave accurate M_n determination. A ^{1}H NMR T1 delay experiment was set up, modifying the parameters of the typical pulse sequence to a 90° pulse, with 16 scans and T1 delay of 15 seconds, to allow all of the proton spins to fully relax before the new scan. Results from the modified NMR showed very little change in the resulting integrals, indicating that the standard ^{1}H NMR spectroscopy was also quantitative, and no correction factor was necessary.

Table 5.3: Polymerisation data from the ROP of *L*-LA with immobilised amines in the melt at 130 °C for 6 hours (entries 1-3), 4 hours (entry 4) and 24 hours (entries 5-6).

Entry	Catalyst	Initiator	[LA]:[Cat]:[I]	Conv. (%)[a]	$M_{n,Theo}$[b]	$M_{n,NMR}$[a]	$M_{n,SEC}$[c]	M_n[d]	$Đ_M$[c]
1	PS-CH_2NH_2	MeBnOH	50:1:1	55	4000	1850	2350	2000	1.12
2	PS-DMAP	MeBnOH	50:1:1	84	3800	3800	2600	1300	2.24
3	PS-DBU	MeBnOH	50:1:1	87	6250	3550	1750	1000	1.40
4	PS-CH_2NH_2	MeBnOH	50:1:2	74	2650	1250	1900	-	1.16
5	PS-CH_2NH_2	MeBnOH	50:1:0.5	57	8200	2050	2300	-	1.13
6	PS-CH_2NH_2	Neopentyl alcohol	50:1:1	61	4400	-	1800	-	1.09

[a] Determined from the ^{1}H NMR spectrum.
[b] Theoretical M_n= ([LA]/[I]) × (144 × equiv. LA) × (conv./100).
[c] As determined by SEC (THF) using RI methods, relative to poly(styrene) standards (multiplied by a factor of 0.58, rounded to the nearest 50).[52]
[d] As determined by MALDI-ToF Mass Spectrometry .

The SEC and MALDI-ToF Mass Spectrometry results supported the M_n values given by NMR analysis. Experiments halving and doubling the amount of initiator used returned the same results ([LA]:[Cat]:[I] = 50:1:2 and 50:1:0.5, entries 4-5, Table 5.3). Changing the initiator to neopentyl alcohol (to monitor the PLA integral against a different initiator peak) also did not provide any explanation for the difference in the expected and obtained M_n (entry 6, Table 5.3). The [LA]:[I] ratio of 50:2 from the ^{1}H NMR implied that instead of each initiating molecule activating one lactide monomer, the initiator would only activate half of the lactide monomers in the reaction, suggesting that perhaps the PLA was also growing straight from the immobilised amine; to verify this, varying the catalyst:initiator ratios could be tested.

In situ ATR-FT-IR Kinetics

Of the three commercially available bases, (aminomethyl)polystyrene was the most promising, with low dispersities ($Đ_M$ 1.12-1.32) and little epimerisation. Due to both the viscosity of the polymer system, high temperatures and heterogeneous nature of the catalyst, the kinetics could not be monitored on the NMR reaction scale. Therefore, using a standard procedure and the same batches of initiator, catalyst and *L*-lactide throughout, parallel (batch) kinetics were carried out at varying times to monitor the changes in molecular weight and dispersity. The ROP of *L*-lactide with PS-CH_2NH_2 was carried out at 2, 4, 6, 8, 16 and 24 hours (Figure 5.3).

An increase in the M_n from both ^{1}H NMR and SEC was detected, reaching a

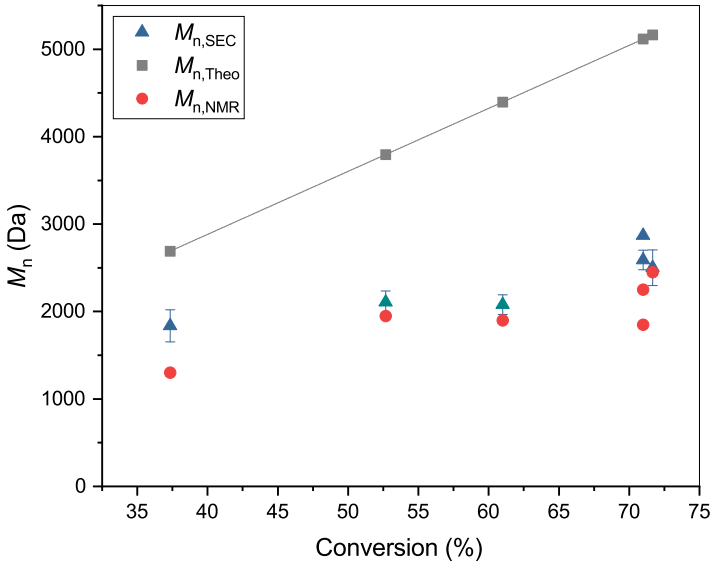

Figure 5.3: Parallel batch kinetics were carried out the melt at 130 °C over 2, 4, 6, 16 and 24 hours, with each time point repeated in triplicate, yielding an overall mean M_n. After 8 hours, conversion visibly plateaus at 70%. [LA]:[Cat]:[I] = 50:1:1.

plateau after 6 hours, where the conversion reached a maximum of 72%. This could be due to the increasing viscosity of the reaction system and mass transfer limitations when using heterogeneous catalysts, such that ROP reached the maximum conversion for this system under these conditions. At times beyond 6 hours, whilst the conversion did not increase, the $Đ_M$ broadened to ~1.30 from the steady dispersity of ~1.15 at shorter times. Once more, the difference between the theoretical and experimental M_n is evident, however the difference becomes prominent at higher reaction times. Coupled with the increase in dispersity, it is suggested that without quenching the reaction system at elevated times (beyond 6 hours), the catalyst can take part in multiple side reactions such as transesterifications and backbiting, causing a significant drop in molecular weight, thereby deviating from the expected molecular weight.

Further investigation by *in situ* ATR-FT-IR was initially conducted at the standard [LA]:[Cat]:[I] ratio of 50:1:1, with the reaction scaled up by three times to ensure coverage of the IR probe. At larger scales, problems emerged due to swell-

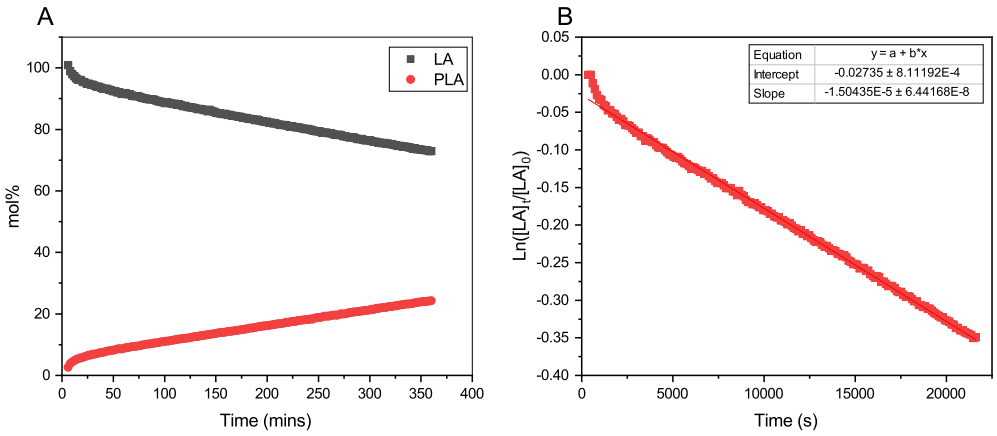

Figure 5.4: (A) Conversion (related to peak area) of lactide and PLA mol% against time, and (B) Semi-logarithmic plot of the concentration of lactide against time, monitored by *in situ* ATR-FT-IR using PS-CH_2NH_2, [LA]:[Cat]:[I] = 50:0.25:1, 130 °C, 6 hours in the melt.

Table 5.4: Comparison of the k_{obs} of each catalyst, extracted from the kinetic data from *in situ* ATR-FT-IR.

Entry	**Catalyst**	$\boldsymbol{k_{obs}}$ **(s^{-1})**	**Relative $\boldsymbol{k_{obs}}$**
1	PS-CH_2NH_2	1.48×10^{-5}	1
2	**PS-L^{H}ZnOAc**	1.38×10^{-4}	9.5
3	**PS-L^{H}SnOct**	7.56×10^{-4}	51

ing of the fine powder catalyst in the molten LA, which solidified significantly once swollen, that magnetic stirring could not mix successfully, blocking the reaction progress. The amount of catalyst was therefore scaled down to 200:1:4 to reduce this problem. A new ATR-FT-IR study over 6 hours was used to extract the observed rate constant for the reaction. While the mol% against time graph could be interpreted as zeroth order, the reaction was assumed to be first order with respect to monomer, in line with literature – a linear semi-logarithmic plot for the reaction was also observed to support this (Figure 5.4A). It was immediately apparent that PS-CH_2NH_2 was far slower in comparison to the metal catalysts described in Section 2.1.4, with a k_{obs} 1.48×10^{-5} s^{-1}. From Table 5.4, it is evident that the **PS-L^{H}ZnOAc** catalyst was ∼9 times faster, whilst the immobilised tin octoate catalyst, **PS-L^{H}SnOct**, was ∼50 times faster than the

amine catalyst, using the same ratios of lactide, catalyst and initiator.

Furthermore, the ROP appeared to occur in two stages involving a fast initiation step (k_{obs} 5.37×10^{-5} s^{-1}, Figure 5.4B), before levelling out to produce a polymer in 28% conversion (M_n 1 300 Da, $M_{n,\,Theo}$ 2 000 Da, $Đ_M$ 1.18). The low conversion was attributed to the decreased catalyst loading used in the *in situ* kinetic study compared to the batch kinetics.

Catalyst recovery

In contrast to the metal imine catalysts, all of the amine catalysts were fine powders, creating difficulty in recovery. Like the amine metals coordinated to ligands **5** and **6**, recovery through filtration was limited, as the catalyst could be trapped in the frit of the sinter or lost in a syringe filter, meaning reuse was prevented. Unlike batch processes, the powdered morphology of the catalyst would not be problematic in a flow set-up, as many catalyst such as zeolites are pelletised prior to use in a catalyst bed.

Table 5.5: Comparison of polymerisation data from the ROP of *L*-LA with various PS$-CH_2NH_2$ catalysts, using [LA]:[Cat]:[I] = 50:1:1 in the melt at 130 °C.

Entry	Catalyst	Loading (mmol/g)	Conv. (%)[a]	$M_{n,Theo}$[b]	M_n[a]	M_n[c]	M_w[c]	$Đ$[c]
1	PS-CH_2NH_2	0.60	86	6200	4650	3250	3900	1.37
2	PS-CH_2NH_2	4.00	27	1950	1450	-	-	-
3	BZA[d]	7.00	12	850	700	-	-	-
4	PS-CH_2NH_2[e]	4.34	38	2750	1250	1700	1800	1.13
5	PS-CH_2Cl	5	4	450	-	-	-	-

[a] Determined from the ^{1}H NMR spectrum.
[b] Theoretical M_n = ([LA]/[I]) × (144 × equiv. LA) × (conv./100).
[c] As determined by SEC (THF) using RI methods, relative to poly(styrene) standards (multiplied by a factor of 0.58, rounded to the nearest 50).[52]
[d] Quadrapure beads obtained from Sigma-Aldrich, where BZA = benzylamine.
[e] PS-CH_2NH_2 beads synthesised *via* the Gabriel synthesis.

Despite the difficulty, the PS-DMAP catalyst was partially recovered; an IR spectrum of the catalyst post-use displayed peaks at 1747 and 1085 cm^{-1} that were absent in the fresh catalyst, suggesting that the PLA had grown from DMAP itself, or become trapped in the cross-linked polymer support, despite thoroughly washing in DCM (Figure B.1). As computational studies have suggested that DMAP is more likely to activate the alcohol over a monomer activation pathway,[11]

the IR suggests that, as with the complexes, the polymer has likely grown from or become trapped in the PS-matrix.

Recovery of PS-CH_2NH_2 was not successful, therefore it was necessary to find alternative morphologies of the catalyst. A more crosslinked equivalent to PS-CH_2NH_2, with a higher loading (4 mmol/g) similar to the "Merrifield's resin" starting material, also proved to be a fine powder, with similar recovery complications as the original catalyst. Further to this, the activity of the new catalyst was far lower than the original catalyst, reaching only 27%, perhaps because access to the extra sites on the catalyst was limited by mass transfer (entries 1-2, Table 5.5). Commercially available (aminomethyl)polystyrene beads ("BZA") were available from Quadrapure, through Sigma-Aldrich; whilst the beads could be recovered, activity was poor, with conversions of only 12% (entry 3, Table 5.5).

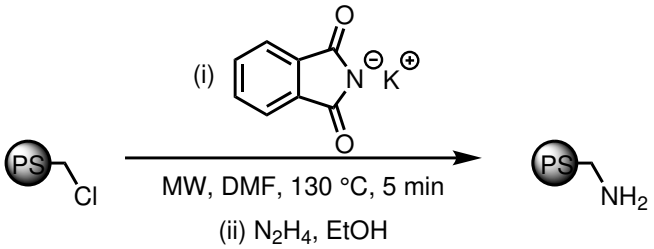

Scheme 5.10: Gabriel synthesis of (aminomethyl)polystyrene, following the procedure described by Kaiz *et al.*[53]

As the commercial options had been exhausted, attempts to synthesise a "homemade" version of the amine catalyst was attempted *via* the Gabriel synthesis using potassium phthalimide salt in DMF, followed by deprotection using hydrazine hydrate, proposed in the literature (Scheme 5.10).[53] Analysis of the IR spectra of the starting material and product, in comparison to the commercial PS-CH_2NH_2 confirmed the success of the synthesis; peaks at 3310 and 1609 cm^{-1} were assigned to the N-H stretches and bends of the amine, respectively, and were similar to the peaks in literature (Figure B.2). When this catalyst was used in ROP, however, only 38% conversion was achieved with a low M_n of 1 250 Da, although the dispersity was far improved after 24 hours compared to the original commercial system ($Đ_M$ 1.13 compared to 1.37, entry 4, Table 5.5). Comparison of the activity to that of the starting material (4% conversion) further confirmed the

Gabriel synthesis had worked to some extent.

In-depth comparison of homogeneous and heterogeneous bases

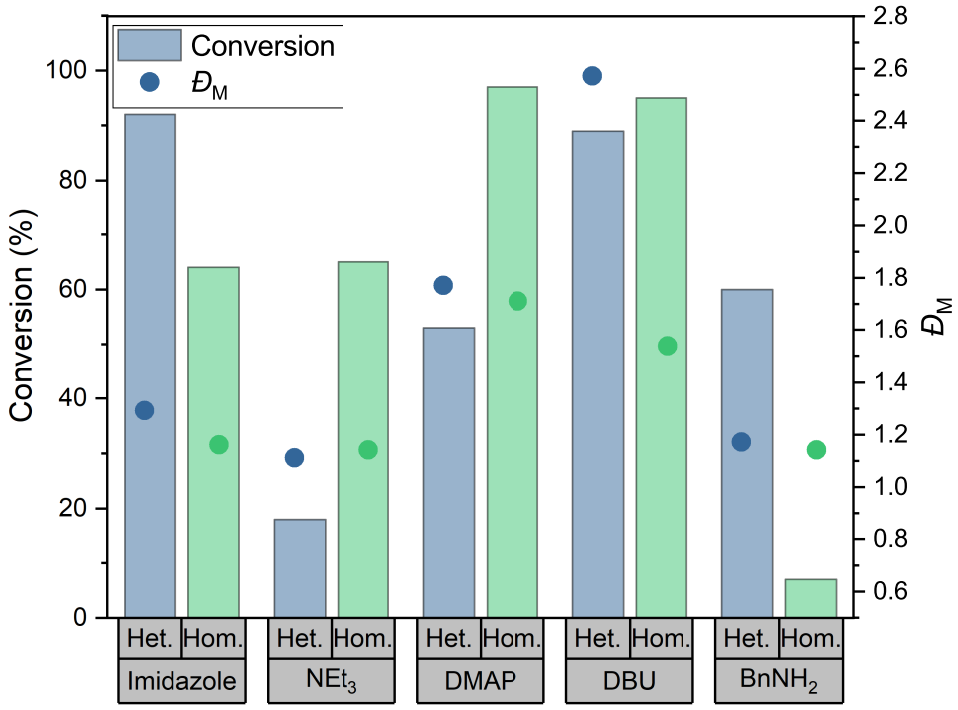

Figure 5.5: Solvent-free ROP of *L*-LA with both homogeneous ("Hom.", green column) and heterogeneous ("Het.", blue column) amine bases (B), at [LA]:[B]:[I] = 50:1:1, over 4 hours at 130 °C, where I = co-initiator (4-methylbenzyl alcohol).

Overall, PS-CH_2NH_2 reached a modest conversion after 6 hours, albeit only at one quarter of the equivalents used in initial studies, and produced polymers with modest M_n and $Đ_M$ of 1.13. Perhaps more interestingly, polymers produced by this catalyst were showed significantly fewer stereoerrors brought about by epimerisation in comparison to the PS-DBU and PS-DMAP. These stronger bases could reach higher conversions more rapidly, but at the expense of dispersity due to competitive epimerisation; this was further supported by a bimodal SEC trace, linked to the lack of control observed in the ^{1}H NMR spectra. Despite this, it is clear from *in situ* kinetics that the current catalysts did not display competitive

rates and selectivity to already commercially available catalysts.

In order to gain a greater understanding of these catalysts, a more in-depth comparison between the heterogeneous catalysts must be carried out. For these studies, imidazole and its heterogeneous counterpart were included, and the PS-support was used throughout (Table 9.1). Maintaining the [LA]:[B]:[I] ratio of 50:1:1 (where B = base), the time of each batch reaction was shortened to 4 hours to remove the potential for all catalysts to reach full conversion (Figure 5.5). This would allow for comparison of catalyst activity without material-intensive *in situ* ATR-FT-IR studies. This was the only viable alternative to NMR kinetic studies which could not be carried out due to the heterogeneous nature of the catalysts and solvent-free, high temperature conditions.

Table 5.6: Polymerisation data from the ROP of *L*-LA with either homogeneous or heterogeneous organocatalytic amine bases (B), using [LA]:[B]:[I] = 50:1:1 in the melt at 130 °C for 4 hours (I = 4-methylbenzyl alcohol).

Entry	**Base**	**Conv. (%)**[a]	$M_{n,Theo}$[b]	$M_{n,NMR}$[a]	$M_{n,SEC}$[c]	$M_{w,SEC}$[c]	$Đ_M$[c]
1	PS-Imidazole	92	6650	4750	2100	2650	1.29
2	Imidazole	64	4600	4000	4200	4850	1.16
3[d]	PS-DMAP	53	3800	3250	1300	2300	1.77
4	DMAP	97	7000	4700	4000	6800	1.71
5[d]	PS-DBU	89	6400	4850	1650	4250	2.57
6	DBU	95	6850	5800	5250	8050	1.54
7	PS-CH_2NH_2	60	4300	2850	2150	2500	1.17
8	$BnNH_2$	7	500	500	250	250	1.14

[a] Determined from the ^{1}H NMR spectrum.
[b] Theoretical M_n= ([LA]/[I]) × (144 × equiv. LA) × (conv./100).
[c] As determined by SEC (THF) using RI methods, relative to poly(styrene) standards (multiplied by a factor of 0.58, rounded to the nearest 50).[52]
[d] Bimodal SEC trace.

Generally, the homogeneous amines tended to have higher conversions compared to their immobilised analogues; the latter also produced polymers of higher dispersities (in green, Figure 5.5)

PS-DBU, for example, did not lower the conversion drastically, yet the dispersity increased significantly on immobilisation ($Đ_M$ 2.57, entry 5, Table 5.6); *in situ* kinetics in future work would be able to distinguish whether this was caused by lengthy reaction times. Excessively long time scales, leaving time for the base to transesterify or epimerise the polymer, for this particular base could

Table 5.7: Example breakdown of the bimodal SEC trace produced by the ROP of *L*-LA with PS-DBU, using [LA]:[PS-DBU]:[I] = 50:1:1 in the melt at 130 °C for 4 hours. 89% conversion, $M_{\mathrm{n,Theo}}$ 6 400 Da.

Entry	SEC Peak	$M_{\mathrm{n,SEC}}$[a]	$M_{\mathrm{w,SEC}}$[a]	$Đ_{\mathrm{M}}$[a]
1	Overall	1650	4250	2.57
2	Peak 1_{main}	2350	3400	1.45
3	Peak 2_{shoulder}	750	850	1.10

[a] As determined by SEC (THF) using RI methods, relative to poly(styrene) standards (multiplied by a factor of 0.58, rounded to the nearest 50).[52]

explain the disparity between the theoretical and experimental molecular weights ($M_{\mathrm{n,Theo}}$ 6 400 Da, $M_{\mathrm{n,SEC}}$ 1650 Da, entry 5, Table 5.6). However, even the 2 hour result had displayed excess epimerisation, with no change over time (Figure 5.2). It is tentatively put forward that more likely, epimerisation could not be avoided at any given time-scale: the base strength was such that the rate of transesterification (k_{trans}) was competitive with the propagation rate (k_{prop}).

Bimodal SEC traces were obtained when both PS-DMAP and PS-DBU were used, even within the shortened time-scale, reaching 53% and 83% conversion, respectively (PS-DMAP: $Đ_{\mathrm{M}}$ 1.77 over both peaks, entry 3, Table 5.6). The disparity between $M_{\mathrm{n,Theo}}$ and $M_{\mathrm{n,SEC}}$ is slightly less once the overall $M_{\mathrm{n,SEC}}$ is broken down into the two constituent peaks. An example of the breakdown is illustrated in Table 5.7. However, a large difference in theoretical and experimental M_{n} remains, echoing results from Figure 5.3. Again, this was attributed to the strength of the base yielding competitive k_{trans}, leading to uncontrolled cyclisation and transesterification side-reactions, as evidenced by the finding of cyclic species in previous MALDI-ToF spectra (Table 5.2).

In contrast, reactions using the free, unbound DMAP and DBU yielded monomodal polymers ($Đ_{\mathrm{M}}{}^{\mathrm{DMAP}}$ 1.71, $Đ_{\mathrm{M}}{}^{\mathrm{DBU}}$ 1.54, entries 4 and 6, Table 5.6). The disparity in $M_{\mathrm{n,Theo}}$ and $M_{\mathrm{n,SEC}}$ was also much lower for some homogeneous bases (imidazole and DMAP) compared to the immobilised bases, supporting the theory that base strength was not the only cause of the difference.

Mass transfer and diffusion limitations, coupled with the solvent-free conditions hampering access to the active sites on the PS-support, might be the root of

epimerisation and the slower polymerisation rates, compared to the homogeneous bases. The added steric bulk of the support could decrease monomer access to the catalyst, and further diffusion limitations imparted by the viscous molten LA are expected to significantly reduce the efficacy of these catalysts. It is also conceivable that a slight change in pKa of the base is possible on immobilisation, potentially altering base activity.

In contrast, both PS-CH_2NH_2 and PS-imidazole produced significantly improved conversions to their homogeneous counterparts (60% and 92%, respectively, entries 1-2 and 7-8, Table 5.6). The low conversion obtained with benzylamine ($BnNH_2$, the homogeneous PS-CH_2NH_2) was potentially due to its physical state: addition of such small amounts of a liquid to a reaction mixture, without the use of stock solutions, means that measurement and addition of the catalyst directly into the reaction medium were not as accurate as with solid bases.

In situ ATR-FT-IR kinetics determined that conversion using PS-CH_2NH_2 reached 20% within 6 hours at [LA]:[B]:[I] = 50:0.25:1, described earlier. A 50:1:1 ratio (*i.e.* with four times the catalyst amount) would be expected to have approximately four times the activity within the same time-frame. Accordingly, conversion reached 60% within 4 hours, which was roughly what would be expected in a first order ROP. A monomodal polymer was again observed, with an excellent dispersity of 1.17 (entry 7, Table 5.6).

The most promising of bases were PS-imidazole and imidazole (64 and 92%, respectively, entries 1-2, Table 5.6). These provided competitive conversions to (PS-)DMAP and (PS-)DBU, whilst retaining narrow, monomodal dispersities not seen with the two stronger bases ($Đ_M$ 1.16-1.29, entries 1-2, Table 5.6). Relatively similar levels of epimerisation were observed in the ^{1}H NMR spectra between PS-CH_2NH_2 and (PS-)imidazole. The pKa of the conjugate acid of imidazole is 6.8; this is slightly lower than that of DMAP, indicating a slightly weaker base and less likely to epimerise the methine proton of the monomer.

Whilst PS-imidazole provided some balance of control and activity, these commercial organocatalysts were not the most suitable for the ROP of *L*-LA in solvent-free conditions due to difficulties in balancing rate, epimerisation and overall control of the reaction. It was therefore necessary to explore more complex or-

ganocatalytic systems to speed up the ROP procedure.

Bifunctional catalysts

Synthesis of immobilised urea

In this regard, ureas have been synthesised *via* reaction of an amine with various iso(thio)cyanates in seconds in anhydrous THF, producing highly selective catalysts. The polymers produced from combination of these (thio)ureas with amines were of narrow dispersity, brought about through a hydrogen-bonding bifunctional mechanism.[15,18,38] Both (thio)urea and amine components were necessary to initiate ROP; uncontrolled ROP, or no conversion at all was observed when the urea and amine were not used in tandem.[15] The so-called "structural flexibility"[15] that is offered by these urea or thiourea/amine catalysts offers a wide array of potential catalysts: Choice of amine and altering of the thiourea substituents can allow for judicious tailoring of the catalyst structure to optimise both the reaction activity and selectivity, whilst surpressing any competing epimerisation and transesterification.

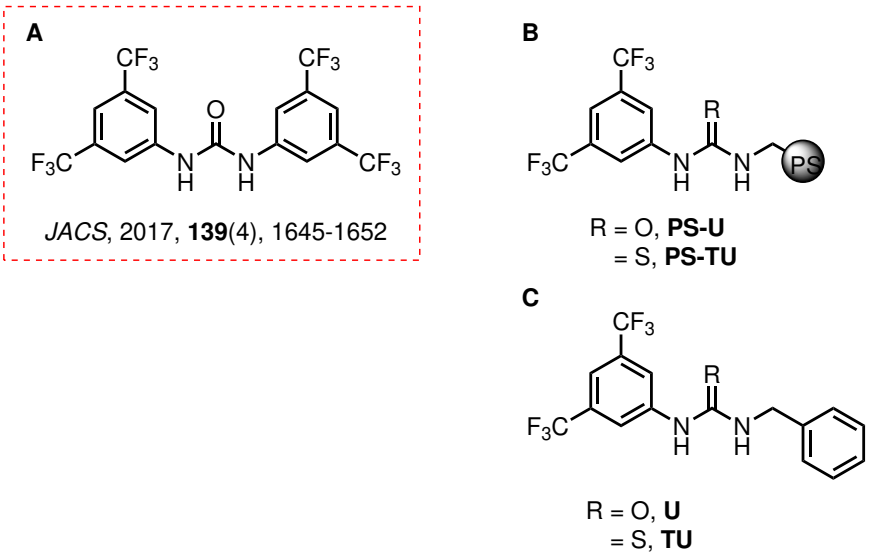

Scheme 5.11: Structures of A) the original Waymouth urea,[42] B) immobilised urea and C) homogeneous analogue synthesised for the following work.

Following the work set out by Lin and Waymouth (Scheme 5.11), addition of an excess of homogeneous urea would modify the activity of KOEt and improve the

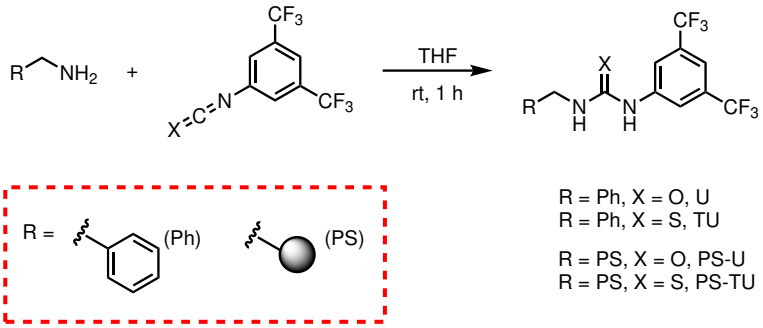

Scheme 5.12: Synthetic route to the free (thio)urea, following the literature procedure.[42] PS denotes the insoluble, heterogeneous poly(styrene) support.

control dramatically.[14] As such, in this work, immobilised (thio)urea derivatives were synthesised to mimic the structures of the successful catalysts reported previously. The synthesis of both heterogeneous and homogeneous catalysts was carried out as described in the literature (Scheme 5.12).[42]

Attempts to immobilise the urea component began with a derivative of the $-CF_3$ functionalised urea reported in literature (Scheme 6.2). As one of the substituents needed to be replaced with an insoluble, crosslinked PS-support to create the heterogeneous catalyst, only one of the two urea substituents was able to contain the two $-CF_3$ groups which imparted the excellent activity onto the urea anion.[42] Since both sets of substituents have an effect on catalyst activity,[54] it was therefore predicted that removing some of the versatility in catalyst design (by having one unchangeable PS substituent) might have some effect on the overall activity of the heterogeneous catalyst. An equivalent homogeneous urea was created using benzylamine as an analogue to the PS substituent.

Consequently, the commercial PS-CH_2NH_2 (amine loading = 4 mmol/g) was reacted with both isocyanate to yield an immobilised urea, similar to those reported in literature,[42] stirring for one hour to ensure all the amine sites had reacted with the isocyanate. A broad peak at 2160 cm^{-1} in the IR spectrum of the product (PS-Urea, or "PS-U") was assigned to the characteristic N−C−O stretch of the urea, whilst two strong peaks at 1385 and 1171 cm^{-1} originated from the C−F stretches (Figure 5.6). CHN analysis revealed that both PS-Urea contained the correct % composition compared to the expected values based on 100% conversion, indicative of near quantitative conversions, and therefore the active site

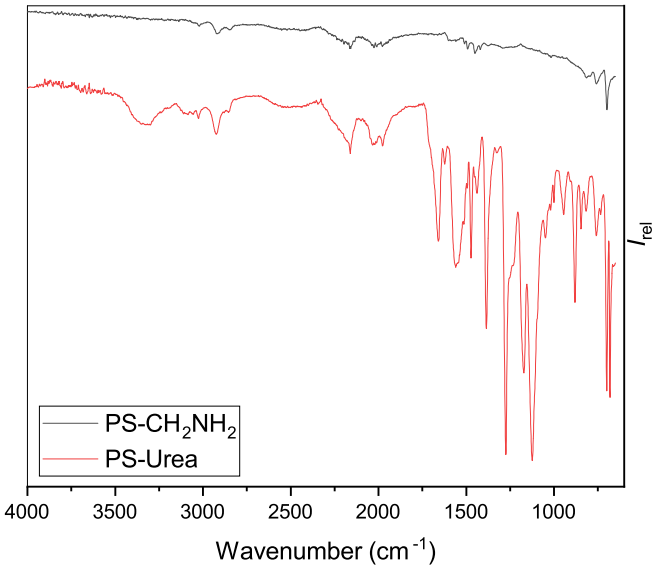

Figure 5.6: IR spectra of PS-Urea (bottom), and the PS-CH_2NH_2 starting material (top).

loading (loading^{cat}) was calculated as 1.98 mmol/g.

A homogeneous urea (labelled "U") was synthesised in a 97% yield using a similar method. The ^{1}H NMR spectrum in DMSO-d_6 showed peaks corresponding to the N−H closest to the $-CF_3$-functionalised aryl group (9.36 ppm) and the $-CH_2$ group of the incorporated benzylamine group (4.32 ppm). The ESI-MS+ in acetonitrile contained a peak at m/z 363.09 (Calcd m/z: 362.09), while analysis of the IR spectrum revealed peaks assigned to the C=O, C−F and C−N stretches at 1654, 1390 and 1178 cm^{-1}, respectively.

Bifunctional organocatalysts in melt ROP

In this work, the bifunctional mechanism was achieved by combining the immobilised urea, PS-Urea (or PS-U), with several homogeneous and heterogeneous bases (B). A ratio of [LA]:[PS-U]:[B]:[I] of 50:1:1:1 was used in the solvent-free ROP of *L*-LA, at 130 °C, in keeping with the ROP reactions carried out earlier in this chapter (Figure 5.7). As no solvent was used, potential suppression of the H-bonding – necessary for the bifunctional mechanism – by polar solvents was

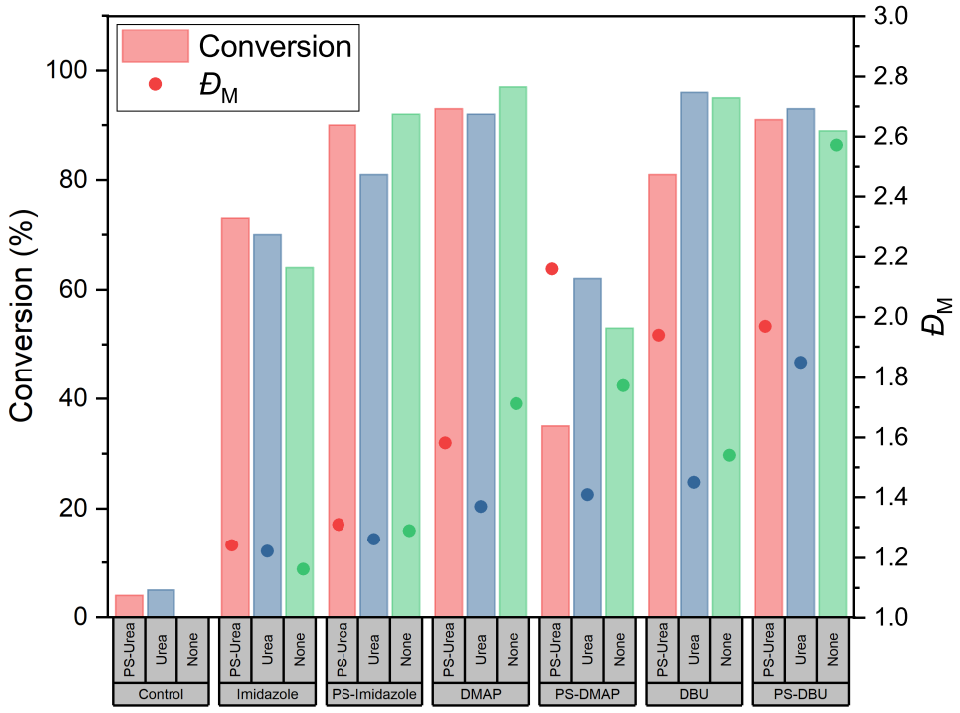

Figure 5.7: Solvent-free ROP of *L*-LA with either the homogeneous urea (U), or heterogeneous urea (PS-U) and an amine base (B), at [LA]:[U]:[B]:[I] = 50:1:1:1, over 4 hours at 130 °C, where I = co-initiator (4-methylbenzyl alcohol). Base coupled with PS-U (pink), Urea (blue) or no catalyst (green, control reaction).

avoided.

Generally, when U was combined with any base, a small improvement in conversion was observed within 4 hours (blue column, Figure 5.7). This was likely a result of the good access of the amine to the homogeneous urea, resulting in an effective bifunctional mechanism due to the proximity between the two co-catalysts allowing for optimal H-bonding. Tables 5.8-5.10 break down individual results for the different combinations of (PS-)U and DMAP, DBU and imidazole.

For combinations of the free U with bases such as PS-DMAP, PS-DBU, DBU and imidazole, the increase in conversion from the bases on their own was accompanied with a decrease in dispersity, potentially resulting from some cooperativity between the two catalysts. Most SEC traces of the various combinations were

monomodal, with relatively narrow dispersities ($Đ_M$ 1.22-1.45). Although the SEC trace of the U/PS-DMAP generated polymer was bimodal, this was not due to two different mechanisms (*i.e.* the original PS-DMAP mechanism, and that stemming from the modification of PS-DMAP by the urea), as the SEC trace of the PS-DMAP control was also bimodal. This strongly suggested that the urea was not modifying the activity of PS-DMAP, and therefore not suppressing the transesterification reactions, as demonstrated in previous work.[15] Rather, it was likely that the two peaks in the SEC trace were either due to this uncontrolled ROP evidenced by signals corresponding to epimerisation in the ^{1}H NMR spectra, or due to the competing nucleophilic and alcohol-initiated H-bonding mechanisms that DMAP has been reported to follow.[11,24]

Table 5.8: Polymerisation data from the ROP of *L*-LA using (PS-)U combined with (PS-)DMAP, using [LA]:[U]:[B]:[I] = 50:1:1:1 in the melt at 130 °C.

Entry	Catalyst	Base (B)	Conv. (%)[a]	$M_{n,Theo}$[b]	$M_{n,NMR}$[a]	$M_{n,SEC}$[c]	$M_{n,SEC}$[c]	$Đ_M$[c]
1	PS-U	-	4	300	350	n.d[d]	n.d	n.d
2	PS-U	DMAP	93	6700	3100	4100	6500	1.58
3[e]	PS-U	PS-DMAP	35	2500	1950	800	1900	2.16
4	U	DMAP	92	6650	2800	5850	8000	1.37
5[e]	U	PS-DMAP	62	4450	2500	1200	1650	1.41
6	U	-	5	350	n.d	n.d	n.d	n.d
7	-	DMAP	97	7000	4700	4000	6800	1.71
8[e]	-	PS-DMAP	63	3800	3250	1300	2250	1.77

[a] Determined from the ^{1}H NMR spectrum.
[b] Theoretical M_n= ([LA]/[I]) × (144 × equiv. LA) × (conv./100).
[c] As determined by SEC (THF) using RI methods, relative to poly(styrene) standards (multiplied by a factor of 0.58, rounded to the nearest 50).[52]
[d] n.d. = Not determined.
[e] Bimodal SEC trace.

In contrast, combination of the bases with the immobilised equivalent of the urea (PS-U) provided unreliable results (pink column, Figure 5.7). The conversion decreased from the base controls when PS-U was combined with PS-DMAP (35% from 63%, entries 3 and 8, Table 5.8) or DBU (81% from 95%, entries 2 and 7, Table 5.9), and an increase in dispersity. The decrease in the activity indicates that the rate of propagation has slowed, potentially allowing for competitive transesterification and epimerisation to occur; indeed, at least some epimerisation was seen in the ^{1}H NMR spectra with both bases upon combination with PS-U, and the dispersity had increased compared to the base control result. For both amines, either the PS-U had some modification on the activity of the base or, more

Table 5.9: Polymerisation data from the ROP of *L*-LA using (PS-)U combined with (PS-)DBU, using [LA]:[U]:[B]:[I] = 50:1:1:1 in the melt at 130 °C.

Entry	Catalyst	Base (B)	Conv. (%)[a]	$M_{n,Theo}$[b]	$M_{n,NMR}$[a]	$M_{n,SEC}$[c]	$M_{n,SEC}$[c]	$Đ_M$[c]
1	PS-U	-	4	300	350	n.d[d]	n.d	n.d
2	PS-U	DBU	81	5850	1150	5750	11100	1.94
3[e]	PS-U	PS-DBU	91	6550	5250	1450	2850	1.97
4	U	DBU	96	6900	3750	3850	5550	1.45
5	U	PS-DBU	93	6700	2550	4850	9000	1.85
6	U	-	5	350	n.d	n.d	n.d	n.d
7	-	DBU	95	6850	5800	5250	8050	1.54
8[e]	-	PS-DBU	89	6400	4850	1650	4250	2.57

[a] Determined from the ^{1}H NMR spectrum.
[b] Theoretical M_n= ([LA]/[I]) × (144 × equiv. LA) × (conv./100).
[c] As determined by SEC (THF) using RI methods, relative to poly(styrene) standards (multiplied by a factor of 0.58, rounded to the nearest 50).[52]
[d] n.d. = Not determined.
[e] Bimodal SEC trace.

likely, the 4 hour time-scale was too long for these bases, leading to uncontrolled side reactions. Again, PS-U/PS-DMAP retained the same bimodality that was observed with PS-DMAP control (entries 3 and 8, Table 5.8), further discounting any potential cooperativity between the two co-catalysts. Neither base displayed any changes relating to a cooperative bifunctional mechanism.

Table 5.10: Polymerisation data from the ROP of *L*-LA using (PS-)U combined with (PS-)imidazole, using [LA]:[U]:[B]:[I] = 50:1:1:1 in the melt at 130 °C.

Entry	Catalyst	Base (B)	Conv. (%)[a]	$M_{n,Theo}$[b]	$M_{n,NMR}$[a]	$M_{n,SEC}$[c]	$M_{n,SEC}$[c]	$Đ_M$[c]
1	PS-U	-	4	300	350	n.d[d]	n.d	n.d
2	PS-U	Imidazole	73	5250	1800	3000	3750	1.24
3	PS-U	PS-imidazole	90	6500	2450	2100	2750	1.31
4	U	Imidazole	81	5850	5150	1850	2350	1.26
5	U	PS-imidazole	70	5050	4400	3200	3900	1.22
6	U	-	5	350	n.d	n.d	n.d	n.d
7	-	Imidazole	64	4600	4000	4200	4850	1.16
8	-	PS-imidazole	92	6650	4750	2100	2650	1.29

[a] Determined from the ^{1}H NMR spectrum.
[b] Theoretical M_n= ([LA]/[I]) × (144 × equiv. LA) × (conv./100).
[c] As determined by SEC (THF) using RI methods, relative to poly(styrene) standards (multiplied by a factor of 0.58, rounded to the nearest 50).[52]
[d] n.d. = Not determined.

Conversions of PS-imidazole and DMAP did not change when these bases were combined with PS-U. The dispersity decreased with the PS-U/DMAP system ($Đ_M$ 1.58, entry 3, Table 5.8), in comparison to the base alone ($Đ_M$ 1.71, entry 7,

Table 5.8). In contrast to previous results, a slight increase in control had been achieved whilst retaining ROP activity, although the SEC trace of the resulting polymer was still slightly bimodal, compared to the monomodal trace obtained with U/DMAP.

For the PS-U/PS-imidazole system, no great improvement in conversion or dispersity was seen (entries 3 and 7, Table 5.10). The unchanged activity and selectivity with the PS-U/PS-imidazole system (compared to the PS-imidazole control) was likely due to the distance between the active sites brought about by the two bulky supports, such that cooperativity between the two components was not possible.

Only one PS-U/B combination significantly improved the conversion, compared to the control reactions with just the bases: PS-U/imidazole. This system seemed like the optimal combination of urea and base, resulting in a higher conversion without compromising the monomodal, narrow dispersity of the polymer product (73%, $M_{\mathrm{n,SEC}}$ 3 000 Da, $Đ_{\mathrm{M}}$ 1.24, entry 2, Table 5.10).

Considered together, these results suggest that tethering of the urea to a bulky PS-support increases the sterics around the urea, leaving little accessible room for the amine and monomer to approach, unlike the homogeneous urea. When two such heterogeneous components are introduced together, the issue becomes two-fold, blocking cooperativity between the PS-U and PS-DMAP. Further, the movement of the heterogeneous catalyst particles against each other during stirring of the reaction medium would also pull the two components away from each other. This increased friction during stirring of the reaction medium pulls the two co-catalysts away from each other, making it impossible for any bifunctional, simultaneous activation to occur. This would indeed explain why marginal changes in activity were observed with some of the heterogeneous bases on combination with PS-U.

Overall, combination of PS-U with heterogeneous bases struggled to achieve the same selectivity observed in literature, or indeed that achieved when combining the same bases with the homogeneous urea. None of the catalysts seemed to affect the selectivity: whilst dispersities were sometimes lowered (*e.g.* with PS-U/DMAP and PS-U/PS-DBU systems), evidence of a high degree of epimer-

isation was still visible in the ^{1}H NMR spectra, indicating that any potential change in activity imparted by PS-U was not enough to control the ROP. When homogeneous U was used, however, the bifunctional system was more readily formed, leading to the more predictable changes seen in the U/B systems.

Bifunctional organocatalysts: changing ratios

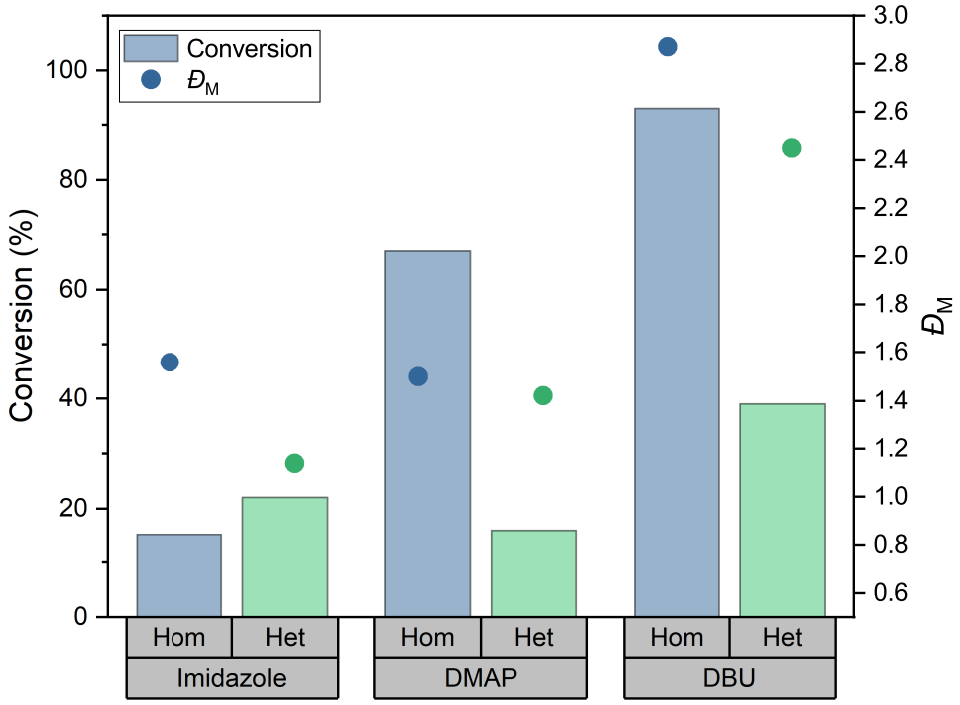

Figure 5.8: Solvent-free ROP of *L*-LA with PS-U combined with either homogeneous ("Hom.", blue column) and heterogeneous ("Het.", green column) amine bases (B), at [LA]:[PS-U]:[B]:[I] = 200:1:1:1, over 4 hours at 130 °C, where I = co-initiator (4-methylbenzyl alcohol).

One of the key issues in distinguishing between the base control reactions and PS-U/B systems was reaction duration, for example with the PS-U/PS-DBU or PS-U/DMAP systems. Slowing down the reaction could potentially help elucidate any differences between the two types of system. This could either be done directly, by quenching the reactions after one hour, or the ratio of LA could be

Table 5.11: Polymerisation data from the ROP of *L*-LA using PS-U combined with either homogeneous or heterogeneous organocatalytic amine bases (B), using [LA]:[PS-U]:[B]:[I] = 200:1:1:1 in the melt at 130 °C for 4 hours.

Entry	**Base**	**Conv. (%)[a]**	$M_{n,Theo}$[b]	$M_{n,SEC}$[c]	$M_{w,SEC}$[c]	$Đ_M$[c]
1	-	2	600	-	-	-
2	PS-DMAP	16	4600	700	1050	1.42
3	DMAP	67	19300	8200	12250	1.50
4*	PS-DBU	39	11250	914	2250	2.45
5	DBU	93	26800	1300	3750	2.87
6	PS-Imidazole	22	6350	1500	1700	1.14
7*	Imidazole	15	4300	1850	2900	1.56
8	PS-EDA	3	900	-	-	-
9	NEt_3	7	2000	-	-	-
10	PS-CH_2NH_2	5	1450	-	-	-
11	$BnNH_2$	2	600	-	-	-

[a] Determined from the ^{1}H NMR spectrum.
[b] Theoretical M_n= ([LA]/[I]) × (144 × equiv. LA) × (conv./100).
[c] As determined by SEC (THF) using RI methods, relative to poly(styrene) standards (multiplied by a factor of 0.58, rounded to the nearest 50).[52]
* Bimodal SEC trace.

increased; the latter would also show if these catalytic systems could reach higher M_n.

At a ratio of 200:1:1:1, combination of the PS-U with the immobilised bases demonstrated lower activity to combinations of PS-U with unsupported bases, after 4 hours in the melt (Figure 5.8, Table 5.11). In most cases, conversions were too low to discern any improvement in M_n arising from the higher ratios used. Interestingly, the PS-U/PS-imidazole system was the only heterogeneous-heterogeneous system which provided a higher conversion to the PS-U/homogeneous base analogue (22%, $Đ_M$ 1.14 versus 15%, $Đ_M$ 1.56, entries 6-7, Table 5.11).

Although conversion only reached 15% when PS-U was combined with imidazole ($M_{n,Theo}$ 4 300 Da, $M_{n,SEC}$ 1 850 Da, $Đ_M$ 1.56), the ratios used were four times higher than in the 50:1:1:1 tests, where conversion reached 73% within the same time-frame. This was the first example of a bimodal SEC trace which was a not seen in prior controls ($M_n^{Overall}$ 1 850 Da, $M_n^{Peak\ 1}$ 8 200 Da, $M_n^{Peak\ 2}$ 1 700 Da). It is tentatively proposed that this change is likely due to an increase in co-operativity between the imidazole and PS-U, yielding a bifunctional mechanism leading to improved catalyst performance. Nevertheless, the epimerisation was

Table 5.12: Polymerisation data from the ROP of *L*-LA using (PS-)U combined with (PS-)imidazole, using [LA]:[PS-U]:[B]:[I] = 200 or 50:1:1:1 in the melt at 130 °C.

Entry	Catalyst	Base (B)	[LA]:[PS-U]:[B]:[I]	Time (h)	Conv. (%)[a]	$M_{n,Theo}$[b]	$M_{n,SEC}$[c]	$Đ_M$[c]
1	PS-U	Imidazole	50:1:1:1	4	73	5250	3000	1.24
2*	PS-U	Imidazole	200:1:1:1	4	15	4300	1850	1.56
3	PS-U	Imidazole	200:1:1:1	24	35	10100	4500	1.32
4	PS-U	PS-Imidazole	50:1:1:1	4	90	6500	2100	1.31
5	PS-U	PS-Imidazole	200:1:1:1	4	22	6350	1500	1.14
6	Urea	Imidazole	50:1:1:1	4	70	5050	3200	1.22
7	Urea	Imidazole	200:1:1:1	4	7	2000	-	-
8	PS-U	-	200:1:1:1	4	2	600	-	-
9	Urea	-	200:1:1:1	4	9	2600	-	-
10	-	Imidazole	200:1:1:1	4	6	1750	-	-

[a] Determined from the ^{1}H NMR spectrum.
[b] Theoretical M_n= ([LA]/[I]) × (144 × equiv. LA) × (conv./100).
[c] As determined by SEC (THF) using RI methods, relative to poly(styrene) standards (multiplied by a factor of 0.58, rounded to the nearest 50).[52]
* Bimodal SEC trace.

still present in the NMR, indicating that the catalyst still did not decrease stereoerror formation, despite excellent dispersities ($Đ_{M,Peak\ 1}$ 1.10, $Đ_{M,Peak\ 2}$ 1.17).

A comparison of these results with a ROP test using imidazole alone revealed that only 7% of the monomer had been converted within the same time-frame (entry 7, Table 5.12). Evidently combination with either the heterogeneous or homogeneous urea allowed for the conversion to double. After 24 hours, however, conversion was still only 35% with PS-U/imidazole, so despite some evidence of bifunctional activity, these are not competitive catalysts with the current urea/base systems reported in literature.

5.4 Conclusions and future work

Several commercially available, immobilised amine bases were tested in the melt ROP of *L*-LA at 130 °C over 24 hours. Kinetic investigations and analysis of the ^{1}H NMR spectra revealed that weaker bases (PS-CH_2NH_2) produced more controlled polymers with less epimerisation and monomodal SEC traces, but reactions took at least 6 hours to reach meaningful conversions. Meanwhile, stronger bases reached high conversions, even in shorter time frames of later experiments, but significant epimerisation and transesterification was still present. Subsequent investigations with other bases revealed that PS-imidazole reached high conver-

sions with minimal epimerisation and monomodal, narrow dispersities within 4 hours (92%, $Đ_M$ 1.29), offering a balance between activity and selectivity.

The activities of these heterogeneous bases were directly compared to those of their homogeneous counterparts. It was clear from these preliminary studies that homogeneous bases typically performed better than their heterogeneous equivalents, leading to higher conversions, narrower dispersities and molecular weights matching theoretical ones predicted from the conversion. In contrast, immobilised catalysts displayed large disparities between theoretical and experimental M_n, due to the epimerisation seen in the ^{1}H NMR spectra. MALDI-ToF Mass Spectrometry analysis revealed catalyst tendency towards transesterification and the resulting formation of cyclic species contributed to the broad dispersities and M_n disparity. A more in-depth MALDI-ToF Mass Spectrometry study is necessary for the comparison to the homogenous amines: do the latter still form cyclic species, and if yes, why is the same M_n disparity not seen?

Notably, a slight improvement in conversion was observed when the immobilised bases were combined with a homogeneous urea. Access of both monomer and amine co-catalyst to the urea were necessary for bifunctional activation; when the urea was immobilised onto a bulky PS-support, this often yielded poor results and lower selectivity in comparison to the fully homogeneous urea/base systems. When both catalysts were heterogenised, this effect was worsened, as shown in the 200:1:1:1 tests, and further problems due to stirring pulling apart active sites contributed to this. Although the modification of activity hinted that the two components were cooperating together, predictable trends were hard to elucidate.

Despite the difficulties in optimising a heterogeneous or semi-heterogeneous system, some successes were still observed. PS-U/PS-imidazole provided good results throughout the study, reaching 90% conversion in 4 hours ($Đ_M$ 1.31, [LA]:[PS-U]:[B]:[I] = 50:1:1:1), while studies at higher ratios revealed a significant improvement on combination of the two components in comparison to controls with PS-imidazole alone.

To improve the current system, future work could focus on several key areas. Initially, shortening of time-scales below 4 hours would be necessary to identify differences between reactions involving the stronger bases such as PS-DBU: are

the high dispersities due to k_{trans} competing with k_{prop} during ROP, or can the transesterification be surpressed? Epimerisation was seen regularly throughout, contradicting previous literature indicating that bifunctional catalysts could be left within the reaction medium without transesterifying the polymer.[38] In the same vein, *in situ* kinetics of successful combinations would identify differences in reaction rates between homogeneous and heterogeneous bases, beyond the preliminary studies in this chapter.

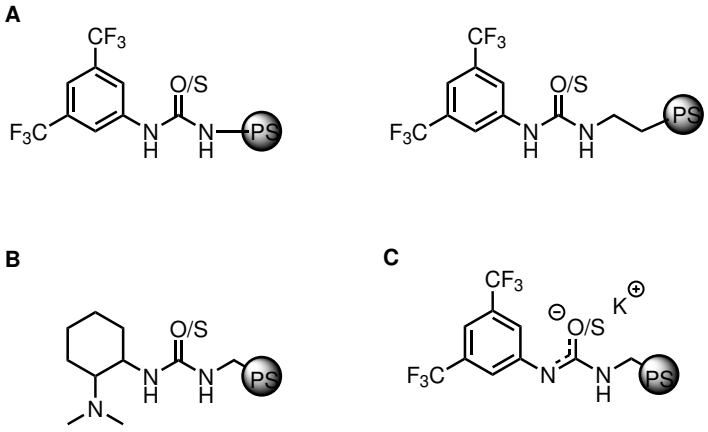

Scheme 5.13: Options for tailoring the PS-(T)U structure. A) Increasing or decreasing the flexibility of the secont substituent (PS-). B) A single-site PS-(T)U with amine incorporated into the structure – this example is adapted from Dove *et al.*[38] C) Maintaining the original PS-(T)U structure, but using KOEt base; this option shall be discussed in Chapter 6.

Secondly, a study of (PS-)U would elucidate how varying the structure could affect the activity of the immobilised catalyst. The original PS-U was designed based on prior studies of the homogeneous bifunctional catalysts, which determined that the electron withdrawing $-CF_3$ groups improved H-bonding activation of the monomer through increasing acidity of the N−H group.[42] Immobilisation of the U on the insoluble PS-support also placed an additional $-CH_2$ group sandwiched between the U and the support, thereby increasing the flexibility of the functional group. Incremental tailoring of the flexibility of the PS-U structure could improve ROP results, to balance flexibility (and therefore monomer access) with activity (to mitigate adduct formation between the U and base, Scheme 5.13A). Similarly, moving from a urea to a thiourea ("TU") might also alter the catalytic activity.

The PS-(T)U catalyst could also be modified further through incorporation of

amine unit within (T)U structure to get a fully heterogeneous system. It is clear that heterogenising both co-catalysts separately does little to provide rapid, controlled ROP. However, immobilisation of a one-site system – where both components are incorporated into the same support – could be an option if a fully heterogeneous bifunctional system was required for further studies into flow ROP (Scheme 5.13B).

Similarly, changing the type of base could also offer an alternative route to controlled heterogeneous ROP. Combination of PS-U with amines under the current conditions did not provide the same selectivity as homogeneous catalysts reported in literature.[15,38] However, another class of "hyperactive" catalysts combining a (T)U motif with KOEt, instead of an amine, increases activity and selectivity through an alternative, zwitterionic bifunctional mechanism. This simple change is the subject of following studies, which focus on solution-phase ROP to maintain excellent interaction between the (T)U and the base, removing any potential mass transfer and diffusion limitations imparted by the viscous medium of solvent-free ROP (Scheme 5.13C).

References

[1] M. C. Tanzi, P. Verderio, M. G. Lampugnani, M. Resnati, E. Dejana and E. Sturani, *J Mater Sci-Mater M*, 1994, **5**, 393–396.

[2] M. K. Kiesewetter, E. J. Shin, J. L. Hedrick and R. M. Waymouth, *Macromolecules*, 2010, **43**, 2093–2107.

[3] A. P. Dove, *ACS Macro Lett*, 2012, **1**, 1409–1412.

[4] W. Jeong, E. J. Shin, D. A. Culkin, J. L. Hedrick and R. M. Waymouth, *J Am Chem Soc*, 2009, **131**, 4884–4891.

[5] H. Li and L. Gu, *J Polym Sci Pol Chem*, 2018, **56**, 968–976.

[6] M. L. Di Lorenzo and R. Androsch, in *Advances in Polymer Science*, Springer, Switzerland, 2018, ch. 279, pp. 67–118.

[7] S. Liu, C. Ren, N. Zhao, Y. Shen and Z. Li, *Macromol Rapid Comm*, 2018, **39**, 1800485.

[8] L. Zhang, F. Nederberg, R. C. Pratt, R. M. Waymouth, J. L. Hedrick and C. G. Wade, *Macromolecules*, 2007, **40**, 4154–4158.

[9] F. Nederberg, E. F. Connor, M. Möller, T. Glauser and J. L. Hedrick, *Angew Chem Int Edit*, 2001, **40**, 2712–2715.

[10] F. Nederberg, E. F. Connor, T. Glausser and J. L. Hedrick, *Chem Commun*, 2001, 2066–2067.

[11] C. Bonduelle, B. Martín-Vaca, F. P. Cossío and D. Bourissou, *Chem - Eur J*, 2008, **14**, 5304–5312.

[12] N. E. Kamber, W. Jeong, R. M. Waymouth, R. C. Pratt, B. G. Lohmeijer and J. L. Hedrick, *Chem Rev*, 2007, **107**, 5813–5840.

[13] I. Kaljurand, A. Kütt, L. Sooväli, T. Rodima, V. Mäemets, I. Leito and I. A. Koppel, *J Org Chem*, 2005, **70**, 1019–1028.

[14] X. Zhang, G. O. Jones, J. L. Hedrick and R. M. Waymouth, *Nat Chem*, 2016, **8**, 1047–1053.

[15] R. C. Pratt, B. G. Lohmeijer, D. A. Long, P. N. Lundberg, A. P. Dove, H. Li, C. G. Wade, R. M. Waymouth and J. L. Hedrick, *Macromolecules*, 2006, **39**, 7863–7871.

[16] M. Baidya and H. Mayr, *Chem Commun*, 2008, 1792–1794.

[17] *Evans pKa Table*, http://evans.rc.fas.harvard.edu/pdf/evans_pKa_table.pdf, Accessed: May 2021.

[18] B. G. Lohmeijer, R. C. Pratt, F. Leibfarth, J. W. Logan, D. A. Long, A. P. Dove, F. Nederberg, J. Choi, C. Wade, R. M. Waymouth and J. L. Hedrick, *Macromolecules*, 2006, **39**, 8574–8583.

[19] S. Naumann, P. B. V. Scholten, J. A. Wilson and A. P. Dove, *J Am Chem Soc*, 2015, **137**, 14439–14445.

[20] A. Alba, O. T. du Boullay, B. Martin-Vaca and D. Bourissou, *Polym Chem*, 2015, **6**, 989–997.

[21] R. C. Pratt, B. G. Lohmeijer, D. A. Long, R. M. Waymouth and J. L. Hedrick, *J Am Chem Soc*, 2006, **128**, 4556–4557.

[22] K. Kaupmees, A. Trummal and I. Leito, *Croat Chem Acta*, 2014, **87**, 385–395.

[23] S. Moins, S. Hoyas, V. Lemaur, B. Orhan, K. Delle Chiaie, R. Lazzaroni, D. Taton, A. P. Dove and O. Coulembier, *Catalysts*, 2020, **10**, 620.

[24] M. K. Kiesewetter, E. J. Shin, J. L. Hedrick and R. M. Waymouth, *Macromolecules*, 2010, **43**, 2093–2107.

[25] M. T. Martello, A. Burns and M. Hillmyer, *ACS Macro Lett*, 2012, **1**, 131–135.

[26] L. Zhang, F. Nederberg, J. M. Messman, R. C. Pratt, J. L. Hedrick and C. G. Wade, *J Am Chem Soc*, 2007, **129**, 12610–12611.

[27] F. Nederberg, B. G. Lohmeijer, F. Leibfarth, R. C. Pratt, J. Choi, A. P. Dove, R. M. Waymouth and J. L. Hedrick, *Biomacromolecules*, 2007, **8**, 153–160.

[28] J. Raynaud, W. N. Ottou, Y. Gnanou and D. Taton, *Chem Commun*, 2010, **46**, 3203–3205.

[29] G. W. Nyce, T. Glauser, E. F. Connor, A. Möck, R. M. Waymouth and J. L. Hedrick, *J Am Chem Soc*, 2003, **125**, 3046–3056.

[30] O. Coulembier, L. Mespouille, J. L. Hedrick, R. M. Waymouth and P. Dubois, *Macromolecules*, 2006, **39**, 4001–4008.

[31] E. F. Connor, G. W. Nyce, M. Myers, A. Möck and J. L. Hedrick, *J Am Chem Soc*, 2002, **124**, 914–915.

[32] D. A. Culkin, W. Jeong, S. Csihony, E. D. Gomez, N. P. Balsara, J. L. Hedrick and R. M. Waymouth, *Angew Chem Int Edit*, 2007, **46**, 2627–2630.

[33] A. P. Dove, R. C. Pratt, B. G. Lohmeijer, D. A. Culkin, E. C. Hagberg, G. W. Nyce, R. M. Waymouth and J. L. Hedrick, *Polymer*, 2006, **47**, 4018–4025.

[34] T. Saito, K. Takojima, T. Oyama, S. Hatanaka, T. Konno, T. Yamamoto, K. Tajima, T. Isono and T. Satoh, *ACS Sustain Chem Eng*, 2019, **7**, 8868–8875.

[35] C. Thomas, F. Peruch, A. Deffieux, A. Milet, J.-P. Desvergne and B. Bibal, *Adv Synth Catal*, 2011, **353**, 1049–1054.

[36] B. Wang, L. Pan, Z. Ma and Y. Li, *Macromolecules*, 2018, **51**, 836–845.

[37] P. Degée, P. Dubois and R. Jérôme, *Macromol Chem Phys*, 1997, **198**, 1973–1984.

[38] A. P. Dove, R. C. Pratt, B. G. G. Lohmeijer, R. M. Waymouth and J. L. Hedrick, *J Am Chem Soc*, 2005, **127**, 13798–13799.

[39] J. Y. C. Lim, N. Yuntawattana, P. D. Beer and C. K. Williams, *Angew Chem Int Edit*, 2019, **58**, 6007–6011.

[40] X. Zhang, G. O. Jones, J. L. Hedrick and R. M. Waymouth, *Nat Chem*, 2016, **8**, 1047–1053.

[41] L. Zhou, Z. Wang, G. Xu, C. Lv and Q. Wang, *Polym Chem*, 2021, **12**, 1806–1815.

[42] B. Lin and R. M. Waymouth, *J Am Chem Soc*, 2017, **139**, 1645–1652.

[43] A. M. Goldys and D. J. Dixon, *Macromolecules*, 2014, **47**, 1277–1284.

[44] A. M. Goldys, M. G. Núñez and D. J. Dixon, *Org Lett*, 2014, **16**, 6294–6297.

[45] R. Feng, S. Jie, P. Braunstein and B. G. Li, *Eur Pol J*, 2019, **121**, 109293.

[46] R. Yuan, G. Xu, C. Lv, L. Zhou, R. Yang and Q. Wang, *Mater Today Commun*, 2020, **22**, 100747.

[47] C. Lv, L. Zhou, R. Yuan, Q. Mahmood, G. Xu and Q. Wang, *New J Chem*, 2020, **44**, 1648–1655.

[48] I. Jain and P. Malik, *Eur Pol J*, 2020, **133**, 109791–109808.

[49] C. Thomas and B. Bibal, *Green Chem*, 2014, **16**, 1687–1699.

[50] I. A. Shuklov, H. Jiao, J. Schulze, W. Tietz, K. Kühlein and A. Börner, *Tetrahedron Lett*, 2011, **52**, 1027–1030.

[51] M. Save, M. Schappacher and A. Soum, *Macromol Chem Phys*, 2002, **203**, 889–899.

[52] J. Baran, A. Duda, A. Kowalski, R. Szymanski and S. Penczek, *Macromol Rapid Comm*, 1997, **18**, 325–333.

[53] Q. M. Kainz, M. Zeltner, M. Rossier, W. J. Stark and O. Reiser, *Chem - Eur J*, 2013, **19**, 10038–10045.

[54] N. Zhu, S. Behzadi, G. Si and C. Tan, *Polymer International*, 2021, **70**, 823–828.

Chapter 6

Immobilised Bifunctional Organocatalysis in Solution-Phase

6.1 Introduction

As we have seen in the previous Chapter, bifunctional organocatalysts involving cooperative activation of both the monomer and the co-initiator have recently also reached exceptional levels of control over ROP, typically through the combination of a urea or thiourea (TU) with a base such as an amine (see Table 6.1 for a summary of (thio)urea/base systems).[1]

Notably, one of the most groundbreaking examples of bifunctional TU systems was discussed by Waymouth and co-workers.[2] Whilst TU/amine systems were typically known to be slower than NHC catalysts, Waymouth and co-workers developed a urea or TU/alkoxide system which lead to controlled ROP, *via* formation of an active zwitterion complex, similar to the pyridyl-urea based catalyst mechanism mentioned in the introduction of Chapter 5.[1,3] Addition of KOMe to the TU (or urea) would tautomerise the TU, generating an alcohol *in situ* which could be activated through the imine nitrogen, while the remaining amine could activate the monomer (Scheme 6.1B). The ROP of LA with [LA]:[TU]:[KOMe] = 100:3:1 was reported to be complete within 90 seconds ($Đ_M$ 1.07, [LA] = 1 mol

L^{-1} in THF). When the TU was replaced by a urea with electron-withdrawing substituents, however, complete monomer conversion to PLA was achieved in just 6 seconds, with a $Đ_M$ of 1.06 and no epimerisation was observed. Further work then demonstrated the application of these catalysts into flow, with the ability to create block copolymers, covered in Chapter 1.[4]

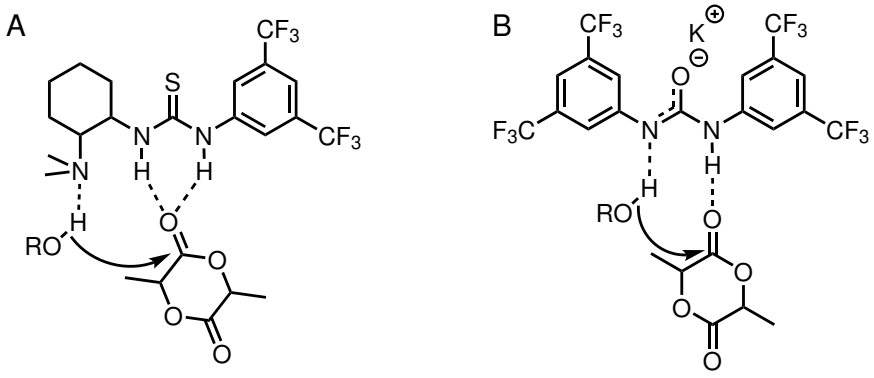

Scheme 6.1: Bifunctional activation mechanisms of (a) TU/amine systems (adapted in Chapter 5),[1] and (b) (T)U/alkoxide systems (discussed herein).[2]

In their subsequent work, Waymouth and co-workers outlined the catalyst selectivities, based on complementary acidities of the TU (or urea) and the pK_aH of the base.[5] A mismatch in acidity nudges the mechanism towards an anionic mechanism (in the case where the B-H$^+$ pK_a is greater than that of the TU), or a cooperative mechanism (in the opposing case); both reduce the ability of a bifunctional mechanism to be exploited (Figure 6.1). They further explored this by forming block copolymers in continuous flow: by matching catalytic activities of the catalysts to the reactivity profiles of various monomers, they were able to get maximal ROP activity with any given monomer in the block copolymer synthesis.[4]

Studies on the importance of the combination of alkoxides with ureas have also led to the development of stereoselective ROP. Stereoblock PLA with P_i values up to 0.93 could be attained when the urea was combined with KOMe, reaching 90% conversion in under two minutes, although low temperatures (−60 °C) were necessary to achieve this ([LA]:[U]:[KOEt] = 100:3:1, M_n 13 900 Da, $Đ_M$ 1.09). When KOMe was switched with NaOMe under the same conditions, PLA was produced with a lower P_i of 0.83.[6] Zhang *et al.* further reported that changing

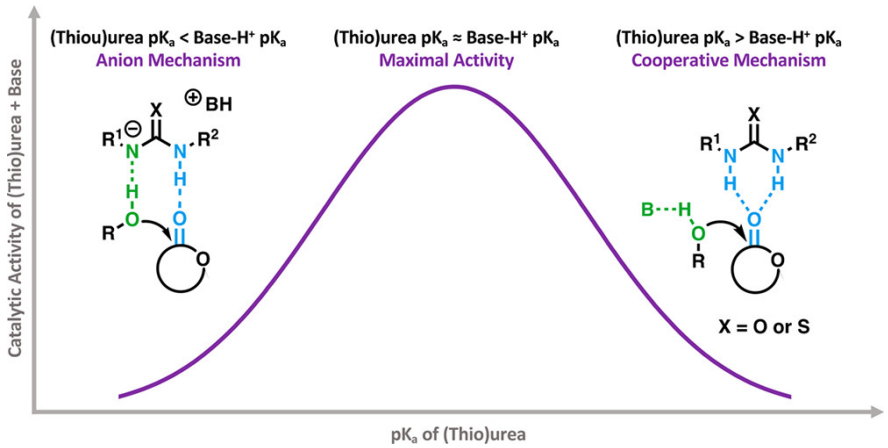

Figure 6.1: Maximal activity is obtained when the pK_a of the (T)U matches that of the conjugate acid of the base, B-H$^+$, according to Waymouth and co-workers.[5]

the alkoxide from KOMe to NaOMe increased the activity of the catalyst, at the expense of the control in dispersity.[3]

Cheap, simple organobases have been proposed as alternatives to KOMe and NaOMe, to form analogous bifunctional architectures, while omitting the use of any metals. A ^{n}Bu$_4$NOH was combined with a urea to give an ionic catalyst, active in ROP.[7] Within minutes at room temperature, quantitative conversion was achieved in excellent control ($Đ_M$ 1.09, [LA]:[U]:[B] = 1000:1:1, where U = urea, B = ^{n}Bu$_4$NOH). When reducing the catalyst loading to just 0.05 mol%, a TOF of 1.2×10^5 h^{-1} was possible. These catalysts were also active in the ROP of other cyclic esters, including ϵ-CL and δ-VL, and both block copolymers and star architectures were demonstrated.

Recently, Tan *et al.* exploited the constrained *cis*-geometry of cyclic amides with alkoxides, coupled with an alcoholic co-initiator to generate a binary catalyst,[8] analogous to the urea/alkoxide system reported by Waymouth and co-workers.[2] The higher the basicity of the cyclic amide improved activation of the alcoholic co-initiator and therefore the activity was increased, however higher stereocontrol was obtained when the nucleophilicity of the alcohol was lowered, leading to lower degree of transesterification. The tunability of the cyclic amide resulted in a balance of the two, with the best result yielding a $Đ_M$ of 1.06, M_n 12 000 Da in 180 seconds. The TU control reaction had a 10% decrease in conversion under the same conditions.

Table 6.1: List of amine-based bifunctional catalysts used in ROP of lactones.

Catalyst	Monomer	Conditions	Time	Conv. (%)	M_n [$Đ_M$]	Reference
NHC-$MgCl_2$	PDL	[M]:[Cat]:[I] = 200:1:1 [M] = 1 mol L^{-1}, Toluene 110 °C	6 h	82	66 200 [1.80]	Dove and co-workers[9]
$Zn(C_6F_6)_2$/DBU	PDL	[M]:[Zn]:[DBU]:[Ph_2CHOH] = 100:1:1:1 [M] = 1.9 mol L^{-1}, Xylene 110 °C	6 h	91	65 300 [1.70]	Wang *et al.*[10]
Phenol/(–)-sparteine	LA	[M]:[ROH]:[Base]:[I] = 20:1:1:1 [M] = 0.7 mol L^{-1}, CH_2Cl_2 20 °C	72 h	95	8 350 [1.08]	Bibal and co-workers[11]
[2]Rotaxane	*rac*-LA	[M]:[Cat]:[B]:[I] = 50:1:1:1 [M] = 1 mol L^{-1}, THF room temp.	96 h	80	5 800 [1.08] P_i = 0.8	Williams and co-workers[12]
Iminophosphorane	*L*-LA	[M]:[Cat]:[I] = 200:1:1 [M] = 2.3 mol L^{-1}, CH_2Cl_2 room temp.	20 min	99	32 900 [1.04]	Goldys, Dixon[13]
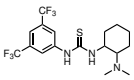	*L*-LA	[M]:[TU]:[I] = 100:1:1 [M] = 0.7 mol L^{-1}, $CDCl_3$ 25 °C	24 h	51	*not determined*	Dove *et al.*[14]
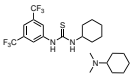	*L*-LA	[M]:[TU]:[I] = 100:1:1 [M] = 0.7 mol L^{-1}, $CDCl_3$ 25 °C	72 h	98	17 800 [1.09]	Hedrick and co-workers[1]
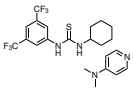	*L*-LA	[M]:[TU]:[I] = 100:1:1 [M] = 0.7 mol L^{-1}, $CDCl_3$ 25 °C	48 h	94	22 900 [1.08]	Hedrick and co-workers[1]
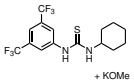	*L*-LA	[M]:[TU]:[KOMe] = 100:3:1 [M] = 1 mol L^{-1}, THF room temp.	90 sec	89	24 500 [1.07]	Waymouth and co-workers[2]
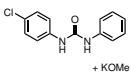	*rac*-LA	[M]:[TU]:[KOMe] = 100:3:1 [M] = 0.2 mol L^{-1}, THF −60 °C	<2 mins	93	13 900 [1.09] P_i = 0.93	Kan *et al.*[6]
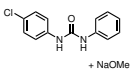	*rac*-LA	[M]:[TU]:[NaOMe] = 100:3:1 [M] = 0.2 mol L^{-1}, THF −60 °C	<2 mins	95	12 700 [1.04] P_i = 0.83	Kan *et al.*[6]
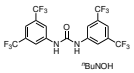	*L*-LA	[M]:[U]:[B] = 1000:1:1 [M] = 0.7 mol L^{-1}, DCM room temperature	2 mins	99	117 400 [1.09]	Jiang *et al.*[7]
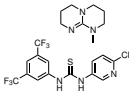	δ-VL	Solvent-free 25 °C	10 mins	99	24 600 [1.10]	Feng *et al.*[15]

6.2 Aims

There is significant precedent for the development of successful organocatalysts grafted onto inert PS-supports for ROP procedures, to exploit the versatility of these catalysts and their potential to avoid contamination of the polymer through

reuse, and recycling opportunities. The work described herein will therefore combine the PS-U (developed in the previous Chapter) with alkoxides, building on work set out by Waymouth. While earlier work with PS-U/amine systems was conducted in the melt, the use of solution-phase ROP throughout the following Chapter aims to encourage cooperativity between the two components, by omitting any complications with viscosity seen earlier. It was also not expected that immobilisation would remove the ability of the urea anion to form upon addition of the base, and further tweaking of the catalyst would allow optimisation of activity.

Although ideally both components would be immobilised, systematic and sequential changes to the known system have been carried out (Scheme 6.2). Given the nature of these (T)U/base systems, our studies have therefore focused on the immobilisation of solely the (T)U, followed by immobilisation of the base.

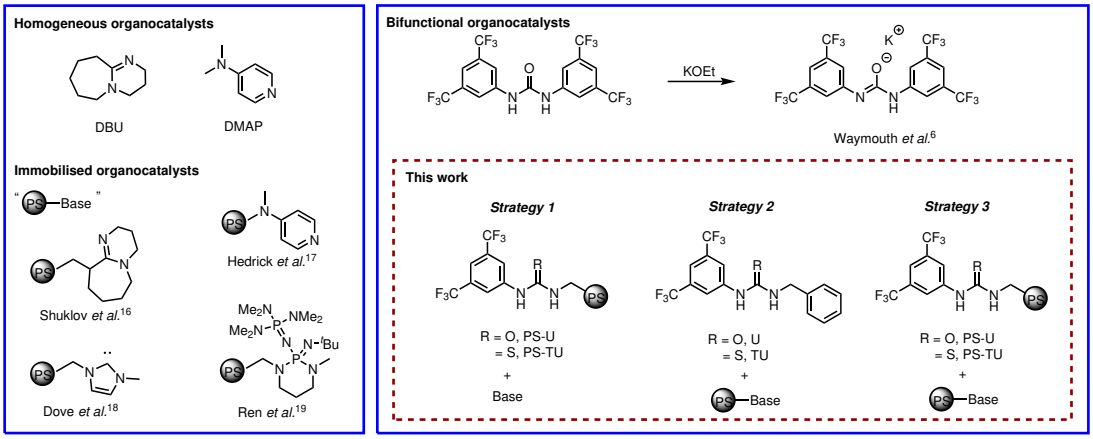

Scheme 6.2: Structures of single site and bifunctional (PS-)organocatalysts which have been used in the ROP of lactones, and immobilised (thio)urea and homogeneous analogues discussed herein.[16–19]

6.3 Results and discussion

ROP initiated by KOEt

In order to obtain optimal cooperativity between KOEt and a suitable co-catalyst, an understanding of the activity of the base itself is necessary. Using a ratio of [LA]:[B]:[KOEt]=100:0:1 (where B = base, [LA] = 1 mol L^{-1}), reactions of KOEt

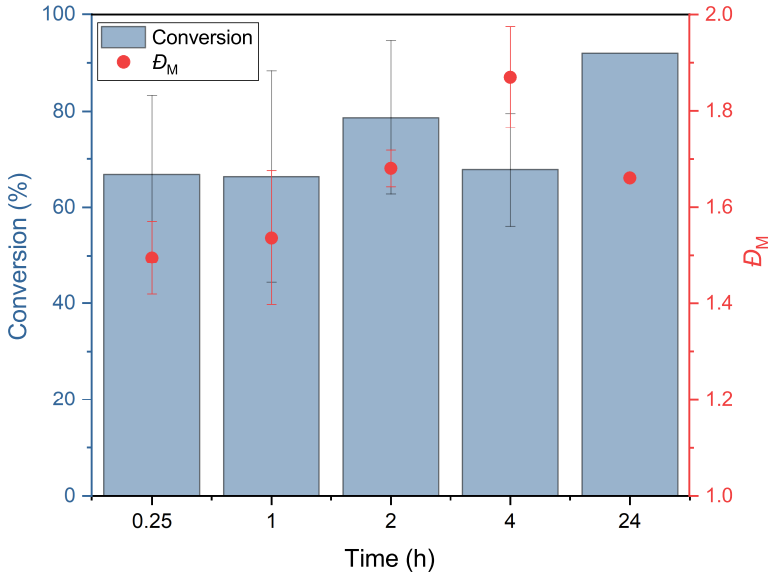

Figure 6.2: Solution-phase ROP of *L*-LA with KOEt without co-catalyst or initiator, at [LA]:[U]:[KOEt] = 100:0:1, [LA] = 1 mol L^{-1} in THF at room temperature.

with *L*-LA in THF at room temperature between 15 minutes and 24 hours, tended to yield high conversions within 15 minutes (>60%), with a general increase in M_n with conversion and monomodal SEC traces (Figure B.31). Although similar to the high conversions reported in literature for these bases,[2] it is clear from triplicate reactions that ROP with KOEt was unreliable (Figure 6.2). A huge variability between the different repeats was observed, indicative of a distinct lack of control over both the conversion itself, but also the dispersity ($Đ_M$), with mean dispersities higher than 1.5, and nearer to 2. Notably, little to no epimerisation was observed in the ^{1}H NMR spectra of all samples. Although unusual for such a strong base, this is perhaps due to the k_{prop} being too fast for the competing k_{trans} required to epimerise the monomer.

ROP catalysed by binary systems comprising KOEt and homogeneous or heterogeneous urea

In order to begin to control the activity, KOEt was paired with a (PS-)Urea described in Chapter 5, to obtain a cooperative mechanism. A series of ROP experiments at different timescales were carried out in THF at room temperature, using a ratio of [LA]:[PS-U]:[KOEt] = 100:3:1 (excess urea having been shown to balance both activity and the dispersity by Waymouth and co-workers).[2] The conversion did increase over time with the PS-U/KOEt system, reaching 87% conversion after 30 minutes (pink triangles, Figure 6.3A), however, the reaction had slowed significantly compared to the ROP with KOEt only. This, combined with the increased predictability of the ROP once a catalyst had been added, hinted that the catalyst had had some effect on KOEt.

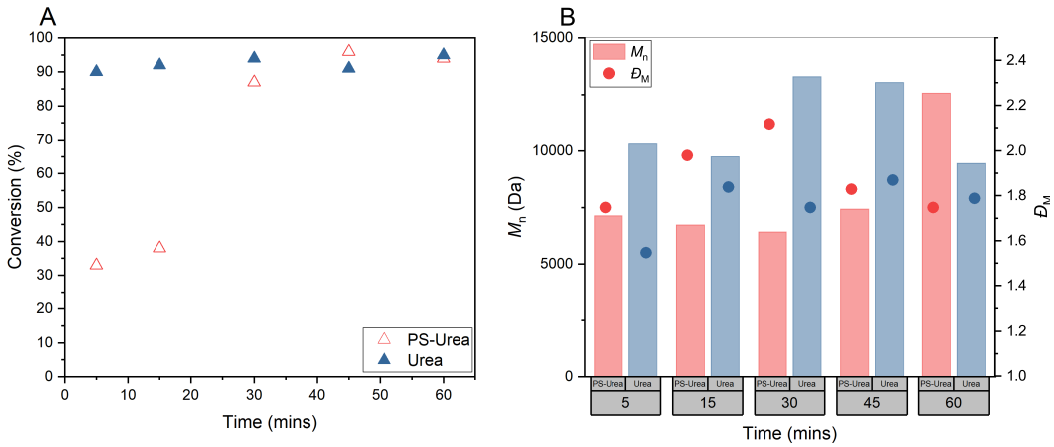

Figure 6.3: Solution-phase ROP of *L*-LA with (PS-)U/KOEt, at [LA]:[U]:[KOEt] = 100:3:1, [LA] = 1 mol L^{-1} in THF at room temperature. (A) Conversion of (PS-)U/KOEt systems over time. (B) M_n and $Đ_M$ over time (Pink: corresponds to KOEt coupled with PS-U; Blue: corresponds to KOEt coupled with homogeneous urea).

When combining of KOEt with the homogeneous urea (U, blue triangles, Figure 6.3A), similar results were obtained, although the rate of reaction was far less compromised than with PS-U/KOEt (Table 6.2). The conversion was also more predictable than KOEt reactions, once more indicating modification of KOEt by the urea, in some capacity.

Table 6.2: Solution-phase ROP of *L*-LA with KOEt in combination with either PS-U or U, at [LA]:[(PS-)U]:[KOEt] = 100:3:1, [LA] = 1 mol L^{-1} in THF at room temperature, in 15 minutes.

Entry	Catalyst	Conv. (%)[a]	$M_{n,Theo}$[b]	$M_{n,SEC}$[c]	$Đ_M$[c]
1[d]	-	67	9600	10550	1.50
2	U	92	13250	9750	1.84
3	PS-U	38	5600	6750	1.98

[a] Determined from the ^{1}H NMR spectrum.
[b] Theoretical M_n = ([LA]/[I]) × (144 × equiv. LA) × (conv./100).
[c] As determined by SEC (THF) using RI methods, relative to poly(styrene) standards (multiplied by a factor of 0.58, rounded to the nearest 50).[20]
[d] Results are mean values, calculated from repeat experiments.

For all these systems, the dispersities were still erratic ($Đ_M$ 1.43-2.12) and monomodal SEC traces were obtained (Figure B.32), although the M_n at each time point did not change significantly with conversion (Figure 6.3B).

Attempts to control the reaction using KOMe as an alternative base were investigated, yielding more promising results: After 1 hour, 96% conversion was reported with a PS-U/KOMe system ($Đ_M$ 1.54), compared to a control without PS-U of only 37% ($Đ_M$ 2.83, entries 4-5, Table A.4). Epimerisation of the monomer was observed in the ^{1}H NMR spectrum of the PS-U/KOMe catalysed reaction, potentially due to k_{trans} becoming competitive when the reaction was slowed down, which was not possible with KOEt systems.

These preliminary results indicate that combination of KOEt or KOMe with (PS)-U enables some extra control over ROP, with marginally more predictable results and longer timescales required to reach similar conversions. It was proving difficult to discern whether PS-U was having any significant effect on the activity of KOEt, it was thought that switching to a weaker base from KOEt would give any indication of cooperativity between PS-U and the base.

When investigating the scope of the PS-U/KOEt system, ROP of *rac*-LA was found to produce mostly atactic polymers, with only a slight skew towards isotactic PLA, through reaction of PS-U/KOEt system (P_r 0.45, 97% in 1 hour, M_n 7 300 Da, $Đ_M$ 1.71, Figure B.28). A beaded version of PS-U (PS-U_{beads}) was created in a similar method to the original PS-U powder, for improved recovery

of the catalyst by filtration, to similar results (97% in 1 hour, M_n 4 600 Da, $Đ_M$ 1.64, entry 3, Table A.4).

Improved control by slowing reaction down? ROP catalysed by binary systems comprising homogeneous or heterogeneous urea and weaker organic bases

Three common amine-containing bases were selected: imidazole, DMAP and DBU, having previously proved to be effective catalysts both in the melt ROP of *L*-LA (Table A.5, Figure A.1) and in combination with TU to create a co-catalytic system.[20,21] Unlike previous experiments, these bases required an initiator (I = 4-methylbenzyl alcohol), which was applied in a 1:1 ratio with the base.

No conversion was observed when PS-U was combined with either imidazole or DMAP, within 24 hours, under various reaction conditions (Table A.6), nor when the ratio was decreased to 50:1:1:1 to speed up the reaction. A solution-phase control with imidazole, for example, showed negligible conversion (4%, 24 hours, entry 1, Table A.6) compared to the melt control with the same base (64%, M_n 4 200 Da, $Đ_M$ 1.16, 4 hours, 130 °C, no solvent, entry 2, Table A.5).

ROP was still possible in solution on combination of PS-U with DBU, a stronger base than the previous two (96%, 4 hours, M_n 5 900 Da, $Đ_M$ 1.61, entry 2, Table 6.3). As with KOEt, it was still difficult differentiating between the bicomponent reaction and the DBU-only reaction. Inspection of the SEC traces was the first indication that there was a differentiation between the two systems: whilst the DBU reaction yielded a monomodal trace, the PS-U/DBU trace was slightly bimodal after 1 hour (Figure B.33), suggesting two separate mechanisms were occurring and the first sign of cooperativity between the base and the supported urea. After only 15 minutes, the bimodality was more pronounced (Figure 6.4); the shorter timescale presumably emphasised the difference between the two mechanisms (cooperative bifunctional and base-catalysed).

In the shorter timescale, PS-U/DBU system also reached a higher conversion (79%, entry 4, Table 6.3) compared to the DBU-only system (60%, entry 3, Table 6.3): this was further evidence of the cooperative mechanism. This suggested that the combination of DBU and PS-U enhanced catalytic activity compared

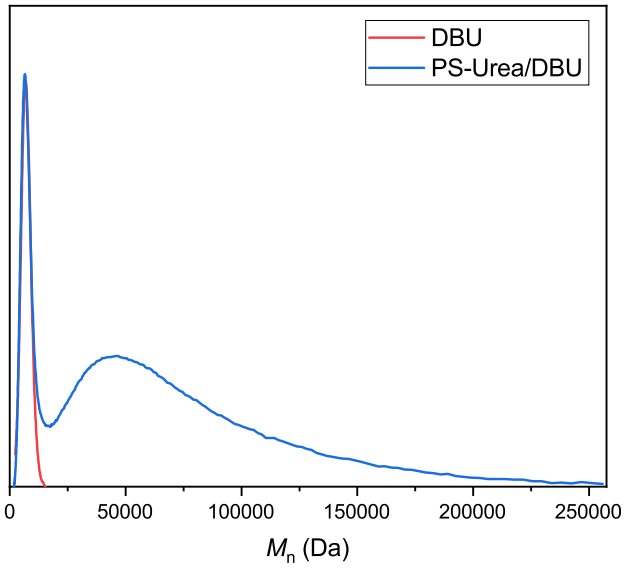

Figure 6.4: SEC traces from the ROP of *L*-LA with PS-U/DBU at [LA]:[PS-U]:[DBU] = 50:1:1, [LA] = 1 mol L^{-1} in THF at room temperature, over 15 minutes.

to the base alone, in accordance with literature reports by both Waymouth and co-workers (for U/KOMe systems),[2] and Hedrick and co-workers (for TU/DBU systems).[22]

The difficulty in monitoring of the rate exactly by NMR studies due to the heterogeneous nature of the co-catalyst, results in the need to monitor the rate by parallel batch tests, each individually quenched at varying time points. These time scales required are challenging to monitor precisely outside of flow chemistry, which can impart excellent control over residence time and reaction conditions, as demonstrated by Waymouth and co-workers.[4] Therefore, in order to work towards a fully heterogeneous system, the reaction must be slowed down to accurately investigate and understand the effects of each component. It is clear that for both KOEt and DBU, the ROP is either too quick and difficult to monitor effectively, or the choice of urea is not optimal to cooperate with KOEt properly, meaning that improvement in control of the ROP is limited.

Table 6.3: Polymerisation data for the ROP of *L*-LA with PS-U/DBU, at [LA]:[PS-U]:[DBU]:[I] = 50:1:1:1, [LA] = 1 mol L^{-1} in THF at room temperature, over 4 hours.

Entry	Catalyst	Time (h)	Conv. (%)[a]	$M_{n,Theo}$[b]	$M_{n,SEC}$[c]	$M_{w,SEC}$[c]	$Đ_M$[c]
1	-	4	98	7050	6350	9200	1.45
2	PS-Urea	4	96	6900	5900	9550	1.61
3	-	0.25	60	4300	3400	3850	1.24
4	PS-Urea[d]	0.25	79	5700	23100[e] 3500[f]	33000[e] 3900[f]	1.43[e] 1.15[f]

[a] Determined from the ^{1}H NMR spectrum.
[b] Theoretical M_n= ([LA]/[I]) × (144 × equiv. LA) × (conv./100).
[c] As determined by SEC (THF) using RI methods, relative to poly(styrene) standards (multiplied by a factor of 0.58, rounded to the nearest 50).[20]
[d] Bimodal SEC trace observed; Overall result as follows: $M_{n,SEC}{}^{Overall}$ = 5 050 [$Đ_M$ 2.87].
[e] $M_{n,SEC}$ of the first peak.
[f] $M_{n,SEC}$ of the second (shoulder) peak.

Slowing down the reaction even more towards better control: ROP catalysed by binary systems comprising homogeneous or heterogeneous thiourea and weaker organic bases

Since attempts to modify the base component of the bifunctional catalyst did not improve ROP with PS-U, switching from a urea to a TU would, according to previous research, yield a slightly slower polymerisation,[2] leaving room to quench accurately and get both good conversion and narrow $Đ_M$. Further, the immobilised TU could potentially offer improved coordination to KOEt, allowing for better modification of activity. This would allow for further investigations on the modification of activity of KOEt when in combination with an immobilised co-catalyst. Accordingly, thiourea analogues of PS-U and U (denoted as "PS-TU" and "TU") were synthesised following the same procedure as PS-U, using 3,5-bis(trifluoro-methyl)phenyl isothiocyanate as the starting material. Both PS-TU and TU were synthesised in good yields according to analysis by ESI-MS, IR and NMR spectroscopy (PS-TU: 94%, loading^{cat} = 1.97 mmol/g; TU: >99%).

ROP using the homogeneous TU/KOEt system produced up to 91% conversion within 15 minutes, with excellent dispersities ($Đ_M$ 1.20, entry 5, Table 6.4), no

Table 6.4: Polymerisation data from the solution-phase ROP of *L*-LA with (PS-) TU/KOEt, at [LA]:[TU]:[KOEt] = 100:3:1, [LA] = 1 mol L^{-1} in THF at room temperature.

Entry	Catalyst (Cat)	Base (B)	[LA]:[Cat]:[KOEt]	Time (h)	Conv. (%)[a]	$M_{n,Theo}$[b]	$M_{n,SEC}$[c]	$M_{w,SEC}$[c]	$Đ_M$[c]
1[d]	-	KOEt	100:0:1	0.25	67	9600	10550	16000	1.50
2	PS-TU	-	100:3:0	1	2	300	-	-	-
3	PS-TU	KOEt	100:3:1	1	57	8200	6850	15200	2.22
4	TU	-	100:3:0	1	2	300	-	-	-
5	TU	KOEt	100:3:1	0.25	91	13100	9700	11650	1.20

[a] Determined from the ^{1}H NMR spectrum.
[b] Theoretical M_n= ([LA]/[I]) × (144 × equiv. LA) × (conv./100).
[c] As determined by SEC (THF) using RI methods, relative to poly(styrene) standards (multiplied by a factor of 0.58, rounded to the nearest 50).[20]
[d] Results are mean values, calculated from repeat experiments.

epimerisation and monomodal SEC traces. A control using just TU yielded no conversion (entry 4, Table 6.4), while KOEt alone reached 67±33% conversion within 15 minutes (entry 1, Table 6.4, Figure 6.2). This is consistent with Waymouth and co-workers' results that demonstrated enhanced activity for the binary system compared to KOEt alone.

On the other hand, ROP using KOEt combined with the supported thiourea (PS-TU) showed a decrease in catalytic rate compared to TU/KOEt and KOEt systems. After one hour, conversions had reached only 57% with PS-TU/KOEt (M_n 6 850 Da, $Đ_M$ 2.22, entry 3, Table 6.4). This was indicative of some level of modification of KOEt activity by PS-TU, if not a cooperative mechanism.

A ^{1}H NMR binding study in THF-d_8 of the homogeneous TU analogue, compared to that of the TU on combination with KOEt (1:1), showed the disappearance of the N−H singlet at 9.20 ppm upon addition of KOEt to the TU, suggestive of deprotonation of the TU and formation of the active thioimidate anion responsible for bifunctional ROP.[3] The appearance of triplet and quartet peaks at 1.10 and 3.54 ppm, respectively, corresponded to the formation of EtOH upon deprotonation of the TU amine by the EtO^- anion (Figure 6.5, see Figures B.26-B.27 for NMR spectra in more detail). The heterogeneous nature of PS-TU made analysis under similar conditions challenging, however since the structure of PS-TU mirrors that of the homogeneous, this suggests that the same activation phenomenon occurs between the homogeneous and heterogeneous TUs.

Combination of the ROP results with the binding studies shows coordination between the two components is indeed the reason for this improved activity and

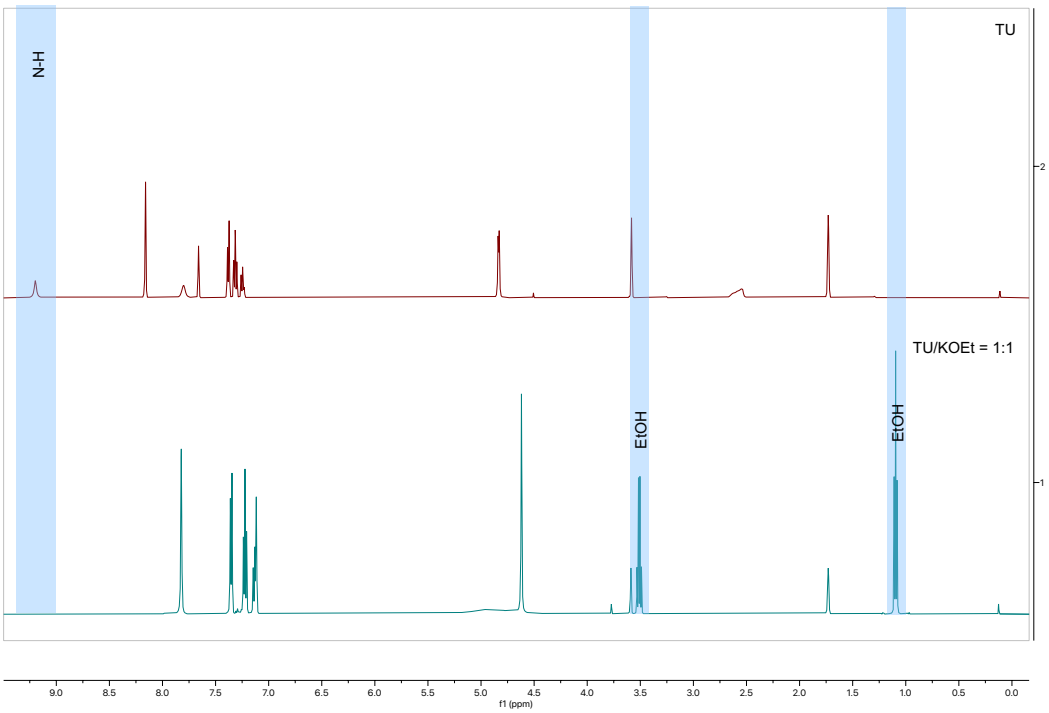

Figure 6.5: ^{1}H NMR (THF-d_8, 500 MHz) study of TU (top) and TU/KOEt (1:1, bottom). Disappearance of the peak at 9.20 ppm corresponds to the N−H abstraction by KOEt.

control. Whilst the PS-TU/KOEt results are not yet competitive with TU/KOEt – potentially due to diffusion limitations of KOEt to TU sites on PS – the initial results are promising.

In terms of polymerisation control, when higher conversions were reached, a small shoulder started to appear in the SEC trace of the PS-TU/KOEt system, which grew over time, eventually becoming a full bimodal peak after 24 hours (green column, Figure 6.6B, Figure B.34). This was evidence of two catalytic mechanisms, similar to that seen with PS-U/DBU (Figure 6.4). These could be the simple or pseudo-anionic ROP (initiated by KOEt alone) as well as the desired bifunctional mechanism involving cooperation between KOEt and the supported TU moiety. If – as observed in the binding study – the KOEt was able to coordinate to the homogeneous TU analogue, then this could be extrapolated to the PS-TU as well, thus explaining the change in activity and SEC bimodality

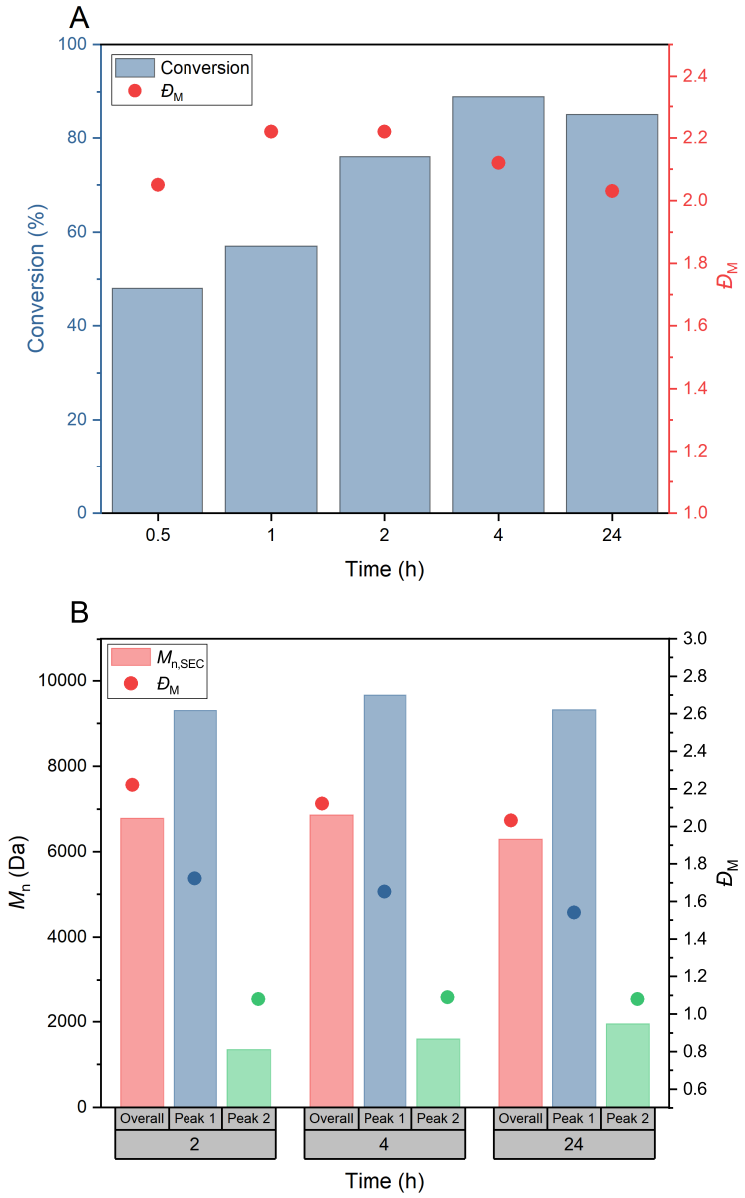

Figure 6.6: A) Solution-phase ROP of *L*-LA with PS-TU/KOEt, at [LA]:[PS-TU]:[KOEt] = 100:3:1, [LA] = 1 mol L^{-1} in THF at room temperature, over 24 hours. B) Breakdown of the M_n from 2-24 hours into the two separate peaks, pink = overall M_n; blue = M_n of first peak (main); green = M_n of second peak (shoulder).

due to a secondary mechanism seen in the ROP catalysed by PS-TU/KOEt.

Changing the reaction conditions

There is clearly a balance between conversion and bimodality; at higher conversions, there is a higher likelihood of oligomers. In order to push the conversions whilst retaining monomodality at timescales which avoided bimodality (1 hour), the ratio and concentration were altered.

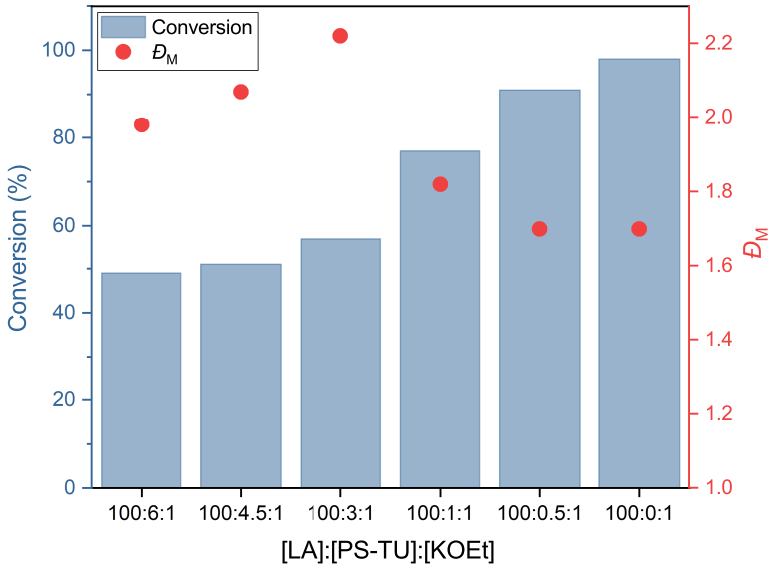

Figure 6.7: ROP of *L*-LA with PS-TU/KOEt at varying ratios, [LA] = 1 mol L^{-1} in THF at room temperature, over 1 hour. When [LA]:[PS-TU]:[KOEt] = 100:0:1, results were unpredictable (Figure 6.2).

It was thought that increasing the excess of PS-TU with respect to KOEt would decrease the likelihood of any free KOEt remaining in the system, thereby slowing down the reaction (leading to lower conversion) and reducing the $Đ_M$ in the process. Reducing the amount of PS-TU would therefore have the opposite effect, leaving an increased concentration of free KOEt available for uncontrolled, fast ROP. While the former was observed when the PS-TU:KOEt ratio was increased to 6:1 (49%, $Đ_M$ 1.98), when the ratio was brought down to 1:1, the conversion and $Đ_M$ improved dramatically (77%, $Đ_M$ 1.82, Figure 6.7). Similar observations

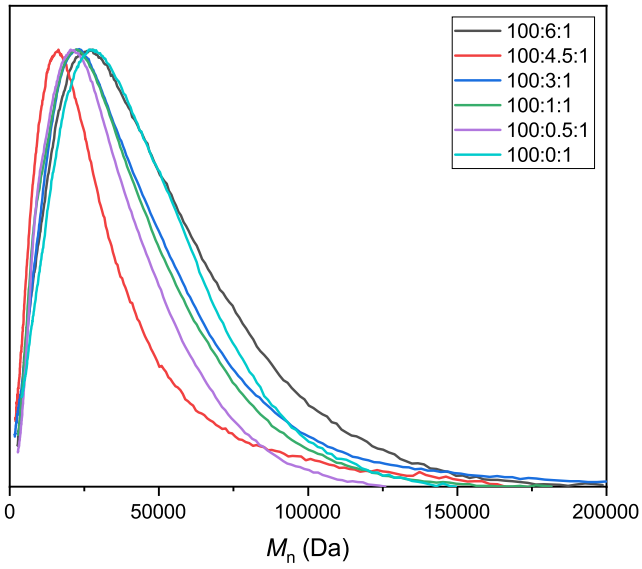

Figure 6.8: SEC traces from the ROP of *L*-LA with PS-TU/KOEt at varying ratios, [LA] = 1 mol L^{-1} in THF at room temperature, over 1 hour. Legend refers to [LA]:[U]:[B] ratio.

were noted by Zhang *et al.*: increasing the TU excess to 5:1 reduced the $Đ_M$ to 1.15 from 1.21 at 1:1.[3]

Notably, none of the SEC traces at ratios below 1:1 (where higher conversions were reached) were bimodal, likely because the secondary mechanism, resulting from cooperativity between the two components, was suppressed at ratios below 1:1 (Figure 6.8). However, previous evidence from the ^{1}H NMR binding study show that all of the TU had coordinated to the KOEt when in a 1:1 ratio, due to the complete disappearance of the N−H singlet. Thus, the ROP result at this ratio seemed to balance both lower dispersity, higher conversion and a monomodal SEC trace, due to coordination between the two components, which could not be achieved at lower ratios. It is worth noting that at 0.5:1 or 0:1, there is not enough PS-TU to coordinate to the KOEt, leaving room for uncontrolled ROP by the free KOEt. Instead, the conversion could be improved past 57% within an hour, without compromising the shape of the SEC curve, if a 1:1 ratio was applied.

Table 6.5: Polymerisation data from the solution-phase ROP of *L*-LA with PS-TU/KOEt, at [LA]:[PS-TU]:[KOEt] = 100:3:1, at various monomer concentrations in THF at room temperature.

Entry	[LA] (mol L^{-1})	Time (h)	Conv. (%)[a]	$M_{n,Theo}$[b]	$M_{n,SEC}$[c]	$M_{w,SEC}$[c]	$Đ_M$[c]
1	0.5	1	22	3150	2950	5350	1.82
					3750	7850	2.10
2	0.5	2	63	9100	5700	8900	1.56
					1200	1300	1.09
3	1	1	57	8200	6850	15200	2.22
4	2	0.5	38	5500	9850	18900	1.91
5	2	1	75	10800	7350	14250	1.95
6	2	1	74	10650	8550	18150	2.13

[a] Determined from the ^{1}H NMR spectrum.
[b] Theoretical M_n= ([LA]/[I]) × (144 × equiv. LA) × (conv./100).
[c] As determined by SEC (THF) using RI methods, relative to poly(styrene) standards (multiplied by a factor of 0.58, rounded to the nearest 50).[20]

When the concentration of LA was reduced to 0.5 mol L^{-1} from the initial polymerisations at 1 mol L^{-1}, the conversion was just under half of the original result within one hour. If the bimodality was a product of concentration, that would mean that either reducing or increasing the concentration of LA would remove the bimodal traces at the equivalent time points. However, at half concentration, but doubled time (two hours), the SEC trace was strongly bimodal, suggesting that the bimodality was not due to the viscosity of the 1 mol L^{-1} solutions, but likely due to the cooperativity between the two components generating an alternative ROP mechanism (63%, M_n 3 750 Da overall, $Đ_M$ 2.10, entries 1-2, Table 6.5).

Despite potential issues in solubility of the LA and KOEt, increasing the concentration to 2 mol L^{-1} resulted in a 75% conversion within 1 hour (entries 4-6, Table 6.5), a significant improvement from the 57% observed at 1 mol L^{-1} (entry 3, Table 6.5), although most importantly, the SEC trace remained monomodal, with no evidence of oligomerisation, so there is some evidence that concentration is an important factor in the ROP with the bifunctional catalyst.

These two studies indicate that pushing up the conversion, without compromising the monomodality, is likely dependent both on a balance between on the ratio between the co-catalysts and the concentration.

Are two heterogeneous components possible?

In an effort to move towards a fully heterogeneous ROP system, the base would also need to be immobilised. Although not immediately possible to immobilise the KOEt component, a commercially available immobilised version of DBU (PS-DBU) was selected (Figure 6.4). At [LA]:[PS-TU]:[Base]:[I]=100:3:1:1, PS-TU was combined with both DBU or PS-DBU, to monitor the differences in using a homogeneous and heterogeneous base.

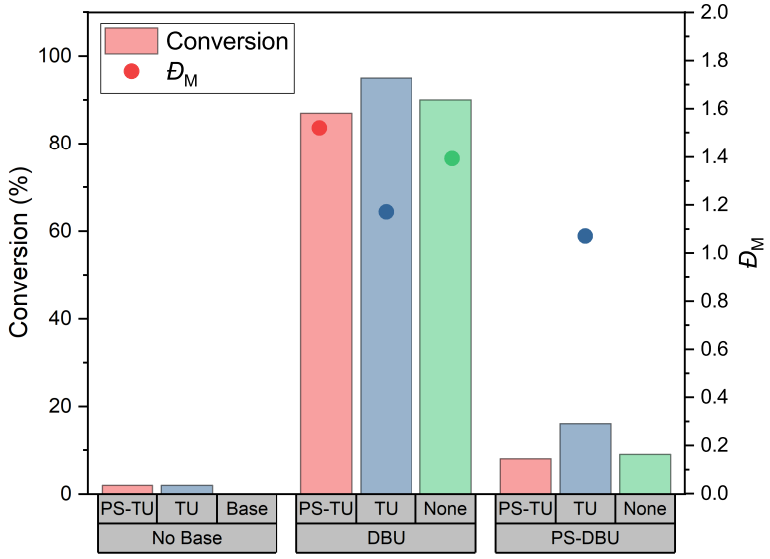

Figure 6.9: Solution-phase ROP of *L*-LA with (PS-)TU and a (PS-)base, at [LA]:[TU]:[B]:[I] = 100:3:1:1, [LA] = 1 mol L^{-1} in THF at room temperature, over 1 hour.

The best results were predictably obtained when both components were homogeneous in nature, with conversions reaching 95% and $Đ_M$ 1.17, which was lower from 1.39 when no TU was used (Figure 6.9, entries 1 and 7, Table A.7). Similarly, when PS-DBU was used, the best result was achieved using the homogeneous TU (16%, $Đ_M$ 1.07, entry 8, Table A.7), compared to <9% achieved in the dual heterogeneous system or the controls (entry 2, Table A.7), suggesting that combination of two heterogeneous co-catalysts reduced the ability of the two to coordinate, due to friction and movement between the catalyst particles which

removes ability to coordinate both components to get bifunctional/cooperative activity, as seen in the previous Chapter. In contrast, the free TU could more easily coordinate to the heterogeneous base, even when the latter was immobilised. SEC traces from both TU/DBU and PS-TU/DBU reactions are bimodal, not seen with DBU alone, confirming similar cooperativity to the PS-TU/KOEt systems (Figure 6.10).

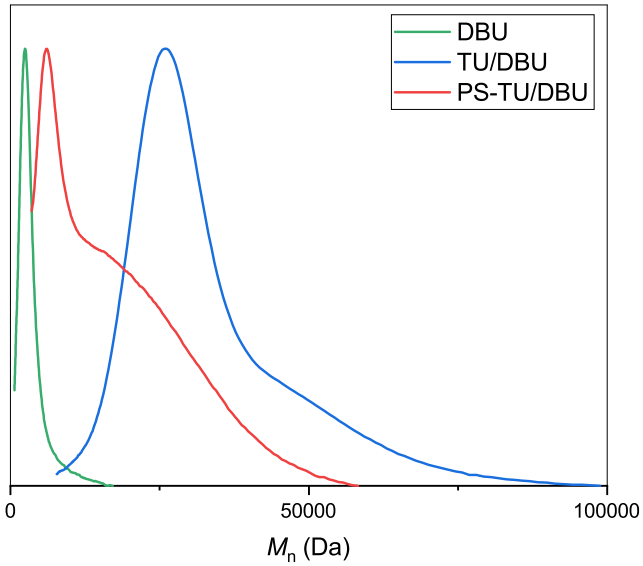

Figure 6.10: SEC traces from the ROP of *L*-LA with (PS-)TU/DBU at [LA]:[TU]:[DBU]:[I] = 100:3:1:1, [LA] = 1 mol L^{-1} in THF at room temperature, over 1 hour.

The same trends were emphasised when the feed ratio was lowered to 50:1:1:1 (Figure A.2). Using a 1:1 ratio of PS-TU to DBU, the conversion dropped from 88% in the DBU control ($Đ_M$ 1.18), to 79% ($Đ_M$ 2.93), whilst TU/DBU had a high conversion and low dispersity (93%, $Đ_M$ 1.25), with reduced epimerisation than the DBU control, suggesting that the TU had effectively improved ROP control. When DBU was replaced with PS-DBU, conversion was increased from 13 to 22% ($Đ_M$ 1.11 for both) upon combination with PS-TU, however when combined with free TU, the conversion reached 70% ($Đ_M$ 1.08). The earlier conclusion that homogeneous components improve cooperativity seems true and it is therefore clear that optimum results are obtained if at least one of the components is

homogeneous.

6.4 Conclusions and future work

Immobilisation of the classic TU/base systems proved challenging and required intricate tailoring of reaction conditions such as catalyst ratio and monomer concentration in order to maximise the conversion without promoting oligomerisation at higher conversions. Reducing the ratio to 100:1:1 or increasing monomer concentration to 2 mol L^{-1} were both found to push the conversion to above 70% within one hour, without resulting in a bimodal SEC, however dispersities remained high in all cases, leaving room for work towards a more controlled heterogeneous catalyst, potentially through modification of the TU structure and substituents themselves.

Immobilisation of the TU is preferred over immobilisation of the base, due to the potentially toxic nature of the TU. Nevertheless, bimodal SEC traces suggested more than one mechanism at play, consisting of either the cooperative bifunctional or the anionic basic mechanism.

In contrast, PLA from solution-phase ROP with immobilised bases and homogeneous (T)Us remained largely monomodal. The activity of the base alone was maintained upon combination with the (T)U, under the same conditions and it was also accompanied by a decrease in dispersity (and therefore an increase in control), potentially due to the better coordination between the two components.

Pushing towards a fully heterogeneous system revealed an order of activity of TU/DBU >TU/PS-DBU>PS-TU/DBU>PS-TU/PS-DBU, which supported the idea that at least one component should remain homogeneous to retain activity, and selection of appropriate combinations of catalyst and base were vital to improvement in ROP activity. This idea was further reinforced when taking into consideration the results from the solvent-free ROP from Chapter 5.

As such, in order to get a working, fully heterogeneous system, a number of routes can be taken: continued catalyst optimisation is one avenue of interest, improving the dispersities and control by altering TU structure for reactions involving PS-TU/PS-Base system. Alternatively, immobilisation of both components on

one single site would be of significant interest. This has already been explored to some degree by Dixon and co-workers, who separately developed a bifunctional iminophosphorane (BIMP) catalyst for ROP of LA, and PS-BIMP catalyst for small molecule synthesis.[13,23] This opens up the possibility of using these immobilised single-site catalysts for ROP, to exploit the bifunctional nature mechanism in a single-site heterogeneous catalyst.

References

[1] R. C. Pratt, B. G. Lohmeijer, D. A. Long, P. N. Lundberg, A. P. Dove, H. Li, C. G. Wade, R. M. Waymouth and J. L. Hedrick, *Macromolecules*, 2006, **39**, 7863–7871.

[2] B. Lin and R. M. Waymouth, *J Am Chem Soc*, 2017, **139**, 1645–1652.

[3] X. Zhang, G. O. Jones, J. L. Hedrick and R. M. Waymouth, *Nat Chem*, 2016, **8**, 1047–1053.

[4] B. Lin, J. L. Hedrick, N. H. Park and R. M. Waymouth, *J Am Chem Soc*, 2019, **141**, 8921–8927.

[5] B. Lin and R. M. Waymouth, *Macromolecules*, 2018, **51**, 2932–2938.

[6] Z. Kan, W. Luo, T. Shi, C. Wei, B. Han, D. Zheng and S. Liu, *Front Chem*, 2018, **6**, 547.

[7] Z. Jiang, J. Zhao and G. Zhang, *ACS Macro Lett*, 2019, **8**, 759–765.

[8] C. Tan, S. Xiong and C. Chen, *Macromolecules*, 2018, **51**, 2048–2053.

[9] S. Naumann, P. B. V. Scholten, J. A. Wilson and A. P. Dove, *J Am Chem Soc*, 2015, **137**, 14439–14445.

[10] B. Wang, L. Pan, Z. Ma and Y. Li, *Macromolecules*, 2018, **51**, 836–845.

[11] C. Thomas, F. Peruch, A. Deffieux, A. Milet, J.-P. Desvergne and B. Bibal, *Adv Synth Catal*, 2011, **353**, 1049–1054.

[12] J. Y. C. Lim, N. Yuntawattana, P. D. Beer and C. K. Williams, *Angew Chem Int Edit*, 2019, **58**, 6007–6011.

[13] A. M. Goldys and D. J. Dixon, *Macromolecules*, 2014, **47**, 1277–1284.

[14] A. P. Dove, R. C. Pratt, B. G. G. Lohmeijer, R. M. Waymouth and J. L. Hedrick, *J Am Chem Soc*, 2005, **127**, 13798–13799.

[15] R. Feng, S. Jie, P. Braunstein and B. G. Li, *Eur Pol J*, 2019, **121**, 109293.

[16] I. A. Shuklov, H. Jiao, J. Schulze, W. Tietz, K. Kühlein and A. Börner, *Tetrahedron Lett*, 2011, **52**, 1027–1030.

[17] F. Nederberg, E. F. Connor, M. Möller, T. Glauser and J. L. Hedrick, *Angew Chem Int Edit*, 2001, **40**, 2712–2715.

[18] A. P. Dove, R. C. Pratt, B. G. Lohmeijer, D. A. Culkin, E. C. Hagberg, G. W. Nyce, R. M. Waymouth and J. L. Hedrick, *Polymer*, 2006, **47**, 4018–4025.

[19] C. Ren, X. Zhu, N. Zhao, Y. Shen, L. Chen, S. Liu and Z. Li, *Eur Pol J*, 2019, **119**, 130–135.

[20] J. Baran, A. Duda, A. Kowalski, R. Szymanski and S. Penczek, *Macromol Rapid Comm*, 1997, **18**, 325–333.

[21] O. I. Kazakov, P. P. Datta, M. Isajani, E. T. Kiesewetter and M. K. Kiesewetter, *Macromolecules*, 2014, **47**, 7463–7468.

[22] B. G. Lohmeijer, R. C. Pratt, F. Leibfarth, J. W. Logan, D. A. Long, A. P. Dove, F. Nederberg, J. Choi, C. Wade, R. M. Waymouth and J. L. Hedrick, *Macromolecules*, 2006, **39**, 8574–8583.

[23] A. M. Goldys, M. G. Núñez and D. J. Dixon, *Org Lett*, 2014, **16**, 6294–6297.

Chapter 7

Flow ROP for Data Encryption Through Defined Molecular Weight Distributions

The following research was carried out at Monash University in the Junkers group, extending their work on data encryption with reversible addition-fragmentation chain transfer (RAFT) to include ROP.

7.1 Introduction

We have already seen the benefits of flow chemistry and various examples of both homogeneous and heterogeneous chemistry, in Chapter 1. More specifically, microreactors (<1 000 μm diameter) have become an attractive option for the application of flow chemistry on a lab scale. Materials covering various tubing materials to syringe pumps are often both widely available and a far cheaper option compared to more industrial scale materials such as stainless steel, which are used in more complex, high pressure reactors. For the majority of small scale chemistry, however, the latter is not necessary, and more simple, flexible tubing which is easier to handle and mould to the reactions requirements, will suffice. The adaptable design of the reactor allows for a huge range of chemistries to be applied to these flow systems.[1]

The high surface-to-volume ratios due to the small microreactor diameters not only allow for excellent heat transfer (thus the ability to translate a wide range of reaction conditions across the reactor almost instantly), but smaller volumes can be used. This in turn decreases potential hazards associated with the reagents, and a "numbering up" approach of aligning several reactors in parallel is an efficient method to scale up the process, without compromising the reaction's efficiency and mitigating any of the traditional economic risks associated with scaling up.

Mixing efficiency and precise control over residence times allow for excellent control of the final product;[2] in the field of polymer chemistry, for example, this translates to an improvement in M_{n} and monodisperse, narrow $Đ_{\mathrm{M}}$ over batch reactions.[3–7]

Whilst many of the basics of flow chemistry were discussed in Chapter 1, the following sections will detail how this technology can be beneficial to polymerisations, and the final properties of the polymers.

Molecular weight distributions and polymer properties

In order to address how microreactors can affect polymer structure, we must first outline how we define polymers. Synthetic polymers typically exist in a range of molecular weights – the distribution of which is typically described by the dispersity ($Đ_{\mathrm{M}}$) and determined by SEC. However, defining a polymer simply in terms of dispersity and M_{n} is reductive and often ignores the overall shape of the distribution, which in itself changes macromolecular properties such as elasticity and viscosity.[8–13]

Molecular weight distributions (MWDs) describe the overall shape of the polymer distribution curve, and are intrinsically related to the dispersity.[14] However, the MWD can provide further information about the polymerisation method: A broad MWD can be indicative of a slow rate of initiation, leading to consumption of the monomer before all initiating molecules have been used up.[7] As a result, the $M_{\mathrm{n,SEC}}$ will be less than the theoretical molecular weight. Alternatively, bimodal MWDs are frequently associated with two separate catalytic mechanisms (potentially due to multiple initiators), each operating at different

rates.

Likewise, the shape of the MWD can be changed through modification of the polymerisation process, to tailor the desired properties. Most research has focussed on narrowing the breadth of the MWD, rather than the shape: Frey and co-workers improved the mixing efficiency by changing the flow rate, such that narrower dispersities were accessible.[15] Other efforts to control the shape of the MWD have included changing the solvent partway through reaction has enabled the production of bimodal SEC traces.[7] Similarly, temporal regulation of initiation periods and concentrations offered an excellent route to control the stiffness of block copolymers of poly(styrene) and poly(isoprene) by modulating the symmetry of the MWD, a method which has been utilised frequently.[8,14,16]

These methods are challenging and require tailoring of the reaction conditions to each individual polymer; application of the same procedure needs laborious optimisation before desired MWD shapes can be obtained, and targeting a wide range of specific MWD shapes through these methods is difficult. Thus, mixing polymer samples with varying dispersities has opened up a new route towards obtaining customised MWDs, although batch synthesis of multiple polymers can be time and labour intensive.[17,18] More recently, Boyer and co-workers utilised the versatility of flow polymerisations to get tailored MWDs, by modifying flow rates, concentrations and light intensities and wavelengths.[19,20] The flow set-up allowed for rapid generation of multiple polymer fractions of different M_{n}, which could then be mixed to obtain customised MWDs.

As seen in the examples outlined above, the increased polymerisation control offered by flow chemistry allows precise modulation over the molecular weight, dispersity and MWD necessary to adapt the polymer properties. Junkers and co-workers developed a predictive framework enabling the determination of which polymer fractions were required to be mixed together to obtain target MWDs.[21,22] Gamma and Gaussian distributions were used to model theoretical MWDs based on polymer fractions with known distributions, such that even multimodal MWDs were predictable, with good experimental consistency. A similar strategy was adopted by Boyer and co-workers: combining raw SEC data with modelling to enable the design of specific MWDs, using a different model.[23] Subsequent automation of the flow reactor – such that several polymer fractions could be accurately

generated in rapid succession – significantly reduced the time intensive process required for this type of MWD modulation.[24] Integration of a feedback loop into the flow reactor, based on in-line benchtop NMR or SEC analysis is also beneficial to speed up the production process of accurate and precise polymer fractions, and enabling self-optimisation.[25,26]

Data encryption: an emerging field in polymer chemistry

The development of software to correctly predict theoretical MWDs from experimental data and extension of this feature to accurately determine which polymers were required in each mixture of polymers to generate desired MWDs, has enabled further advancements in the field of polymer chemistry. Not only does this new capability and software enable generation of multimodal polymers with the goal of altering polymer properties, but a new field has emerged as a result.

If the "forward process" is defined as the act of obtaining discrete polymer fractions with differing properties (through batch or flow) and mixing of these to create random or predicted MWDs, then the "backward process" can be defined as the act of going in the opposite direction, deconstructing overall MWDs to identify which polymer fractions have been used in what ratio. Junkers and co-workers recently exploited this feature, utilising the individual poly(styrene) samples within an overall MWD to store data, thereby developing a method of data encryption.[27]

Unique MWDs were obtained using the mixture of five polymers, including one

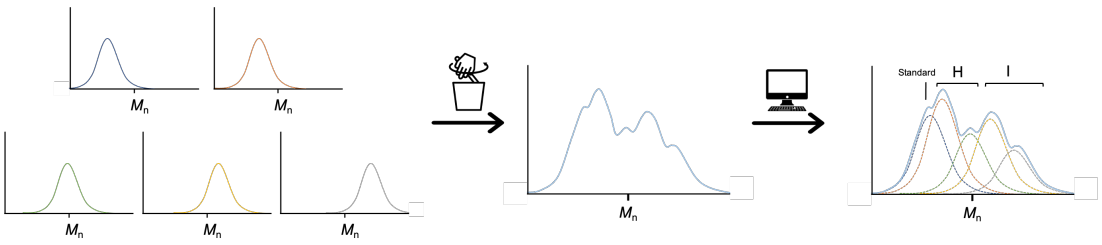

Scheme 7.1: The encryption keys (5 polymers of different M_n) are mixed together in different mass ranges to generate a unique MWD. This can then be deconvoluted by an algorithm, which reads out the mass ranges of the polymers in order against an internal standard, to reveal the encrypted letters – in this case, the word "Hi".

internal standard (polymer 1); the remaining four polymers were grouped into two separate encoded letters (polymers 2-3 and 4-5). The mixture of two polymers in different mass ratios determined which letter had been encoded – a more in depth description of the process is defined in this research. Thus, unique MWDs would result from the mixture of all five polymer fractions together (Scheme 7.1).

These could then be de-convoluted using software based on the Gaussian distribution software developed in their earlier research, described in the previous section. The decryption process enabled the extrapolation of the individual polymer mass fractions from the overall MWD, but could only occur if the properties (M_n and $Đ_M$) of the individual polymers in the mixture were known. The individual macromolecules act as so-called "encryption keys", which are used to unlock the overall MWD, revealing the mass fractions of each polymer. Since couples of polymers in specific mass range combinations described specific characters, the de-convolution of the MWD revealed a sequence of letters. Decryption of MWDs was possible across continents, proving the ability of the polymers to act as reliable "barcodes" to store data.

7.2 Aims

The ability for the size and shape of a polymer's MWD to affect the polymer properties, and tailoring the distribution, has proven a successful method of harnessing the desired properties. The application of polymers to the field of data encryption, by manipulating MWDs, has opened a new area of research and developed a novel use for polymers. Coupled with the vast array of different polymers – accessible not only through different polymerisation methods, but also through increased polymer design to modify existing polymers and creating block copolymers – the data density possible in data encryption seems exponential.

Importantly, synthesis of multiple different polymers with different MWD targets can be labour intensive and impractical and as such, there are some key requirements for the polymers in order for this field to be competitive with other methods of data encryption. Namely, rapid generation of encrypted datasets would be impossible with slow polymerisation reactions; it is imperative that

rapid reactions are selected to avoid the synthetic step becoming rate limiting in the encryption process. For this reason, research has focused on radical polymerisation techniques such as RAFT polymerisation. However, equally important is the need to have narrow dispersities, to allow the decryption software to readily identify which polymer corresponds to the MWD. While RAFT provides polymers of decent dispersity, ROP often provides rapid generation of polymers of far narrower dispersities, and is thus an interesting and reliable candidate.

Initial discussion will focus on the application of ROP of *L*-LA into a flow microreactor. Rapid production of polymer was possible under these conditions, such that future development of a robust system to access various poly(lactones) might also be possible, with potential to couple it to an automated system. The second part will focus on the use of the different polymers in data encryption, through the creation of unique MWDs and attempts to deconvolute them.

7.3 Results and discussion

Reactor set-up

A 250 μL reactor was constructed using a 1.27 m length of PFA tubing (internal diameter, I.D. = 0.5 μm; outer diameter, O.D. = 1/16"), and wrapped into a coil; the length of the tubing (L) was calculated using Equation 7.1, where V = total volume and D = internal diameter of tubing.

$$V = \frac{\pi D^2}{4} \cdot L \tag{7.1}$$

The tubing was placed in an oil bath to maintain a constant temperature. One end of the tubing was inserted through the rubber septum of an SEC vial for sample collection. The other end of the coiled reactor was connected to a Y-piece mixing unit (PEEK, P-512, Upchurch Scientific). This was attached to two gastight 1 mL syringes (SGE) using short tubing (10 cm) of the same dimensions as the reactor. The syringes were attached to a Chemyx syringe pump to control the flow rates. Flow rates were calculated using Equation 7.2.

$$\text{Total Flow Rate } (\mu L\ min^{-1}) = \frac{\text{Reactor Volume } (\mu L)}{\text{Residence Time}, \tau_{\text{r}}\ (min)} \tag{7.2}$$

Once the flow rate had been set for the reaction, the reaction was allowed to reach steady state (so reached a consistent conversion indicating the monomer has spent the appropriate residence time in the reactor) prior to sample collection (Equation 7.3). An illustration of the reactor components is shown in Scheme 7.2 and Figure 7.1.

$$\text{Steady State } (min) = 1.5 \times \text{Residence Time } (min) \tag{7.3}$$

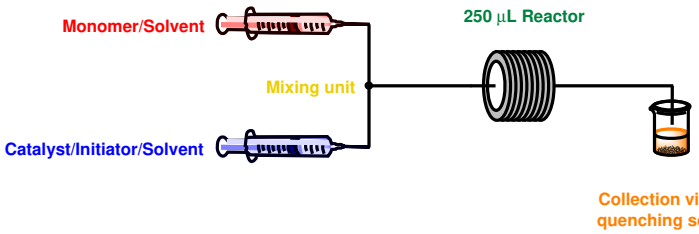

Scheme 7.2: Schematic representation of the flow reactor, set up with two 1 mL syringes, containing either the monomer or the catalyst/initiator stock solutions. The two streams merge through a Y-piece mixing unit.

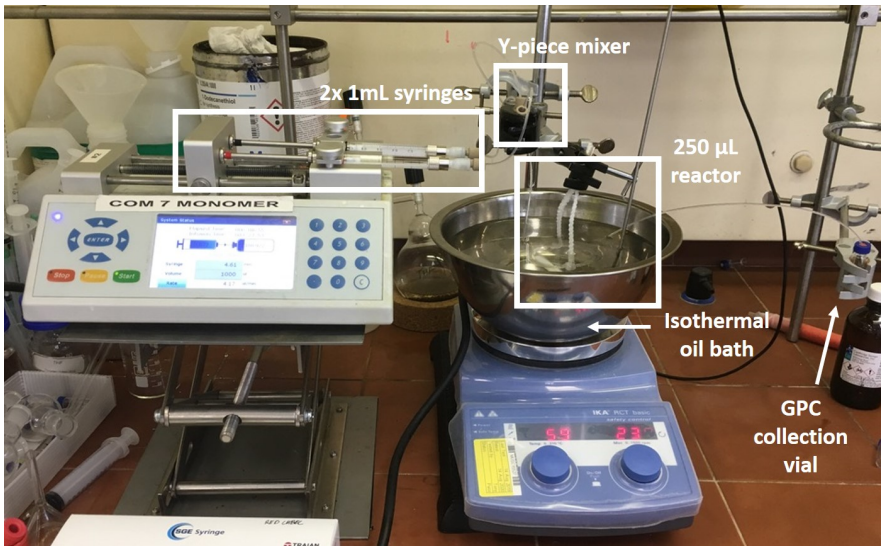

Figure 7.1: Reactor set for the ROP of lactones in flow.

Test on ϵ-caprolactone

Preliminary studies focused on using stock solutions of ϵ-caprolactone (CL) and benzyl alcohol (BnOH). Reactions were catalysed by TBD and carried out at [CL]:[Cat]:[I] = 50:1:1, with a starting concentration of [CL] = 1 mol L^{-1} in anhydrous toluene.

Although the conversion was poor at 60 °C, it could be increased to 62% in 30 minutes at 8.33 μL min^{-1}, by increasing the temperature to 80 °C, maintaining a $Đ_M$ of around 1.25 (entries 1 and 3, Table 7.1). At 80 °C, M_n increased linearly with conversion, indicative of a living polymerisation. 88% conversion was achieved upon increasing the residence time to 60 minutes (entry 4, Table 7.1).

The dispersity increased to 1.43, presumably due to the increased adverse effects of laminar flow patterns on dispersity at longer residence times, which would leave more room for the central "column" of fluid to travel further than the fluid in contact with the reactor wall – this could also explain the increased difference between the theoretical and experimental M_n.[2] The slow manual quenching method also contributed to the higher dispersity, although this was not such an issue with slower reactions at higher temperatures.

Despite excellent preliminary results, quicker rates were required in order to work towards a fully automated system, with quick changes to flow rates and concentrations to modify the molecular weights. Moving to other, more reactive monomers such as lactide could remedy this issue. Further tests were therefore carried out

Table 7.1: Polymerisation data from the ROP of ϵ-CL with TBD, using [CL]:[Cat]:[I] = 50:1:1 in anhydrous toluene ($[CL]_{final}$ = 1 mol L^{-1}), with varying reaction conditions.

Entry	Temp. (°C)	Residence time, τ_r (min)	Flow rate (μL min^{-1})	Conv. (%)[a]	$M_{n,Theo}$[b]	$M_{n,SEC}$[c]	$M_{w,SEC}$[c]	$Đ_M$[c]	DP_{SEC}[c]
1	60	30	8.33	49	2800	800	950	1.25	4
2	80	15	16.67	45	2550	2000	2500	1.23	10
3	80	30	8.33	62	3550	2350	2900	1.23	12
4	80	60	4.17	88	5000	3200	4600	1.43	16

[a] Determined from the ^{1}H NMR spectrum.
[b] Theoretical M_n= ([CL]/[I]) × (114 × equiv. CL) × (conv./100).
[c] As determined by SEC (THF).

with this goal in mind.

Screening conditions in the ROP of *L*-LA with TBD

Table 7.2: Polymerisation data from the ROP of *L*-LA, using [LA]:[Cat]:[I] = 50:1:1 at 25°C, with varying reaction conditions.

Entry	Solvent	Catalyst	[LA] (mol L^{-1})	Mixer	Quench	τ_r range (min)	Conv. (%)[a]	$M_{n,SEC}$[b]	$Đ_M$[b]
1	Toluene	TBD	1	Y	Benzoic acid (BA)[c]	-	-	-	-
2	Toluene/THF	TBD	1	Y	Benzoic acid (BA)[c]	2 - 5	> 90	2300 - 5100	1.74 - 2.25
3	THF	TBD	1	Y	BA[c]	30 s - 2	> 96	700 - 1050	2.09 - 2.25
4	THF	TBD	1	Y	BA (1 mg/mL)	30 s - 2	> 93	4700 - 8150	2.14 - 2.24
5	THF	TBD	1	Y	BA + THF[d]	5 s - 2	> 90	3600 - 6550	2.04 - 2.36
6	THF	TBD	1	Static[e]	BA + THF	10 s - 2	> 92	2550 - 2900	1.71 - 1.74
7	DCM	TBD	1	Y	BA + THF	2.5 s - 1	> 89	3700 - 4950	1.72 - 2.22
8	DCM	TBD	0.5	Y	BA + THF	2.5 s - 1	> 88	3800 - 4900	1.35 - 2.15
9	DCM	DBU	1	Y	BA + THF	5 s - 60	36 - 99	1350 - 4650	1.19 - 1.55
10[f]	DCM	DBU	1	Y	BA + THF	30 s - 5	77 - 96	2700 - 4150	1.19 - 1.31

[a] Determined from the ^{1}H NMR spectrum.
[b] Ranges determined by SEC (THF), with applied Mark-Houwink parameters.
[c] BA delayed addition by spatula.
[d] 3 drops of BA in THF (1 mg mL^{-1}) + 0.5 mL THF.
[e] Static mixer causes leaking in the reactor due to lactide crystallisation out of solution, which blocked the mixing ball in the static mixer.
[f] Temperature = 35 °C.

Subsequent work focussed on optimising the ROP of *L*-LA over ϵ-CL, keeping the original ROP conditions explored in the ROP of ϵ-CL ([LA]:[Cat]:[I] = 50:1:1 where Cat = TBD, [LA] = 1 mol L^{-1} in toluene). Solubility issues of *L*-LA in toluene were present, so ROP was not possible (entry 1, Table 7.2). When a 50:50 mix of toluene and THF (by creating a solution of *L*-LA in THF, whilst the catalyst/initiator solution remained in toluene) the LA would crystallise out of solution once the two streams combined, so SEC data from these tests were not reliable (entry 2, Table 7.2).

Similar uncontrolled results were obtained in THF – despite the improved solubility – and although conversions consistently reached above 96%, all $Đ_M$ exceeded 2.09 (entry 3, Table 7.2). This was likely due to transesterification occurring at high conversions reached in short timescales to the speed of reaction. No change to the dispersity was seen when the quenching method was improved: creating a solution of benzoic acid in THF, then placing the latter into the collection vial to get a more immediate, effective and controlled quenching method which removed any human errors in quench timings (entry 4, Table 7.2). Shortened residence times of 5 seconds also did not improve control (96%, $M_{n,Theo}$ 6 300 Da, $M_{n,SEC}$ 3 600 Da, $Đ_M$ 2.36, entry 5, Table 7.2).

Although no correlation between flow rate, conversion and dispersity was evident,

Table 7.3: Polymerisation data from the ROP of *L*-LA with TBD, using [LA]:[Cat]:[I] = 50:1:1, [LA] = 1 mol L^{-1} in THF, 1 minute residence time at 25 °C, with different quenching methods.

Entry	Quench	Conv. (%)[a]	$M_{n,Theo}$[b]	$M_{n,SEC}$[c]	$Đ_M$[c]
1	Benzoic acid (BA)[d]	98	7050	1850	2.14
2	Benzoic acid (BA)/THF[e]	90	6500	6550	2.16

[a] Determined from the ^{1}H NMR spectrum.
[b] Theoretical M_n= ([LA]/[I]) × (144 × equiv. LA) × (conv./100).
[c] As determined by SEC (THF), with applied Mark-Houwink parameters.
[d] drops of BA in THF (1 mg mL^{-1}) + 0.5 mL THF.
[e] Static mixer causes leaking in the reactor due to lactide crystallisation out of solution, which blocked the mixing ball in the static mixer.

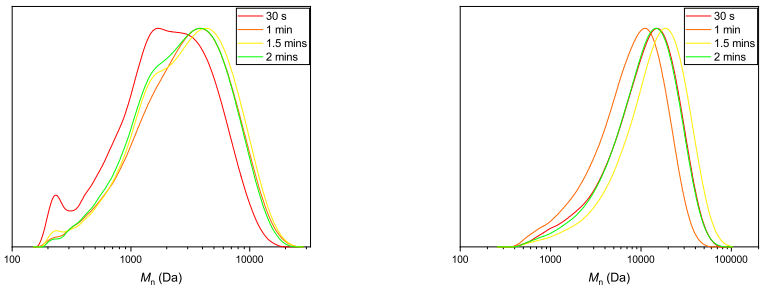

(a) Indirect benzoic acid addition. (b) Direct benzoic acid addition.

Figure 7.2: SEC traces from the ROP of *L*-LA with TBD in THF ([LA] = 1 mol L^{-1}; [LA]:[Cat]:[I] = 50:1:1) at 25 °C, with varying residence times. a) Quenching by delayed addition of benzoic acid to the collected sample. b) Direct quenching of the mixture flow into a vial containing 3 drops of benzoic acid (1 mg/mL in THF) + 0.5 mL THF.

SEC traces became notably more monomodal with the new quenching method, which preventing bimodality from developing due to delayed addition of benzoic acid (Figure 7.2). This was accompanied by an improved correlation between $M_{n,Theo}$ and $M_{n,SEC}$, which could be explained by the new quenching method, removing the opportunity for side reactions to occur (Table 7.3).

Since increasing flow rates did not improve dispersity, it was necessary to see if improved mixing from the mixing unit itself would improve dispersity, to balance out the speed of the reaction at room temperature. To this point, a simple Y-mixing unit had been used, combining the two incoming streams, likely to result in laminar flow, with mixing between the two streams occurring through diffusion.[28]

Due to the narrow channels of a microreactor, this diffusion is typically rapid, allowing for efficient mixing, which must be balanced with flow rate to prevent unwanted side reactions. However, mixing is not typically instigated within the Y-piece itself; rather, diffusion occurs throughout the length of the reactor. Further, a laminar flow pattern results in a gradient of residence times due to friction between the reactor walls and the reaction solution slowing down the flow rate by comparison to the central channel of solution, which moves faster. This results in a gradient of residence times, and thus a broader dispersity. To prevent a broad dispersity, this can be balanced out with high flow rates.

(a) Y-Piece. (b) Static Mixer.

Figure 7.3: The Y-piece mixer was replaced with a static mixer (Upchurch Scientific), equipped with a ball bearing to induce turbulent mixing.

The Y-piece mixer was therefore replaced with a static mixing unit, equipped with a ball bearing to encourage turbulent mixing from within the mixer (Figure 7.3). Dispersities immediately dropped to between 1.71-1.74 using residence times under 2 minutes, maintaining high conversions (entry 6, Table 7.2). However, leaking of the mixing unit due to high reactor pressures afforded by the high flow rates (typical of a static mixer) meant that results were not reliable. Whilst leaking could be mitigated by using much slower flow rates and a shorter reactor length (to obtain the same residence time), the benefits in dispersity were not significant enough to merit redesigning the reactor.

Dispersities dropped when the solvent was changed to DCM, by potentially suppressing H-bonding between the solvent and the amine moiety of the catalyst that was possible with THF, preventing monomer activation by the catalyst ($Đ_{\mathrm{M}}$ 1.72, entry 7, Table 7.2). In another effort to slow down the reaction, ROP reached 96% conversion, $Đ_{\mathrm{M}}$ 1.35 within 2.5 seconds at 0.5 mol L^{-1} ($M_{\mathrm{n,SEC}}$ 6 900 Da, $M_{\mathrm{n,NMR}}$ 6 100 Da, $M_{\mathrm{n,SEC}}$ 4 200 Da, entry 8, Table 7.2). Differences in the $M_{\mathrm{n,Theo}}$ and $M_{\mathrm{n,SEC}}$ were still present, although calculations based on the

methine proton in the ^{1}H NMR suggested that this difference was not so extreme; differences in SEC calibrations and application of the Mark-Houwink K and α parameters into the processing software (which was not carried out in the majority of the research where correction factors were applied) meant that further correction of the M_{n} values was not required.

A direct comparison with the batch reaction further confirmed the unsuitability of TBD in DCM due to the speed at which it reached high conversion and therefore the difficulty in controlling the reaction time to obtain reliably low dispersities: After two minutes at 25 °C, the dispersity of the polymer was 1.98 (96% conversion, Figure 7.4). Nevertheless, this was promising evidence that excellent control was possible using TBD at the ultra-rapid timescales that were possible in flow.

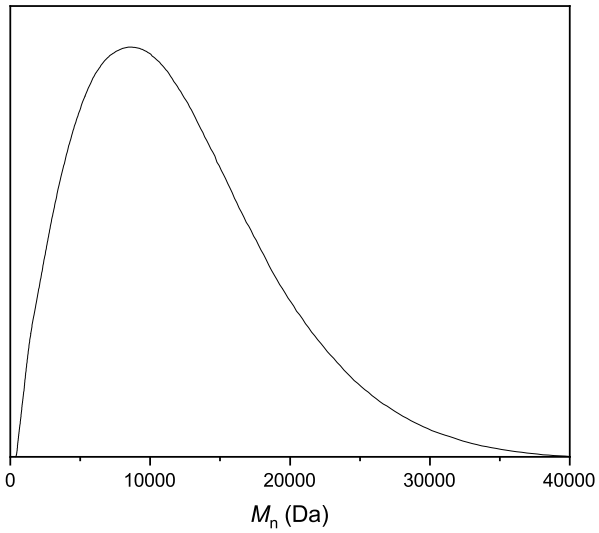

Figure 7.4: SEC trace from the batch ROP of *L*-LA with TBD in DCM ([LA] = 0.5 mol L^{-1}, [LA]:[Cat]:[I] = 50:1:1) at 25 °C. 96% conversion after 2 minutes, $M_{\mathrm{n,\ Theo}}$ 6 900 Da, $M_{\mathrm{n,\ SEC}}$ 3 900 Da, $Đ_{\mathrm{M}}$ 1.98.

Changing the catalyst, monomer concentration or initiator

Thus, switching the catalyst from TBD to weaker base, DBU, was necessary to improve control, both through slowing the reaction down and as reducing the

likelihood for the weaker base of participating in transesterification side reactions with an appropriately optimised system.

Dispersities as low as 1.19 were possible in 30 seconds (36%), however the reaction rate was significantly slower than with earlier tests using TBD, only reaching 99% after 30 minutes (entry 9, Table 7.2). Increasing the temperature to 35 °C significantly improved the rate, this time reaching 97% conversion within two minutes, while maintaining a good dispersity ($Đ_M$ 1.25, entry 10, Table 7.2, Figure 7.5).

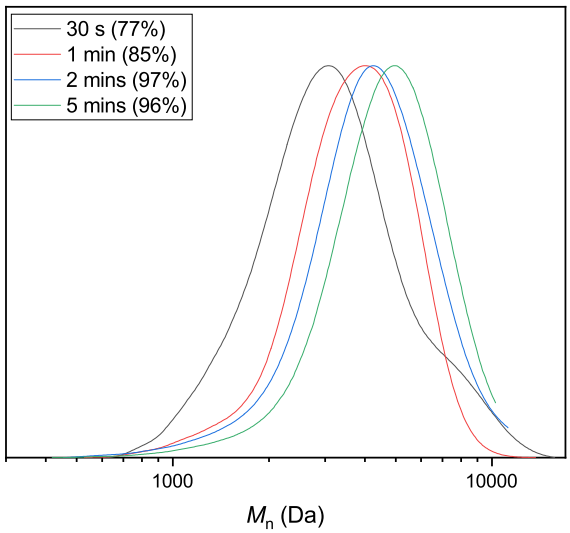

Figure 7.5: SEC traces from the ROP of *L*-LA with DBU in DCM ([LA] = 1 mol L^{-1}; [LA]:[Cat]:[I] = 50:1:1) at 35 °C, providing the optimal results from the screening study by balancing speed (τ_r = 1 min) with narrow $Đ_M$ (1.20, 85%). The tailing could be due to early termination events from residual water impurities – which could be removed by purification of the polymer – or due to initiaton from other species.

Subsequent reactions at half concentration of catalyst ([LA]:[Cat]:[I] = 50:0.5:1, Table 7.4) to improve control further were unsuccessful, and conversions did not exceed 33%, with no visible improvement in dispersity.

A similar conversion profile with residence time was observed when BnOH was replaced 4-MeBnOH, to see if a change of initiator would lead to more improved

control (due to increased accuracy of mass with a solid catalyst). However, the dispersity increased far more predictably with the new initiator, rising from 1.21 (30 seconds) to 1.48 (5 minutes, Figure 7.6), whereas BnOH provided variable results, rising to $Đ_M$ 1.33 after 6 minutes, before dropping to 1.22 in 8 minutes (Table 7.4).

Table 7.4: Polymerisation data ROP of *L*-LA with DBU, using BnOH as the initiator. Conditions: DCM at 35 °C ([LA] = 1 mol L^{-1}), [LA]:[Cat]:[I] = 50:0.5:1.

Entry	Residence Time (min)	Conv. (%)[a]	$M_{n,Theo}$[b]	$M_{n,SEC}$[c]	$Đ_M$[c]
1	2	21	1500	800	1.25
2	6	33	2400	150	1.33
3	8	28	2000	1500	1.22

[a] Determined from the ^{1}H NMR spectrum.
[b] Theoretical M_n= ([LA]/[I]) × (144 × equiv. LA) × (conv./100).
[c] As determined by SEC (THF), with applied Mark-Houwink parameters.

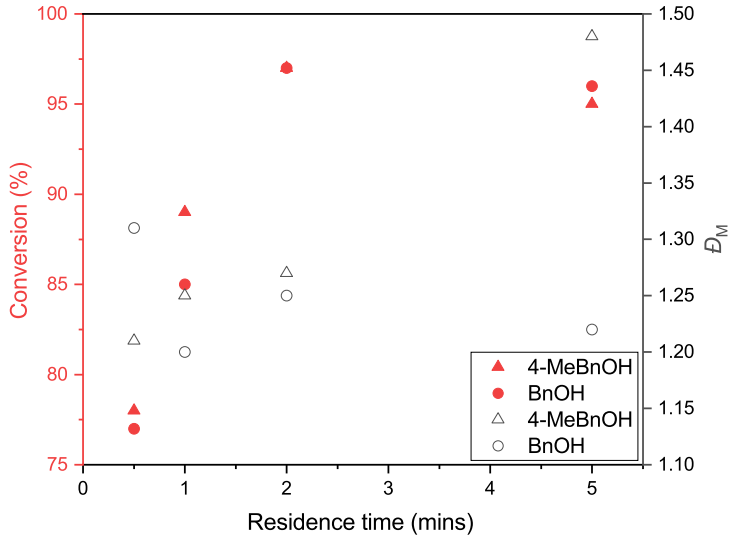

Figure 7.6: Varying the residence time from 30 s to 5 minutes in the ROP of *L*-LA with DBU, in DCM ([LA] = 1 mol L^{-1}, [LA]:[Cat]:[I] = 50:1:1) at 35 °C, using either BnOH or 4-MeBnOH as initiator.

Rac-lactide production in batch and continuous flow

The successful conditions discovered in the previous section were applied to the ROP of *rac*-LA. Reactions were carried out at 35 °C in DCM, however, the

Table 7.5: Polymerisation data ROP of *rac*-LA with DBU in DCM, at 35 °C, with varying ratios.

Entry	[LA]:[Cat]:[I]	[LA] (mol L^{-1})[a]	Residence time (min)	Conv. (%)[b]	$M_{n,Theo}$[c]	$M_{n,SEC}$[d]	$Đ_M$[d]
1	50:1:1	1	1	66	4750	3750	1.23
2	50:1:1	0.5	1	43	3100	1850	1.23
3	100:1:1	0.5	1	24	3450	750	1.19

[a] Concentration of L
[b] Determined from the ^{1}H NMR spectrum.
[c] Theoretical M_n= ([LA]/[I]) × (144 × equiv. LA) × (conv./100).
[d] As determined by SEC (THF), with applied Mark-Houwink parameters.

concentration of monomer feed solution was reduced from 2 to 0.5 and 1 mol L^{-1}, as the lower solubility of *rac*-lactide over *L*-LA did not allow for higher concentrations.

Predictable decreases in conversion were possible through tuning of flow rates and concentrations. Conversions reached 66% with a residence time of 1 minute at 1 mol L^{-1}, which decreased to 43% once the concentration was halved (entries 1-2, Table 7.5). Similarly, halving the catalyst loading to 100:1:1 halved the conversion again, to only 24% (entry 3, Table 7.5). The high discrepancy in $M_{n,Theo}$ 3 450 Da and $M_{n,SEC}$ 750 Da could be due to the high transesterification seen in earlier chapters, using the same catalyst (Chapter 5).

The residence time was varied from one to five minutes, with increases in M_n with conversion, reaching 65% conversion within five minutes ($M_{n,SEC}$ 3 550 Da, $Đ_M$ 1.25, [LA] = 0.5 mol L^{-1}, Figure 7.7). Similar results were obtained in the 100:1:1 tests, ranging from one to 18 minutes residence time (Figure 7.8). Conversions proved erratic such that full control of the ROP had not been achieved, even with the lower concentration of LA and lower catalyst loadings used to slow the reaction down.

In flow, 43% conversion was possible within one minute residence time, due to the high surface area-to-volume ratio allowing for efficient mixing and heat transfer, leading to rapid reactions ($Đ_M$ 1.23, [LA] = 0.5 mol L^{-1}, entry 2, Table 7.5). By comparison, batch ROP of *rac*-LA provided excellent conversion (93%) and low, monomodal dispersity ($Đ_M$ 1.05) in one hour (entry 4, Table 7.6, Figure 7.9), highlighting the benefits of both batch and flow systems: high conversions and low dispersities in batch were both possible, despite the longer reaction time. Batch allowed for effective quenching of the reaction before dispersity increased,

although this was dependent on accurate sampling to identify the appropriate time to quench the reaction. In contrast, the high flow rates and accurate residence times in flow, coupled with good mixing enabled rapid conversions and controllable dispersities.

It was clear that the additional issues encountered when using the less soluble *rac*-LA provided unreliable or slow results in comparison to *L*-LA, particularly in flow. Therefore, future work only considered the ROP of *L*-LA.

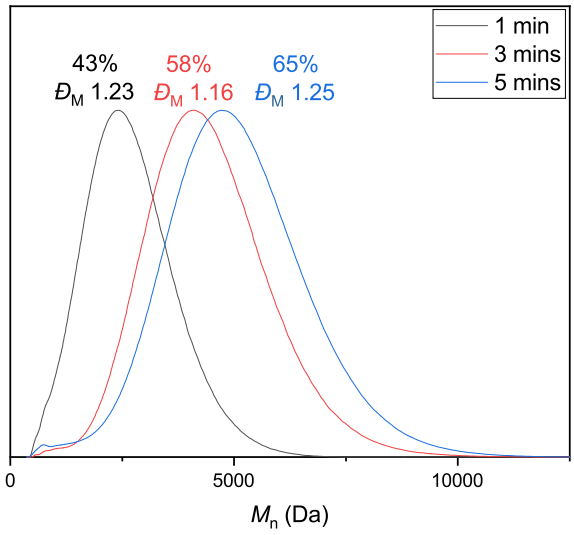

Figure 7.7: Varying the residence time from 1 minute to 5 minutes in the ROP of *rac*-LA with DBU, in DCM ([LA] = 0.5 mol L^{-1}, [LA]:[Cat]:[I] = 50:1:1) at 35 °C. Conversions are expressed as % above the SEC traces.

Table 7.6: Polymerisation data large-scale batch solution-phase ROP of *rac*-LA with DBU in DCM, using [LA]:[Cat]:[I] = 50:1:1, at 35 °C (I = BnOH).

Entry	**[LA] (mol L^{-1})**	**Time (min)**	**Conv. (%)[a]**	$M_{n,Theo}$[b]	$M_{n,NMR}$[a]	$M_{n,SEC}$[c]	$Đ_M$[c]
1	1	2	2	150	-	-	-
2	0.5	2	2	150	-	-	-
3	0.5	30	14	1000	250	-	-
4	0.5	60	93	6700	2100	8750	1.05

[a] Determined from the ^{1}H NMR spectrum.
[b] Theoretical M_n= ([LA]/[I]) × (144 × equiv. LA) × (conv./100).
[c] As determined by SEC (THF), with applied Mark-Houwink parameters.

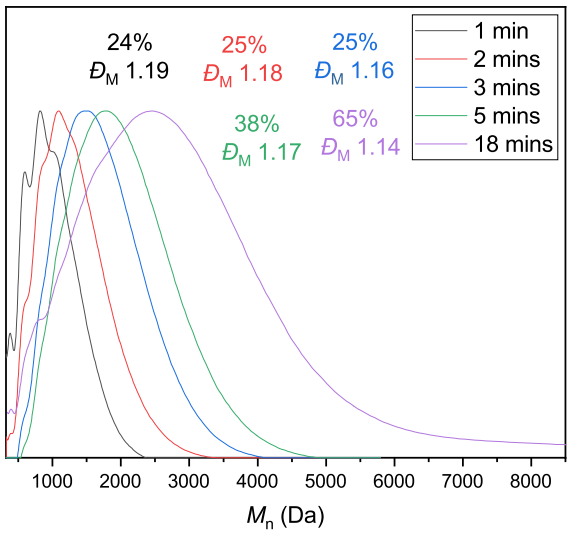

Figure 7.8: Varying the residence time from 1 minute to 18 minutes in the ROP of *rac*-LA with DBU, in DCM ([LA] = 0.5 mol L^{-1}, [LA]:[Cat]:[I] = 100:1:1) at 35 °C. Conversions are expressed as % above the SEC traces.

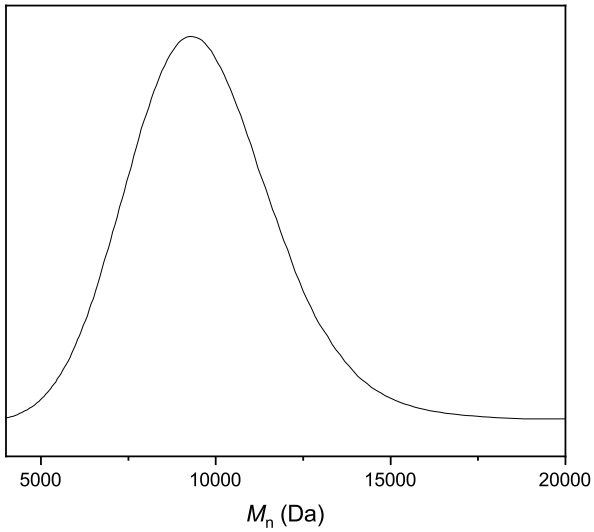

Figure 7.9: SEC trace from the batch ROP of *rac*-LA with DBU in DCM ([LA] = 0.5 mol L^{-1}, [LA]:[Cat]:[I] = 50:1:1) at 35 °C (entry 4, Table 7.6). 93% conversion, $M_{n,\,Theo}$ 6 700 Da, $M_{n,\,SEC}$ 8 750 Da, $Đ_M$ 1.05.

Batch ROP of *L*-LA with DBU toward data encryption

Excellent progress had been achieved in the flow ROP of *L*-LA, concluding that use of a DBU catalyst, in DCM at 35 °C, were the optimal conditions to achieve rapid, controlled ROP of *L*-LA in flow. However, although ratios of 100:1:1 were tested, higher ratios to afford industrially relevant molecular weights have not been carried out; future work should therefore focus on the application of high ratios into flow, without compromising activity or control.

For the following work, it was necessary to generate several PLA batches of varying molecular weights, before it was possible to combine the study with the flow work described in the previous sections. To achieve this, several parallel batch ROP were set up, using the same conditions as described earlier, to prepare for a readily transferable system to flow. Eight polymerisations were prepared, with increasing equivalents of LA, with reaction times increasing sequentially to enable higher conversions for polymerisations with higher ratios (Table 7.7).

All reactions displayed excellent dispersities ($Đ_M$ 1.05-1.18) and the majority reached above 70% conversion (entries 1-5, Table 7.7). Above 300:1:1, however, conversions started dropping significantly, with DBU evidently struggling to achieve high conversions at higher ratios; despite increasing the reaction time to one hour, the 500:1:1 test only reached 10% conversion (entry 8, Table 7.7). The apparent limit on the maximum number of equivalents of LA meant that only a select number of molecular weights were available for the following studies. Nevertheless, molecular weights of up to 17 900 Da were still possible at only 38% conversion ($Đ_M$ 1.05, entry 7, Table 7.7), indicating that further ROP optimisation to promote higher conversions at higher ratios would generate improved M_n.

While some organocatalysts are known to struggle to produce high molecular weight PLA, the low conversions and molecular weights seen in this work are likely due to deactivation of the DBU at higher reaction times. The sensitivity of this particular catalyst to trace impurities has previously been reported.[29] Reaction of DBU with acid residues from water or lactic acid (which are difficult to remove, even through extensive purification) leads to progressive deactivation of the catalyst. These impurities can also be introduced through exposure to

Table 7.7: Polymerisation data large-scale batch solution phase ROP of *L*-LA with DBU, in DCM ([LA] = 1 mol L^{-1}), using varying [LA]:[Cat] ratios ([Cat]:[I] = 1), at 35 °C.

Entry	[LA]:[Cat]	Time (min)	Conv. (%)[a]	$M_{n,Theo}$[b]	$M_{n,NMR}$[a]	$M_{n,SEC}$[c]	$Đ_M$[c]	DP[d]
1	10	1	91	1300	95	8450	1.11	74
2	25	1	76	2750	500	3650	1.09	32
3	50[e]	2	78	11250	1400	2050	1.18	18
4	100	4	70	10100	3100	5500	1.09	48
5	200	8	90	25950	9800	10400	1.08	91
6	300	12	42	18150	12550	15100	1.07	132
7	400	16	38	21900	22450	17900	1.05	157
8	500	60	10	7200	9800	8700	1.12	77

[a] Determined from the ^{1}H NMR spectrum.
[b] Theoretical M_n= ([LA]/[I]) × (144 × equiv. LA) × (conv./100).
[c] As determined by SEC (THF), with applied Mark-Houwink parameters.
[d] DP (degree of polymerisation) = $MW_{PLA} \div MW_{LA}$
[e] [LA]:[Cat]:[I] = 100:0.5:1.

air, if tightly controlled air sensitive conditions are difficult to achieve. This is particularly prevalent at higher reaction times, leaving more room for the deactivation pathway to occur, thus leading to low conversions seen in Table 7.7. Transferring this work into flow would therefore require meticulous control of reaction conditions and air sensitive techniques, or a move to a less moisture sensitive catalyst.

However, for the purpose of the following work, only five polymers of defined molecular weights and narrow dispersities were necessary. Therefore, polymers defined by entries 2 and 4-7 were carried through, due to their high conversions and low dispersities. For increased accuracy in the data encryption process, the polymers were twice purified before use in the following research.

Encoding polymer distributions

Previous work in the group demonstrated the mixing of polymers of varying molecular weights enabled precise engineering of the MWD shape.[24] A predictive framework was developed in order to easily compute which combination of M_n are required to achieve desired MWDs.[21] This streamlines the procedure towards achieving predictable MWDs, by removing the need to synthesise large libraries of polymers of varying M_n and $Đ_M$, and painstakingly mixing them in varying ratios until the desired MWD has been found.

Table 7.8: Mass ranges for mixtures of PLA of different M_n, assembled in a random distribution.

Level	**Mass ranges (mg)**
1	0-1
2	1-2
3	2-3
4	3-4
5	4-5
6	5-6
7	6-7
8	7-8
9	8-9
10	9-10

Further software enabled the deconvolution – or decryption – of MWDs of polymer mixtures, working backwards to identify which polymer samples make up any given MWD.[27] It is the combination of these processes that has allowed for data encryption through MWD "fingerprints", formed through mixing of polymers of varying M_n. Each macromolecular component thus acts as a specific encryption key, and knowledge of this key enables the user to "unlock" the encrypted code. Thus, the encoded data can only be de-convoluted if the user is in possession of the encryption keys, enabling a two-fold security measure, or symmetric encryption, whereby the code (MWD of the polymer mixture, determined by SEC) cannot be decrypted without the key (M_n and $Đ_M$ of the individual polymers).

This type of deconvolution works only if the polymers are different enough in M_n that they do not lead the software to mistakenly allocate more weighting to the wrong polymer, thereby reading out the wrong code. On the other hand, there would be no need to know the encryption keys if the M_n of the various polymers are spaced too far apart from one another.

The work described herein concerns the theory and development of the encoded data, whilst fitting and decoding of the final MWDs (obtained through SEC analysis) was carried out by Vrijsen *et al.* in Hasselt University. The reader is referred to work by Junkers and co-workers for further information about the specific workings of the algorithm.[21,22,27]

Theory and practice: deconvoluting random distributions

To begin, a random distribution of polymer molecular weights was made up for decoding. To achieve this, mass ranges separated by 1 mg, were defined such that 0-1 mg was designated as 'Level 1', and so on until a maximum level of 10 mg, *i.e.* the average amount of polymer in an SEC sample (Table 7.8).

The 5 polymers with different M_n were then randomly assigned a distribution range by a generator to give mixtures 1 ('Code 0') and 2 ('Code 1'). In Code 0, for example, polymer 2 was assigned to level 2 *i.e.* 1-2 mg of polymer 2 was required in that mixture (Tables 7.9 and 7.10).

Accurate concentrations were prepared using stock solutions, so the algorithm could accurately read out the distributions of each component polymer, generating the two mixtures (Figure 7.10). The SEC traces of the two mixtures were obtained, and the normalised number distribution was overlaid with the normalised number distributions of the individual polymers. This data was sent to Hasselt University for decoding.

The SEC trace decoding software operates by measuring the distribution of a mixture of five polymers. Subsequently, it can de-convolute the SEC trace of the mixture to identify the how much of each individual polymer is in the mixture. This is achieved by curve-fitting combinations of the individual polymers' distributions to match the experimental curve of the mixture. The software requires one polymer with a known mass (standard mass of 5 mg) as an internal standard, against which it can calculate the mass of the other polymers, based off their contribution to the SEC curve of the mixture.

Table 7.9: Amounts of polymer required for the random distribution of Code 0. The mass is determined from the middle of the distribution that each level corresponds to.

Mixture 1	**Code 0**	
	Use	**mass (mg)**
Polymer 1	Standard	5
Polymer 2	level 2	1.5
Polymer 3	level 2	1.5
Polymer 4	level 9	9.5
Polymer 5	level 5	4.5

Table 7.10: Amounts of polymer required for the random distribution of Code 1. The mass is determined from the middle of the distribution that each level corresponds to.

Mixture 2	**Code 1 Use**	**mass (mg)**
Polymer 1	Standard	5
Polymer 2	level 5	4.5
Polymer 3	level 4	6.5
Polymer 4	level 7	3.5
Polymer 5	level 4	1.5

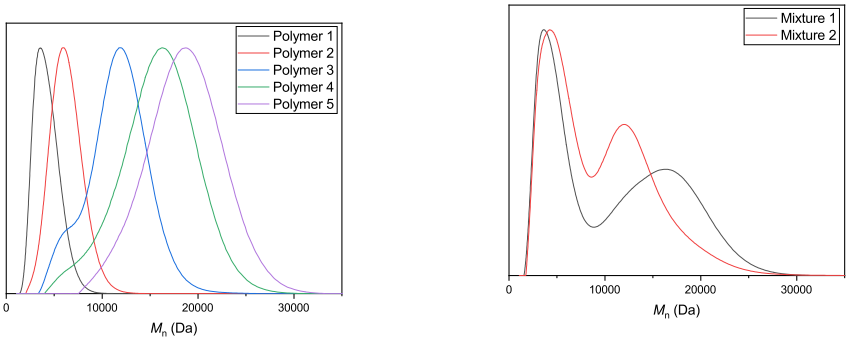

(a) Overlay of the individual polymers. (b) Mixtures 1 and 2, each in random distributions.

Figure 7.10: Normalised number distributions of the SEC traces of the mixtures. (a) Black = 3 650 Da, Red = 5 500 Da, Blue = 10 400 Da, Green = 15 100 Da, Lilac = 17 900 Da. (b) Black = Mixture 1, Red = Mixture 2.

Theory: encoding words

With the purified polymers from the batch solution phase ROP of *L*-LA, combinations of these polymers could be prepared to encode letters. This was achieved by assigning distribution ranges to the molecular weights up to 10 mg, as described above. In this case, level 1 would be in the 1.5-3.0 mg range, whilst level 2 would cover 3.0-4.5 mg (Table 7.11). In contrast to the random distributions, only 6 different mass levels were required rather than 10, to allow for any error in measurement of the polymer and therefore increase the likelihood that the software could identify each letter. 5 polymers with varying molecular weights were prepared and there are 6 levels of possible mass distributions. If each letter was to be described by one polymer, this would require 36 individual polymers

with distinct dispersities and molecular weight distributions (MWDs) with no significant overlap. However, this would be synthetically challenging and labour intensive, therefore each letter was defined by a combination of two polymers in different mass distributions. With two polymers (per letter) in 6 different levels, this accounts for 36 possibilities (= 6^2), translating to 36 different characters. It is therefore possible to encode all 26 letters of the alphabet and some basic punctuation.

Table 7.11: Distribution ranges for PLA.

Level	**Mass ranges (mg)**
N/A	0-1.5
1	1.5-3.0
2	3.0-4.5
3	4.5-6.0
4	6.0-7.5
5	7.5-9.0
6	9.0-10.5

Each letter could be encoded by two of the 5 polymers, in different combinations of distribution. The letter 'a' would, for example, be encoded by polymer 1 (level 1, *i.e.* 1.5-3.0 mg) and polymer 2 (level 1, *i.e.* 1.5-3.0 mg). The letter 'b' would then be encoded by polymer 1 (level 1, *i.e.* 1.5-3.0 mg) and polymer 2 (level 2, *i.e.* 3.0-4.5 mg), and so on for the rest of the letters (Table 7.12). The fifth polymer would be the internal standard, which the algorithm would recognise and calculate the relative amounts of the other four polymers from. The algorithm could then read out the mass ranges of the polymers in sequence, starting from the internal standard and combining the remaining four polymers into groups of two, corresponding to one letter per group, as defined above.

Since each mixture was made up of 5 polymers, accounting for one internal standard and four remaining polymers, the latter could therefore be assembled into two distinct combinations. Each combination would describe one discrete letter, *i.e.*, four separate polymers encoding two letters. Using the decoding software, it would then be possible to deconstruct the overall trace into its individual components, and identify the amounts of each polymer in the sample. By reading out the different amounts (mass ranges) of the four polymers in order, the letters could be re-extracted from the SEC mixture.

Table 7.12: Each letter is described by a combination of two letters, each in a distinct'level' *i.e.* mass distribution defined in Table 7.11. Polymer 1 is always used as an internal standard (5 mg).

First letter	Polymer 2	Polymer 3	Second letter	Polymer 4	Polymer 5
a	Level 1	Level 1	a	Level 1	Level 1
b	Level 1	Level 2	b	Level 1	Level 2
c	Level 1	Level 3	c	Level 1	Level 3
d	Level 1	Level 4	d	Level 1	Level 4
e	Level 1	Level 5	e	Level 1	Level 5
f	Level 1	Level 6	f	Level 1	Level 6
g	Level 2	Level 1	g	Level 2	Level 1
h	Level 2	Level 2	h	Level 2	Level 2
i	Level 2	Level 3	i	Level 2	Level 3
j	Level 2	Level 4	j	Level 2	Level 4
k	Level 2	Level 5	k	Level 2	Level 5
l	Level 2	Level 6	l	Level 2	Level 6
m	Level 3	Level 1	m	Level 3	Level 1
n	Level 3	Level 2	n	Level 3	Level 2
o	Level 3	Level 3	o	Level 3	Level 3
p	Level 3	Level 4	p	Level 3	Level 4
q	Level 3	Level 5	q	Level 3	Level 5
r	Level 3	Level 6	r	Level 3	Level 6
s	Level 4	Level 1	s	Level 4	Level 1
t	Level 4	Level 2	t	Level 4	Level 2
u	Level 4	Level 3	u	Level 4	Level 3
v	Level 4	Level 4	v	Level 4	Level 4
w	Level 4	Level 5	w	Level 4	Level 5
x	Level 4	Level 6	x	Level 4	Level 6
y	Level 5	Level 1	y	Level 5	Level 1
z	Level 5	Level 2	z	Level 5	Level 2
.	Level 5	Level 3	.	Level 5	Level 3
?	Level 5	Level 4	?	Level 5	Level 4
!	Level 5	Level 5	!	Level 5	Level 5
,	Level 5	Level 6	,	Level 5	Level 6
space	Level 6	Level 1	space	Level 6	Level 1

As described, this method offered a way of "double encryption"; a word or phrase may be encrypted into a mixture of polymers, generating an SEC 'code'. The latter could only then be decoded if the individual had the original individual SEC traces of each polymer.

Practice: encoding words

To demonstrate the capability of the software, the phrase 'PRD!' (an acronym of the Polymer Reaction Design group at Monash University) was prepared into a distribution of polymers. Based on the distributions described above, the phrase was encoded into two separate mixtures: the first described letters 'P' and 'R',

Table 7.13: Amounts of polymer required to code the letters 'P' and 'R' into the phrase 'PRD!'. The mass is determined from the middle of the distribution that each level corresponds to.

Mixture 1 'PR'	**Use**	**Mass (mg)**	**Character encoding**
Polymer 1	Standard	5	-
Polymer 2	(D1, level3)	5.25	P
Polymer 3	(D2, level4)	6.75	
Polymer 4	(D1, level3)	5.25	R
Polymer 5	(D2, level6)	9.75	

Table 7.14: Amounts of polymer required to code the letter 'D' and '!' into the phrase 'PRD!'. The mass is determined from the middle of the distribution that each level corresponds to.

Mixture 2 'D!'	**Use**	**Mass (mg)**	**Character encoding**
Polymer 1	Standard	5	-
Polymer 2	(D1, level1)	2.25	D
Polymer 3	(D2, level4)	6.75	
Polymer 4	(D1, level5)	8.25	!
Polymer 5	(D2, level5)	8.25	

while the second described the 'D' and '!'. Tables 7.13-7.14 illustrate which polymers and their distributions were required for this phrase. The same process was carried out for the phrase 'BUCHARD!' (Tables 7.15-7.18).

The Gaussian (Gauss) method predicts the final MWD, by scanning a range of M_{n}, ideally covering the range described by the experimental MWD, and curve-fitting a distribution to satisfy the experimental characteristics (M_{n} and $Đ_{\mathrm{M}}$).[21] For each polymer mixture, the overall MWD is modelled through the combination several Gaussian distributions pertaining to each polymer component. This method was initially applied to the polymers synthesised from 100:1:1 and 200:1:1 ratios, and the Gauss method successfully fitted the shape and dispersity of the distributions of these two individual polymers (Figure 7.11). As the method was able to track the MWD of polymers produced through ROP, thus tracking the MWD of mixtures of polymers should also be possible, enabling data encryption.

Table 7.15: Amounts of polymer required to code the letters 'B' and 'U' into the phrase 'BUCHARD!'. The mass is determined from the middle of the distribution that each level corresponds to.

Mixture 1 'BU'	Use	Mass (mg)	Character encoding
Polymer 1	Standard	5	-
Polymer 2	(D1, level1)	2.25	B
Polymer 3	(D2, level2)	3.50	
Polymer 4	(D1, level4)	6.75	U
Polymer 5	(D2, level3)	5.25	

Table 7.16: Amounts of polymer required to code the letters 'C' and 'H' into the phrase 'BUCHARD!'. The mass is determined from the middle of the distribution that each level corresponds to.

Mixture 2 'CH'	Use	Mass (mg)	Character encoding
Polymer 1	Standard	5	-
Polymer 2	(D1, level1)	2.25	C
Polymer 3	(D2, level3)	5.25	
Polymer 4	(D1, level2)	6.75	H
Polymer 5	(D2, level2)	3.75	

Table 7.17: Amounts of polymer required to code the letters 'A' and 'R' into the phrase 'BUCHARD!'. The mass is determined from the middle of the distribution that each level corresponds to.

Mixture 3 'AR'	Use	Mass (mg)	Character encoding
Polymer 1	Standard	5	-
Polymer 2	(D1, level1)	2.25	A
Polymer 3	(D2, level1)	2.25	
Polymer 4	(D1, level3)	5.25	R
Polymer 5	(D2, level6)	9.75	

Table 7.18: Amounts of polymer required to code the letter 'D' and '!' into the phrase 'BUCHARD!'. The mass is determined from the middle of the distribution that each level corresponds to.

Mixture 4 'D!'	Use	mass (mg)	Character encoding
Polymer 1	Standard	5	-
Polymer 2	(D1, level1)	2.25	D
Polymer 3	(D2, level4)	6.75	
Polymer 4	(D1, level5)	8.25	!
Polymer 5	(D2, level5)	8.25	

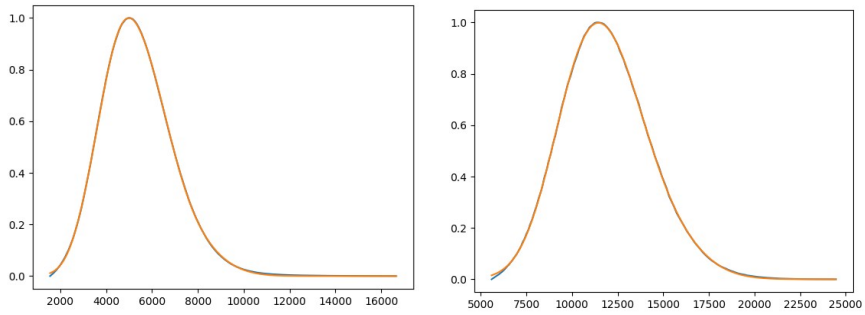

(a) [LA]:[Cat]:[I]=100:1:1. (b) [LA]:[Cat]:[I]=200:1:1.

Figure 7.11: Experimental SEC trace (blue) and fitted SEC trace (5 Gauss, orange) using the software that was developed at Hasselt University for decoding of SEC traces.

Figures 7.10-7.12 show the MWDs obtained through mixing of the five polymer fractions in varying amounts to encrypt a random distribution, the word "PRD!" and the word "BUCHARD!", respectively. Unfortunately, when the Gaussian method was applied, deconvolution of the MWD was unsuccessful, despite the excellent tracking of the distributions of the individual polymers. A short discussion of the issues encountered has, however, opened up new directions that the research could work towards to address these difficulties.

What is immediately clear is that each distribution is ill-defined, only displaying two peaks (effectively a bimodal SEC trace), rather than a multimodal MWD with several shoulder peaks, as was used for data encryption in previous research in the group.[27] This is likely due to the proximity of the distributions of each polymer fraction, meaning that the individual distributions are too merged together, forming one broad peak rather than several identifiable shoulder peaks – this would make it easier for the software to recognise which distributions to allocate to each polymer. While some overlap is necessary for the encryption process (totally discrete polymer distributions would omit the need for an encryption key), enough separation is needed for the algorithm to correctly deconvolute the data and assign the right weighting to each polymer fraction.

Prior research has indicated that a difference of 20 monomer units is required between the DP (degree of polymerisation) of polymer fractions; this was determined for poly(styrene) samples which possessed dispersities over 1.20 and

thus higher differences in DP are necessary to counteract the higher degree of overlap between distributions.[27] Since it is possible to achieve narrow dispersities (<1.20) with PLA, the DP difference of 20 units is theoretically not as important for the Gauss method to deconvolute the MWD and extract the mass fractions of each component of the mixture of polymers. Nevertheless, it is clear that the choices of polymers for this particular study are still too close in DP (Table 7.7), and future studies could look towards developing a larger spread in M_n range.

Further, the light tailing and appearance of small shoulder peaks in the SEC traces of polymers 3 and 4 (10 400 and 15 100 Da, respectively, Figure 7.10) could also challenge the algorithm, as these imperfections seemed difficult to predict using the Gaussian method. Therefore, control over the reaction conditions to provide monomodal polymers, as well as access to a broader range of M_n was required to enable deconvolution of the encrypted data.

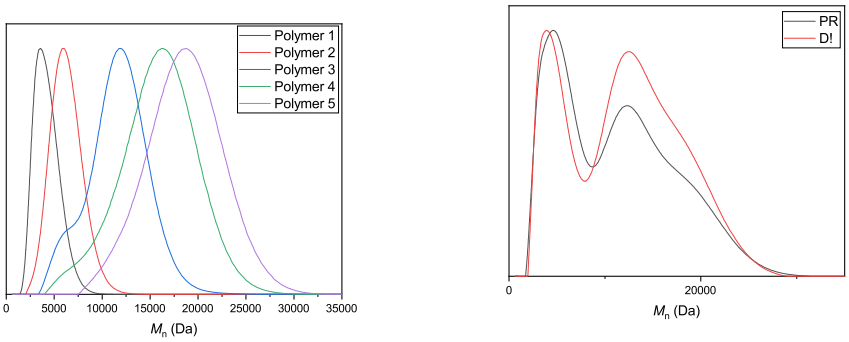

(a) Overlay of the individual polymers. (b) Mixtures 1 and 2, making the word 'PRD!'.

Figure 7.12: Normalised number distributions of the SEC traces of the mixtures encoding the phrase 'BUCHARD!'. (a) Black = 3 650 Da, Red = 5 500 Da, Blue = 10 400 Da, Green = 15 100 Da, Lilac = 17 900 Da. (b) Black = Mixture 1, Red = Mixture 2.

7.4 Conclusions and future work

The study encompassed two key areas: development of a continuous flow system for a rapid, controlled and reliable solution-phase ROP, and using polymer produced under these conditions to use PLA as a method of data encryption.

In the first instance, alternative mixing units, concentrations, initiators, catalysts and solvents were used to optimise the ROP of LA in flow. A successful method of synthesising PLA using DBU in DCM was found, using a [LA]:[Cat]:[I] ratio of 50:1:1, at 35 °C ([LA] = 1 mol L^{-1}). High activities were possible under these conditions, reaching 97% conversion in two minutes ($M_{n,SEC}$ 3 650 Da, $Đ_M$ 1.25).

Attempts to increase the $M_{n,target}$ were carried out by decreasing the catalyst loading, to limited success, likely resulting from catalyst deactivation by trace impurities. Nevertheless, batch ROP under the same conditions reached up to 17 900 Da in 16 minutes, with consistently narrow dispersities ($Đ_M$ 1.05, [LA]:[Cat]:[I] = 400:1:1). Five polymer samples at varying ratios were obtained to carry through to the next stage of the research.

The five polymers from the batch synthesis were combined together in varying mass fractions, with one polymer acting as an internal standard, while the remaining four were attributed to two separate characters (two polymers per character). Each mixture with different mass fractions generated a unique MWD, which could be deconvoluted by a Gaussian method. The SEC trace of the mixture and the encryption keys (characteristics of each individual polymers) were sent to Hasselt University to decode the encrypted data. While the Gaussian method accurately predicted the distribution of individual polymers, it encountered difficulties when deconvoluting the MWDs of the mixtures. This was in part because the distributions of each individual polymer were not separated enough in M_n, but also due to slight shoulder peaks and tailing in the SEC traces of the polymers.

Higher M_n – or rather, a broader range of accessible M_n – was therefore necessary in order to mitigate these issues. The success of the batch ROP compared to the flow set-up suggests that higher degree of control over the inert reaction conditions in flow was required to prevent any catalyst deactivation. As discussed earlier, DBU may not be the ideal catalyst to achieve this, due to its high sensitivity to trace impurities and moisture. Thus, other catalysts should be identified to not only balance activity and control, but also catalyst sensitivity. $Sn(Oct)_2$ is an obvious choice due to its relative stability and notable ROP activity (although accompanied by its own issues, covered in Chapter 8), however the focus on organocatalysts in these studies were part of an effort to move away from metal based catalysts, so alternative organocatalysts should be the focus of upcoming

studies to access polymers of higher molecular weight.

Once a reliable system is found which can access a broader range molecular weights in continuous flow, a move towards automated polymer synthesis can be explored. This has been the subject of previous studies with acrylate-based polymers from RAFT polymerisation.[24,25] Analysis of the resulting polymers M_n through on-line SEC monitoring linked up to an in-built feedback loop built into the reactor; the latter can then automatically modify monomer concentrations and flow rates in order to obtain precise, defined molecular weights. As this software has already been developed and tested with other polymers, the same procedure should be readily applied to PLA, when an appropriate range of M_n can be obtained. Thus, the rapid synthesis of a wide library of polymers of varying distributions would be possible, to obtain a greater selection of combinations for a greater data density. Similarly, the use of other lactone-based polymers and co-polymers would add to the number of possible combinations.

References

[1] T. Junkers, *J Flow Chem*, 2017, **7**, 106–110.

[2] M. H. Reis, T. P. Varner and F. A. Leibfarth, *Macromolecules*, 2019, **52**, 3551–3557.

[3] T. Junkers, *Macromol Chem Phys*, 2017, **218**, 1600421.

[4] M. Seo, Z. Nie, S. Xu, M. Mok, P. C. Lewis, R. Graham and E. Kumacheva, *Langmuir*, 2005, **21**, 11614–11622.

[5] N. Zhu, W. Feng, X. Hu, Z. Zhang, Z. Fang, K. Zhang, Z. Li and K. Guo, *Polymer*, 2016, **84**, 391–397.

[6] T. Honda, M. Miyazaki, H. Nakamura and H. Maeda, *Lab Chip*, 2005, **5**, 812–818.

[7] A. F. Johnson, M. A. Mohsin, Z. G. Meszena and P. Graves-Morris, *J Macromol Sci-Pol R*, 1999, **39**, 527–560.

[8] V. Kottisch, D. T. Gentekos and B. P. Fors, *ACS Macro Lett*, 2016, **5**, 796–800.

[9] D. Maier, A. Eckstein, C. Friedrich and J. Honerkamp, *J Rheol*, 1998, **42**, 1153–1173.

[10] M. W. Collis and M. R. Mackley, *J Non-Newton Fluid*, 2005, **128**, 29–41.

[11] D. Nichetti and I. Manas-Zloczower, *Polym Eng Sci*, 1999, **39**, 887–895.

[12] O. Dragostin and L. Profire, in *Characterization of Polymeric Biomaterials*, Elsevier, 2017, pp. 101–121.

[13] N. A. Lynd and M. A. Hillmyer, *Macromolecules*, 2007, **40**, 8050–8055.

[14] D. T. Gentekos, L. N. Dupuis and B. P. Fors, *J Am Chem Soc*, 2016, **138**, 1848–1851.

[15] J. Morsbach, A. H. Müller, E. Berger-Nicoletti and H. Frey, *Macromolecules*, 2016, **49**, 5043–5050.

[16] S. Domanskyi, D. T. Gentekos, V. Privman and B. P. Fors, *Polym Chem*, 2020, **11**, 326–336.

[17] G. Hadziioannou, A. Skoulios and G. Hadziioannou, *Macromolecules*, 1982, **15**, 267–271.

[18] J. Listak, W. Jakubowski, L. Mueller, A. Plichta, K. Matyjaszewski and M. R. Bockstaller, *Macromolecules*, 2008, **41**, 5919–5927.

[19] N. Corrigan, A. Almasri, W. Taillades, J. Xu and C. Boyer, *Macromolecules*, 2017, **50**, 8438–8448.

[20] N. Corrigan, R. Manahan, Z. T. Lew, J. Yeow, J. Xu and C. Boyer, *Macromolecules*, 2018, **51**, 4553–4563.

[21] M. Rubens and T. Junkers, *Polym Chem*, 2019, **10**, 5721–5725.

[22] T. Junkers and J. H. Vrijsen, *Eur Pol J*, 2020, **134**, 109834.

[23] K. Liu, N. Corrigan, A. Postma, G. Moad and C. Boyer, *Macromolecules*, 2020, **53**, 8867–8882.

[24] M. Rubens and T. Junkers, *Polym Chem*, 2019, 6315–6323.

[25] M. Rubens, J. H. Vrijsen, J. Laun and T. Junkers, *Angew Chem Int Edit*, 2019, **58**, 3183–3187.

[26] M. Rubens, J. Van Herck and T. Junkers, *ACS Macro Lett*, 2019, **8**, 1437–1441.

[27] J. H. Vrijsen, M. Rubens and T. Junkers, *Polym Chem*, 2020, **11**, 6463–6470.

[28] M. B. Plutschack, B. Pieber, K. Gilmore and P. H. Seeberger, *Chem Rev*, 2017, **117**, 11796–11893.

[29] N. J. Sherck, H. C. Kim and Y. Y. Won, *Macromolecules*, 2016, **49**, 4699–4713.

Chapter 8

Thesis Outlook

8.1 Working towards a flow reactor for heterogeneous ROP

Background

Thus far, empirical developments in the fields of heterogeneous ROP catalysts and homogeneous ROP in continuous flow have been carried out, establishing a series of robust PS-immobilised metal complexes and bases. From here, work towards the coupling of the heterogeneous catalysts and continuous production of polymers can begin, which itself feeds into the overall direction of future work.

Importantly, in contrast to the homogeneous flow ROP developed previously (Chapter 7), heterogeneous ROP must be considerate of several factors. For example, the insoluble heterogeneous catalyst is often compacted into a short segment of tubing creating a packed-bed reactor; this way, only one stream of monomer solution is required (in comparison to the two streams which are combined together *via* a mixing unit in homogeneous reactions). Separately, robust reactor design must be developed such that the continuous flow reactor could eventually accommodate melt conditions (*i.e.* solvent free, high viscosities and temperatures).

These considerations and others shall be covered in the following discussion, which

shall describe the overall reactor design and preliminary results. For the purposes of reactor development, all decisions were made with the ultimate goal of immobilising one of the catalysts that have been developed in this work. Preliminary tests, however, used homogeneous catalysts as a model for heterogeneous ROP, to test the efficacy of the reactor without complications added by heterogeneous catalysts (increased pressures, reactor blocking and catalyst waste or degradation during preliminary testing).

Following this, a global outlook of the project will be considered, emphasising future developments related to ROP of lactones in flow.

Reactor development

Reactor design

The initial reactor design was based upon previous reactors established by Hammond and co-workers.[1,2] Choice of the overall reactor design and initial testing were carefully selected to maximise the productivity of the reactor without complicating the set-up, and were thus dependent on numerous factors, detailed in the following paragraphs.

While homogeneous ROP was conducted in a small scale reactor made out of PEEK tubing and a syringe pump, these would not be sufficient to cope with additional pressures encountered in melt ROP with a heterogeneous catalyst immobilised in a packed-bed reactors. Next, due to the moisture-sensitivity of ROP materials, relatively impermeable materials were necessary, particularly in the cases were slower ROP is observed (leaving more time for water permeability through the reactor tubing). Equally, appropriate materials were required to accommodate high temperatures and viscosities, for both homogeneous and heterogeneously catalysed ROP (depending on reagents used).

These combined reasons meant that more robust materials and pumps were necessary. For this reason, a stainless steel reactor was built from typical Swagelok materials, with flexible PTFE tubing in areas out of contact with heating sources. A HPLC reciprocating pump with synchronised dual pistons was selected to enable a constant flow of reaction mixture at high exit pressures.

The final set-up is illustrated in Figure 8.1. A PTFE tube channelled the feed solution (stirred under an argon atmosphere in a Schlenk tube) to the HPLC pump. From here the solution was pumped through a segment of 1/16 inch tube (SS-T1-S-014-6ME-S, 1/16 in. OD × 0.14 in. wall), connecting to the main tubing (1/8 inch stainless steel tubing, SS-T2-S-028-6ME-S, 1/8 in. OD × 0.028 in. wall), before connecting to a 5 cm segment of 1/4 inch stainless steel tubing (SS-T2-S-028-6ME-S, 1/4 in. OD × 0.049 in. wall) placed in an oil bath. The latter segment would eventually accommodate the packed-bed heterogeneous catalyst. The reactor was subsequently connected to a 1/8 inch sampling tube (Teflon tubing, TFE, 1.5 mm × 3.2 mm OD, Sigma Aldrich) to monitor the reaction. In future work where heterogeneous catalysts will be tested, this final 1/8 tube would be connected to a back pressure regulator to ensure constant pressure would be maintained. Narrow tubing was selected for the majority of the reactor to reduce to total volume necessary for the reaction, while a wider segment was required for the "packed-bed" segment to enable addition of catalyst.

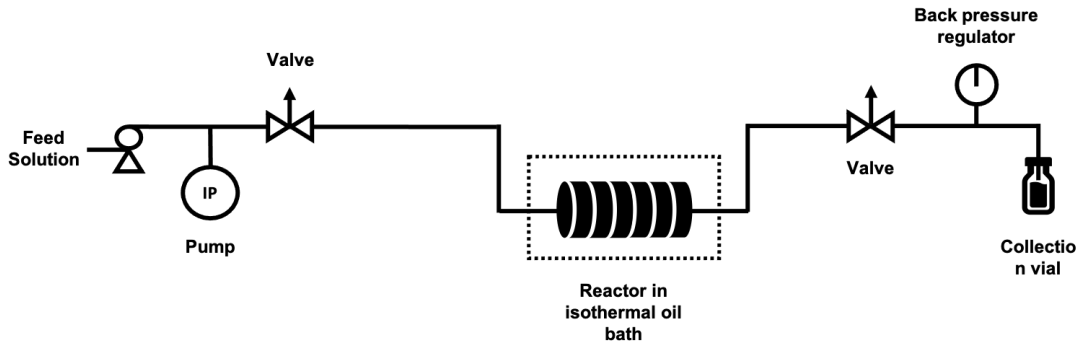

Scheme 8.1: Schematic representation of the flow reactor design. The feed solution (monomer, initiator in solvent) is pumped through 1/8 inch tubing, then passes through the reactor (1/4 inch tubing) in an isothermal oil bath. A back pressure regulator at the end monitors the pressure throughout the reactor.

Flow rates were calculated using the same method described in Chapter 7 (Equations 8.1-8.2). The volume of reactor in this case referred to the segment of 1/4 inch tubing that was heated, rather than the full length of the tubing.

$$V = \frac{\pi D^2}{4} \cdot L \tag{8.1}$$

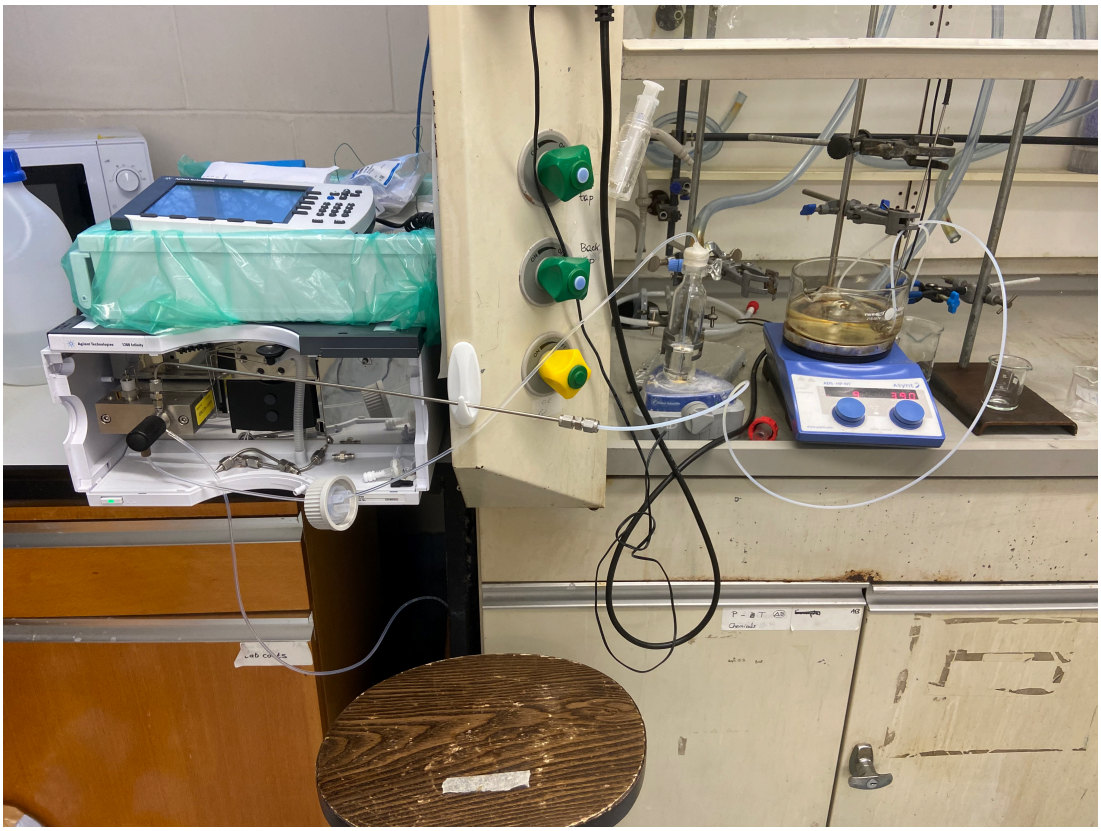

Figure 8.1: Reactor set for the ROP of lactones in flow. For preliminary homogeneous studies, the design from 8.1 was simplified by removing valves and BPR.

$$\text{Total Flow Rate } (\mu L\ min^{-1}) = \frac{\text{Reactor Volume } (\mu L)}{\text{Residence Time}, \tau_{\text{r}}\ (min)} \tag{8.2}$$

Reagent choice and preliminary results

Choice of reagents was paramount to obtain a system that worked within the parameters of the reactor. As mentioned, preliminary tests were conducted with homogeneous catalysts as a model for future heterogeneous work. Solution-phase ROP was also first tested to avoid complications with increased viscosities, as developing methods to heat the full length of the reactor tubing to keep the monomer from crystallising out would add additional challenges.

Toluene was selected as a suitable solvent to access a wide temperature range. ϵ-CL was therefore used to avoid crystallisation issues that LA displays due to

poor solubility in this solvent at room temperature.

Since rigorously anhydrous conditions were not possible given the design and scale of the reactor, a robust catalyst had to be selected to enable efficient ROP. Indeed, the feed solution of a test of the ROP of ϵ-CL with TBD deactivated rapidly ([CL]:[TBD]:[I] = 100:1:1, τ_r = 1 hour, toluene, 80 °C). As such, the catalyst was switched to $Sn(Oct)_2$, as this was readily available and a common catalyst for ROP. The catalyst was also compatible with both toluene and ϵ-CL at high temperature, and thus a good model for future **PS-L^{H}SnOct** and **PS-L^{Cl}SnOct** catalysed reactions.

As the reactor is maintained using a 50:50 mixture of IPA and water in between uses, the tubing was primed by washing thoroughly with dry toluene (5 minutes at 5 mL min^{-1}) to remove water residues leading to increased transesterification and early termination events during the reaction. Subsequent conditioning of the reactor with the monomer (feed) solution at a high flow rate (5 mL min^{-1}, 5 minutes) was performed prior to setting the desired flow rate.

Once an appropriate combination of reagents and reactor materials was established, initial tests were performed at low ratios and long residence times were selected to maximise conversion to the polymer ([CL]:[$Sn(Oct)_2$]:[I] = 25:1:1, τ_r = 4 hours, 0.006 mL min^{-1}). Once the reactor had been conditioned, sampling of the reactor output was performed at regular intervals until the conversion had stabilised, indicating steady state had been reached.

A gradual increase in conversion was observed over the first five hours of monitoring, reaching a maximum of 40% conversion (Figure 8.2A). The different conversions at hours 1-4 were indicative of the different residence times, with earlier results corresponding to segments of PCL which had spent part of the time in the reactor segment at one flow rate (the priming flow rate, 5 mL min^{-1}), and part of the time in the reactor at the set flow rate (0.006 mL min^{-1}). After this, however, the conversion began to decrease once more, indicating that the feed solution (monomer and catalyst) had started to degrade, presumably due to exposure to air and moisture leaking through the seal of the feed solution.

The flow rate was doubled to 0.012 mL min^{-1}, halving the final residence time to 2 hours, but theoretically decreasing the time taken to reach steady state

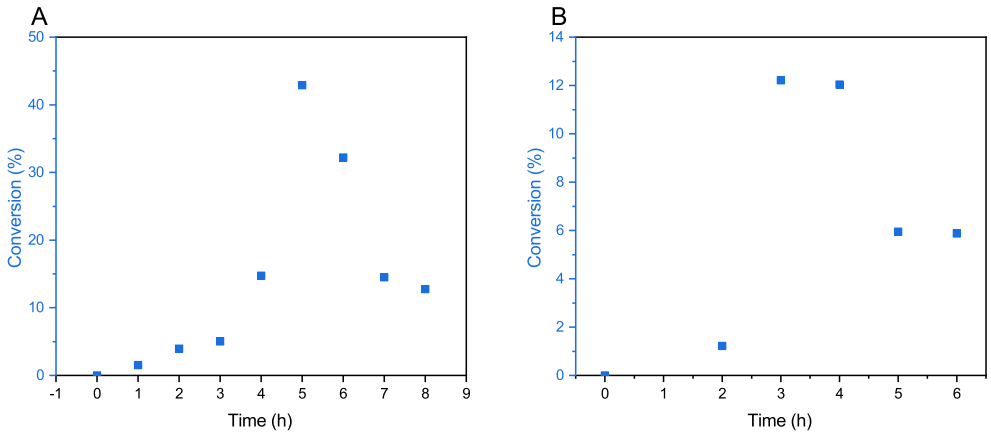

Figure 8.2: Reactor tests of the ROP of ϵ-CL in flow, using $Sn(Oct)_2$ as catalyst and 4-methylbenzyl alcohol as the initiator, at 100 °C in toluene ([CL]:[$Sn(Oct)_2$]:[I] = 25:1:1, [CL] = 1 mol L^{-1}). Residence time (τ_r) = 4 hours (A) and 2 hours (B).

(Figure 8.2B). This was indeed the result, with a total conversion of 12% reached after only 2 hours (under half the time needed to reach maximum conversion at 0.006 mL min^{-1}), which plateaued for three hours before degradation of the feed solution due to exposure to air and moisture.

The feed solution of both tests were continuously stirred at room temperature to ensure a homogeneous mixture was fed into the reactor. Sampling of the feed solution was also carried out at each time point as a baseline, and no conversion to polymer was identified in the ^1H NMR spectra of these samples at earlier time points in the reaction (*i.e.* prior to the degradation seen in the reactor output). This was further evidence that passing the feed solution through the heated reactor segment promoted ROP of the monomer, although further adjustments were required to optimise the process prior to switching to a heterogeneous catalyst.

8.2 Thesis outlook and focus points for future work

This thesis set out to lay the foundation for heterogeneously-catalysed ROP in continuous flow, with the idea that polymer could be produced continuously. In the long-term, the reactor could be tuned towards the synthesis of customised block copolymers, *via* implementation the catalysts in several reactor beds connected in sequence, with the addition of a new monomer after each bed of catalyst. Simultaneously, if a heterogeneous catalyst could be developed with competitive rates and selectivity to $Sn(Oct)_2$ but also be recoverable and reuseable, this could reduce the metal content and toxicity of the polymer. Thus, any extra purification steps could be avoided, which could also be of interest for industrial use.

Indeed, the second goal was achieved, as both classes of catalysts (metal-based and organocatalysts) were heterogenised and readily recovered from the ROP mixture. Reuse studies with the **PS-L^{X}MO$_2$CR** catalysts showed that it was possible to reuse the catalysts, although regeneration of the active site is necessary to maintain catalytic activity. Future work on appropriate regeneration techniques would improve the conversion in each subsequent reuse cycle.

In terms of flow reactors, melt ROP in a PFR would be challenging due to high temperatures, pressures and viscosities, but solution-phase ROP is conceivable and was the focus of preliminary testing. Early results from the tests confirm that flow ROP could be carried out in the reactor, opening up the option of implementing a packed-bed reactor with the catalysts developed throughout this research. It is also clear that the residence times required for $Sn(Oct)_2$ catalysed ROP under these conditions are too long, leading to the eventual degradation of the feed solution.

Nevertheless, due to the versatility of the system that was designed, it should possible to alter many of the variables in order to optimise the reactor to promote rapid and reliable ROP in continuous flow. Addition of titanium isopropoxide (TTIP) to the feed mixture could potentially reduced the moisture sensitivity as demonstrated in the batch ROP of ϵ-CL,[3] (or indeed through addition of molecular sieves) thereby keeping the feed solution fresh for longer, and avoiding the

degradation seen in the tests so far. Control experiments could also be performed to test if it was the feed solution which had degraded, where the feed solution could be heated up to promote ROP once the reactor output conversion began to decrease.

Improvements in the selection of the reagents and conditions are also key for successful ROP in flow on the scale that is appropriate for heterogeneous catalysts. Changing initiators is one way to enable calculation of the $M_{\mathrm{n,NMR}}$, and appropriate solvent selection is also vital to enable $M_{\mathrm{n,NMR}}$ analysis. In the latter case, toluene overlaps significantly with not only the $CDCl_3$ peak, but also the initiator peaks in the aromatic region, making extraction of any molecular weight data impossible. This could be done in tandem with finding the appropriate solvent to solubilise *L*-LA, to increase the range of useable monomers in flow ROP.

Importantly, preliminary tests were also conducted with homogeneous catalysts, although the reactor was primarily built for heterogeneous work. Implementation of the immobilised catalysts into a packed-bed reactor would be the next line of research once the optimal combination of reagents was obtained. Both metal-based and metal-free heterogeneous catalysts developed throughout this project could be coupled with the reactor with some modifications, which shall be discussed in the following paragraphs. These robust metal-based catalysts, for example, have the advantage of providing rapid and reproducible results, which could hopefully be translated into flow.

However, the long reaction times (and therefore slow flow rates) needed in the preliminary tests with $Sn(Oct)_2$ suggested that the activity of the heterogeneous catalysts must be optimised further. Whilst the current **PS-L$^{\mathbf{X}}$MO$_2$CR** catalysts developed in this work were rapid in the melt and achieved the low metal content in the polymer target, their speeds were not comparable to $Sn(Oct)_2$ and they were not rapid enough in solution-phase ROP to enable reasonable flow rates in a PFR. As discussed in Chapter 3, both of these goals (to make flow a viable option with these catalysts and be competitive in the melt to the industrial catalyst) could potentially be achieved using alternative ligand frameworks. This could include tripodal ligands with a fluxional arm to accommodate entry of the lactone, such as those developed by Kol and co-workers.[4,5]

The catalyst support must also be considered: pelletisation of the catalyst could offer a way to avoid pressure drops across the reactor, but the successful metal complexes have only been tested using crosslinked PS beads. Studies looking at the relative activity of powder catalysts to those immobilised on beads could be of interest, or exploring other supports including monoliths, with channels to accommodate a flow of monomer feed solution.

For this reason, the PS-TU and PS-U catalysts (developed in Chapters 5-6) could be implemented into a flow reactor more readily; the powder morphology of these catalysts is optimal for pelletisation. The solution-phase ROP was explored extensively in Chapter 6, with excellent results at room temperature in under one hour – suitable for higher flow rates. The high activity of these catalysts in solution would also be significantly beneficial to flow work compared to the **PS-L$^{\mathbf{X}}$MO$_{\mathbf{2}}$CR** catalysts, as higher flow rates (thus shorter residence times) could be used, so the feed solution would have less time to degrade. Previous work with (thio)ureas by Waymouth and co-workers has extended to continuous flow ROP, and the formation of copolymers with the reactors in sequence;[6] this could potentially be replicated with the immobilised equivalents, by altering the (thio)urea side arm to match the activity of the catalysts.[7]

Throughout Chapters 5-6, it became clear that the success of the bifunctional catalysts was only possible when the two components were proximal to each other, so must consist of one heterogeneous (T)U and a homogeneous base. In a PFR, this creates an additional challenge, as the homogeneous component would be unable to remain in place as the feed solution flows through the reactor channel. Studies investigating immobilised bifunctional (thio)ureas with tethered amines should be able to tackle this challenge. Not only would both components be immobilised (and thus useable in reactors or recovered by filtration), but this method would ensure that both components remain close to each other to exploit the bifunctional activation of the monomer and initiator. The utility of a longer tethering carbon chain between the active site and the support should also be investigated, to create an immobilised bifunctional catalyst with a "pseudo-homogeneous" active site, while reducing the sterics around the site to accommodate monomer approach.

Although the development of a flow reactor has several fundamental steps to

tackle before it becomes a viable option, this thesis work has provided strong foundations to continue this work and identified key areas of interest for future studies. Both classes of immobilised catalyst that were explored have proved robust and reliable catalysts, leaving significantly less metal residue in the polymer with excellent ROP rates in the melt, and are made using widely available materials and as such, are of industrial interest. The development of heterogeneous catalysts and flow processes for the ROP of cyclic esters has opened up a new window of opportunity to couple these two processes together. Although still in its infancy, it is clear that many routes stem from these two fields, from furthering catalyst development to improve selectivity, to the continuous production of polymers and copolymers with heterogeneous catalysts.

References

[1] C. Hammond, *Green Chem*, 2017, **19**, 2711–2728.

[2] L. Botti, D. Padovan, R. Navar, S. Tolborg, J. S. Martinez-Espin and C. Hammond, *ACS Catalysis*, 2020, **10**, 11545–11555.

[3] S. Atta, J. Cohen, J. Kohn and A. J. Gormley, *Polym Chem*, 2021, **12**, 159–164.

[4] T. Rosen, Y. Popowski, I. Goldberg and M. Kol, *Chem - Eur J*, 2016, **22**, 11533–11536.

[5] I. D'Auria, M. C. D'Alterio, C. Tedesco and C. Pellecchia, *RSC Adv*, 2019, **9**, 32771–32779.

[6] B. Lin, J. L. Hedrick, N. H. Park and R. M. Waymouth, *J Am Chem Soc*, 2019, **141**, 8921–8927.

[7] N. Zhu, S. Behzadi, G. Si and C. Tan, *Polymer International*, 2021, **70**, 823–828.

Chapter 9

Experimental

9.1 Materials

Reagents and solvents were purchased from commercial suppliers and used without further modification unless specified. *L*-LA was recrystallised in dry toluene three times and stored under argon prior to use. 4-methylbenzyl alcohol was recrystallised in diethyl ether and stored under argon. All dry solvents were used directly from an MBraun solvent purification system and dried further over molecular sieves (3 Å).

^{1}H and ^{13}C{^{1}H} NMR spectra were collected using a Bruker Avance 400 or 500 MHz spectrometer (the latter set to a 128 scan run for ^{1}H NMR). Chemical shifts (δ) are expressed in parts per million (ppm) and relative to residual protonated solvent. Coupling constants are expressed in Hertz (Hz). Notation of signals are as follows: s = singlet, d = doublet, t = triplet, q = quartet and m = multiplet. Polymer tacticity was obtained through analysis of the methine region in the homonuclear decoupled (^{1}H{^{1}H}) NMR of the polymer dissolved in $CDCl_3$.[1,2]

Diffusional Ordered Spectroscopy (DOSY) NMR was conducted in $CDCl_3$, on a Bruker Avance III 500 MHz spectrometer, using the ledbpgp2s pulse sequence. The diffusion delay (D1) was set to 4 seconds, with a diffusion gradient length (P30) of 3000 μs and diffusion time (Δ, D20) of 0.07 s. Ten gradient strengths between 2 and 95% were used, with 4 scans per gradient level. Data processing using DOSY methods.[3–5]

Electronspray-Ionisation-Mass-Spectrometry (ESI-MS) was conducted on a MicroToF electrospray quadrupole time-of-flight mass spectrometer, using a positive loop injection mode and a range of 50–500 m/z. 1 μg L^{-1} solutions of samples were made up in acetonitrile (MeCN).

Attenuated total reflectance infra-red (ATR-IR) spectra were recorded on a Perkin Elmer Spectrum 100 FT-IR spectrometer.

CHN microanalysis was carried out at the Science Centre at the London Metropolitan University by Mr. Stephen Boyer and Exeter Analytical Laboratories.

Inductively coupled plasma-Optical Emission Spectrometry (ICP-OES) was conducted by Exeter Analytical Ltd.

Scanning Electron microscopy (SEM) and Energy Dispersive X-Ray (EDX) analysis were performed on a JEOL JSM-6480LV SEM spectrometer, with an Oxford INCA X-ray analyser. A low vacuum mode was applied to the samples for EDX, using a back scattered electron (BSE) detector. The samples were gold coated (70 nm) prior to SEM imaging in high vacuum mode, using a secondary electron detector.

Thermogravimetric analysis (TGA) was performed on a Setaram Setys Evolution TGA 16/18 between 30 and 600 °C (10 °C min^{-1}) under a flow of argon.

Differential Scanning Calorimetry (DSC) analysis was conducted using a TA Instruments DSC Q20 instrument. After holding at 40 °C, the polymer sample was heated to 200 °C at a heating rate of 10 °C min^{-1}. The sample was held at 200 °C for 1 minute then cooled to 40 °C once more at 10 °C min^{-1}, where it was held for a further minute. A second heating cycle was performed, heating the sample at 5 °C min^{-1} to 200 °C. The melting temperature (T_m) value was obtained from the second heating cycle.

Size exclusion chromatography (SEC) data was collected using an Agilent 1260 Infinity Gel Permeation Chromatography (GPC) instrument equipped with PLgel 5 μm MIXED-D column (300 × 7.5 mm) at 1 μL min^{-1} flow rate at 35 °C, using the desired sample dissolved in THF (1 mg mL^{-1}). M_n and M_w data was calculated using refractive index (RI) methods against polystyrene standards, and the values were corrected by multiplying by 0.58 and 0.56 to account for

PLA and PCL, respectively.[6,7] Molecular weights for PDL were reported relative to polystyrene standards. SEC data collected in Chapter 7 was performed on a PSS SECcurity2 GPC, using three SDV 5 μm analytical columns (1000-100 000 Å50 $\times$ 8 mm) and coupled to a differential RI and viscosity detector, and calibrated to polystyrene standards. THF was used as the eluent at 40 °C, with the same flow rate as above.

Matrix-assisted laser-desorption time-of-flight (MALDI-ToF) analysis was performed using a Bruker Autoflex speed instrument using a DCTB matrix (trans-2-[3-(4-tertbutylphenyl)-2-methyl-2-propenylidene]malononitrile) and NaTFA to ionise the sample.

Attenuated-Total-Reflection-Fourier-Transform-Infra-Red (ATR-FT-IR) monitored ROP of *L*-LA with immobilised metal complexes (Chapter 3) and organocatalysts (Chapter 5) was carried out using a model IN350-T IR probe, connected to a Bruker Matrix-MF spectrometer, with continual monitoring of the C−O−C peaks. Data was processed using Opus 7.5 software (Bruker), with further processing performed in Microsoft Excel. ATR-FT-IR conducted in Chapter 4 was performed using the Mettler Toledo ReactIR 700, equipped with a TE MCT Detector and AgX 9.5mm $\times$ 1.5m Fibre (Silver Halide) diamond probe, with a resolution every 8 wavenumbers, , with continual monitoring of the C=O peaks. Data was processed using the iC IR 7.1 software.

9.2 Methods

Chapter 3

Synthesis of Complexes

Synthesis of immobilised metal Schiff-base complexes

Following the literature procedures: In a typical PS functionalisation, a commercially available (chloromethyl)polystyrene resin, crosslinked with 5.5% DVB (divinylbenzene) (Merrifield's resin, 5.5 mmol g^{-1}, 11 mmol), and $NaHCO_3$ (11 mmol) were stirred in DMSO (20 mL) at 155 °C for 6 hours. The solvent was removed by vacuum filtration, and light-yellow PS-CHO beads were washed with DMSO until the filtrate ran clear. The PS-CHO beads were dried *in vacuo* at

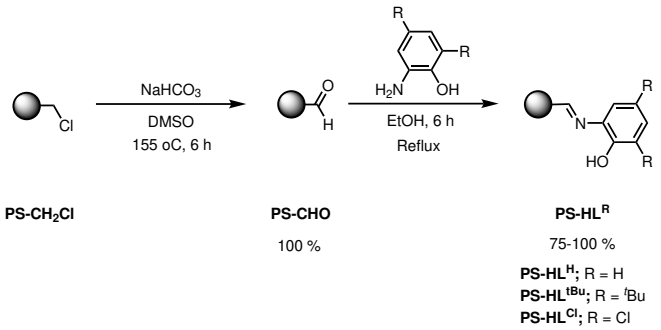

Scheme 9.1: Synthetic route to the immobilised ligands on (chloromethyl)polystyrene (PS) resin.

100 °C for two hours.

PS-CH_2Cl starting material **IR (ATR, cm^{-1})** 2919 ν(C−H), 1604 ν(C=C),1264 ν(C−Cl), 825 ν(C=C), 673 ν(C−Cl).

PS-CHO IR (ATR, cm^{-1}) 2918 ν(C−H), 2746 ν(C−H, aldehyde), 1697 ν(C=O), 826 ν(C=C). **PS-CHO (29.02 g/mol):** calcd. C 83.10, H 6.99, N 0.00, O 9.91; found C 56.46, H 6.16, N 0.00. **Loading:** calcd. 6.20 mmol/g; found 6.20 mmol/g. 100% yield.

PS-CHO (5.5 mmol) was then stirred with the appropriate amine (5.5 mmol) in ethanol at reflux for 6 hours, to produce ligand **PS-HL^H**. The orange product was collected by vacuum filtration, washed with ethanol until the filtrate ran clear, then dried *in vacuo* at 50 °C for two hours.

PS-HL^H IR (ATR, cm^{-1}) 3381 ν(O−H), 2920 ν(C−H), 1698 ν(C=O), 1623 ν(C=N), 1598 ν(C=C), 1285 ν(C−N), 1247 ν(C−O), 827 ν(C=C). **PS-C_7H_6NO (120.13 g/mol):** calcd. C 81.65, H 6.47, N 5.55, O 6.33; found C 76.36, H 6.43, N 2.28. **Loading:** calcd. 3.96 mmol/g; found 4.24 mmol/g. >100% yield (note that yields greater than 100% indicate residual salts or impurities on the catalyst surface).

PS-HL^{tBu} IR (ATR, cm^{-1}) 3675 ν(O−H), 2952 ν(C−H), 1699 ν(C=O), 1624 ν(C=N), 1605 ν(C=C), 1267 ν(C−N), 1247 ν(C−O), 825 ν(C=C). **PS-$C_{15}H_{22}NO$ (232.37 g/mol):** calcd. C 84.74, H 8.68, N 3.07, O 3.51; found C 80.70, H 7.23, N 2.63. **Loading:** calcd. 6.20 mmol/g; found 1.88 mmol/g. 77% yield.

PS-HL^{Cl} IR (ATR, cm^{-1}) 3378 ν(O−H), 2921 ν(C−H), 1698 ν(C=O), 1604 ν(C=N), 1573 ν(C=C), 1269 ν(C−N), 1269 ν(C−O), 1168 ν(C−O, 3°alcohol), 842 ν(C−Cl), 827 ν(C=C). **PS-$C_7H_4Cl_2NO$ (189.01 g/mol):** calcd. C 64.13, H 4.45, N 4.36, O 4.97, Cl 22.09; found C 74.29, H 6.30, N 1.16. **Loading:** calcd. 3.11 mmol/g; found 0.84 mmol/g. 16% yield.

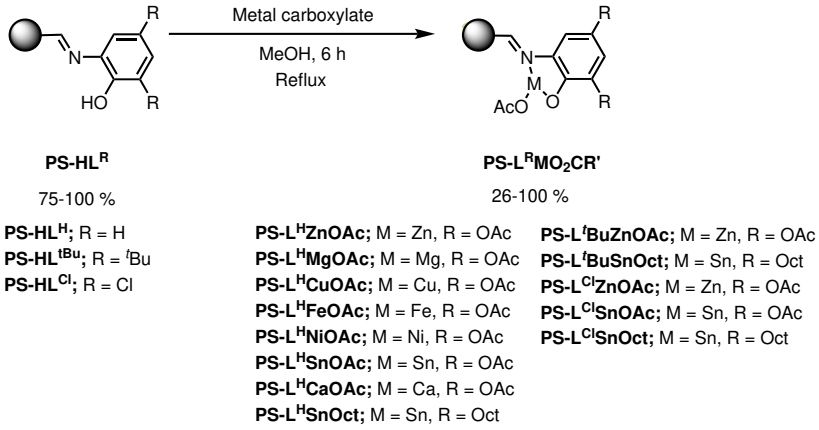

Scheme 9.2: Synthetic route to the immobilised complexes on (chloromethyl)polystyrene (PS) resin.

PS-HL^{H} (1.7 mmol) was stirred with a metal carboxylate source (1.7 mmol) in methanol (15 mL) under reflux for 6 hours. The complex was collected by vacuum filtration and washed with methanol until the filtrate ran clear, then dried *in vacuo* at 50 °C for two hours.

PS-L^{H}ZnOAc IR (ATR, cm^{-1}) 2920 ν(C−H), 1698 ν(C=O), 1604 ν(br, C=N), 1574 ν(complexed COO^{-}), 1453 ν(C−H, methyl), 1282 ν(C−N), 1259 ν(C−O). **PS-$C_9H_8NO_3Zn$ (243.56 g/mol):** calcd. C 59.80, H 4.75, N 3.90, O 13.35, Zn 18.21; found C 68.14, H 6.37, N 1.36. Loading: calcd. 2.78 mmol/g; found 1.68 mmol/g. 50% yield.

PS-L^{H}MgOAc IR (ATR, cm^{-1}) 2922 ν(C−H), 1698 ν(C=O), 1604 ν(C=N), 1576 ν(complexed COO^{-}), 1286 ν(C−N), 1248 ν(C−O). **PS-$C_9H_8NO_3Mg$ (202. 46 g/mol):** calcd. C 68.75, H 5.48, N 4.18, O 14.33, Mg 7.26; found C 77.37, H 6.35, N 1.54. **Loading:** calcd. 2.78 mmol/g; found 0.99 mmol/g. 27% yield.

PS-L^{H}CuOAc IR (ATR, cm^{-1}) 2920 ν(C−H), 1697 ν(C=O), 1603 ν(br, C=N),

1574 ν(complexed COO^-), 1453 ν(C−H, methyl), 1286 ν(C−N), 1245 ν(C−O). **PS-$C_9H_8NO_3Cu$ (241.70 g/mol):** calcd. C 61.54, H 4.91, N 3.75, O 12.82, Cu 16.99; found C 71.34, H 5.73, N 1.41. **Loading:** calcd. 2.78 mmol/g; found 1.26 mmol/g. 38% yield.

PS-L^HNiOAc IR (ATR, cm^{-1}) 2919 ν(C−H), 2158-1974 ν(C−H), 1698 ν(C=O), 1604 ν(C=N), 1572 ν(complexed COO^-), 1451 ν(C−H, methyl), 1289 ν(C-N), 1251 ν(C-O). **PS-$C_9H_8NO_3Ni$ (236.84 g/mol):** calcd. C 62.35, H 4.97, N 3.79, O 12.99, Ni 15.90; found C 72.32, H 5.80, N 1.41. **Loading:** calcd. 2.71 mmol/g; found 1.21 mmol/g. 36% yield.

PS-L^HSnOAc IR (ATR, cm^{-1}) 2921 ν(C−H), 1698 ν(C=O), 1603 ν(C=N), 1574 ν(complexed COO^-), 1452 ν(C−H, methyl), 1287 ν(C−N), 1259 ν(C−O). **PS-$C_9H_8NO_3Sn$ (296.86 g/mol):** calcd. C 53.63, H 4.27, N 3.26, O 11.18, Sn 27.65; found C 69.66, H 5.45, N 1.74. **Loading:** calcd. 2.33 mmol/g; found 1.08 mmol/g. 34% yield.

PS-L^HCaOAc IR (ATR, cm^{-1}) 3373 ν(O−H), 2921 ν(C−H), 1697 ν(C=O), 1602 ν(C=N), 1573 ν(br, complexed COO^-), 1451 ν(C−H, methyl), 1287 ν(C−N), 1248 ν(C−O). **PS-$C_9H_8NO_3Ca$ (218.23 g/mol):** calcd. C 65.66, H 5.23, N 4.00, O 13.68, Ca 11.43; found C 73.06, H 6.07, N 1.69. **Loading:** calcd. 2.71 mmol/g; found 0.92 mmol/g. 26% yield.

PS-L^HSnOct IR (ATR, cm^{-1}) 2926-2859 ν(C−H), 1699 ν(C=O), 1623 ν(br, uncomplexed C=N), 1599 ν(C=C), 1583 ν(complexed COO^-), 1453 ν(C−H, methyl), 1290 ν(C−N), 1251 ν(C−O). **PS-$C_{15}H_{20}NO_3Sn$ (381.04 g/mol):** calcd. C 58.87, H 5.93, N 2.73, O 9.34, Sn 23.12; found C 69.66, H 5.45, N 1.74. Loading: calcd. 1.95 mmol/g; found 1.03 mmol/g. 35% yield.

The same procedure was used to complex $Zn(OAc)_2 \cdot 2\,H_2O$ and $Sn(Oct)_2$ to ligand **PS-HL^{tBu}**, and **PS-HL^{Cl}**.

PS-L^{tBu}ZnOAc IR (ATR, cm^{-1}) 2952 ν(C−H), 1702 ν(remaining C=O), 1604 ν(C=N), 1576 ν(complexed COO^-), 1267 ν(C−N), 1248 ν(C−O). **PS-$C_{17}H_{24}NO_3$-Zn (355.80 g/mol):** calcd. C 59.25, H 6.86, N 3.73, O 12.76, Zn 17.40; found C 80.95, H 7.15, N 1.15. **Loading:** calcd. 2.71 mmol/g; found 2.36 mmol/g. 84% yield.

PS-L^{tBu}SnOct IR (ATR, cm^{-1}) 2952 ν(C−H), 1697 ν(remaining C=O), 1604 ν(C=N), 1605 ν(C=C), 1573 ν(complexed COO$^-$), 1265 ν(C−N), 1247 ν(C−O). **PS-$C_{23}H_{37}NO_3Sn$ (494.29 g/mol):** calcd. C 57.31, H 7.57, N 2.72, O 9.32, Sn 23.08; found C 78.07, H 6.95, N 1.19. **Loading:** calcd. 1.94 mol/g; found 1.94 mmol/g. 100% yield.

PS-L^{Cl}ZnOAc IR (ATR, cm^{-1}) 2921 ν(C−H), 1698 ν(remaining C=O), 1602 ν(C=N), 1571 ν(complexed COO$^-$), 1454 ν(C−H, methyl), 1260 ν(C−N), 1213 ν(C−O), 842 ν(C−Cl), 826 ν(C=C). **PS-$C_9H_6Cl_2NO_3Zn$ (312.43 g/mol):** calcd. C 79.83, H 6.87, N 0.74, O 2.53, Cl 3.75, Zn 6.27; found C 72.66, H 6.20, N 0.93. **Loading:** calcd. 0.76 mmol/g; found 0.43 mmol/g. 54% yield.

PS-L^{Cl}SnOAc IR (ATR, cm^{-1}) 2921 ν(C−H), 1698 ν(remaining C=O), 1602 ν(C=N), 1571 ν(complexed COO$^-$), 1264 ν(C−N), 1213 ν(C−O), 1448 ν(C−H, methyl), 842 ν(C−Cl), 826 ν(C=C). **PS-$C_9H_6Cl_2NO_3Sn$ (365.76 g/mol):** calcd. C 53.91, H 5.03, N 2.29, O 7.83, Cl 11.58, Sn 19.37; found C 68.34, H 5.80, N 0.94. **Loading:** calcd. 2.01 mol/g; found 1.94 mmol/g. >100% yield.

PS-L^{Cl}SnOct IR (ATR, cm^{-1}) 2923 ν(C−H), 1697 ν(remaining C=O), 1602 ν(C=N), 1571 ν(complexed COO$^-$), 1450 ν(C−H, methyl), 1266 ν(C−N), 1213 ν(C−O), 842 ν(C−Cl), 826 ν(C=C). **PS-$C_{15}H_8Cl_2NO_3Sn$ (450.02 g/mol):** calcd. C 51.90, H 4.89, N 2.41, O 8.24, Cl 12.19, Sn 20.38; found C 66.70, H 5.92, N 0.95. **Loading:** calcd. 1.72 mol/g; found 2.99 mmol/g. >100% yield.

Synthesis of immobilised amine complexes

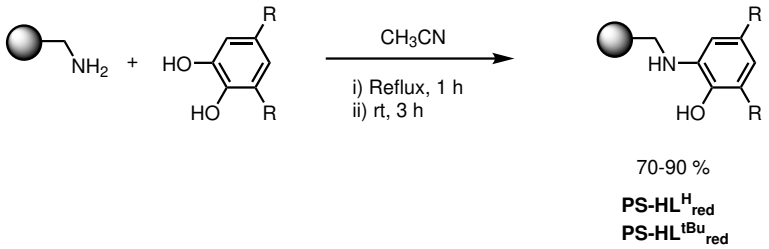

Scheme 9.3: Synthetic route to immobilising the amine (reduced) analogue ligands.

The immobilised amine ligands were synthesised as follows: Aminomethyl(polystyrene) (1 g, 4 mmol/g, 4 mmol) was stirred with the appropriate catechol (4 mmol) in CH_3CN (10 mL) at reflux for one hour. The mixture was then cooled

to room temperature and stirred for a further three hours. The resulting product PS-HL^{H}_{red} was a green powder, characterised by IR.

PS-HL^{H}_{red} IR (ATR, cm^{-1}) 3358 ν(O−H), 3023 ν(N−H), 2922 ν(C−H), 1596 ν(C=C), 1484 ν(C=C), 1254 ν(C−N), 1028 ν(C−O). **PS-C_7H_8NO (122.15 g/mol):** calcd. C 83.88, H 7.35, N 4.10, O 4.67; found C 81.59, H 7.12, N 4.11. **Loading:** calcd. 2.92 mmol/g; found 2.89 mmol/g. 99% yield.

PS-HL^{tBu}_{red} IR (ATR, cm^{-1}) 3350 ν(O−H), 3024 ν(N−H), 2950-2863 ν(C−H), 1599 ν(C=C), 1492 ν(C=C), 1251 ν(C−N), 1225 ν(C−N), 1018 ν(C−O). **PS-$C_{15}H_{24}NO$ (234.39 g/mol):** calcd. C 84.31, H 9.09, N 3.08, O 3.52; found C 87.21, H 8.36, N 3.56. **Loading:** calcd. 2.20 mmol/g; found 1.79 mmol/g. 70% yield.

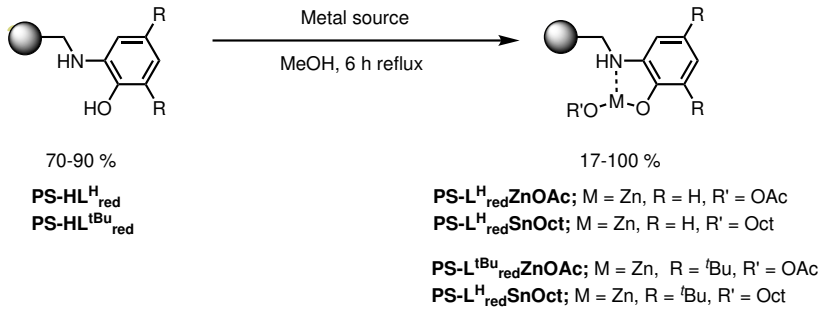

Scheme 9.4: Synthetic route to complexing the amine (reduced) ligands.

Complexation of the amine tethered ligands were achieved as with the Schiff-base complexes.

PS-L^{H}_{red}ZnOAc IR (ATR, cm^{-1}) 2952 ν(C−H), 1552 ν(complexed COO^{-}), 1489 ν(C−N), 1441 ν(C−H, methyl), 1256 ν(C−N), 1018 ν(C−O). **PS-$C_9H_{10}NO_3Zn$ (245.58 g/mol):** calcd. C 67.01, H 5.85, N 2.98, O 10.22, Zn 13.93; found C 58.81, H 5.52, N 2.88. **Loading:** calcd. 2.34 mmol/g; found 1.79 mmol/g. >100% yield.

PS-L^{H}_{red}SnOct IR (ATR, cm^{-1}) 2922 ν(C−H), 1580 ν(complexed COO^{-}), 1475 ν(C−N), 1450 ν(C−H), 1241 ν(C−N). **PS-$C_{15}H_{22}NO_3Sn$ (383.06 g/mol):** calcd. C 63.59, H 6.52, N 2.32, O 7.93, Sn 19.64; found C 70.18, H 6.35, N 3.28. **Loading:** calcd. 2.34 mmol/g; found 1.12 mmol/g. 54% yield.

PS-L^{tBu}_{red}ZnOAc IR (ATR, cm^{-1}) 3024 ν(N−H), 2924 ν(C−H), 1601 ν(C=C),

1566 ν(complexed COO^-), 1450 ν(C−H, methyl), 1305 ν('ceC-N), 1026 ν(C−O). **PS-$C_{17}H_{26}NO_3Zn$ (357.82 g/mol):** calcd. C 73.79, H 7.54, N 2.05, O 7.03, Zn 9.59; found C 82.14, H 6.94, N 3.02. **Loading:** calcd. 1.47 mmol/g; found 0.45 mmol/g. 26% yield.

PS-L^{tBu}_{red}SnOct IR (ATR, cm^{-1}) 3024 ν(N−H), 2922 ν(C−H), 1603 ν(C=C), 1480 ν(C=C), 1245 ν(C−H), 1305 ν(C−N), 1016 ν(C−O). **PS-$C_{23}H_{38}NO_3Sn$ (495.30 g/mol):** calcd. C 70.20, H 7.75, N 1.71, O 5.85, Sn 14.48; found C 82.14, H 6.94, N 3.02. **Loading:** calcd. 1.22 mmol/g; found 0.29 mmol/g. 17% yield.

Synthesis of 2,4-di-*tert*-butyl-6-aminophenol[8]

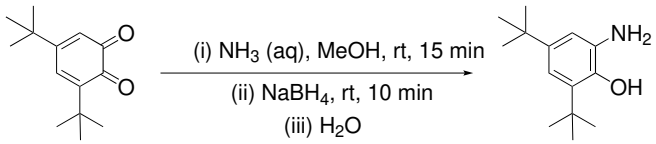

Aqueous ammonia (3.61 mL, 32.8 mmol) was added dropwise to a dark yellow solution of 3,5-di-*tert*-butyl-*o*-benzoquinone (1 g, 4.6 mmol) in methanol (12 mL), and the reaction was left to stir at room temperature for 15 minutes.[9] The reaction turned dark red, and on addition of $NaBH_4$ (0.1717 g, 4.6 mmol) the reaction instantly turned a light orange colour. The mixture was stirred for 10 minutes, after which the reaction was quenched with DI water and a light yellow/green product precipitated out. The product was separated out between diethyl ether and DI water, and the combined organic phases were dried with Mg_2SO_4. The solvent was removed *in vacuo* to give a yellow/orange crude product which was washed with pentane to dissolve out any impurities. The product was dried under vacuum for 1 hour (54%). **^{1}H NMR ($CDCl_3$, 400 MHz)** δ 6.92 (d, J_{HH} = 2.3 Hz, 1H, Ar), 6.82 (d, J_{HH} = 2.3 Hz, 1H, Ar), 5.67 (s, 1H, OH), 3.15 (s, 2H, NH), 1.41 (s, 9H, $C(CH_3)_3$), 1.27 (s, 2 H, $C(CH_3)_3$).

Synthesis of 2,4-dichloro-6-aminophenol[10]

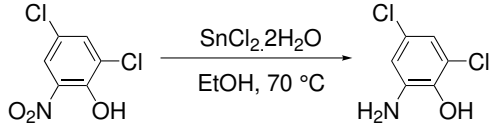

2,4-dichloro-6-nitrophenol (1g, 5 mmol, 1 equiv.) was stirred under reflux in ethanol (20 mL) with $SnCl_2 \cdot 2\,H_2O$ (5.42 g, 25 mmol, 5 equiv.) for 30 minutes. The solution was then cooled to room temperature, then poured into ice (50 mL). $NaHCO_3$ was added to neutralise the mixture. The residual white solid was removed by vacuum filtration, and the filtrate was washed with ethyl acetate (3×30 mL) to extract the organic phase. The combined organic phases were washed with brine (3×20 mL), then dried with $MgSO_4$. The latter was removed by gravity filtration, and the solvent was removed *in vacuo* to produce an off-white solid (35%). **^{1}H NMR ($CDCl_3$, 400 MHz)** δ 6.72 (s, 1H, Ar-H), 6.61 (s, 1H, Ar-H), 5.36 (s, 1H, OH), 3.75 (s, 2H, NH2); **ESI-MS+ (CH_3CN):** $[C6H5Cl2NO]^+$ theoretical: 176.97, found: 177.98; **IR (ATR, cm^{-1})** 3397 ν(N−H), 3310 ν(N−H), 2925 ν(br, O−H), 1584 ν(C=C), 1477 ν(N−H), 1320 ν(C−N), 1227 ν(C−N), 1162 ν(C−O), 834 ν(C=C), 708 ν(C=C).

ROP procedures in the melt

Melt ROP of *L*-lactide (*L*-LA) with immobilised catalysts

A 50:1:1 ratio of *L*-Lactide (1 g, 6.9 mmol), 4-methylbenzyl alcohol and the catalyst were added to a Schlenk flask and stirred at 130 °C for the required reaction time. Once complete, the polymerisation was quenched with technical grade *n*-hexane (∼1 mL) to precipitate the polymer, and the reaction was dissolved in dichloromethane (DCM, 10 mL). The heterogeneous catalysts were recovered from the solubilised polymer *via* vacuum filtration, then dried and characterised by IR (ATR, cm^{-1}) once recovered. The solvent was removed from the reaction mixture *in vacuo*, yielding the crude polymer. Purification of PLA was achieved by dissolving the crude polymer in the minimum amount of DCM. Dropwise addition of the sample to a stirred solution of technical grade *n*-hexane (ten times the amount of DCM) precipitated out the polymer. The latter was collected by vacuum filtration and dried *in vacuo*. Analysis of the methine region of the crude polymer by ^{1}H NMR ($CDCl_3$, 400 MHz) gave the conversion (the $-CHCH_3$ proton in the monomer: 5.05 ppm, polymer: ca. 5.16 ppm). GPC (1-2 mg sample dissolved in 1 mL THF; analysis by refractive index and corrected by a factor of 0.58 for PLA, 0.56 for PCL)[6,7] was used to determine M_n, M_w and $Đ_M$, and was compared to the theoretical value (Equation 1). The $M_{n,NMR}$ was calculated from

the aromatic proton signal of the 4-MeBnO$^-$ end group at 7.18 ppm. MALDI-ToF (using NaTFA and a DCTB matrix in THF) enabled determination of end groups.

In Situ Attenuated Total Reflection-Fourier Transform-Infrared (ATR-FT-IR) monitored ROP of *L*-LA

A Schlenk flask was charged with *L*-LA (3 g, 20.8 mmol, 1 equiv.), immobilised catalyst (0.1 mmol, 0.005 equiv.), 4-methylbenzyl alcohol (50.9 mg, 0.4 mmol, 0.02 equiv.) and a magnetic stirrer in the glovebox, in a [LA]:[Cat]:[I] ratio of 200:1:4. The flask was sealed and removed from the glovebox. Under a flow of argon, the stopper was removed and replaced by an ATR-FT-IR probe (model IN350-T, connected to a Bruker Matrix-MF spectrometer). A background spectrum was obtained prior to positioning the probe into the reaction mixture so that the mechanical stirrer did not interfere with the probe. The flask, equipped with the probe, was placed into a pre-heated oil bath set to 130 °C to melt the *L*-LA, upon which real-time ATR-FT-IR data collection on the Opus 7.5 software (Bruker) began. Kinetic information was collected by integrating the *L*-LA and PLA peaks at 1160-1200 cm^{-1} and 1203-1265 cm^{-1} respectively, in the absorption spectrum, then plotting the natural logarithm of $[LA]_t$ against time (t), to obtain a linear, first order reaction with respect to monomer. Conversion was obtained using a calibration of the IR signals at 174 °C. Measurements were obtained of samples of varying PLA:LA mol% ratios, then the peak areas of each of LA and PLA were plotted against concentration to find a relationship in the form of y=mx+c (Figures B.4 - B.4).

Solution phase ROP of *L*-LA with immobilised catalysts

A 50:1:1 ratio of *L*-Lactide (1 g, 6.9 mmol, 0.69 mol L^{-1}), 4-methylbenzyl alcohol and the catalyst were added to a Schlenk flask and stirred at 80 °C in dry toluene or tetrahydrofuran (THF, 10 mL) for the required reaction time. Once complete, the polymerisation was quenched with technical grade *n*-hexane (1 mL), and the immobilised catalysts were recovered *via* vacuum filtration. The solvent was removed *in vacuo*, yielding the crude polymer.

Sheldon test for heterogeneity

A 50:1:1 ratio of *L*-Lactide (1 g, 6.9 mmol), 4-methylbenzylalcohol and **PS-**

L^{H}SnOct was stirred at 130 °C under an argon atmosphere for 30 minutes. The reaction was removed from the heat and brought into an argon filled glovebox, by which time the monomer/polymer mixture had crystallised out. Some of the mixture was transferred to a second Schlenk flask, taking care to avoid transfer of the catalyst over. A ^{1}H NMR in $CDCl_3$ was obtained at this point. The two batches of reaction mixture (one with catalyst and one without) were then allowed to react for a further two hours until the full reaction time had elapsed. The reactions were quenched with technical grade *n*-hexane (∼0.5 mL) and a work-up was carried out as described above. Adapted from Aguilera *et al.*[11]

Chapter 4

Copolymer synthesis through sequential addition

ϵ-CL (0.77 mL, 6.9 mmol, 50 equiv.), 4-methylbenzyl alcohol (0.0170 g, 0.1 mmol, 1 equiv.) and **PS-L^{H}SnOct** (0.0712 g, 0.1 mmol, 1.95 mmol/g, 1 equiv.) were added to a flask under an argon atmosphere. The reaction was stirred at 130 °C for 2.5 hours, after which a sample was extracted under a flow of argon. *L*-LA (1 g, 6.9 mmol, 50 equiv.) was added from a second flask under a flow of argon. The mixture was stirred for a further 2.5 hours, then quenched with technical grade *n*-hexane (ca. 1 mL) and dissolved in DCM (10 mL) to filter catalyst out by vacuum filtration. The solvent was removed *in vacuo* to yield the copolymer, which was analysed with the same methods as the homopolymers, including ^{1}H (128 scan), ^{13}C{^{1}H} and ^{1}H DOSY NMR. % Composition of the polymers was calculated based on ratios of the two blocks obtained from ^{1}H NMR (calculations found below).

The ABC triblock copolymer $PDL_{50}-b-PCL_{50}-b-PLA_{50}$ was synthesised using the same method, with a third addition of *L*-LA, using [DL]:[CL]:[LA]:[Cat]:[I] = 50:50:50:1:1. Reactions were left for 24 hours, 2.5 hours and 2.5 hours for each monomer, respectively.

The ABA triblock was synthesised using 1,4-benzenedimethanol (0.0186 g, 0.1 mmol, 1 equiv.) as the central unit, off which two arms of PCL could grow. ϵ-CL (1.5 mL, 13.5 mmol, 100 equiv.) was added as the first monomer with **PS-L^{H}SnOct** (0.0692 g, 0.1 mmol, 1.95 mmol/g, 1 equiv.). After 2.5 hours, the

reaction was sampled under an argon flow, and a second monomer was added (*L*-LA, 0.97 g, 6.7 mmol, 50 equiv.). The reaction was left for a further 2.5 hours and then worked up as above.

Copolymer synthesis through a one-pot method: *in situ* ATR-FT-IR monitored ROP

A short, wide Schlenk flask was charged with *L*-LA (3 g, 20.8 mmol, 50 equiv.) and 4-methylbenzyl alcohol (0.0510 g, 0.4 mmol, 1 equiv.). ϵ-CL (2.31 mL, 20.8 mmol, 50 equiv.) was added to a separate flask. The probe was placed into the flask containing the mixture of monomers under an argon flow, such that the end of the probe was submerged in the reaction mixture. The flask was submerged into the oil bath set to 130 °C and monitoring of the reaction established when the temperature had stabilised. Under a flow of argon, ϵ-CL was added *via* syringe once all the *L*-LA had melted **PS-L$^{\mathbf{H}}$SnOct** (0.2136 g, 0.4 mmol, 1.95 mmol/g, 1 equiv.) was added in through the side arm of the Schlenk containing the monomers, using anti-static weighing paper as a funnel, then the side-arm was sealed. Progress of reaction was carried out by collecting a spectrum every minute, with continuous monitoring of the C=O peak areas of the monomer and polymer until these stopped changing. Work up followed the same process as with sequential copolymerisations.

The same procedure was used for [LA]:[CL]:[Cat]:[I] = 50:50:0.25:1 reactions and LA/ϵ-DL copolymerisation. It was also applied to the "small scale" one-pot copolymerisation, where amounts of reagents were scaled to 1 g *L*-LA, and the ATR-FT-IR was not used.

Calculation of % content of monomer 1 (M_1) and monomer 2 (M_2) in the polymer

The following calculations assume 100 % incorporation of the monomers into the final copolymer.

$$\%M_2 = \left(\frac{(\text{Conversion } M_2 \times \text{equiv. } M_2)}{(\text{Conversion } M_1 \times \text{equiv. } M_1) + (\text{Conversion } M_2 \times \text{equiv. } M_2)}\right) \times 100$$

$$\%M_1 = 100 - \%M_2$$

Chapter 5

Synthesis of immobilised urea(U) and thiourea (TU) catalysts[12]

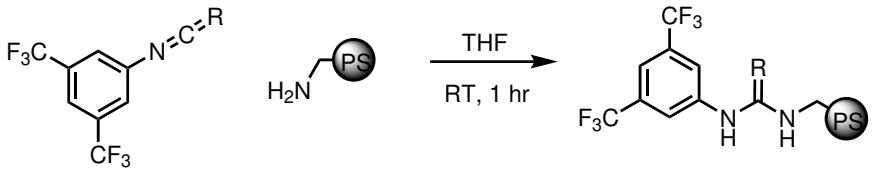

R = O, **PS-Urea**
= S, **PS-TU**

In an argon filled glovebox, a Schlenk flask was charged with 3,5-bis((tri fluoromethyl)phenyl isocyanate (0.35 mL, 2 mmol) and (aminomethyl)polystyrene (0.5 g, 2 mmol, 4 mmol/g) were stirred in anhydrous THF (12 mL) at room temperature for 1 hour. The resulting catalyst was collected by vacuum filtration, then dried *in vacuo* at 50 °C for 2 hours.

PS-Urea IR (ATR, cm^{-1}) 3300 ν(N−H), 2160 ν(br, N=C=O), 1658 ν(C=O), 1385 ν(C−F), 1274 ν(strong, C−N), 1171 ν(medium, C−N), 1123 ν(strong, C−F). **PS-$C_{10}H_7F_6N_2O$ (285.17 g/mol):** calcd. C 63.94, H 4.78, N 5.55, O 3.17, F 22.57; found C 62.48, H 4.56, N 5.59. **Loading:** calcd. 1.98 mmol/g; found 2.10 mmol/g. 112% yield.

PS-Thiourea IR (ATR, cm^{-1}) 3245 ν(N−H), 2156 ν(C−H), 2028 ν(N−C=S), 1380 ν(C−F), 1274 ν(strong, C−N), 1169 ν(medium, C−N), 1125 ν(strong, C−F). **PS-$C_{10}H_7F_6N_2S$ (301.23 g/mol):** calcd. C 61.97, H 4.63, N 5.38, S 5.96, F 21.21; found C 62.70, H 4.56, N 5.38. **Loading:** calcd. 1.98 mmol/g; found 1.86 mmol/g. 94% yield.

Synthesis of homogeneous urea (U)/thiourea (TU) catalysts

In an argon filled glovebox, a vial, equipped with a magnetic stirrer, was charged with 3,5-bis((trifluoromethyl)phenyl isocyanate (0.81 mL, 4.67 mmol) and anhydrous THF (12 mL). Benzylamine (0.51 mL, 4.67 mmol) was added dropwise and

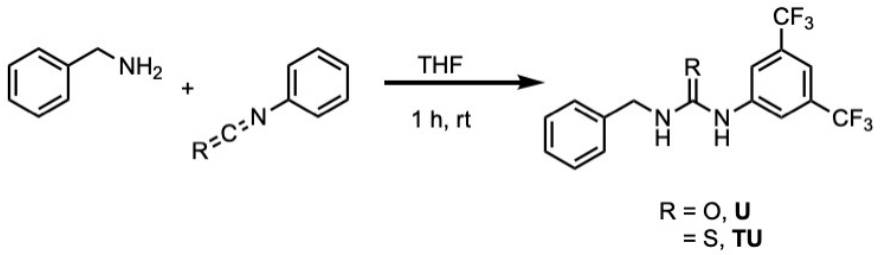

the reaction mixture was stirred at room temperature for 1 hour. The solvent was removed *in vacuo*, yielding a light yellow solid powder urea. The same process was repeated with 3,5-bis((trifluoromethyl)phenyl isothiocyanate to yield the TU.

Urea (U) ^{1}H NMR (DMSO-d_6, 400 MHz): δ = 9.36 (s, 1H, N−H), 8.10 (s, 2H, Ar−H), 7.55 (s, br, 1H, N−H), 7.38-7.28 (m, 4H, Ar−H), 7.28-7.21 (m, 1H, Ar−H), 7.01 (t, J_{HH} = 6.0 Hz, 1H, Ar−H), 4.32 (d, J_{HH} = 6.0 Hz, 2H, $-CH_2$); **IR (ATR, cm^{-1})** 3331 ν(N−H), 1654 ν(strong, C=O), 1390 ν(C−F), 1269 ν(strong, C−N), 1178 ν(medium, C−N), 1122 ν(strong, C−F); **ESI-MS+ (CH_3CN):** theoretical m/z $[C_{16}H_{12}F_6N_2O]^+$ 362.09, found m/z: 363.09; Yield = 1.64 g, 97%.

TU ^{1}H NMR (DMSO-d_6, 400 MHz): 8.67 (s, br, 1H, N−H), 8.24 (s, 2H, Ar−H), 7.73 (s, 1H, Ar−H), 7.39-7.19 (m, 5H, Ar−H), 4.77 (s, 2H, $-CH_2$), 3.30 (s, 1H); **IR (ATR, cm^{-1})** 3217 ν(N−H), 3034 ν(N−H), 1545 ν(strong, C=S), 1382 ν(N=C=S),[13] 1262 ν(strong, C−N), 1170 ν(strong, C−N), 1124 ν(strong, C−F), 1106 ν(strong, N=C=S); **ESI-MS+ (CH_3CN):** theoretical m/z $[C_{16}H_{12}F_6N_2S]^+$ 378.06, found m/z: 379.07; Yield = 1.19 g, >99%.

Gabriel synthesis of PS-CH_2NH_2 beads

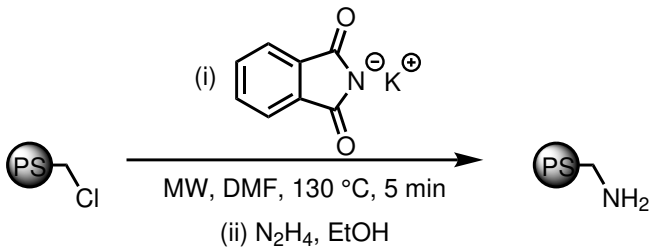

Following the literature procedure,[14] cream coloured beads of Merrifield's resin (PS-CH_2Cl, 0.2 g, 0.1 mmol, 5.5 mmol/g), potassium phthalimide salt (7.9645

g, 43 mmol) and DMF (20 mL) were combined in a microwave vial equipped with a mechanical stirrer. The reaction was carried out in a microwave reactor at 130 °C for 10 minutes. The pale yellow intermediate was collected by vacuum filtration and washed with copious amounts of DI water to remove any unreacted phthalimide salt. The intermediate was stirred at reflux in air, with hydrazine monohydrate (5.4 mL, 87 mmol) in ethanol for 20 hours. The grey amine product was collected by vacuum filtration and washed with acetone to remove any unreacted hydrazine and DI water, and then dried under vacuum at 50 °C for 2 hours. **IR (ATR, cm^{-1})** 3310 ν(N−H), 2917 ν(C−H), 1609 ν(bend, N−H), 1450 ν(bend, C−H).

Solution phase ROP of *L*-LA with PS-CH_2NH_2

A 50:1:1 ratio of *L*-Lactide (1 g, 6.9 mmol), 4-methylbenzyl alcohol (0.1 mmol) and the catalyst (0.1 mmol) were added to a Schlenk flask and stirred at 80 °C in dry toluene (10 mL) for the required reaction time. Once complete, the polymerisation was quenched with technical grade *n*-hexane (∼1 mL) to precipitate the polymer. The solvent was removed *in vacuo*, yielding the crude polymer. Analysis of the crude polymer by ^{1}H NMR ($CDCl_3$, 400 MHz) gave a conversion of 10%. The same method was repeated using DCM (10 mL) and stirring for 72 hours at room temperature.

General melt bifunctional ROP of *L*-LA with (PS-)U and (PS-)Bases

The following procedure was consistent between ROP with both immobilised and free bases and (thio)ureas.

Under an argon atmosphere, *L*-LA (1 g, 6.9 mmol, 50 equiv.), PS-Urea (0.0704 g, 1.97 mmol/g, 0.1 mmol, 1 equiv.), PS-imidazole (0.1388 g, 1 mmol/g, 0.1 mmol, 1 equiv.) and 4-methylbenzyl alcohol (0.0170 g, 0.1 mmol, 1 equiv.) were added to a Schlenk flask. The reaction mixture was stirred at 130 °C for four hours, then quenched with technical grade *n*-hexane (ca. 1 mL) and solubilised in DCM (10 mL). The heterogeneous catalyst was removed by syringe filtration, and the solvent was removed *in vacuo* to obtain the polymer. The same procedure was used in the ROP of *L*-LA with organobases, but the (T)U was omitted. Table outlines the various immobilised organobases and their catalyst loading on the PS surface.

Table 9.1: Functional group loading of PS-immobilised bases; for catalyst with a loading range, it was assumed that the lowest end of the range was the true loading.

Catalyst	Catalyst loading (mmol/g)
PS-CH_2NH_2	0.6
PS-CH_2NH_2	4
PS-DMAP	3
PS-DBU	1.5-2.5
PS-Imidazole	1-1.5
PS-NEt_2	1.5-2

Chapter 6

Solution phase bifunctional ROP of *L*-LA with (PS-)U and KOEt

Following a similar procedure described by Waymouth and co-workers,[12] the ROP of *L*-LA was carried out as follows. The immobilised urea (or TU) catalyst was dried under vacuum at 50 °C for 2 hours prior to use. A solution of *L*-LA (288.3 mg, mmol, [LA] = 1 mol L^{-1}) in anhydrous THF (1.5 mL) was added to a Schlenk flask containing a preprepared solution of dried catalyst (29.4 mg, 0.1 mmol) KOEt (1.7 mg, 2×10^{-2} mmol) in anhydrous THF (0.5 mL) under argon, obtaining a ratio of [LA]:[U]:[KOEt] = 100:3:1. After stirring at room temperature for the desired amount of time, the reaction was quenched with benzoic acid (40 mg). The solvent was removed *in vacuo*, and the crude polymer was analysed by ^{1}H NMR in $CDCl_3$ and GPC (THF).

Chapter 7

Flow ROP of *L*-LA with TBD in a microreactor

The following describes the general procedure using *L*-LA; the same procedure was used for ϵ-caprolactone.

Anhydrous DCM (10 mL) was added to a flame-dried Schlenk flask containing *L*-LA (2.8826 g, 10 mmol, [LA] = 2 mol L^{-1}), creating stock solution 1. In a separate Schlenk flask, TBD (0.0557 g, 0.2 mmol) was added under a flow of argon. The flask was flushed with argon three times to remove any air in the flask. 1 mL benzyl alcohol stock solution in DCM (0.4 mol L^{-1}, 0.041 mL benzyl

alcohol, 0.2 mmol) was syringed through a rubber septum, and DCM (9 mL) was added to the mixture to create the second stock solution (10 mL total volume, [TBD] = 0.04 mol L^{-1}, [BnOH] = 0.04 mol L^{-1}).

The two 1 mL gastight syringes were loaded with dry solvent and connected to the PFA tubing. The solvent (2 mL total volume) was run through the reactor at a high flow rate (500 μL min^{-1}) to purge the reactor and create a dry environment for the reaction. 1 mL of each stock solution was taken up into a gastight syringe and attached to the reactor tubing. A high flow rate was set for approximately 0.1 mL (per syringe) to flush out any air bubbles. The desired flow rate was then set and the reaction was left to run until steady state before sample collection into the SEC vial containing 0.5 mL THF and benzoic acid to quench the reaction.

The solvent was removed under a flow of N_2, and a small drop of the concenrated product was taken for ^{1}H NMR. The remaining solid was dissolved in SEC grade THF spiked with toluene as an internal standard (150 μL per 250 mL THF).

Flow ROP of *L*-LA with DBU in a microreactor

Anhydrous DCM (10 mL) was added to a flame-dried Schlenk flask containing *L*-LA (2.8826 g, 10 mmol, [LA] = 1 mol L^{-1}), creating stock solution 1. Separately, a DBU stock solution in DCM (0.4 mol L^{-1}, 0.0598 mL DBU, 0.2 mmol) and was prepared. This was added to 1 mL of the benzyl alcohol stock solution in DCM (0.4 mol L^{-1}, 0.041 mL benzyl alcohol, 0.2 mmol). DCM (8 mL) was added to the catalyst/initiator mixture to create the second stock solution ($[DBU]_{final}$ = 0.04 mol L^{-1}, $[BnOH]_{final}$ = 0.04 mol L^{-1}).

The flow polymerisation then followed the same pocedure as described in the previous section.

Batch Solution phase ROP of *L*-LA

The catalyst/initiator stock solution was prepared by adding 0.5 mL of each of benzyl alcohol stock in DCM (0.4 mol L^{-1}, mmol) and of DBU in DCM (0.4 mol L^{-1}, mmol). The initiator/catalyst stock was added quickly to a Schlenk submerged in a 35 °C oil bath, containing *L*-LA (1.4413 g, 1 mol L^{-1}, 6.9 mmol) in DCM (10 mL), *via* Schlenk techniques, to create a 100:1:1 ratio of [LA]:[Cat]:[I].

The reaction was allowed to stir for the desired amount of time. Once complete, the polymerisation was quenched with technical grade *n*-hexane (ca. 1 mL) to precipitate the polymer, and the reaction was dissolved in DCM (ca. 10 mL). The solvent was removed under a flow of N_2, yielding the crude polymer.

Purification of PLA was achieved by dissolving the crude polymer in the minimum amount of DCM. Dropwise addition of the sample to a stirred solution of hexane (ca. 30 mL) precipitated out the polymer. The latter was collected by vacuum filtration, purified once more, then dried under vacuum.

The solvent was removed under a flow of N_2, and a small drop of the concentrated product was taken for ^{1}H NMR. The remaining solid was dissolved in SEC grade THF spiked with toluene as an internal standard (150 μL per 250 mL THF).

Preparation of mixtures for data encryption

For each mixture (either a mixture of random amounts of polymer, or a mixture with specific letters encoded), each of the five polymers was added into the mixture in different mass ranges, outlined in Table 7.11.

Once the amounts per SEC sample were determined, stock solutions were prepared for increased accuracy of concentrations within the final mixtures. The total weight of each polymer was calculated, and an error in measurement of 20% was added as an allowance for SEC calibration differences. As an example, the total mass of polymer 2 that was required was 7.2 mg (6 mg + 20%). The polymer was dissolved in 5 mL SEC grade THF (ca. 4.44 g), generating a w/w concentration of polymer.

For example, for mixture 1 ('Code 0'), in order to obtain 1.5 mg of polymer 2, 0.90 g of the stock solution of polymer 2 was measured out; separately, 2.70 g was measured out to give 4.5 mg in mixture 2 ('Code 1'). The same procedure was repeated for the other polymers within the mixture, and SEC traces were obtained .

Chapter 8

General procedure for homogeneous ROP using the reactor

In an argon filled glovebox, a Schlenk containing a magnetic stirrer was charged with ϵ-CL (4.43 mL, 40 mmol, 25 equiv.), $Sn(Oct)_2$ (0.51 mL, 1.6 mmol, 1 equiv.), 4-methylbenzyl alcohol (0.1955 g, 1.6 mmol, 1 equiv.) and anhydrous toluene (40 mL, [CL] = 1 mol L^{-1}). Under an argon flow outside of the glovebox, the reactor tubing was washed through with a separate batch of anhydrous toluene (5 minutes at 5 mL min^{-1}) to remove any residual IPA:Water. Once the reactor had been primed, the inlet tubing was then transferred from the toluene flask to the flask containing the feed solution; the stopper was switched for the inlet PTFE tube to direct the feed solution to the pump, and held in place with a suba-seal. The flow rate was set to 5 mL min^{-1} once again to fill the reactor with feed solution (3-5 minutes), then adjusted to 0.006 mL min^{-1} to achieve the desired residence time (τ_r = 4 hours). Sampling was started from this point, and continued hourly until a steady state had been reached; sampling was achieved by collection of the exit solution in a vial containing a few drops of $CDCl_3$ for ^{1}H NMR analysis. The flow rate was adjusted to change the total residence time.

References

[1] B. M. Chamberlain, M. Cheng, D. R. Moore, T. M. Ovitt, E. B. Lobkovsky and G. W. Coates, *J Am Chem Soc*, 2001, **123**, 3229–3238.

[2] J. Coudane, C. Ustariz-Peyret, G. Schwach and M. Vert, *J Polym Sci Pol Chem*, 1997, **35**, 1651–1658.

[3] R. Evans, Z. Deng, A. K. Rogerson, A. S. McLachlan, J. J. Richards, M. Nilsson and G. A. Morris, *Angew Chem Int Edit*, 2013, **52**, 3199–3202.

[4] H. Kato, T. Saito, M. Nabeshima, K. Shimada and S. Kinugasa, *J Magn Reson*, 2006, **180**, 266–273.

[5] R. Evans, G. Dal Poggetto, M. Nilsson and G. A. Morris, *Anal Chem*, 2018, **90**, 3987–3994.

[6] J. Baran, A. Duda, A. Kowalski, R. Szymanski and S. Penczek, *Macromol Rapid Comm*, 1997, **18**, 325–333.

[7] G. Gontard, A. Amgoune and D. Bourissou, *J Polym Sci Pol Chem*, 2016, **54**, 3253–3256.

[8] F. Dulong, O. Bathily, P. Thuéry, M. Ephritikhine and T. Cantat, *Dalton Trans*, 2012, **41**, 11980–11983.

[9] J. Vinsova, K. Cermakova, A. Tomeckova, M. Ceckova, J. Jampilek, P. Cermak, J. Kunes, M. Dolezal and F. Staud, *Bioorganic and Medicinal Chemistry*, 2006, **14**, 5850–5865.

[10] F. D. Bellamy and K. Ou, *Tetrahedron Letters*, 1984, **25**, 839–842.

[11] D. A. Aguilera, L. Spinozzi Di Sante, A. Pettignano, R. Riccioli, J. Roeske, L. Albergati, V. Corti, M. Fochi, L. Bernardi, F. Quignard and N. Tanchoux, *Eur J Org Chem*, 2019, **2019**, 3842–3849.

[12] B. Lin and R. M. Waymouth, *J Am Chem Soc*, 2017, **139**, 1645–1652.

[13] C. N. Rao and R. Venkataraghavan, *Spectrochim Acta*, 1962, **18**, 541–547.

[14] Q. M. Kainz, M. Zeltner, M. Rossier, W. J. Stark and O. Reiser, *Chem - Eur J*, 2013, **19**, 10038–10045.

Appendix A

Additional ROP Data

Chapter 3

Table A.1: Polymerisation data from the recycling study of **PS-L^{H}MOR'** (M = Zn, Mg, Ca and Sn and R' = OAc or Oct) in the ROP of *L*-LA. Conditions: [LA]:[Cat]:[I] = 50:1:1 in the melt at 130 °C for 24 hours.

Entry	Catalyst	Conv. (%)[a]	$M_{n,\ Theo}$[b]	$M_{n,NMR}$[a]	$M_{n,SEC}$[c]	$Đ_M$[c]
1	**PS-L^{H}ZnOAc**	84	6050	5800	4650	1.23
2	**PS-L^{H}ZnOAc Reused**	33	2400	2150	2750	1.25
3	**PS-L^{H}MgOAc**	30	2150	1350	1150	1.05
4	**PS-L^{H}MgOAc Reused**	4	300	-	-	-
5	**PS-L^{H}CaOAc**	30	2150	1350	1150	1.05
6	**PS-L^{H}CaOAc Reused**	18	1300	1000	-	-
7	**PS-L^{H}SnOct**	93	6700	3150	5900	1.49
8	**PS-L^{H}SnOct Reused**	82	5900	3000	9750	1.51

[a] Determined from the ^{1}H NMR spectrum.

[b] Theoretical M_n= ([LA]/[I]) × (144 × equiv. LA) × (conv./100).

[c] As determined by SEC (THF) using RI methods, relative to poly(styrene) standards (multiplied by a factor of 0.58, rounded to the nearest 50, according to *Macromol. Chem. Phys.*, 2002, **203**, 889–899).

Table A.2: Polymerisation data from the solution-phase ROP of *L*-LA with **PS-L^{H}MOR'** catalysts (R' = OAc or Oct) and control reactions over 24 hours, using [LA]:[Cat]:[I] = 50:1:1 ([LA] = 0.69 mol L^{-1}).

Entry	Catalyst	Solvent	Temp. (°C)	Conv. (%)[a]	$M_{n,Theo}$[b]	$M_{n,SEC}$[c]	$M_{w,SEC}$[c]	$Đ_M$[c]
1	**PS-L^{H}SnOct**	THF	rt	3	200	-	-	-
2	**PS-L^{H}ZnOAc**	THF	rt	0	0	-	-	-
3	**PS-L^{H}SnOct**	Toluene	80	77	5550	4400	4800	1.09
4	**PS-L^{H}ZnOAc**	Toluene	80	19	1350	2000	2100	1.07
5	$Sn(Oct)_2$	Toluene	80	93	6700	5200	6050	1.16

[a] Determined from the ^{1}H NMR spectrum.
[b] Theoretical M_n= ([LA]/[I]) × (144 × equiv. LA) × (conv./100).
[c] As determined by SEC (THF) using RI methods, relative to poly(styrene) standards (multiplied by a factor of 0.58, rounded to the nearest 50, according to *Macromol. Chem. Phys.*, 2002, **203**, 889–899).

Chapter 5

Table A.3: Polymerisation data from the ROP of *L*-LA with PS-DBU, using [LA]:[B]:[I] = 50:1:1 in the melt at 130 °C for 2, 6, 16 and 24 hours.

Entry	Time (h)	Conv. (%)[a]	$M_{n,Theo}$[b]	$M_{n,NMR}$[a]	$M_{n,SEC}$[c]	$M_{w,SEC}$[c]	$Đ_M$[c]
1	24	87	6250	3550	1750	2450	1.40
2	16	88	6350	4250	7900	9350	1.23
3	6	87	625	4050	1550	2500	1.65
4	2	81	5850	2600	2650	4000	1.49

[a] Determined from the ^{1}H NMR spectrum.
[b] Theoretical M_n= ([LA]/[I]) × (144 × equiv. LA) × (conv./100).
[c] As determined by SEC (THF) using RI methods, relative to poly(styrene) standards (multiplied by a factor of 0.58, rounded to the nearest 50, according to *Macromol. Chem. Phys.*, 2002, **203**, 889–899).

Chapter 6

Table A.4: Polymerisation data for the ROP of *L*-LA with PS-U/KOEt or KOMe, at [LA]:[PS-U]:[KOEt] = 100:3:1, [LA] = 1 mol L^{-1} in THF at room temperature, 1 hour.

Entry	Catalyst	Base	Conv. (%)[a]	$M_{n,Theo}$[b]	$M_{n,SEC}$[c]	$Đ_M$[c]
1	PS-U	-	0	-	-	-
2	PS-U	KOEt	94	13550	9150	1.75
3	PS-U_{beads}	KOEt	97	14000	4600	1.64
4	PS-U	KOMe	96	13850	4600	1.54
5	-	KOMe	37	5350	5700	2.83
6	Urea	KOEt	93	13400	7700	1.46

[a] Determined from the ^{1}H NMR spectrum.
[b] Theoretical M_n= ([LA]/[I]) × (144 × equiv. LA) × (conv./100).
[c] As determined by SEC (THF) using RI methods, relative to poly(styrene) standards (multiplied by a factor of 0.58, rounded to the nearest 50, according to *Macromol. Chem. Phys.*, 2002, **203**, 889–899).

Table A.5: Polymerisation data for the solvent-free ROP of *L*-LA with a commercially available amine base, at [LA]:[B]:[I] = 50:1:1, at 130 °C, over 4 hours. This data also appears in Chapter 5, but has been compiled here for reference to Chapter 6.

Entry	Base	Conv. (%)[a]	$M_{n,Theo}$[b]	$M_{n,NMR}$[a]	$M_{n,SEC}$[c]	$M_{w,SEC}$[c]	$Đ_M$[c]
1	PS-BDZ	92	6650	4750	2100	2650	1.29
2	Imidazole	64	4600	4000	4200	4850	1.16
3	PS-DMAP	53	3800	3250	1300	2300	1.77
4	DMAP	97	7000	4700	4000	6800	1.71
5	PS-DBU	89	6400	4850	1650	4250	2.57
6	DBU	95	6850	5800	5250	8050	1.54

[a] Determined from the ^{1}H NMR spectrum.
[b] Theoretical M_n= ([LA]/[I]) × (144 × equiv. LA) × (conv./100).
[c] As determined by SEC (THF) using RI methods, relative to poly(styrene) standards (multiplied by a factor of 0.58, rounded to the nearest 50, according to *Macromol. Chem. Phys.*, 2002, **203**, 889–899).

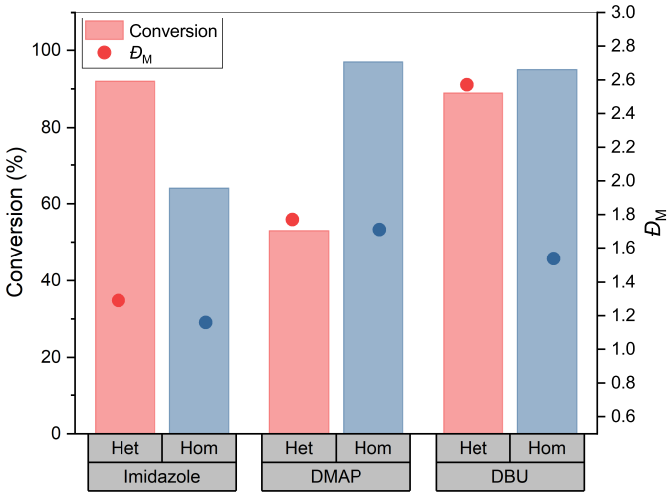

Figure A.1: Solvent-free ROP of *L*-LA with homogeneous and heterogeneous commercially available bases (B), including imidazole, DMAP and DBU, at [LA]:[B]:[I] = 50:1:1, at 130 °C, over 4 hours.

Table A.6: Polymerisation data for the ROP of *L*-LA with PS-U/Amine base, at varying ratios and reaction conditions, [LA] = 1 mol L^{-1}.

Entry	Catalyst	Base	[LA]:[U]:[B]:[I]	Temp. (°C)	Solvent	Time (h)	Conv. (%)[a]
1	-	Imidazole	50:0:1:1	rt	THF	24	4
2	PS-Urea	-	100:3:1:0	rt	THF	1	0
3	PS-Urea	Imidazole	100:3:1:1	rt	THF	1	3
4	PS-Urea	Imidazole	100:3:1:1	rt	THF	24	3
5	-	Imidazole	50:0:1:1	rt	THF	1	3
6	PS-Urea	Imidazole	50:1:1:0	rt	THF	24	2
7	PS-Urea	Imidazole	50:1:1:1	rt	THF	24	3
8	PS-Urea	Imidazole	50:1:1:1	60	THF	24	5
9	PS-Urea	Imidazole	50:1:1:1	rt	DCM	24	5
10	PS-Urea	Imidazole	50:1:1:1	35	DCM	24	7
11	Urea	Imidazole	50:1:1:1	rt	THF	4	7
12	PS-Urea	Imidazole	50:0:1:1	rt	THF	4	5
13	PS-Urea	Imidazole	50:1:1:1	rt	THF	4	8
14	-	DMAP	50:0:1:1	rt	THF	4	5
15	PS-Urea	DMAP	50:1:1:1	rt	THF	4	8

[a] Determined from the ^{1}H NMR spectrum.

Table A.7: Polymerisation data for the fully heterogeneous ROP of *L*-LA with (PS-)TU/(PS-)DBU, at [LA]:[TU]:[DBU]:[I] = 100:3:1:1 or 50:1:1:1, [LA] = 1 mol L^{-1} in THF at room temperature.

Entry	**Catalyst**	**Base**	**[LA]:[Cat]:[B]:[I]**	**Conv. (%)**[a]	$M_{n,NMR}$[a]	$M_{n,SEC}$[b]	$M_{w,SEC}$[b]	$Đ_M$[b]
1	-	DBU	100:0:1:1	90	6500	1100	1550	1.39
2	-	PSDBU	100:0:1:1	9	650	-	-	-
3	PS-TU	-	100:1:0:0	2	150	-	-	-
4	TU	-	100:1:0:0	2	150	-	-	-
						4750	7200	1.52
5	PS-TU	DBU	100:3:1:1	87	6250	10450[c]	12150[c]	1.16[c]
						3400[d]	3700[d]	1.07[d]
6	PS-TU	PS-DBU	100:3:1:1	8	600	-	-	-
7	TU	DBU	100:3:1:1	95	6850	14150	16550	1.17
8	TU	PS-DBU	100:3:1:1	16	1150	6650	7050	1.07
9	-	DBU	50:0:1:1	88	6350	5750	6800	1.18
						4250	12400	2.93
10	PS-TU	DBU	50:1:1:1	79	5700	24100[c]	35550[c]	1.48[c]
						3250[d]	4050[d]	1.25[d]
11	TU	DBU	50:1:1:1	93	6700	7300	9000	1.25
12	-	PS-DBU	50:0:1:1	13	950	1700	1900	1.11
13	PS-TU	PS-DBU	50:1:1:1	22	1600	2300	2550	1.11
14	TU	PS-DBU	50:1:1:1	70	5050	5400	5850	1.08

[a] Determined from the ^{1}H NMR spectrum.

[b] As determined by SEC (THF) using RI methods, relative to poly(styrene) standards (multiplied by a factor of 0.58, rounded to the nearest 50, according to *Macromol. Chem. Phys.*, 2002, **203**, 889–899).

[c] $M_{n,SEC}$ of Peak 1.

[d] $M_{n,SEC}$ of Peak 2 (shoulder).

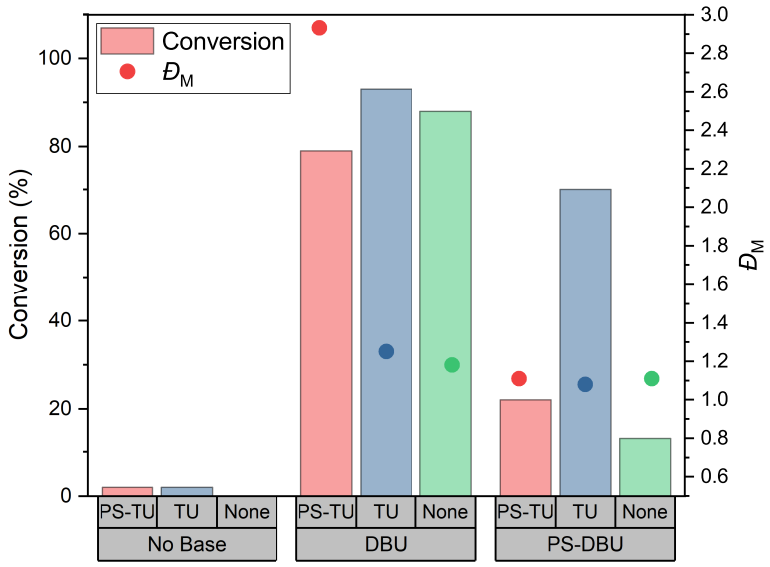

Figure A.2: ROP of *L*-LA with (PS-)TU/(PS-)DBU at [LA]:[TU]:[DBU]:[I] = 50:1:1:1, [LA] = 1 mol L^{-1} in THF at room temperature, over 1 hour.

Appendix B

Additional Characterisation Data

B.1 Example calculation of the catalyst functional group loading and elemental % composition for PS-CHO (step 1 of complex synthesis)

1. Starting from 1 g PS-CH_2Cl resin (5.5 mmol/g), the weight of PS in the resin must be calculated:

$$5.5 \text{ mmol amine} \times 49.48 \text{ g/mol } CH_2Cl = 272.14 \text{ mg of } CH_2Cl \text{ in resin}$$

$$1000 \text{ mg resin} - 272.24 \text{ mg} = 727.86 \text{ mg PS}$$

2. Calculation of the weight remaining CH_2Cl when conversion = X%; assume X = 50% (for example):

$$50\% \times 5.5 \text{ mmol } CH_2Cl = 2.75 \text{ mmol } CH_2Cl \text{ remaining}$$

$$2.75 \text{ mmol } CH_2Cl \times 49.48 \text{ g/mol} = 136.07 \text{ mg } CH_2Cl \text{ remaining}$$

3. Calculation of the weight of CHO (product) groups when X = 50%, 2.75 mmol

CHO have formed:

$$2.75 \text{ mmol CHO} \times 29.02 \text{ g/mol CHO} = 79.805 \text{ mg of CHO groups in resin}$$

4. Calculation of the total (new) weight of the resin:

$$\sum \text{mg}_{\text{PS}} + \text{mg}_{\text{CH}_2\text{Cl remaining}} + \text{mg}_{\text{CHO}} = 943.74 \text{ mg resin (total)}$$

5. Calculation of **CHO loading** from conversion (where X = 50%)

$$\text{mmol/g CHO loading} = \frac{\left(\text{weight CHO at X \%} \div \text{Total resin weight}\right)}{\text{Mr CHO}}$$

$$\text{mmol/g CHO loading} = \frac{\left(79.805 \text{ mg}_{\text{CHO}} \div 943.74 \text{ mg}_{\text{resin}}\right)}{29.02 \text{ g/mol}_{\text{CHO}}}$$

$$= 2.91 \text{ mmol/g}$$

6. Calculation of **mass % of each component** within the resin (e.g. mass % PS):

$$\text{mass \% PS} = \frac{727.86 \text{ mg PS}}{943.74 \text{ mg resin (total)}} \times 100 = 77.13\%$$

Complete for the CH_2Cl and CHO, using values from (2) and (3).

7. Calculation of the % composition of elements in each of the three components (e.g. carbon):

a. PS chemical formula (repeat unit): C_8H_8

$$\%\text{C in PS} = \frac{\text{Mr}_{\text{C}} \times \text{ratio of C}}{\left(\sum \text{Mr}_{\text{All Elements}} * \text{ratio element}\right)}$$

$$\%C \text{ in PS} = \frac{12.01 \text{ g/mol} \times 8}{104.16} = 92.24\%$$

b. CH_2Cl chemical formula: CH_2Cl

$$\%\text{C in } CH_2Cl = \frac{12.01 \text{ g/mol} \times 1}{49.48} = 24.27\%$$

c. CHO chemical formula: CHO

$$\% \text{ C in CHO} = \frac{12.01 \text{ g/mol} \times 1}{29.01} = 41.40\%$$

8. Final resin composition (e.g. total % C in resin):

$$\% \text{ C (total)} = \big(\% \text{ C in PS} \times \text{mass \% PS}\big) + \big(\% \text{ C in } CH_2Cl \times \text{mass \% } CH_2Cl\big)$$
$$+\big(\% \text{ C in CHO} \times \text{mass \% CHO}\big)$$
$$\% \text{ C (total)} = 78.14\%$$

Steps (6)-(8) should be completed for each element present in the different components of the resin. These mass% can then be compared to those obtained through ICP analysis using the "Solver" function in Microsoft Excel to obtain the experimental loading based on the elemental mass %, through a back calculation. In the above example, the total % carbon in the resin at 100% conversion would be 83.10%, making the loading 6.20 mmol/g.

B.2 IR spectra

Chapter 5

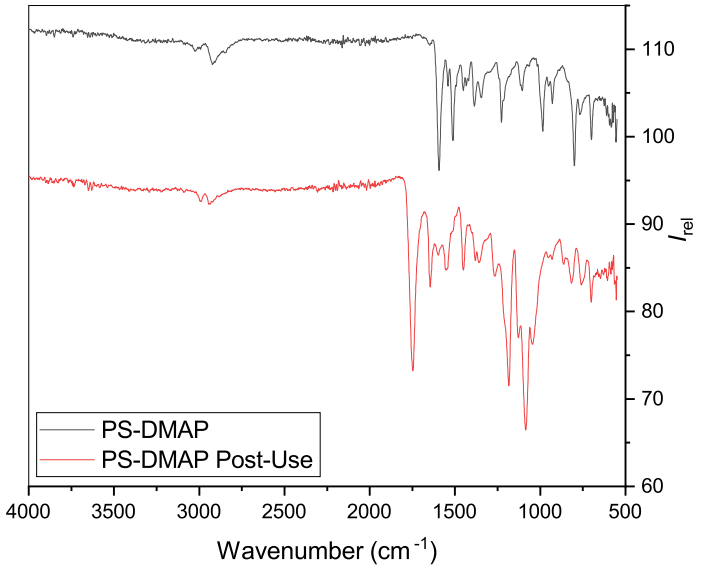

Figure B.1: IR spectrum of immobilised DMAP pre- and post-use in ROP of *L*-lactide, displaying peaks at 1747 and 1085 cm^{-1}, corresponding to the lactone C=O and C−O stretches, respectively.

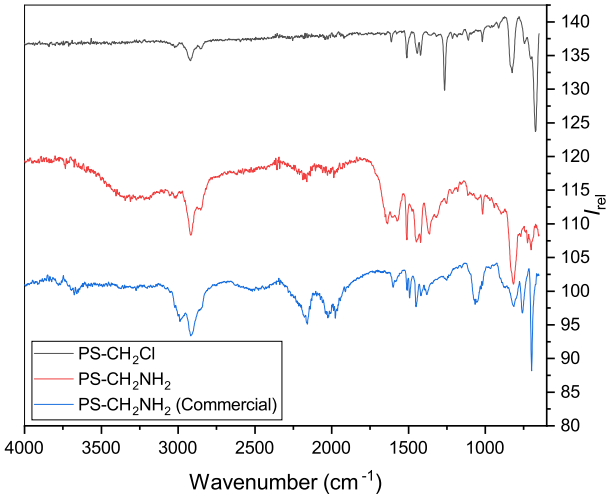

Figure B.2: IR spectrum of the starting material and product from the Gabriel synthesis (top and middle traces, respectively), compared to the commercial (aminomethyl)polystyrene (bottom).

B.3 *In situ* ATR-FT-IR

Chapter 3

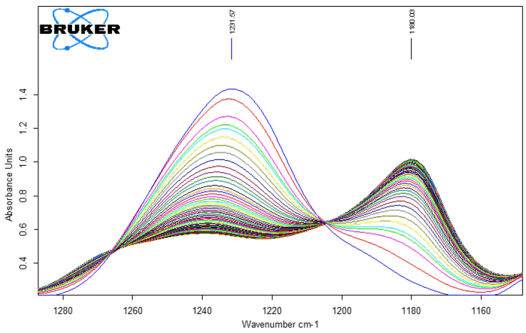

Figure B.3: FT-IR stretches of the C−O−C bonds of PLA (right, 1185 cm^{-1}) and lactide (left, 1240 cm^{-1}).

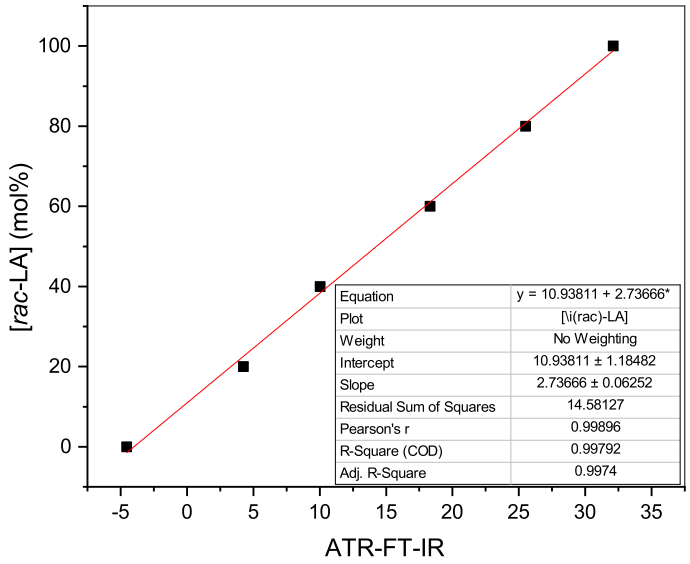

Figure B.4: Calibration curve at 174 °C to correlate the ATR-FT-IR integrated peak area of lactide to the concentration.

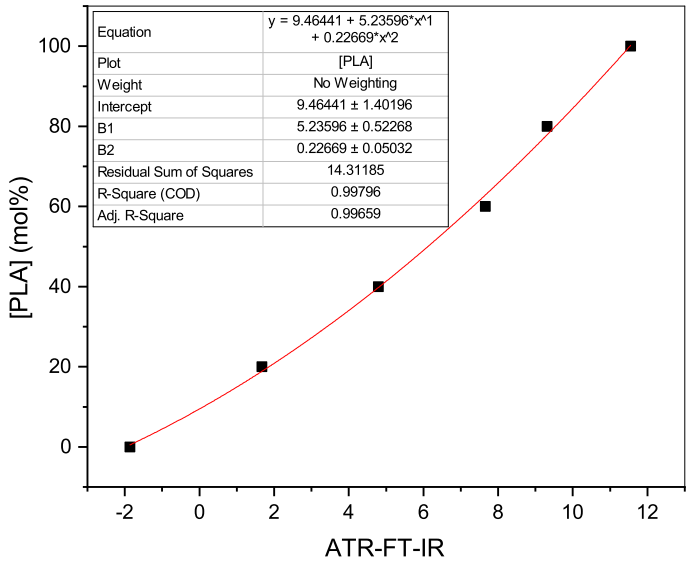

Figure B.5: Calibration curve at 174 °C to correlate the ATR-FT-IR integrated peak area of PLA to the concentration.

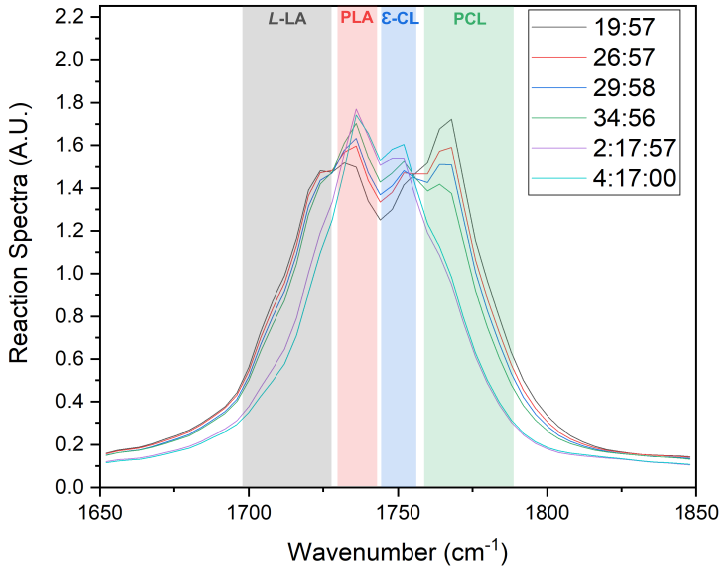

Figure B.6: C=O region of selected IR spectra from the *in situ* ATR-FT-IR monitored one-pot copolymerisation of ϵ-CL and *L*-LA ([LA]:[CL]:[Cat]:[I] = 50:50:1:1, melt, 130 °C). Kinetic analysis carried out by monitoring the area beneath the LA (grey), PLA (red), PCL (blue) and CL (green) peaks at 1766, 1750, 1735, 1723 cm^{-1}, respectively. Legend refers to time during reaction.

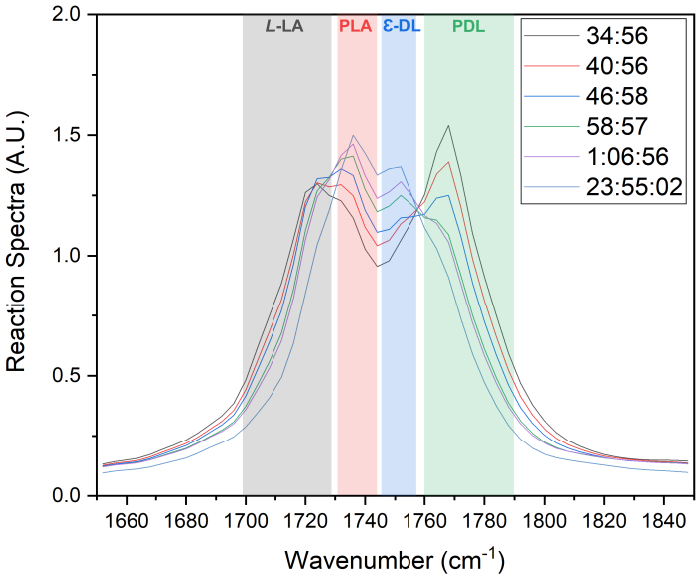

Figure B.7: C=O region of selected IR spectra from the *in situ* ATR-FT-IR monitored one-pot copolymerisation of ϵ-DL and *L*-LA ([LA]:[CL]:[Cat]:[I] = 50:50:1:1, melt, 130 °C). Kinetic analysis carried out by monitoring the area beneath the LA (grey), PLA (red), PDL (blue) and DL (green) peaks at 1766, 1750, 1733, 1722 cm^{-1}, respectively. Legend refers to time during reaction.

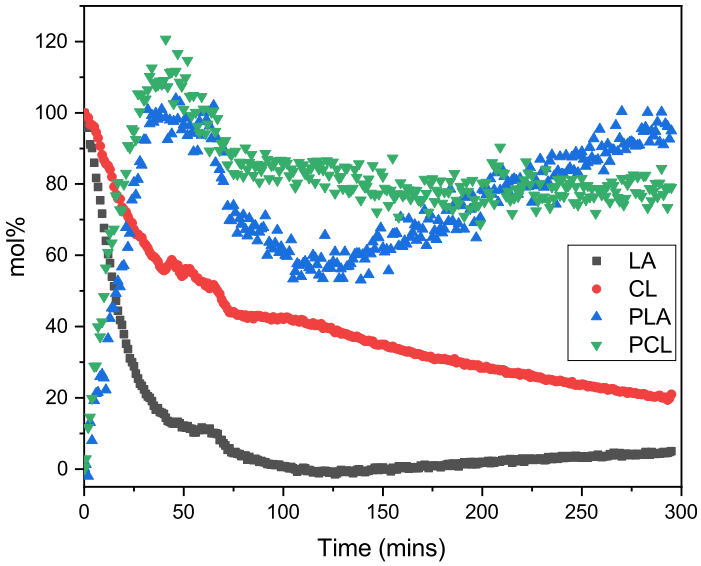

Figure B.8: Full time-scale of one-pot copolymerisation of *L*-LA and ϵ-CL in the melt, 5 hours ([LA]:[CL]:][Cat]:[I] = 50:50:1:1, 130 °C, entry 2, Table 4.6).

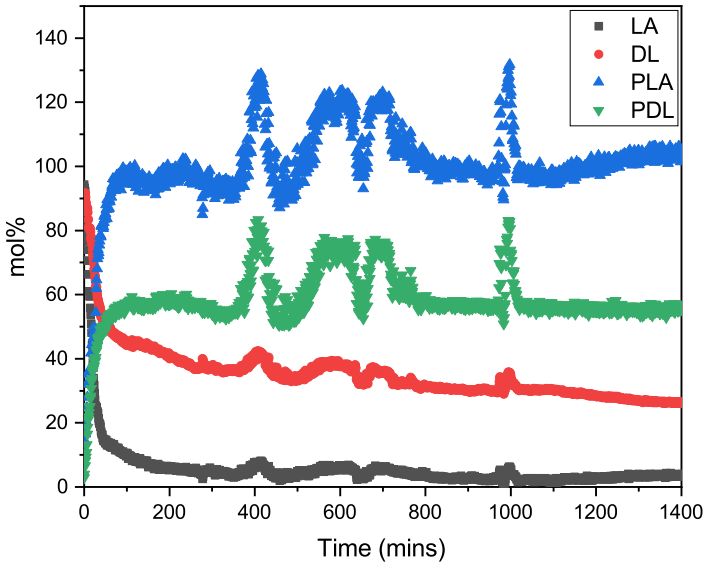

Figure B.9: Full time-scale of one-pot copolymerisation of *L*-LA and ϵ-DL in the melt, 24 hours ([LA]:[DL]:][Cat]:[I] = 50:50:1:1, 130 °C, entry 3, Table 4.6).

B.4 NMR spectra

Chapter 3

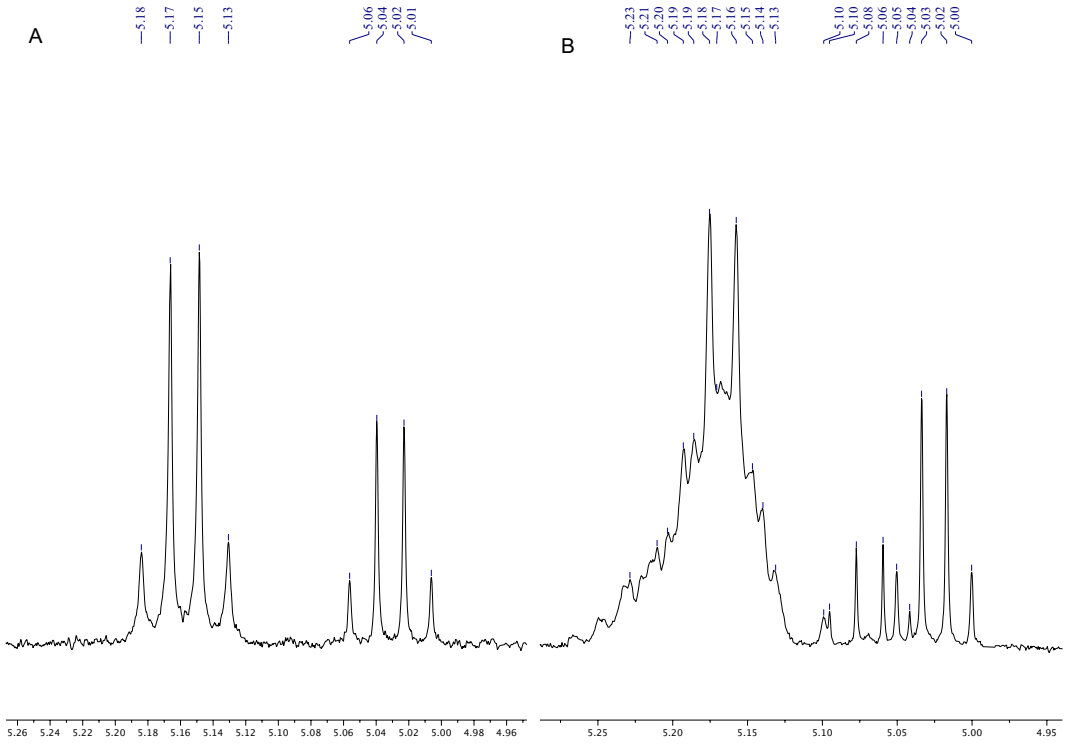

Figure B.10: Methine region of PLA (ca. 5.19 ppm) and lactide (5.05 ppm) in the ^{1}H NMR ($CDCl_3$, 400 MHz) of the crude PLA formed with (A) **PS-L^{tBu}SnOct** and (B) PS-DMAP which participates in epimerisation. The scrambled quartet at 5.19 and 5.05 ppm in (B) shows that the strength of the base resulted in a high degree of epimerisation of the lactide.

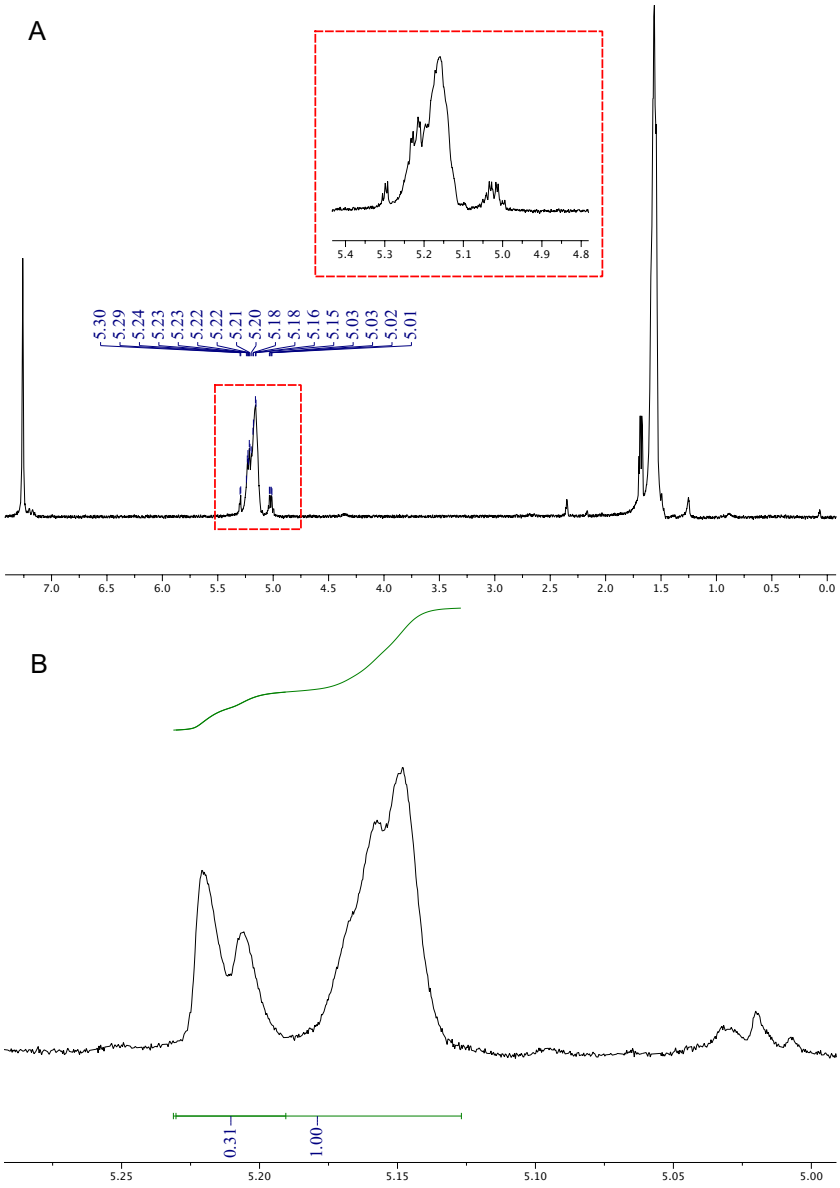

Figure B.11: Example of PLA produced by the **PS-L$^{\mathbf{H}}$SnOct** catalysed ROP of *rac*-LA. (A) ^{1}H NMR ($CDCl_3$, 400 MHz) of the crude polymer, (B) Homonuclear Decoupled ^{1}H{^{1}H} NMR ($CDCl_3$, 500 MHz). Conditions: [LA]:[Cat]:[I] = 50:1:1, 2.5 h in the melt at 130 °C. Probability of heterotactic enchainment calculated by $P_r = \sqrt{2 \times isi}$.

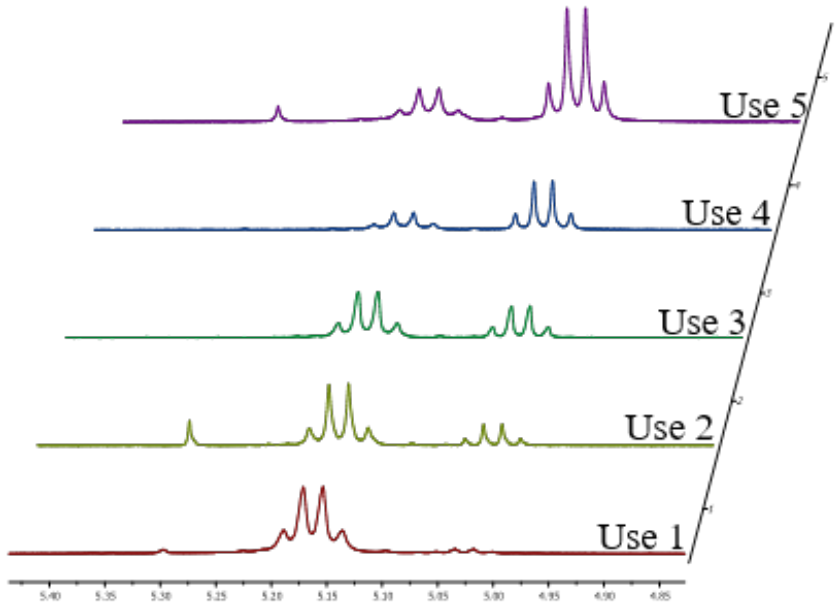

Figure B.12: Methine region in the ^{1}H NMR ($CDCl_3$, 400 MHz) spectra of crude PLA after 6 reuse cycles using **PS-L^{H}SnOct** (Conditions: [LA]:[Cat]:[I] = 50:1:1, 2.5 hours in the melt at 130 °C).

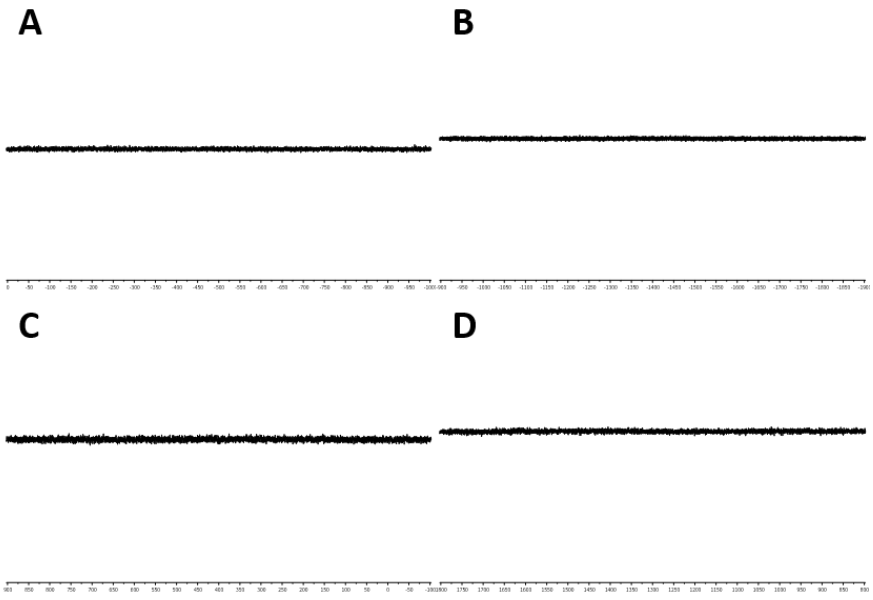

Figure B.13: ^{119}Sn NMR ($CDCl_3$, 187 MHz) spectra of a PLA sample produced with $Sn(Oct)_2$. (A) 0 to -1000 ppm (780 scans), (B) -1000 to -2000 ppm (512 scans), (C) 900 to -100 ppm (599 scans) and (D) 1800 to 800 pm (1847 scans).

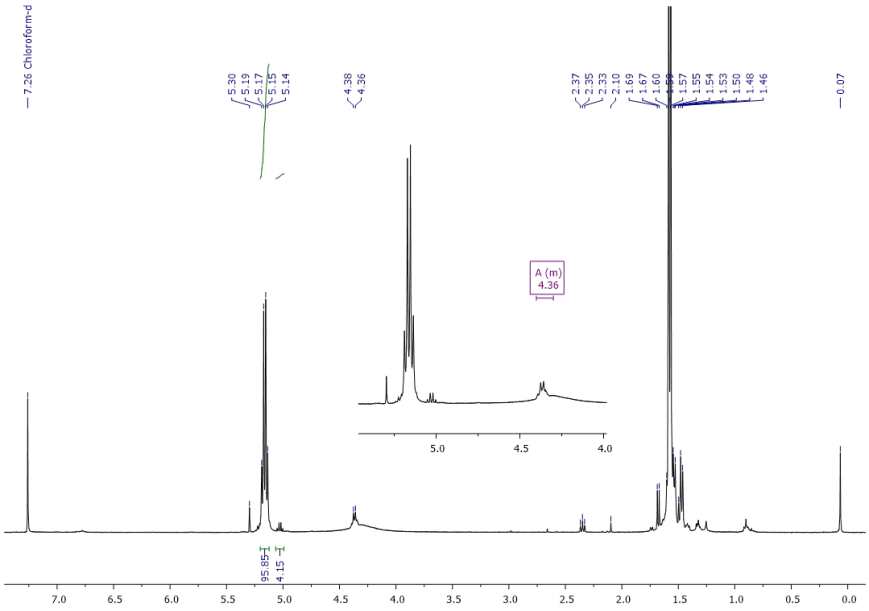

Figure B.14: ^{1}H NMR ($CDCl_3$, 400 MHz) of residual PLA collected after attempting to regenerate the catalyst by stirring the latter in DCM and acetic acid for 72 hours. Depolymerisation is evidenced by the generation of a lactic acid quartet at 4.36 ppm arising from the methine hydrogen.

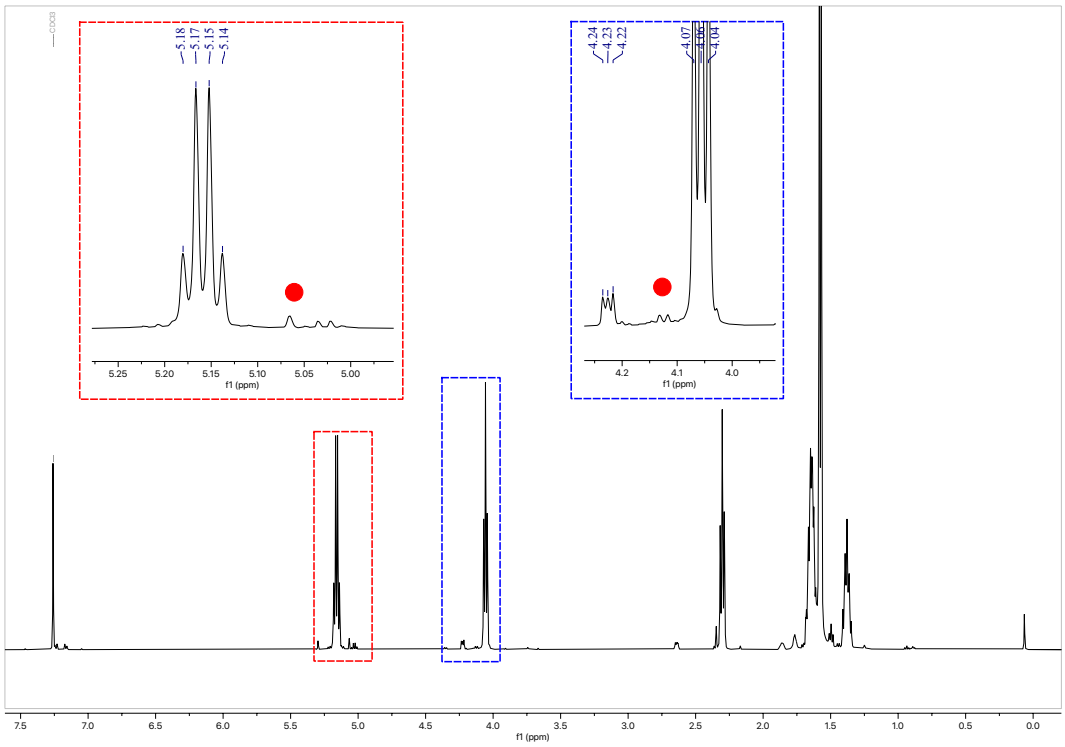

Figure B.15: ^{1}H NMR (500 MHz, 128 scans) in $CDCl_3$ for $PCL_{50}-b-PLA_{50}$.

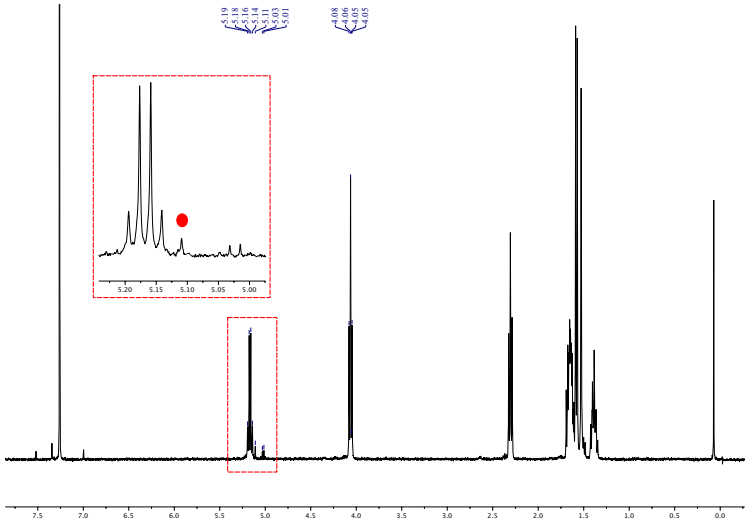

Figure B.16: ^{1}H NMR (500 MHz, 128 scans) in $CDCl_3$ for ABA triblock $PLA_{25}-b-PCL_{50}-o-PCL_{50}-b-PLA_{25}$.

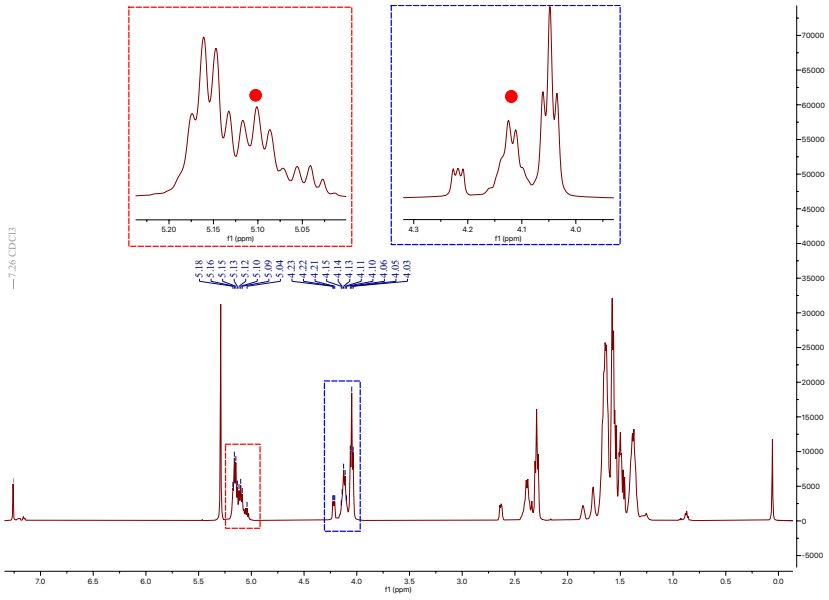

Figure B.17: ^{1}H NMR (500 MHz, 128 scans) in $CDCl_3$ for $PLA_{50}-PCL_{50}$, produced through the one-pot copolymerisation method.

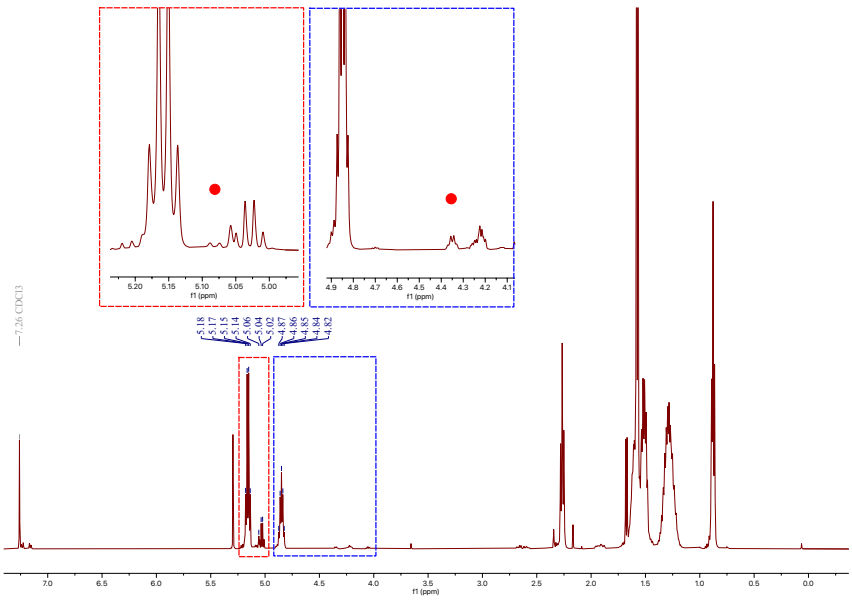

(a) ^{1}H NMR (128 scans)

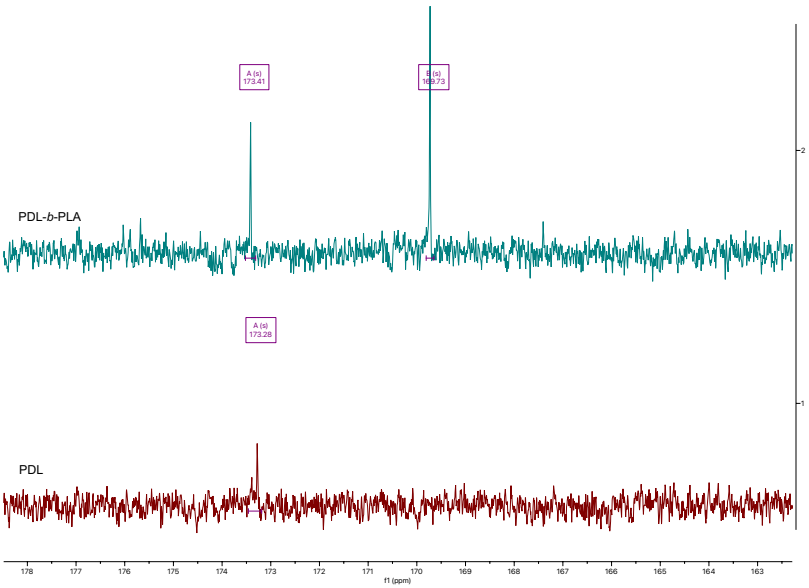

(b) ^{13}C{^{1}H} NMR

Figure B.18: NMR spectra in $CDCl_3$ of $PDL_{50}-b-PLA_{50}$ ([LA]:[DL]:[Cat]:[I] = 50:50:1:1], 130 °C in the melt).

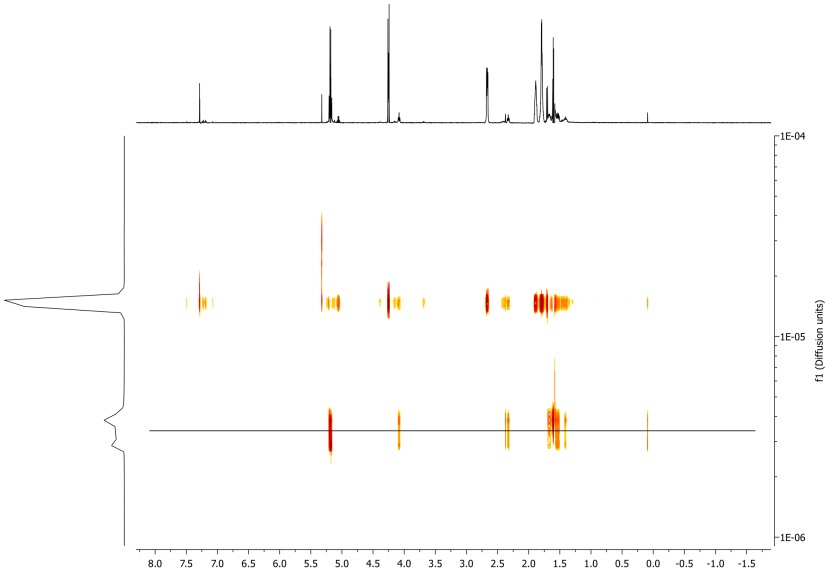

Figure B.19: ^{1}H DOSY NMR spectra in $CDCl_3$ of $PLA_{50}-b-PCL_{50}$, 130 °C in the melt. $D_{sol} = 1.54 \times 10^{-5}$ cm^2 s^{-1}, $D_{poly} = 3.28 \times 10^{-6}$ cm^2 s^{-1}.

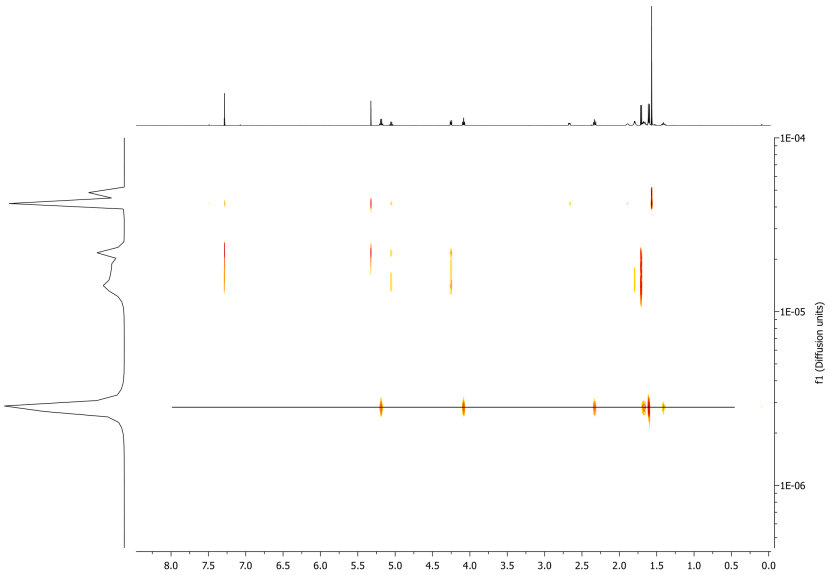

Figure B.20: ^{1}H DOSY NMR spectra in $CDCl_3$ of $PCL_{50}-b-PLA_{50}$, 130 °C in the melt. $D_{sol} = 2.04 \times 10^{-5}$ cm^2 s^{-1}, $D_{poly} = 2.71 \times 10^{-6}$ cm^2 s^{-1}.

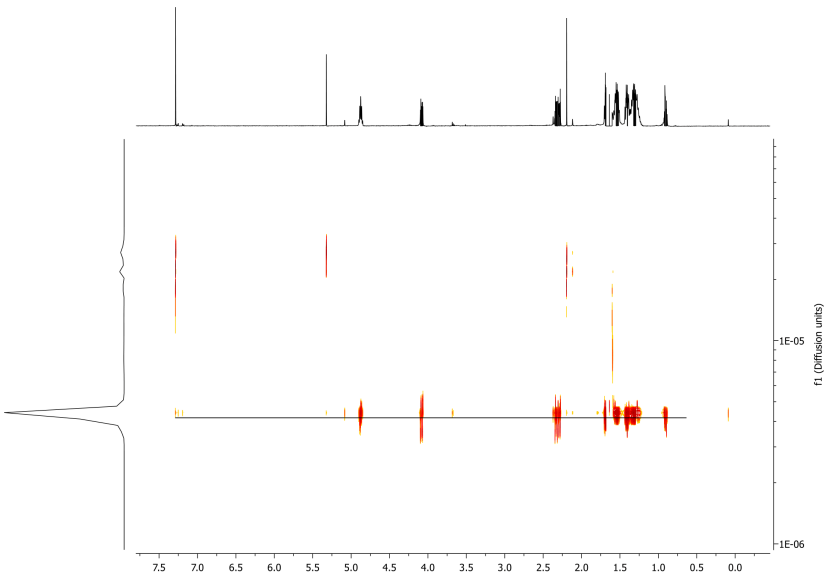

Figure B.21: ^{1}H DOSY NMR spectra in $CDCl_3$ of $PDL_{50}-b-PCL_{50}$, 130 °C in the melt. $D_{sol} = 2.48 \times 10^{-5}$ cm^2 s^{-1}, $D_{poly} = 4.30 \times 10^{-6}$ cm^2 s^{-1}.

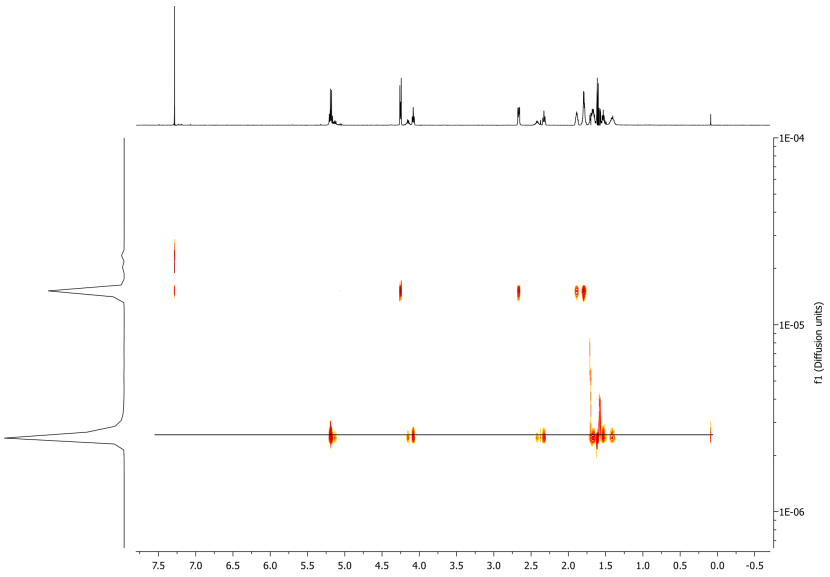

Figure B.22: ^{1}H DOSY NMR spectra in $CDCl_3$ of the one-pot$PLA_{50}-PCL_{50}$,([LA]:[CL]:[Cat]:[I] = 50:50:0.25:1], 130 °C in the melt). $D_{sol} = 2.31 \times 10^{-5}$ cm^2 s^{-1}, $D_{poly} = 2.55 \times 10^{-6}$ cm^2 s^{-1}.

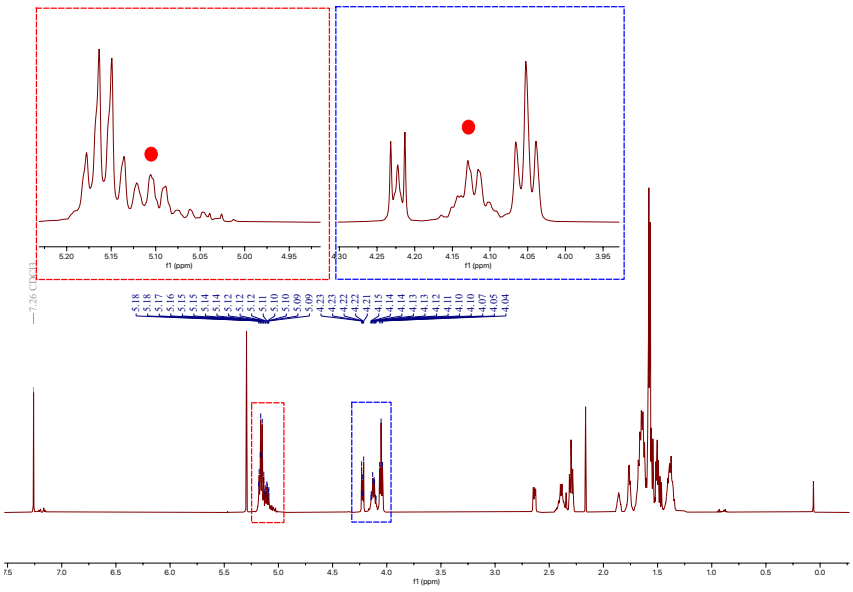

(a) ^{1}H NMR (128 scans)

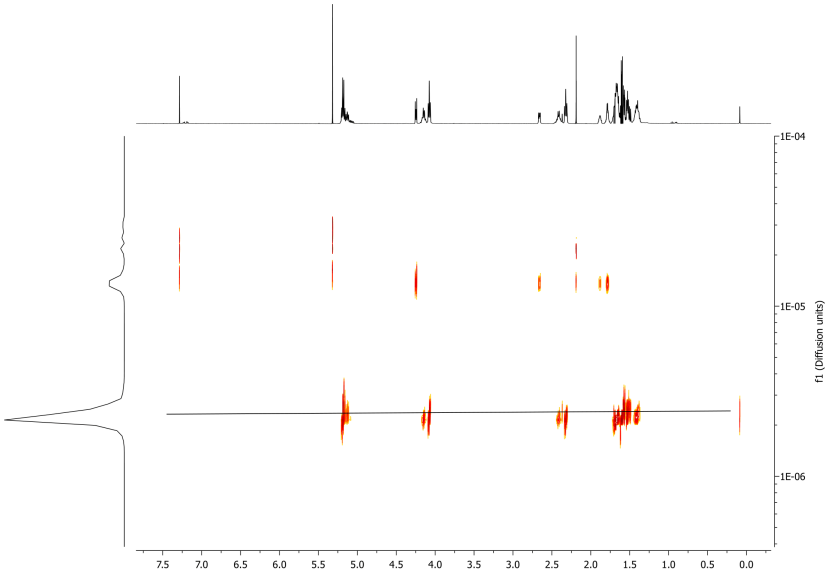

(b) ^{1}H DOSY

Figure B.23: NMR spectra in $CDCl_3$ of the one-potPLA_{50}−PCL_{50} ([LA]:[CL]:[Cat]:[I] = 50:50:1:1], 130 °C in the melt). $D_{sol} = 2.05 \times 10^{-5}$ cm^2 s^{-1}, $D_{poly} = 2.27 \times 10^{-6}$ cm^2 s^{-1}.

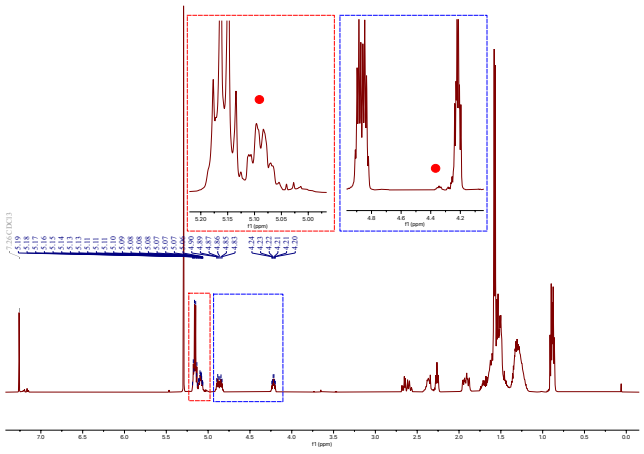

(a) ^{1}H NMR (128 scans)

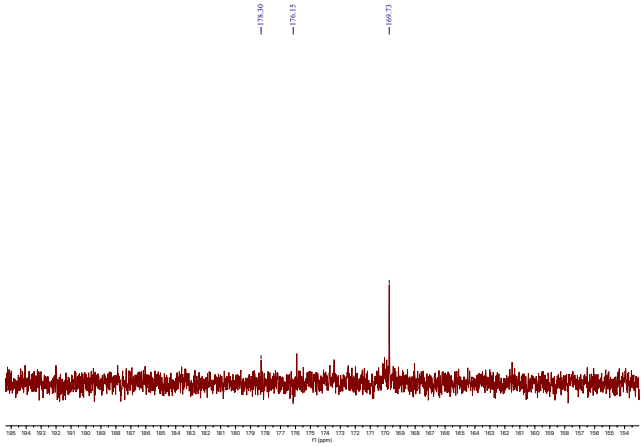

(b) ^{13}C{^{1}H} NMR

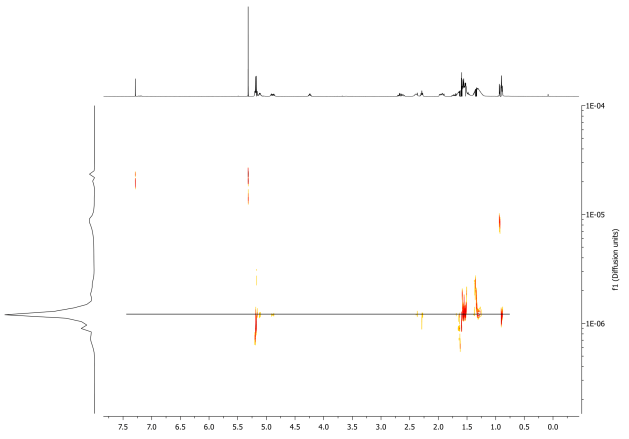

(c) ^{1}H DOSY

Figure B.24: NMR spectra in $CDCl_3$ of the one-pot PLA_{50}−PDL_{50} ([LA]:[DL]:[Cat]:[I] = 50:50:1:1], 130 °C in the melt). $D_{sol} = 2.05 \times 10^{-5}$ cm^2 s^{-1}, $D_{poly} = 2.27 \times 10^{-6}$ cm^2 s^{-1}.

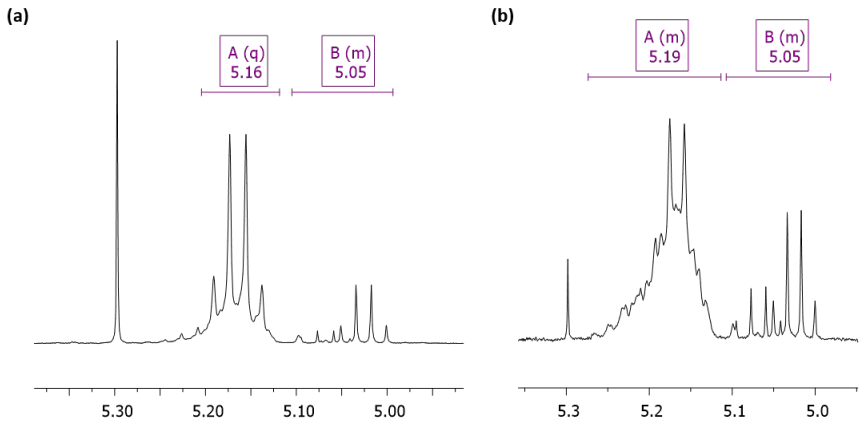

Figure B.25: Methine region of PLA (ca. 5.19 ppm) and lactide (5.05 ppm) in the ^{1}H NMR ($CDCl_3$, 400 MHz) of the crude PLA formed with (a) PS-CH_2NH_2 and (b) PS-DMAP. The scrambled quartet in (b) shows that the strength of the base resulted in a high degree of epimerisation.

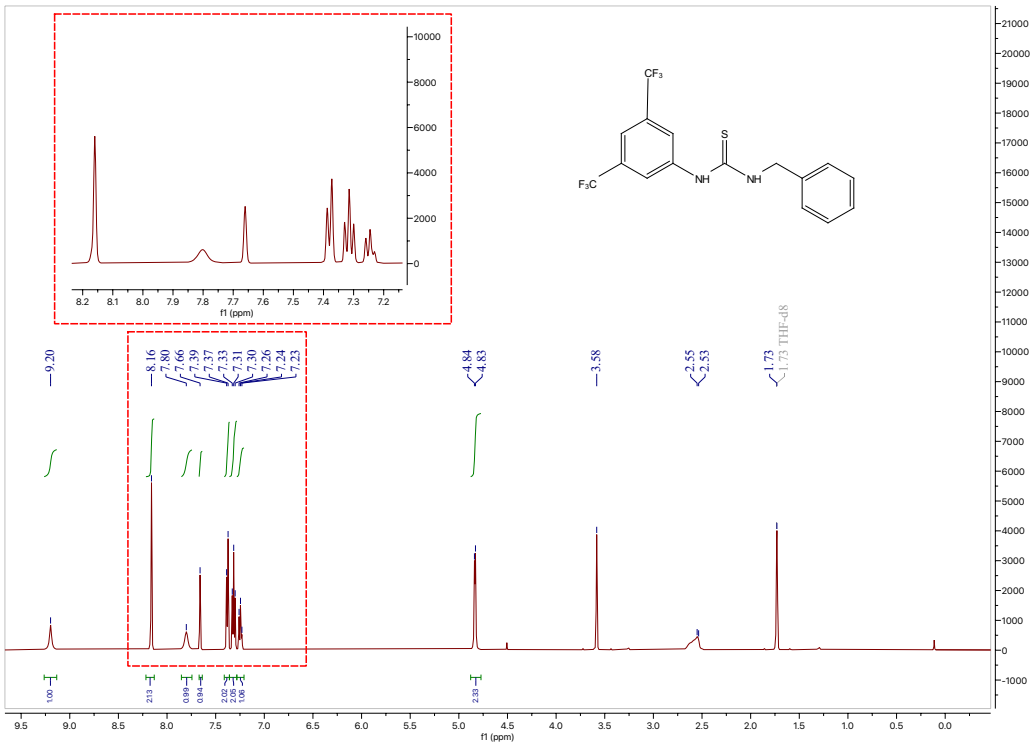

Figure B.26: NMR Study of TU, ^{1}H NMR (THF-d_8, 500 MHz) δ 9.20 (s, broad, 1H, N−H), 8.16 (s, 2H, Ar−H), 7.80 (s, broad, 1H, N−H), 7.66 (s, 1H, Ar−H), 7.38 (d, J_{HH} = 7.6 Hz, 1H, Ar−H), 7.31 (t, J_{HH} = 7.4 Hz, 1H, Ar−H), 7.24 (t, J_{HH} = 7.3 Hz, 1H, Ar−H), 4.83 (d, J_{HH} = 5.3 Hz, 1H, $-CH_2$).

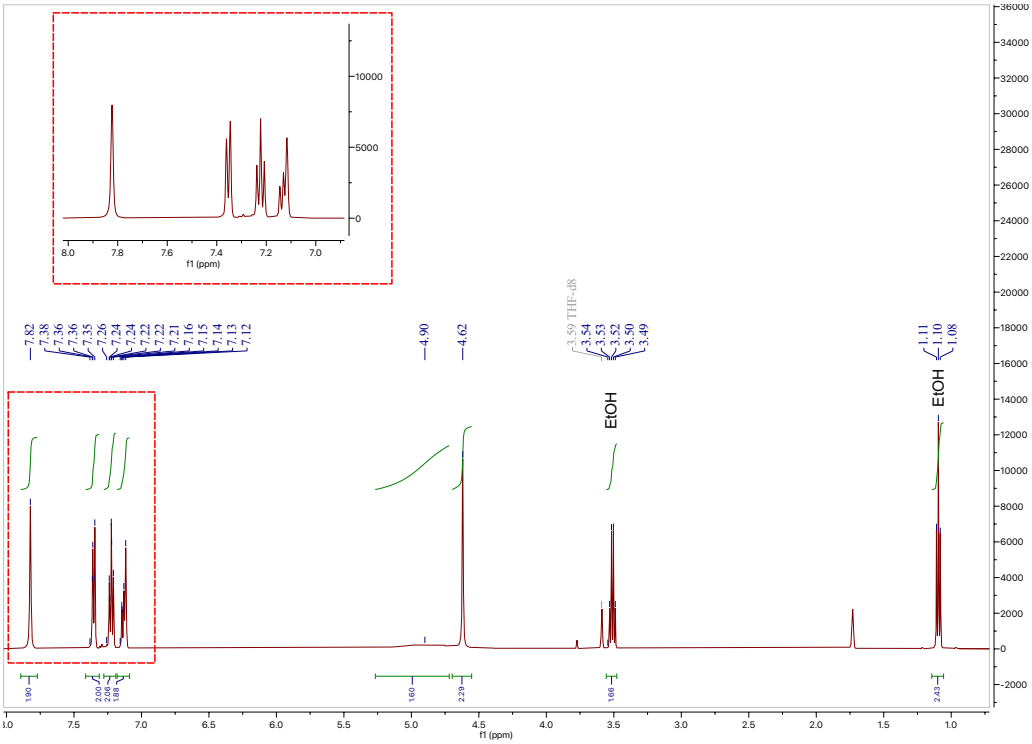

Figure B.27: NMR Study of TU/KOEt (1:1), ^{1}H NMR (THF-d_8, 500 MHz) δ 7.82 (s, 2H, Ar−H), 7.35 (d, J_{HH} = 7.4 Hz, 1H, Ar−H), 7.22 (t, J_{HH} = 7.4 Hz, 1H, Ar-H), 7.16-7.10 (m, 1H, Ar−H), 4.90 (s, broad, 1H, N−H), 4.62 (s, 1H, $-CH_2$), 3.51 (q, J_{HH} = 7.0 Hz, $-CH_2$ EtOH), 1.10 (t, J_{HH} = 7.0 Hz, $-CH_3$ EtOH).

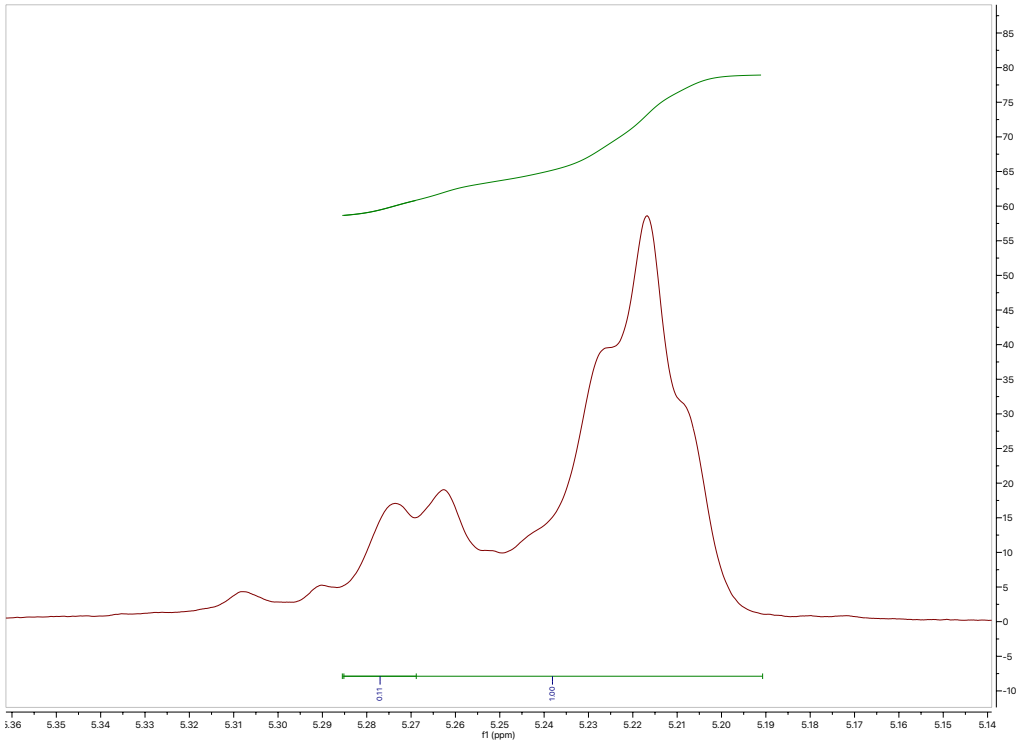

Figure B.28: Homonuclear decoupled ^{1}H{^{1}H} NMR of PLA produced from *rac*-LA, using PS-U/KOEt. [LA]:[Cat]:[KOEt] = 100:3:1, [LA] = 1 mol L^{-1} in THF, 1 h at room temperature (97%, $M_{\mathrm{n,Theo}}$ 7 000 Da, $M_{\mathrm{n,SEC}}$ 7 300 Da, $Đ_{\mathrm{M}}$ 1.71). Probability of heterotactic enchainment (P_{r}) found to be 0.45, calculated by $P_{\mathrm{r}} = \sqrt{(2 \times sis)}$.

B.5 SEC data

Chapter 3

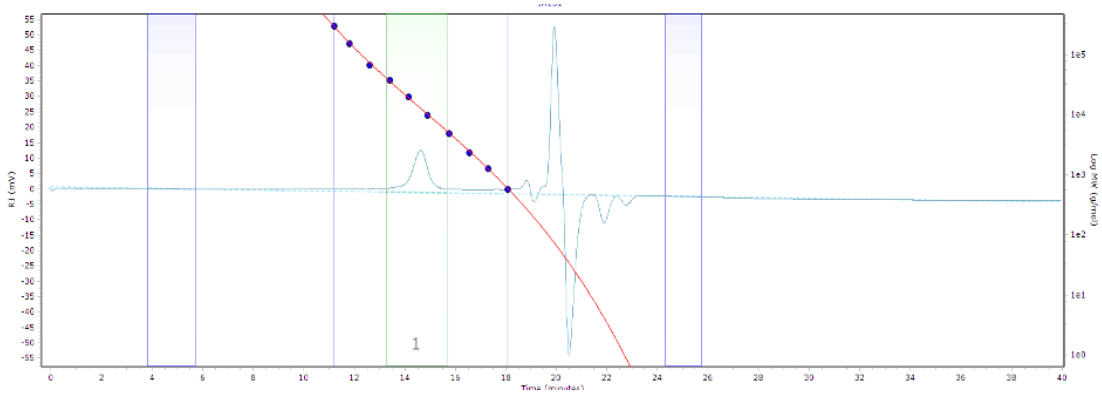

Figure B.29: Size exclusion chromatography (SEC) trace of PLA produced by **PS-L^{H}SnOct**. Conditions: [LA]:[Cat]:[I] = 200:1:4, 2.5 h in the melt at 130 °C (87%, M_n 6 300, $Đ_M$ 1.17).

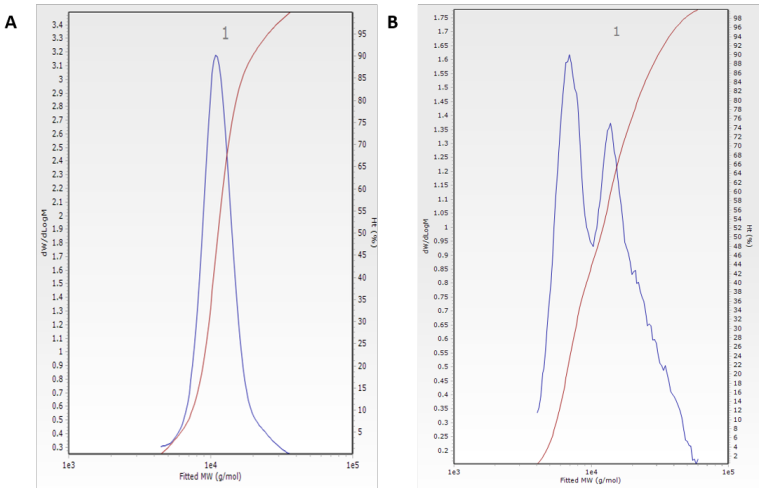

Figure B.30: SEC dispersity trace of PLA produced with **PS-L^{H}SnOct** in the melt (130 °C) after (A) 2.5 h ([LA]:[Cat]:[I] = 200:1:4, 87%, M_n 6 300 Da, $Đ_M$ 1.17), and (B) 24 h ([LA]:[Cat]:[I] = 50:1:1, 93%, M_n 6 000 Da, $Đ_M$ 1.49).

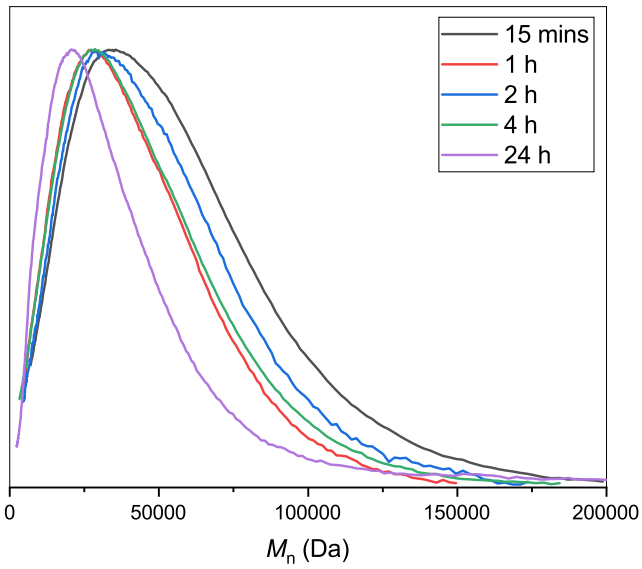

Figure B.31: SEC traces from the ROP of *L*-LA with KOEt at [LA]:[Cat]:[KOEt] = 100:0:1, [LA] = 1 mol L^{-1} in THF at room temperature.

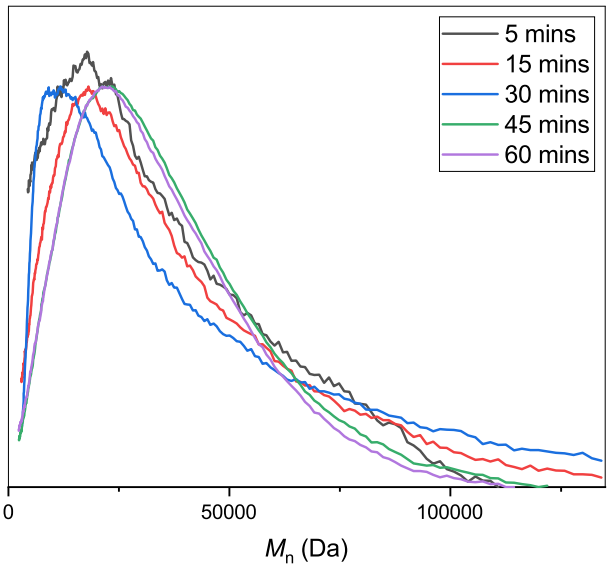

Figure B.32: SEC traces from the ROP of *L*-LA with PS-U/KOEt at [LA]:[PS-U]:[KOEt] = 100:3:1, [LA] = 1 mol L^{-1} in THF at room temperature.

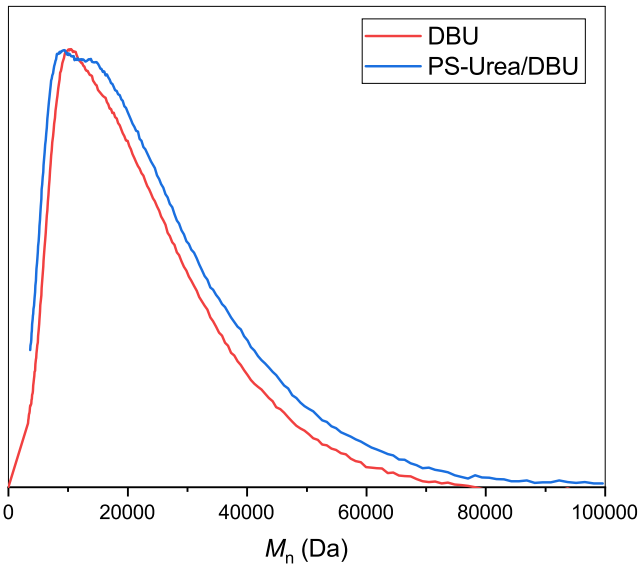

Figure B.33: SEC traces from the ROP of *L*-LA with PS-U/DBU at [LA]:[PS-U]:[DBU] = 50:1:1, [LA] = 1 mol L^{-1} in THF at room temperature, 1 hour.

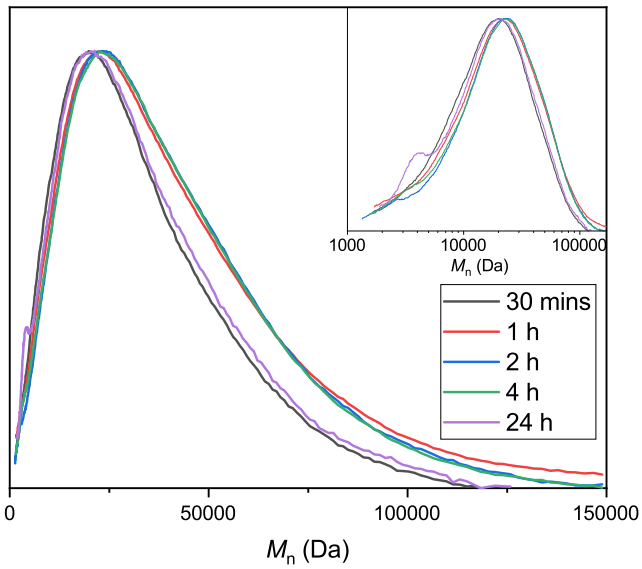

Figure B.34: SEC traces from the ROP of *L*-LA with PS-TU/KOEt at [LA]:[PS-TU]:[KOEt] = 100:3:1, [LA] = 1 mol L^{-1} in THF at room temperature. Development of the bimodal trace over time is emphasised in the logarithmic scale in the inset.

B.6 MALDI-ToF mass spectrometry data

Chapter 3

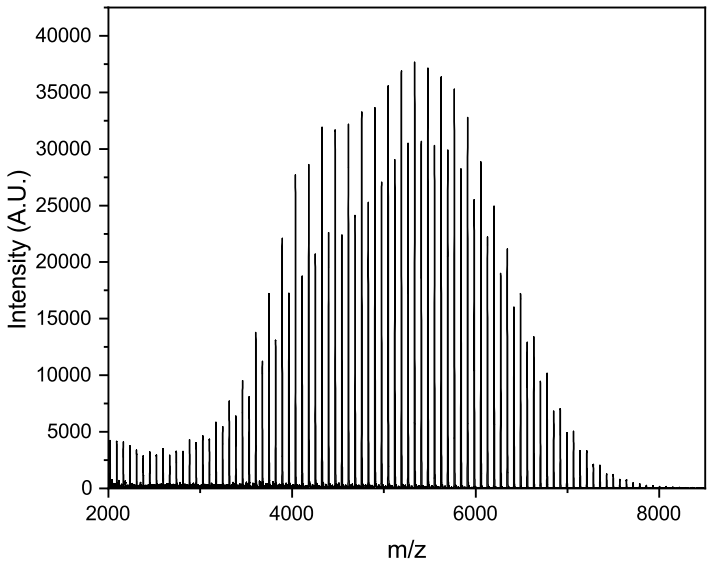

Figure B.35: MALDI-ToF spectrum of PLA from **PS-L$^{\mathbf{H}}$ZnOAc**. Conditions: [LA]:[Cat]:[I] = 50:1:1, 24 hours in the melt at 130 °C (84%, M_{n} 6450, $Đ_{\mathrm{M}}$ 1.23, major series: degree of polymerisation (DP) = 39).

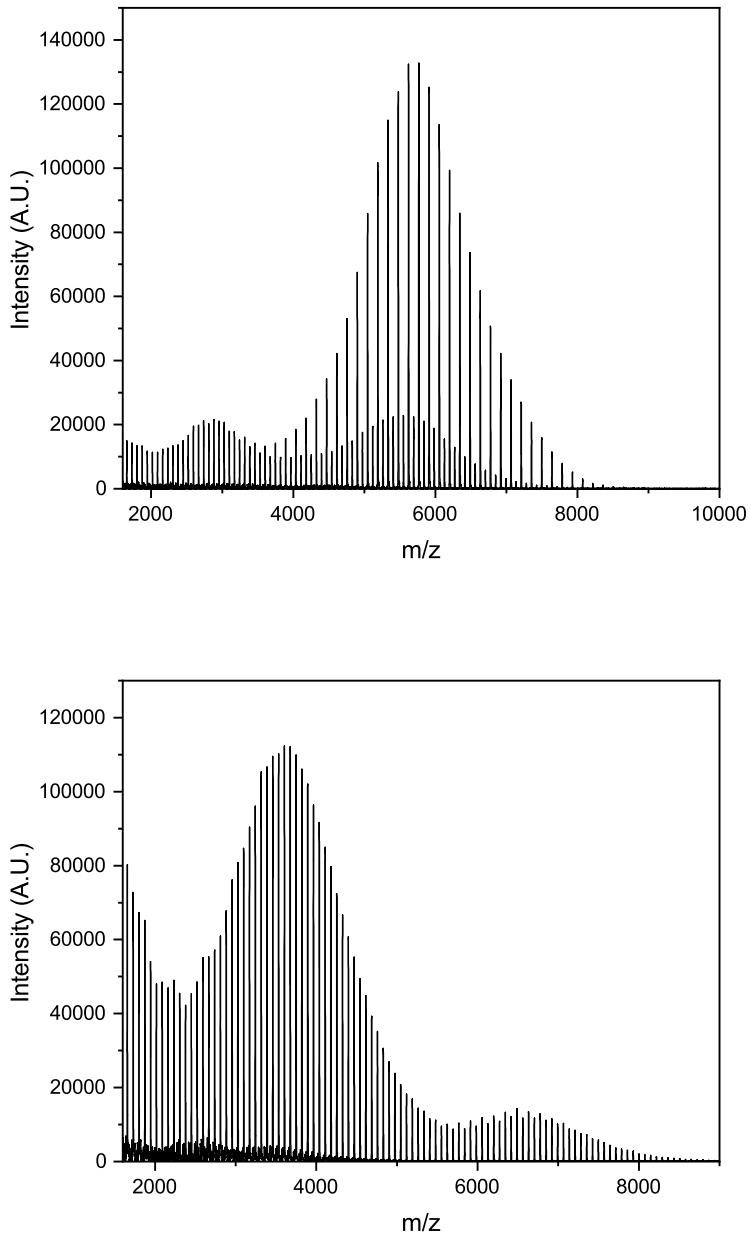

Figure B.36: MALDI-ToF spectrum of PLA from **PS-L$^{\mathbf{H}}$SnOct** after (A) 2.5 h (87%, M_{n} 6300, $Đ_{\mathrm{M}}$ 1.17, major series: DP = 40) and (B) 24 h (93%, M_{n} 6000, $Đ_{\mathrm{M}}$ 1.49, major series: DP = 24). Conditions: [LA]:[Cat]:[I] = 50:1:1, in the melt at 130 °C.

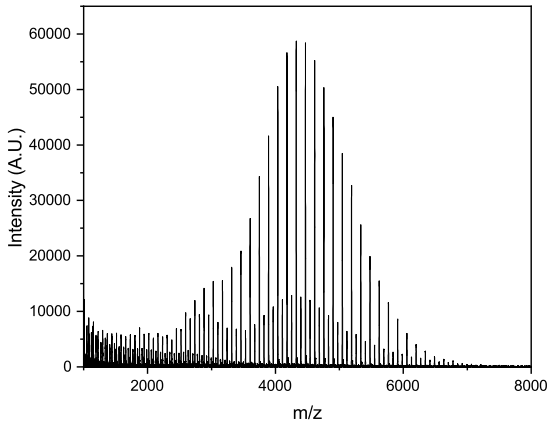

Figure B.37: MALDI-ToF spectrum of PLA from **PS-L$^{\mathbf{tBu}}$SnOct**. Conditions: [LA]:[Cat]:[I] = 50:1:1, 24 hours in the melt at 130 °C (69%, M_{n} 6250, $Đ_{\mathrm{M}}$ 1.48, major series: degree of polymerisation (DP) = 29).

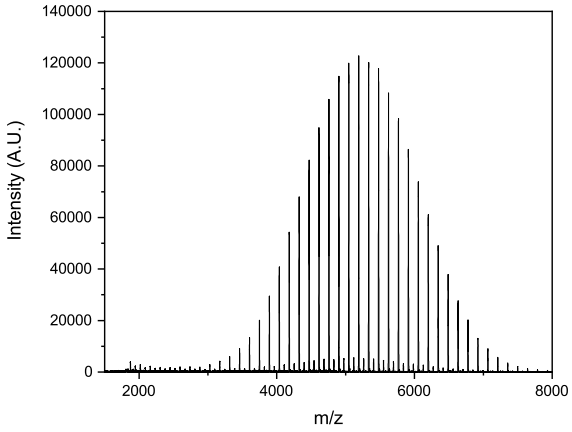

Figure B.38: MALDI-ToF spectrum of PLA from **PS-L$^{\mathbf{Cl}}$SnOct**. Conditions: [LA]:[Cat]:[I] = 50:1:1, 55 minutes in the melt at 130 °C (83%, M_{n} 6000, $Đ_{\mathrm{M}}$ 1.05, major series: degree of polymerisation (DP) = 35).

Chapter 5

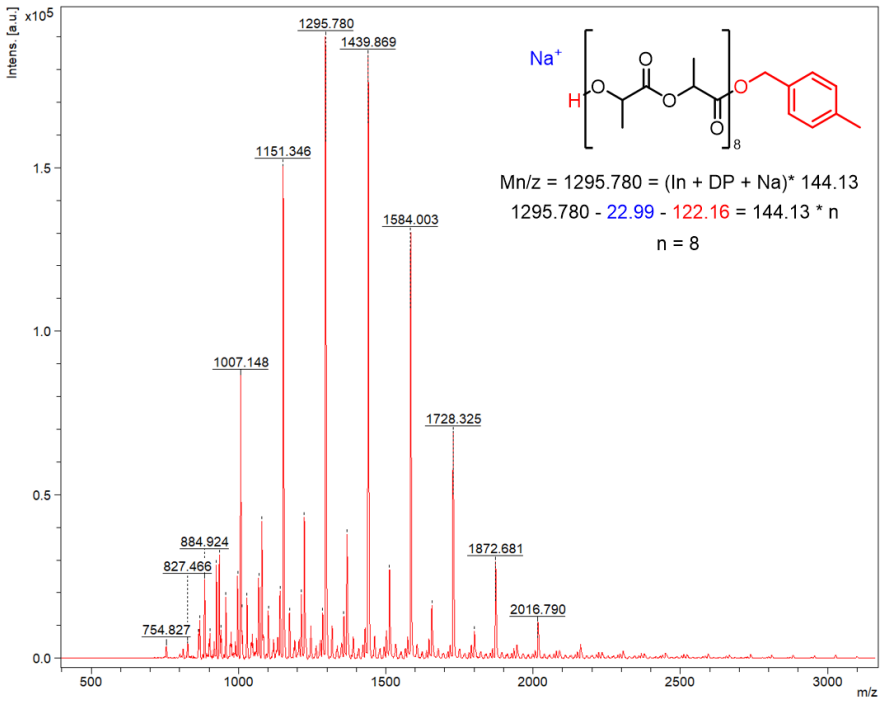

Figure B.39: MALDI-ToF of PLA produced using PS-DMAP in the melt shows high degree of transersterification, with a cyclic series.

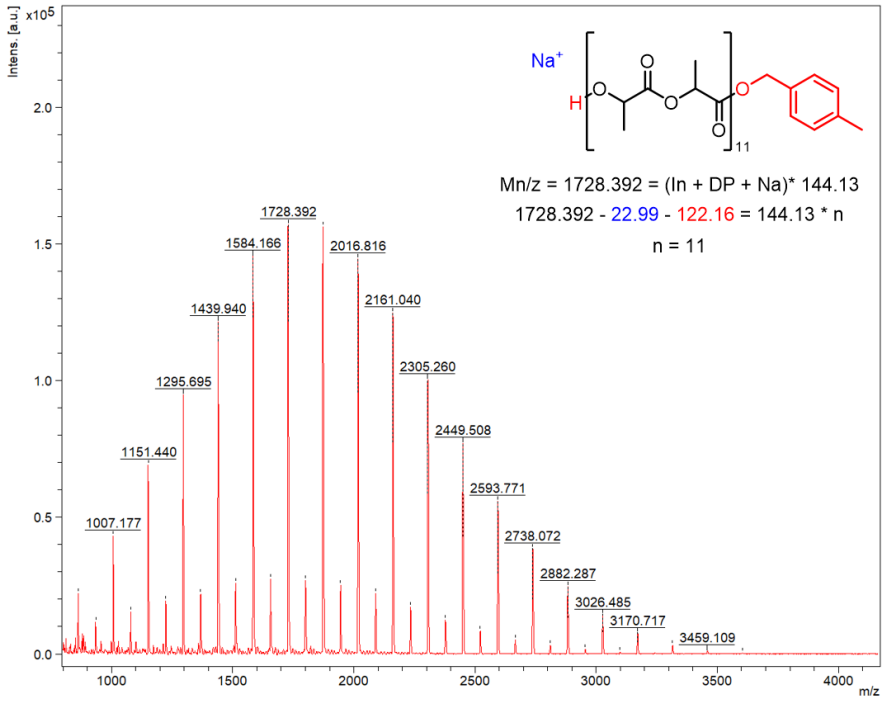

Figure B.40: MALDI-ToF of PLA produced using PS-CH_2NH_2 in the melt shows high degree of transersterification, with a cyclic series.

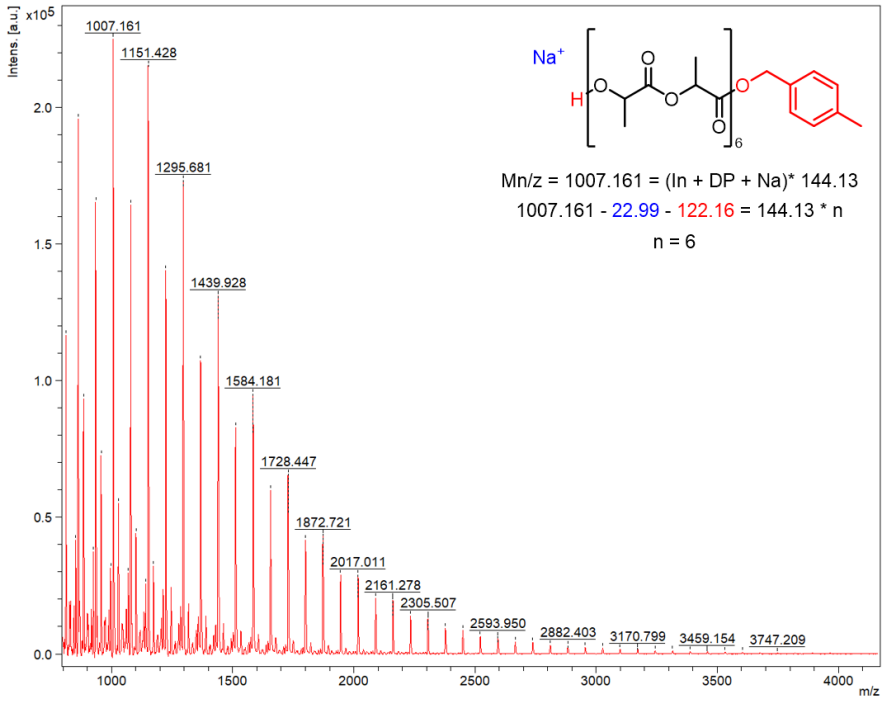

Figure B.41: MALDI-ToF of PLA produced using PS-DBU in the melt shows high degree of transersterification, with a cyclic series.

B.7 EDX data

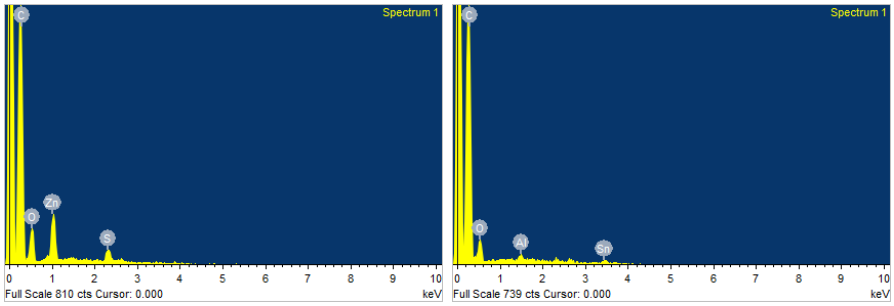

Figure B.42: EDX spectrum of (A) **PS-L$^{\mathbf{H}}$ZnOAc**, showing the lack of Cl in the complex, and prespresence of Sn and O, indicating successful immobilisation of the complex.

B.8 DSC data

Chapter 3

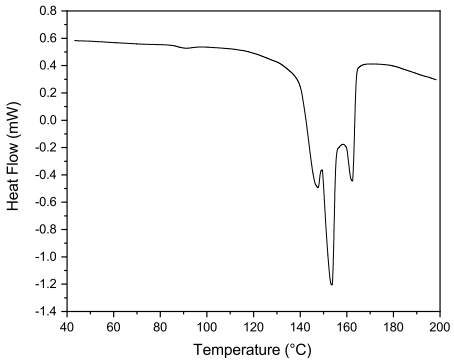

Figure B.43: DSC trace of PLA formed by **PS-L$^{\mathbf{H}}$ZnOAc** (89%, M_n 6 100 Da, $Đ_M$ 1.15). Conditions: [LA]:[Cat]:[I] = 200:1:4, hours in the melt at 130 °C. Three discernable melting temperatures during the second heating cycle (150, 153 and 162 °C), potentially due to the disrupted crystallinity from the first heating and cooling cycles.

B.9 BET data

Chapter 3

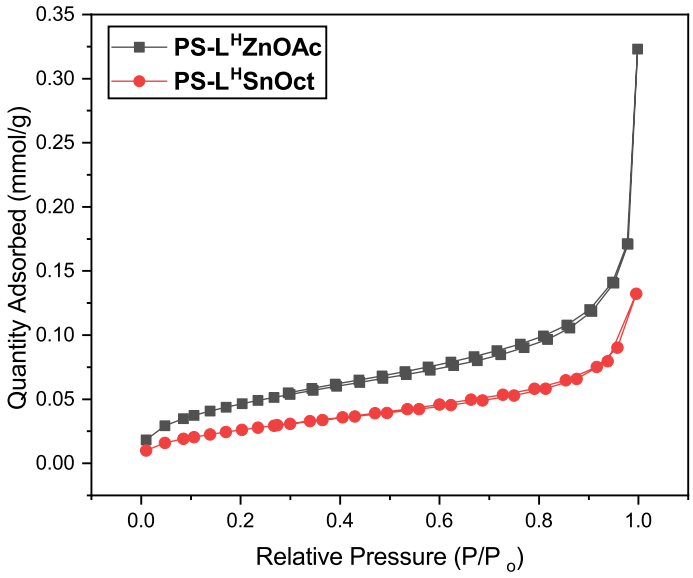

Figure B.44: N_2 adsorption-desorption isotherms of **PS-L^{H}ZnOAc** and **PS-L^{H}SnOct** catalysts.

B.10 TGA data

Chapter 3

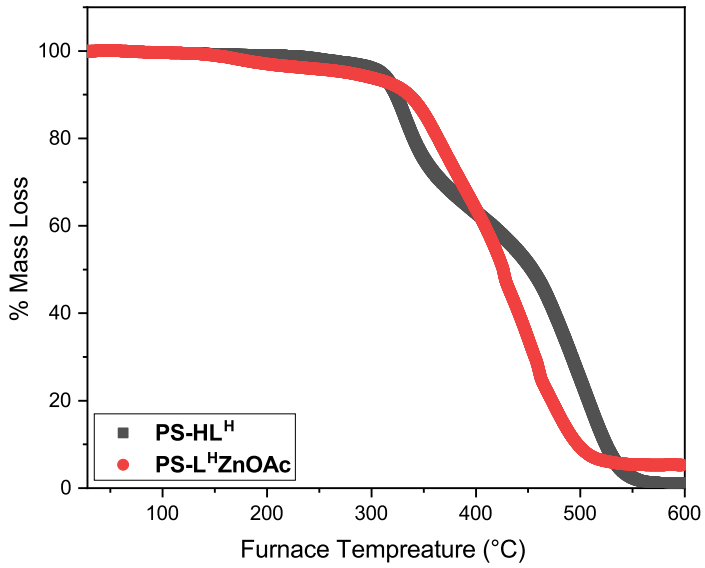

Figure B.45: Thermogravimetric analysis (TGA) of ligand **PS-HL^{H}** (grey) and its metal complex, **PS-L^{H}ZnOAc** (red).

Table B.1: TGA mass loss list for **PS-HL^{H}**, **PS-L^{H}ZnOAc** and **PS-L^{H}SnOct**.

Sample	Mass Loss Event	Δm (mg)	Δm (%)	Time (min)	Temp. (°C)	mg PS in sample (% of resin)	mg ligand in sample (% of resin)	mg M-OR in sample (% of resin)
PS-HL^{H}	1	4.168	34.45	24-37	332	-	5.76 (47.60)	-
	2	7.497	61.96	37-57	509	6.3 (52.40)	-	-
PS-L^{H}ZnOAc	1	0.246	3.28	11-21	174	-	-	3.82 (51.09)
	2	2.112	28.23	27-37	370	-	2.59 (34.60)	-
	3	4.550	60.82	37-57	427	2.41 (32.21)	-	-
PS-L^{H}SnOct	1	0.507	4.61	22-29	280	-	-	5.60 (50.82)
	2	3.664	33.31	29-44	388	-	2.55 (23.20)	-
	3	4.678	42.53	44-57	2.86 (25.98)	-	-	